MOLECULAR DYNAMICS OF BREAST CANCER RESPONSE TO AROMATASE INHIBITORS TREATMENT

Ph.D. THESIS

Gemma Santacana Font

Salamanca, 2024

Centro de Investigación del Cáncer

Instituto de Biología Molecular y Celular del Cáncer

Universidad de Salamanca

Centro de Investigación del Cáncer
IBMCC-FICUS
(University of Salamanca – CSIC)
Miguel de Unamuno Campus
37007 Salamanca (Spain)
Tel.: (+34) 923 294 720
www.cicancer.org

El **Dr. ANTONI HURTADO RODRIGUEZ**, Científico Titular del Consejo Superior de Investigaciones Científicas,

CERTIFICA

Que el trabajo de tesis titulado **"Molecular dynamics of breast cancer response to aromatase inhibitors treatment"**, presentado por **Dª GEMMA SANTACANA FONT** para optar al Grado de Doctor por la Universidad de Salamanca, ha sido realizado bajo nuestra dirección en el Centro de Investigación del Cáncer de Salamanca (USAL/CSIC). Considerando que cumple con las condiciones necesarias, autorizo su presentación a fin de que pueda ser defendido ante el tribunal correspondiente.

Y para que conste a los efectos oportunos, expedimos y firmamos el presente certificado en Salamanca, a 1 de diciembre de 2023.

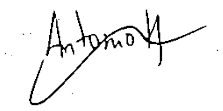

Fdo.: Dr. Antoni Hurtado Rodríguez

The research conducted in this Ph.D. thesis has been supported by:

I. Fundings from The European Union's Horizon 2020 Research as part of the RESCUER-Resistance Under Combinatorial Treatments in ER+ and ER- Breast Cancer (No. 402156).

II. Funding from the Innovation Program awarded by the Spanish Ministry of Economy and Competitiveness under Grant agreement No. 847912, from the RyC 2017 program (RYC-2017-22715).

III. Fundings from the Programa de generación de concocimiento del MIN Ciencia y Tecnologia.

IV. Funding to support the strategic plan of the Salamanca Research Center (CLC-2017-01) from Castilla y León Autonomous Government.

A totes les persones que han cregut en mi i m'han recolzat,

però en especial a les meves fonts de motivació

Elsa, Iaia Mercè i Oski

ABSTRACT

This research investigates the complex mechanisms of response and resistance to aromatase inhibitors (AIs) in luminal breast cancer patients. By exploring two AIs, namely exemestane and letrozole, the study identifies a subset of patients exhibiting distinct response to these drugs. Utilizing both human samples and *in vitro* data, the study reveals that a combination of exemestane (Exe) and its primary metabolite, 17β-hydroxyexemestane (17-HEXE), exerts strong inhibitory effects on tumor growth when both are present in patients' serum. The research establishes a crucial threshold set at 20% of 17-HEXE metabolite of total exemestane in patient serum, leading to better clinical responses, evident through reduction in Ki67 staining levels. Mechanistically, both 17-HEXE and Exe bind to the Androgen Receptor (AR), inducing a synergistic activation leading to cell death and diminishing Ras oncogene-driven signaling. Patients with tumors exhibiting at least 20% AR-positive cells are most responsive to exemestane and 17-HEXE. Interestingly, AR binding to chromatin in tumors offers a molecular signature capable of distinguishing responsive from non-responsive patients to these compounds. The study indicates a dual therapeutic role for exemestane: suppressing estrogen-driven proliferation and inducing cell death by interacting with AR at the genomic level. These insights suggest that both Exe and 17-HEXE are crucial for optimal therapeutic effects in ER+/AR+ breast cancer tumors. Moreover, this thesis delves into metastatic mechanisms, elucidating transcription factors contributing to AI resistance in luminal breast cancer patients by identifying disparities between primary and metastatic tumors. Epigenetic analyses in paired samples depicted chromatin binding site reorganization between primary and metastatic tumors. Gene set enrichment analysis identified pathways related to repression, methylation, and histone modification altered due to therapy, converging on GATA3, a key component of the NuRD complex. Furthermore, the study highlights the impact of the NuRD on the epithelial-mesenchymal transition (EMT), providing insights into the mechanisms underlying metastatic evolution. Targeting HDACs of the NuRD complex has emerged as a potential strategy with significant therapeutic implications. In summary, this thesis provides substantial insights into the complex mechanisms involved in treatment response and development of resistance to AIs in luminal breast cancer. It sets the stage for potential targeted therapeutic interventions to optimize treatment outcomes and mitigate resistances.

ABSTRACT EN ESPAÑOL

Este trabajo investiga los mecanismos de respuesta y resistencia a los inhibidores de aromatasa (IAs) en pacientes con cáncer de mama luminal. Al explorar dos IAs, específicamente exemestano y letrozol, el estudio ha identificado un subconjunto de pacientes que muestran una respuesta distinta a estos fármacos. Utilizando muestras humanas y datos *in vitro*, el estudio ha revelado que una combinación de exemestano (Exe) y su metabolito principal, 17β-hidroxiexemestano (17-HEXE), ejerce fuertes efectos inhibitorios sobre el crecimiento tumoral cuando ambos están presentes en el suero de los pacientes. La investigación establece un umbral crucial de un 20% de 17-HEXE como metabolito de exemestano en el suero del paciente, lo que conduce a mejores respuestas clínicas, evidenciadas por la reducción en los niveles de Ki67. De hecho, tanto 17-HEXE como el exemestano se unen al Receptor de Andrógenos (AR), induciendo una activación sinérgica que conduce a la muerte celular y a la disminución de la señalización impulsada por Ras. Los pacientes con tumores que muestran, al menos, un 20% de células AR-positivas son los más receptivos al exemestano y al 17-HEXE. Curiosamente, la unión del AR a la cromatina en los tumores ofrece una firma molecular capaz de distinguir a los pacientes responsivos de los no responsivos a estos compuestos. El estudio indica un papel terapéutico dual para el exemestano: suprimir la proliferación impulsada por el estrógeno e inducir la muerte celular mediante la interacción con el AR a nivel genómico. Estos conocimientos sugieren que tanto el exemestano como 17-HEXE son cruciales para obtener efectos terapéuticos óptimos en los tumores de cáncer de mama ER+/AR+. Además, esta tesis profundiza en los mecanismos metastásicos, elucidando los factores que contribuyen a la resistencia a los IAs en pacientes con cáncer de mama luminal mediante la identificación de disparidades entre tumores primarios y metastásicos. Los análisis epigenéticos en muestras emparejadas presentan una reorganización de los sitios de unión de la cromatina entre tumores primarios y metastásicos. El análisis de enriquecimiento de conjuntos génicos identificó vías relacionadas con la represión, la metilación y la modificación de histonas alteradas debido a la terapia, convergiendo en GATA3, un componente clave del complejo NuRD. Además, el estudio destaca los impactos del NuRD en la Transición Epitelial-Mesenquimal (EMT), brindando conocimientos sobre los mecanismos subyacentes a la evolución metastásica. El enfoque en los HDACs del complejo NuRD ha surgido como una estrategia potencial con importantes implicaciones terapéuticas.

TABLE OF CONTENT

LIST OF FIGURES

LIST OF TABLES

LIST OF ABBREVIATIONS

16-OHE1	16-hydroxyestrone
17-HEXE	17β-hydroxyexemestane
2-OHE1	2-hydroxyestrone
3-MA	3-methyladenine
AA	Abiraterone acetate
AIs	Aromatase inhibitors
AKR	Aldoketoreductases
ANOVA	Analysis of variance
AR	Androgen receptor
BAH	Bromo adjacent homology
BC	Breast cancer
Bic	Bicalutamide
BMI	Body mass index
bp	Base pairs
BPM	Bases per million
BSA	Bovine serum albumin
cDNA	Complementary DNA
CEA	Carcinoembryonic antigens
CERAN	Complete estrogen receptor antagonist
ChIP	Chromatin immunoprecipitation
CT	Computed tomography
CTCs	Circulating tumor cells
ctDNA	Circulating tumor DNA
Cts	Cycle thresholds
CYP	Cytochrome P450
DBD	DNA-binding domain
DCIS	Ductal carcinoma *in situ*
DFS	Disease-free survival
DHT	Dihydrotestosterone
DMEM	Dulbecco's modified eagle medium
DMSO	Dimethyl sulfoxide
DNA	Deoxyribonucleic acid
DNMTi	DNA methyl transferase inhibitors
DTT	Dithiothreitol
E1	Estrone
E1s	Estrone sulfate
E2	17β-estradiol
E3	Estradiol
EDTA	Ethylenediaminetetraacetic acid
EMT	Epithelial-mesenchymal transition
ER	Estrogen receptor
ERE	Estrogen response elements
ESR1	Estrogen receptor 1
EtOH	Ethanol
EV	Extracellular vehicles
Exe	Exemestane
FBS	Fetal bovine serum
FDR	False discovery ratio
FF	Fresh-frozen
FFPE	Formalin-fixed paraffin-embedded
Fit	Fixed-tissue chromatin immunoprecipitation
FSH	Follicle-stimulating hormone
Ful	Fulvestrant
GAPDH	Glyceraldehyde 3-phosphate dehydrogenase
GBM	Glioblastoma multiforme
GnRH	Gonadotropin-releasing hormone
GSEA	Gene set enrichment analysis
H&E	Hematoxylin & eosin
H3	Histone 3
HAT	Histone acetyltransferase

HDAC	Histone deacetylase
HDACi	HDAC inhibitors
HDM	Histone demethylase
HER2	Human epidermal growth factor receptor 2
hg19	Human genome 19
HMT	Histone methyltransferase
HPC	High performance computing
HR	Hormone receptor
HRP	Horseradish peroxidase
HRT	Hormone replacement therapy
HSD	Honestly-significant-difference
HSP	Heat shock proteins
IBC	Inflammatory breast cancer
IDC	Invasive ductal carcinoma
IHC	Immunohistochemistry
ILC	Invasive lobular carcinoma
IP	Immunoprecipitation
LBD	Ligand-binding domain
LCIS	Lobular carcinoma *in situ*
Let	Letrozole
LH	Luteinizing hormone
LN2	Liquid nitrogen
MET	Mesenchymal-to-epithelial transition
miRNA	MicroRNAs
MRI	Magnetic resonance imaging
MSigDB	Molecular signatures database
MTA	Metastatic tumor antigen
mTORC1	Mammalian target of rapamycin complex 1
MUC-CA	Mucinous carcinoma
NES	Net enrichment score
NST	Non-special type
NT	Non-targeted
NuRD	Nucleosome remodeling and deacetylase
PBS	Phosphate buffered saline
PCA	Principal component analysis
pCR	Pathological complete responses
PET	Positron emission tomography
PFS	Progression-free survival
PROTAC	Proteolysis-targeting chimeric
RNA	Ribonucleic acid
RR	Relative risk
RT	Room temperature
RTK	Receptor tyrosine kinase
SDS	Sodium dodecyl sulfate
SE	Standard error
SEM	Standard error mean
Seq	Sequencing
SERCA	Selective estrogen receptor covalent antagonists
SERD	Selective estrogen receptor degraders
SERM	Selective estrogen receptor modulators
siRNA	Short interfering RNA
SNEC	Small cell neuroendocrine carcinoma
SNP	Single nucleotide polymorphism
SPECT	Single photon emission computerized tomography
TAM	Tumor-associated macrophages
TF	Transcription factor
TME	Tumor microenvironment
TNBC	Triple-negative breast cancer
TSS	Transcription start site
VPA	Valproic acid
WB	Western blot
WT	Wild-type

INTRODUCTION

1. Breast Cancer (BC): Overview

1.1. BC Epidemiology

1.1.1. Incidence and mortality of breast cancer today

Breast cancer (BC) is the leading cause of cancer in women worldwide, and it is also the most frequent when total population is considered. In 2022, around 2.3 million women were diagnosed with breast cancer, making it the cancer with the highest incidence (47.8 per 100000). In 2020, with 7.8 million women alive 5 years after being diagnosed with breast cancer, it is the world's most prevalent cancer. In 2022 breast cancer also caused 685000 deaths worldwide, being the fifth cause of cancer death, but it is also the second leading cause of cancer mortality (13.6 per 100000) [1]. However, in men, breast cancer represents only 1% of cancer cases and deaths from this cause [2].

Breast cancer is the most common cancer diagnosed in women worldwide (diagnosed in 159 countries), and it affects women at any age after puberty, with rates increasing with age, with only 5% of cases diagnosed before the age of 40 [2]. Female breast cancer occurs in developed and developing countries, but the incidence rate varies worldwide from less than 30 per 100000 women to more than 70 per 100000 women [1, 3]. Overall, the highest incidence rates occur in Europe, North America, Australia and New Zealand, intermediate rates happen in South America and Eastern Europe, and the lowest incidence takes place in most of the African and Asian countries (Figure 1) [4]. The age-standardized incidence and mortality rates by areas of the world are detailed below (Figure 2).

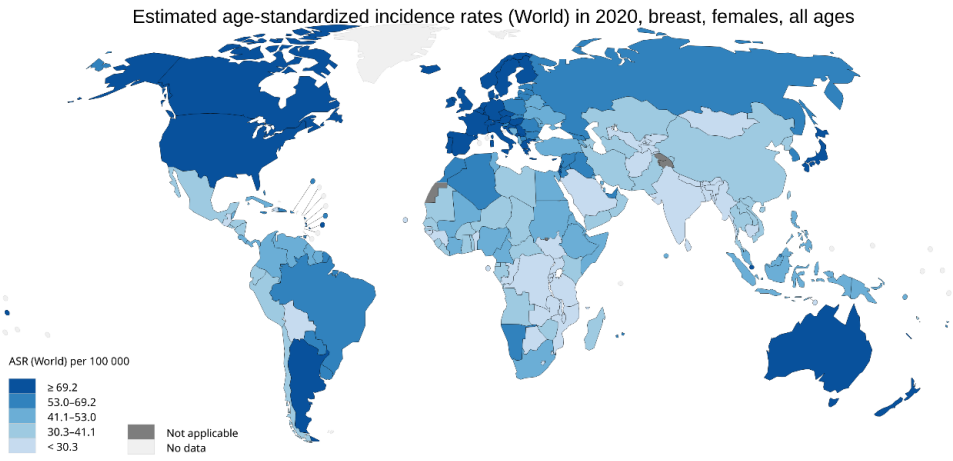

Figure 1. Female breast cancer estimated age-standardized incidence rate by country per 100000 women. World map showing the incidence rates per 100000 women per country. The color codes go from the lightest blue for incidence rates lower than 30.3 to the darkest blue for rates higher than 69.2 [1].

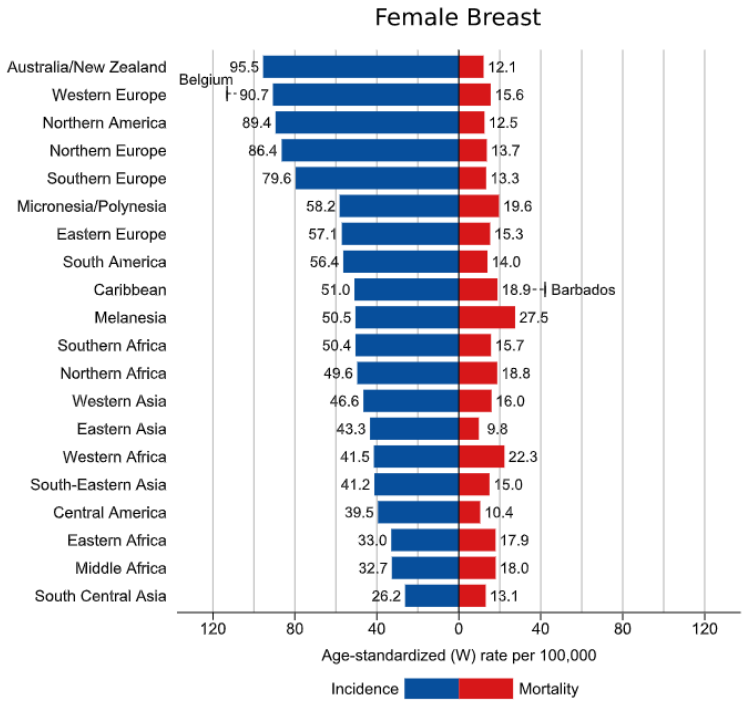

Figure 2. Female breast cancer incidence and mortality age-standardized rates by region in 2020. Barplot displaying the incidence and mortality rates per 100000 cases for different regions across the world [1].

1.1.2. Breast cancer incidence and mortality: historical evolution

During the 1980s and 1990s, breast cancer incidence increased in developed countries like North America, Oceania and Europe and this is likely to be associated with widespread mammography screening increment [1]. In the 2000s, breast cancer incidence dropped or stabilized in Western countries in women aged more than 65 (Figure 3) [5]. This shift was attributed to a reduction usage of menopausal hormone replacement therapy (HRT) [6].

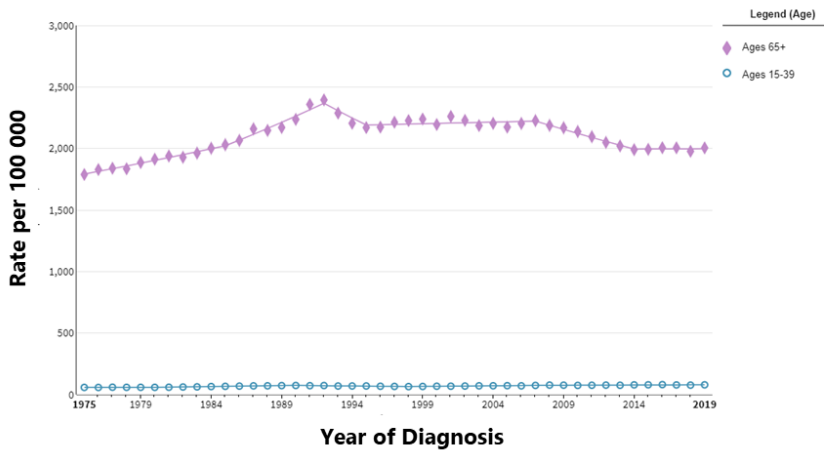

Figure 3. Annual age-adjusted incidence rate of breast cancer in women in the United States between 1975 and 2019. Plot showing the annual incidence rate per 100000 women divided by women 65 years-old or older (purple) and women between 15 and 39 years-old (blue) [7].

In recent years, breast cancer incidence is rising faster in developing regions like South America, Africa, or Asia, but also in high-income Asian countries where rates were previously low [8]. This has been linked to changes in lifestyle and sociocultural habits, which have influenced the prevalence of associated risk factors such as obesity, having fewer children, and physical inactivity [1].

Age-standardized breast cancer mortality in high-income countries decreased by 40% between the 1980s and 2020 due to mammography screening and better treatments [9]. However, mortality rates have increased in developing countries, which is likely due to higher incidence rates and limited access to early detection and treatment [10, 11]. This results in breast cancer having a higher survival rate than other cancers, especially in developed countries with an 80% survival rate after 5 years and a 40% survival in low-income countries [12, 13].

1.2. Breast cancer pathogenesis

1.2.1. Breast anatomy

The breast is an organ located between the second and sixth/seventh ribs and chest muscles. It is composed mainly by fat, glands and connective tissue (stroma) that are surrounding the lobules and ducts [14]. In more detail, breasts are made up of the following components (Figure 4):

- **Skin**: is the breast's most superficial layer and merges with the superficial fascia [15].
- **Superficial fascia**: is a layer beneath the skin that envelopes the breast parenchyma with the deep facia [15].
- **Breast parenchyma**: is composed of fat and three different types of tissue: glandular epithelium, fibrous stroma and supporting structures [14].
    - Glandular epithelium: accounts for 10-15% of the adult female breast and it is composed of 15-20 lobes, known as terminal ductules or acini, that are arranged in a radial pattern around the nipple [16]. These lobes divide into smaller lobules, which are the milk-producing glands, and are connected by ductiles that merge and culminate in one main duct. This duct widens beneath the nipple areola complex to form a lactiferous sinus to exits the milk through the nipple [14].

- Fibrous stroma and supporting structures: most commonly referred to as the suspensory ligaments of Cooper. These are fibrous bands of connective tissue that travel through the breast and insert into the dermis [14].
- Adipose tissue: is the remainder of the breast and it raises with age and is maximal in postmenopausal breast [14]. It is supplied by network of nerves, blood vessels, lymph vessels, and lymph nodes, and is also composed of fibrous connective tissue and ligaments [17].

- **Nipple (areola complex):** is composed of sebaceous, sweat, and accessory glands that form the Montgomery tubercles. The nipple is the opening in the skin of the breast where the lactiferous sinuses ducts join to form larger ducts that allow milk to exit the breast through the 10-15 orifices. It is surrounded by a thicker, darker skin called the areola [14].
- **Deep fascia**: is a layer of tissue deeper than the breast parenchyma [14].

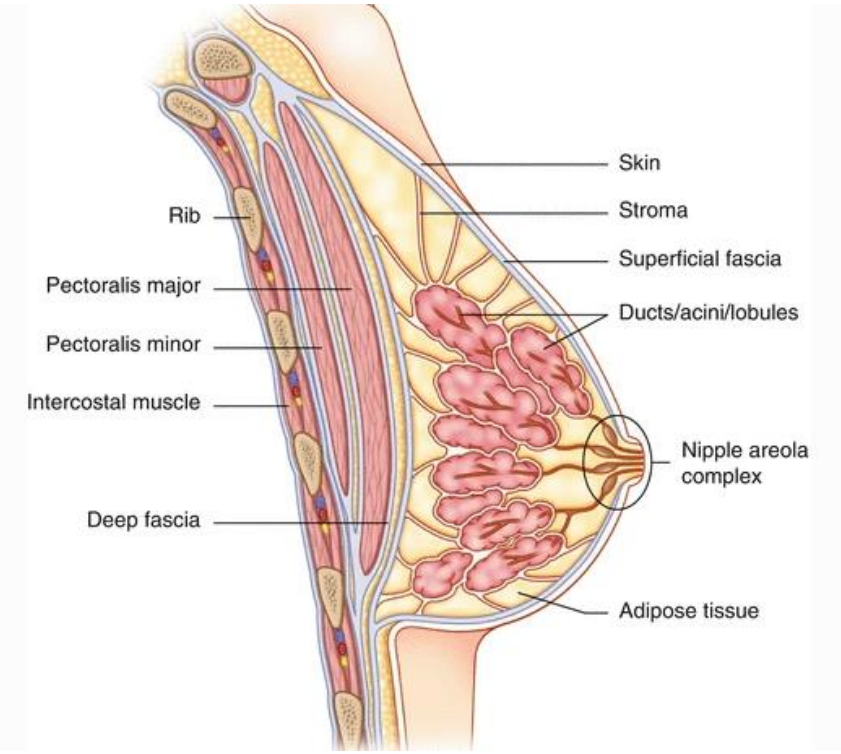

Figure 4. Anatomy and components of the breast. Illustration of the breast anatomy with its most significant components highlighted [14].

1.2.2. Breast physiology

Before puberty there are no discernible functional or structural differences between male and female breasts. The pre-pubertal breast, in both males and females, consists of multiple poorly developed rudimentary ducts arranged circumferentially and converging towards the nipple. However, during puberty, female breast undergoes a remarkable transformation in both its structure and function, leading to a sexual dimorphism. These changes are a direct consequence of the breast's distinctive reaction to various hormonal influences which will be elaborated in this section. It is important to note that the following description of the breast's physiology will be specific to the female breast, as its primary function is lactation and encompassing the synthesis, secretion, and ejection of the milk [18].

1.2.2.1. Female breast from birth to puberty

Breast development begins in the fifth and sixth week of fetal development and continues until puberty. During puberty, the ducts begin to proliferate, and the terminations of these ducts form solid cell masses that will eventually develop into breast lobules. At that time, the breast is made up of dispersed ducts that are lined with epithelium and a dense fibrous stroma. This initial growth during the early phases of puberty is influenced by increased levels of estrogen and progesterone via the hypothalamic-pituitary axis, which are responsible for breast growth and development. When puberty begins, the hypothalamic-pituitary axis becomes less sensitive to estrogen's negative feedback. This desensitization causes the hypothalamus to produce more gonadotropin-releasing hormone (GnRH) that stimulates the anterior pituitary to release luteinizing hormone (LH) and follicle-stimulating hormone (FSH). Consequently, there is an increase in estrogen and progesterone release, which, in turn, triggers female breast development [14].

Estrogen promotes ductal system proliferation and branching, as well as the maturation and prominence of the nipples. Progesterone, on the other hand, promotes the development of breast lobules and the differentiation of epithelial cells. The growth and multiplication of acini at the areolar ends of the ducts are the combined result of estrogen and progesterone acting synergistically. The breast after puberty consists of fat, stroma, lactiferous ducts, and lobular units. From that point, the breast has several functional and supportive structures, but some of these do not fully develop until pregnancy and lactation, and then regress, or involute, after lactation and at menopause [14, 18].

1.2.2.2. Female breast physiology in menstrual cycle

The menstrual cycle has an impact on both the uterus and the breast. In the follicular phase (days 4-14), estrogen levels rise, leading to epithelial proliferation and increased cell division. In the luteal phase (days 15-28), progesterone levels increase while estrogen decreases. During this phase, mammary ducts expand, and alveolar epithelial cells differentiate into secretory cells. Lipid droplets may accumulate, and some secretion may occur within the ducts. Additionally, estrogen causes histamine-like effects, resulting in increased blood flow and breast swelling before menstruation [14].

1.2.2.3. Female breast physiology during pregnancy and lactation

During pregnancy, the breast suffers multiples changes, for example, the number of new acini (milk-producing units) increases while the fibrous stroma decreases. In the first trimester, the alveoli start to develop, and the ducts grow and branch out. Lobules also form due to the increase in estrogen. Additionally, the nipple-areola complex darkens and enlarges. In the second trimester, progesterone levels rise, leading to further lobule formation. The alveoli now displays a lumen surrounded by secretory cells and begins to produce colostrum, which consists of eosinophilic cells, plasma cells, leukocytes, and epithelial cells that will be replaced by true secretion of milk. In the third trimester, the alveoli continue to produce colostrum. During this time, epithelial cell differentiation is complete, resulting in the development of secretory cells that produce and secrete milk proteins. Oxytocin levels rise, especially in the third trimester, causing myoepithelial cells to proliferate around the ductal structures. These myoepithelial cells contract, assisting in the movement of milk towards the nipple-areola complex [14, 18].

Following birth, there is a sudden decrease in the levels of estrogen, progesterone, and placental lactogen, while prolactin levels increase. Prolactin, which stimulates the production and secretion of milk, in conjunction with other growth factors, results in the accumulation of colostrum and, later, milk in the alveoli and ducts. The stimulation of the nipple-areola complex causes oxytocin release and contraction of the myoepithelial cells surrounding the ductal system facilitating the flow of milk from the breast. When lactation ceases, prolactin and oxytocin levels decrease. Any remaining secretions are cleared through phagocytosis. The glandular, ductal, and stromal elements of the breast undergo atrophy, and the secretory cells responsible for milk production undergo apoptosis [14].

1.2.2.4. Female breast physiology in menopause

The beginning of menopause is characterized by a natural and steep decline in the body's production of estrogen and progesterone. This lack of hormonal stimulation causes a progressive decrease in glandular tissue in the breast, as well as an increase in fatty tissue. As a result, tissue density is reduced [18]. After menopause, the glandular tissue atrophies, and the connective tissue becomes less cellular and has a lower collagen content. Some women have significant fatty infiltration in the breast, whereas, in others, the breasts shrink significantly. At this stage, the breast parenchyma regresses and is replaced by adipose tissue. This transformation occurs as the breast's ductal, glandular, and connective tissue elements undergo involution. Although the ductal system is intact, there is atresia, which causes the lobular units to collapse. The number of lymphatic channels within the breast parenchyma also decreases [14].

1.2.3. Breast cancer pathogenesis

Healthy cells have limited growth promotion and regulation, which serves to maintain tissue function and structure. Cancerous cells, on the other hand, proliferate indefinitely and continuously even in the absence of external stimuli and outcompete growth suppressor genes [19, 20]. Therefore, breast cancer is a disease characterized by uncontrolled cell growth in the breast and its development and progression involves various factors and processes. There are different types of breast cancer based on which cells in the breast develop into cancerous ones, more detail in Section 1.3.2. (Introduction) [21].

Healthy cells are tightly controlled by complex signaling pathways that allow cells to communicate with one another and with their surrounding environment. Not surprisingly, many of these signaling pathways are disrupted or hijacked by cancer cells. In essence, cancer is primarily caused by genetic and epigenetic alterations that grant cells the ability to bypass the mechanisms that normally limit their growth, survival, and migration. Many of these changes affect signaling pathways responsible for essential functions such as cell proliferation, division, death, differentiation, fate, and motility. In this context, activating mutations in proto-oncogenes can lead to the hyperactivation of these signaling pathways, while the inactivation of tumor suppressors eliminates crucial signaling pathways regulators [22].

1.2.4. Risk factors

A risk factor is defined as anything that increases an individual's likelihood of developing a disease, in this section breast cancer risk factors will be detailed [23]. It is estimated that 90-95% of breast cancers are caused by environmental or reproductive hormonal factors, with only 5-10% associated to hereditary genetic causes [24]. The primary risk factors for breast cancer development are as follows:

- **Gender**: women are about 100 times more likely than men to develop the disease [23].
- **Aging:** Breast cancer incidence is strongly correlated with advancing age, with the majority of cases being diagnosed in women around menopause (55 years of age and older). Women under the age of 45 have a significantly lower risk of developing breast cancer [23, 25].
- **Family history**: A woman's risk of developing breast cancer nearly doubles if she has a first-degree relative (mother, sister or daughter) with the disease, and having two first-degree relatives diagnosed with breast cancer nearly triples her risk [26]. Interestingly, women also have a higher risk of developing breast cancer if their father or brother have the disease. However, less than 15% of breast cancer patients have a family member who also has the disease, as the vast majority (approximately 85%) of breast cancers occur in women who have no apparent family history of breast cancer [23, 27].
- **Reproductive factors**: Women's reproductive life can have a role by having a protective effect against breast cancer or by increasing the risk of developing the disease. For instance, Hsieh et al. [28] noted that early menarche (first menstruation), particularly before the age of 12, is linked to a slightly increased risk of developing breast cancer [23]. However, for every two years that menarche is delayed, the risk of developing breast cancer is reduced by 10% [25]. Additionally, the age at which menopause occurs also affects the likelihood of developing breast cancer. The risk is higher in women who experience menopause later in life, especially after the age of 55 [23]. It has been estimated that the risk increases by 3% per year of continued menstruation [29]. The age of pregnancy, parity, or breastfeeding also has a correlation (risk or protection) with breast cancer occurrence [30]. A slightly higher overall risk of breast cancer exists in women who have never given birth or who have their first child after reaching the age of 30. Conversely, early pregnancy and/or

having multiple pregnancies are linked to a lower risk of breast cancer [23]. Each extra birth reduces the risk of breast cancer by 10% [31]. In addition, prolonged breast feeding provides similar protection, lowering the risk of breast cancer occurrence by 4.3% per year [25].

- **Estrogen**: Estrogens, both endogenous and exogenous, are linked to an increased risk of breast cancer. In pre and post-menopausal women, high levels of circulating estrogen are linked to a higher incidence of estrogen receptor (ER) positive breast cancer [32]. The main sources of exogenous estrogen are oral contraceptives and hormone replacement therapy (HRT). Many birth control methods rely on hormones, which have a slightly increased risk of breast cancer. Although, once the regimen is discontinued, the risk appears to return to normal within 10 years [29]. HRT usually consists on the administration of exogenous estrogen, or other hormones, to (post)-menopausal women to relieve menopausal symptoms and prevent osteoporosis [23]. Its use in postmenopausal women increases the risk of breast cancer, but is correlated with the length of therapy. With 5 years of HRT usage, the risk is 15% higher and it increases to 34% with 10 years of therapy. However, as in birth control methods, this risk is also reversible within 5 years of discontinuing HRT [33].
- **Lifestyle**: The risk of breast cancer can be increased by modern lifestyle factors like excessive alcohol consumption, a high-fat diet, obesity, and a lack of physical activity [30]. Alcohol consumption is undoubtedly associated with a higher risk of developing breast cancer, and the risk increases by 7% for each additional 10 grams of alcohol consumed per day [34]. Dietary habits, especially in developed countries, are based on fat-rich products as well as processed food containing chemical substances for flavoring or preservation that can promote neoplastic processes in the mammary glands [25]. Indeed, excess saturated fat consumption is associated with mortality with a relative risk (RR) of 1.3 and is also related with poor prognosis in breast cancer patients [35]. Nevertheless, consuming antioxidants or vitamin D-rich foods may reduce the relative risk of breast cancer by 20% [36]. In addition, obesity raises the risk of breast cancer in postmenopausal women. This increased risk is primarily caused by heightened circulating estrogen levels as the majority of estrogen in postmenopausal women comes from fat tissue. Thus, having more fat tissue raises estrogen levels and increases the risk of developing breast cancer. To a lesser extent, obesity is linked to higher insulin levels which are also associated with an increased

risk of breast cancer. However, physical activity in women after menopause may lower the risk of developing breast cancer due to its effect on body weight [23].

- **Inherited susceptibility to breast cancer:** The most common cause of hereditary breast cancer is an inherited susceptibility caused by a pathogenic mutation in BRCA1 and BRCA2 (breast cancer gene 1 and 2) genes. Women with a BRCA1 mutation have a 55-65% lifetime risk of developing breast cancer, whereas women with a BRCA2 mutation have a 45% lifetime risk [23].

1.3. Diagnosis, molecular subtypes and staging

1.3.1. Breast cancer diagnosis

Breast cancer is diagnosed by using various diagnostic tools, including physical examination, mammography, breast ultrasound, and, occasionally, breast magnetic resonance imaging (MRI), as well as a comprehensive medical and personal history. The physical examination comprises clinician examination as well as self-examination of the breasts. Early stages of breast cancer, on the other hand, are generally symptomless and are typically diagnosed by the existence of a palpable tumor or alterations in mammography. This technique is considered as the gold standard for early detection of breast cancer. Ultrasound breast imaging is frequently used as an additional screening method, particularly when mammography alone fails to detect a breast tumor. Nonetheless, the definitive diagnosis is primarily determined through a core needle biopsy of the tumor, which is typically guided by radiological techniques in the case of non-palpable tumors [37].

Immunohistochemistry (IHC) has become an important tool for molecular diagnostic. IHC staining, when used in combination with diagnostic techniques, gives essential information and plays an important role in the diagnosis of breast cancer. For example, estrogen receptor (ER) and progesterone receptor (PR) are key breast cancer markers. Testing for these receptors, together with the human epidermal growth factor 2 (HER2) antigen, offers information regarding the disease's aggressiveness and responsiveness to breast cancer treatment. These molecular biomarkers, like ER, PR, HER2 and Ki67 (proliferation index) help classify breast cancer into subtypes and guide targeted therapies. Moreover, automated gene expression platforms have been developed over the last few decades to promote breast cancer molecular profiling [38]. These platforms have been

designed to either determine the prognosis at 5 or 10 years in a biologically robust way (Oncotype Dx, MammaPrint, EndoPredict, PAM50/Prosigna), directly determine the tumor subtype (PAM50/Prosigna, BluePrint) and/or to predict the benefit of adjuvant chemotherapy (OnctypeDx) in hormone receptor (HR)-positive and HER2-negative patients [39]. Although the genes investigated by the different platforms vary, the information provided is relatively consistent [40].

In cases where metastasis is suspected, laboratory testing such as complete blood count, biochemistry parameters test, and tumor markers, such as carcinoembryonic antigens (CEA), Ca 15.3, and Ca 27.29, are conducted. These markers are substances produced by cancer cells, or normal cells in response to cancer, that can be found at low levels in the bloodstream of patients. They are used to monitor disease progression, recurrence, or response to treatment. Finally, in cases with clinical suspicion or laboratory abnormalities, further imaging approaches such as nuclear medicine techniques including single photon emission computerized tomography (SPECT), positron emission tomography (PET), computed tomography (CT), or bone scintigraphy are performed [21].

More recently, liquid biopsies have emerged as a novel tool to detect and monitor breast cancer. This technique involves testing blood samples for circulating tumor cells (CTCs) or tumor DNA (ctDNA). These tests can provide information about the tumor's genetic makeup, monitor treatment response, and detect the presence of minimal residual disease or recurrence [41].

1.3.2. Breast cancer types based on pathology, invasiveness and prevalence

Breast cancer has traditionally been classified based on its location, pathology, invasiveness, and prevalence. Breast cancer can be originated in a variety of areas, and its type is determined by the cell that is affected. Based on that, breast cancers are classified into two types: sarcomas and carcinomas. Sarcomas are rare cancers (<1%) that develop from the stromal components of the breast, which include myofibroblasts and blood vessel cells. Carcinomas, on the other hand, develop from the breast's epithelial component, which includes cells in the lobules and ducts. The vast majority of breast cancers are carcinomas. Within carcinomas, there are various subtypes based on the pathological features and invasiveness of the primary tumor: non-invasive (or *in situ*), invasive, and metastatic [23, 42].

Non-invasive breast cancers, such as ductal carcinoma *in situ* (DCIS) and lobular carcinoma *in situ* (LCIS), are cancers that have not spread beyond the ducts (DCIS) or the lobules (LCIS) in which they are located. Although they are restricted to the ducts or lobules, they have the potential to spread and invade other areas over time. Invasive breast cancer, on the other hand, occurs when cancer cells spread beyond the ducts or lobules and infiltrate the surrounding breast stromal tissue. Invasive breast cancers are further classified into two kinds based on the tissue and cell types involved: invasive ductal carcinoma (IDC) and invasive lobular carcinoma (ILC). IDC accounts for the 80% of breast cancers and it can be subdivided into different carcinoma subtypes: medullary, mucinous, papillary, tubular and cribriform carcinoma. ILC accounts for 10-15% of breast cancers and tends to occur in older women. These types of carcinomas grow in a pattern in which individual cells are grouped in a single file or sheet and they differ molecularly and genetically, from IDC.

Less frequent types of invasive breast cancer include inflammatory breast cancer (IBC) (1-5%), Paget's disease (<3%), phyllodes tumor (<1%) and angiosarcoma of the breast (<1%) [21, 23]. When invasive breast carcinomas spread beyond the breast and form metastases in the lymph nodes or in other organs of the body, they are classified as metastatic breast cancer. Breast cancer metastases can occur in a variety of locations, including lymph nodes in the armpit and distant sites such as the lung, liver, bone, and brain. In these areas, they can expand and form new tumors. Even after the primary tumor has been removed, microscopic tumor cells or micro-metastases may remain in the body, allowing the cancer to return and spread. The risk of breast cancer recurrence and metastasis is approximately 30% of the women who have been diagnosed with early-stage breast cancer [43].

1.3.3. Clinical staging

Once breast cancer has been diagnosed, tests are carried out to establish the stage of the disease. The clinical staging of breast cancer is the same for all breast cancer subtypes. Staging is essential for predicting prognosis and guiding treatment [44]. The TNM classification system, developed by Pierre Denoix [45], and later published by the American Joint Commission on Cancer (AJCC) [46], divides tumors into three categories based on primary tumor size (T), regional lymph node involvement (N), and the presence or absence of distant metastases (M) [45]. Tables 18-21 in Annex show the T, N, and M classifications in abbreviated form.

The staging system has evolved over time, with the most recent edition (8th) considering grading, IHC biomarkers, and anatomical progression of the disease for prognostic stage grouping [44, 47]. This prognostic stage classification (Table 1) has prognostic implications and influences the therapeutic strategy. The prognostic stages of breast cancer, ranging from 0 to IV, indicate the characteristics and progression of the tumor. Each stage, from non-invasive (stage 0) to metastatic (stage IV), represents the tumor's size, involvement of lymph nodes and invasiveness (metastatic state)[21].

- **Stage 0** represents non-invasive tumors within the breast, such as DCIS [48].
- **Stage I** breast cancer is classified into two subtypes based on tumor size and lymph node involvement [49].
- **Stage II** is divided into two categories: axillary or sentinel lymph node involvement and bigger tumors without lymph node involvement [50].
- **Stage III** is further subdivided into three subgroups based on the amount of tumor and lymph node involvement, which includes inflammatory breast cancer [51].
- **Stage IV** cancer is characterized by advanced metastatic cancer that has spread to other organs [52].

Table 1. TNM staging: Classification by prognostic stages [53].

Stage	T	N	M
0	Tis	N0	M0
IA	T1	N0	M0
IB	T0	N1mi	M0
	T1	N1mi	M0
IIA	T0	N1	M0
	T1	N1	M0
	T2	N0	M0
IIB	T2	N1	M0
	T3	N0	M0
IIIA	T3	N1	M0
	T1	N2	M0
	T2	N2	M0
	T3	N2	M0
	T0	N2	M0
IIIB	T4	N0	M0
	T4	N1	M0
	T4	N2	M0
IIIC	Any T	N3	M0
IV	Any T	Any N	M1

1.3.4. Breast cancer types based on molecular classification

Breast cancer is a heterogeneous disease with different biological subtypes that exhibit distinct behaviors and therapeutic responses. A novel molecular classification of breast cancer has emerged in the last decade, based on tumor gene expression profiles rather than traditional histopathological characteristics. Perou et al. were the first to use microarray gene expression data to classify breast cancer, revealing four intrinsic or molecular subtypes: Luminal, HER2-enriched, Basal-like, and Normal Breast-like [54].

Further research refined this classification, dividing the luminal subtype into two subgroups (Luminal A and B) and the Normal breast-like subtype was later removed due to potential contamination by normal mammary glands. Later, The Cancer Genome Atlas (TCGA) project confirmed the existence of four main intrinsic breast cancer subtypes based on gene expression levels: Luminal A, Luminal B, HER2-enriched, and Basal-like or Triple negative (Table 2) [55, 56].

- **Luminal** breast cancer is estrogen receptor (ER) positive, and is the most common subtype of breast cancer, accounting for nearly 70% of cases in western populations [7]. Luminal-like tumors, according to proliferation markers and luminal-regulated pathways, can be further classified into two subtypes: Luminal A and Luminal B.
    - **Luminal A** tumors are characterized by the presence of ER and/or PR, absence of HER2, and low levels of Ki67, a marker of cell proliferation. They are usually of low grade, grow slowly and have the best prognosis. Luminal A tumors account roughly for 40% of all breast cancers [23]. This subtype presents a low expression of genes related to cell proliferation and treatment typically involves hormonal therapy [57].
    - **Luminal B** tumors are ER-positive, may be PR-negative and/or HER2-positive, with high levels of Ki67. They have higher grades, worse prognosis, and higher expression of proliferation-related genes. This subtype accounts for <20% of all breast cancers [58]. This particular subtype exhibits lower expression of genes typically associated to luminal epithelium such as the PR [59] and Forkhead Box A1 (FOXA1) [60]. However, ER is expressed similarly in A and B subtypes and serves to distinguish luminal tumors [47].
- **HER2-enriched** breast cancer accounts for around 10-15% of all incidences of breast cancer. It is characterized by high HER2 protein expression and the absence

of ER and PR [47]. HER2-enriched cancers tend to grow faster than luminal tumors and, before the emergence of HER2-targeted therapies, had worse prognosis [23]. It is important to highlight that the HER2-enriched breast cancer subtype is not the same as clinically diagnosed (using IHC techniques) HER2-positive. While around 50% of tumors clinically diagnosed as HER2-positive fall into the HER2-enriched subtype, the remaining 50% can belong to any molecular subtype [61].

- **Basal-like or Triple-Negative Breast Cancer (TNBC)** is a heterogeneous collection of breast tumors characterized by the absence of ER, PR and HER2. It accounts for around 20% of all breast cancer cases and is more common in women with BRCA1 gene mutations, as well as younger women (under 40 years old) and in African-American women. TNBC tends to be biologically aggressive and has a poor prognosis when compared to other kinds of breast cancers [62]. Although the term basal-like and TNBC have been used interchangeably, not all TNBC are basal. Based on gene expression profiling, TNBC can be classified into six subtypes: basal-like, mesenchymal, mesenchymal stem-like, immunomodulatory, luminal androgen receptor and an unidentified group [63].

Table 2. Summary of breast cancer molecular subtypes according to the IHC markers [54].

Molecular subtype	Molecular markers (IHC)
Luminal A	ER-positive (>1%) and/or PR-positive (>1%) HER2-negative Low Ki67 (<14%)
Luminal B	ER-positive (>1%) and/or PR-positive (>1%) HER2-negative High Ki67 (>14%)
	ER-positive (>1%) and/or PR-positive (>1%) HER2-positive Any value of Ki67
HER2-enriched	ER-negative (<1%) PR-negative (<1%) HER2 amplification
Basal-like or Triple-negative breast cancer	ER-negative (<1%) PR-negative (<1%) HER2-negative

2. Estrogen-Estrogen Receptor signaling pathway

The Estrogen-Estrogen Receptor (ER) signaling pathway regulates different physiological functions in the body through the interaction of estrogens with ER, primarily in tissues such as the breast, uterus, and bone. This pathway is essential for normal development as well as the progression of hormone-dependent disorders such as breast cancer. The Estrogen-ER signaling pathway plays a critical role in the development, growth, and progression of hormone receptor-positive (HR+) breast cancers by activating the ER when estrogen enters the cell and binds to it, either in the cytosol or on the cell membrane [64].

Excessive or prolonged exposure to estrogen has been associated with breast cancer development and progression, especially in HR+ breast cancers. ER-positive breast cancer cells exploit estrogen signaling to drive uncontrolled proliferation, evade apoptosis and promote angiogenesis. As previously mentioned, in Section 1.2.4. (Introduction), elevated estrogen levels, whether endogenous or exogenous, are linked to an increased risk of breast cancer [65].

2.1. Estrogen

Estrogens are cholesterol-derived steroidal molecules with 18 carbon atoms arranged into three hexane rings and one pentane ring [66]. They have four rings (A, B, C, and D) with a hydroxyl group (OH) on carbon 3 (C3) and either an OH or a ketone group on carbon 17 (C17) (Figure 5). The primary estrogens are 17β-estradiol (E2), estrone (E1), and estradiol (E3) [67]. Estrogens are predominantly synthesized in the ovaries through a complex enzymatic process, but they can also be synthesized in the adrenal gland and other peripheral tissues such as fat tissue, liver, breast, and brain tissue [68]. In premenopausal women, E2 is the predominant type, with the greatest biological capacity, whereas in postmenopausal women, E1 and estrone sulfate (E1s) account for the majority of circulating estrogens. E1 exhibits significantly lower estrogenic effectiveness compared to E2 due to the absence of the OH group at the position 17β position. E3, on the other hand, is a feeble estrogenic factor that briefly interacts to the ER [69].

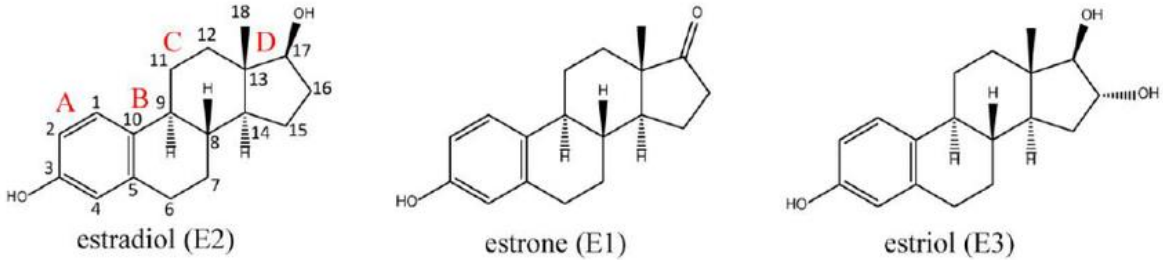

Figure 5. Structures of natural estrogens: 17β-estradiol (E2), estrone (E1), and estriol (E3) [70].

Regarding estrogen production, in premenopausal women with normal ovulatory cycles, the ovarian follicle secretes between 15 to 300 pg/mL of E2 per day. In a postmenopausal woman, on the other hand, the production of estrogens by the ovary is greatly reduced and falls to less than 15 pg/mL of E2 and 7 to 40 pg/mL of E1 [71]. The ovary is the primary source of E2 in premenopausal women, while the liver synthesizes the majority of E1 and E3 from E2, or other peripheral organs generate them from androstenedione. However, androstenedione synthesis is reduced in half during menopause due to a decrease in ovarian steroid production. After menopause, peripheral tissues rely on androstenedione, testosterone, and E1 as primary estrogen precursors. In premenopausal women, the adrenal glands and ovaries share equal responsibility for producing androstenedione, which then is transformed into estrogens in peripheral tissues by the aromatase enzyme. The ovarian production of androstenedione is attributed to theca cells which then release it into the bloodstream. In contrast, ovarian estrogen production culminates within the granulosa cells, which contain the aromatase enzyme (CYP19) [68].

The biosynthesis of estrogen from cholesterol is mediated by several enzymes and specific molecular structures (Figure 6). The process involves the conversion of cholesterol to pregnenolone, followed by androgen synthesis. The aromatase enzyme, encoded by the CYP19A1 gene, is responsible for the final step, converting androgens to estrogens. Aromatase is a member of the cytochrome P450 superfamily and is found on the endoplasmic reticulum membrane. It catalyzes the conversion of C19 androgens into C18 estrogens, which involves the removal of the 19-methyl group and the aromatization of the steroid A-ring. This process requires oxygen and NADPH. Therefore, aromatase specifically converts androgens like androstenedione, testosterone and 16-α-hydroxytestosterone into estrogens like estrone, 17β-estradiol and 17β-16α-estriol [66, 68].

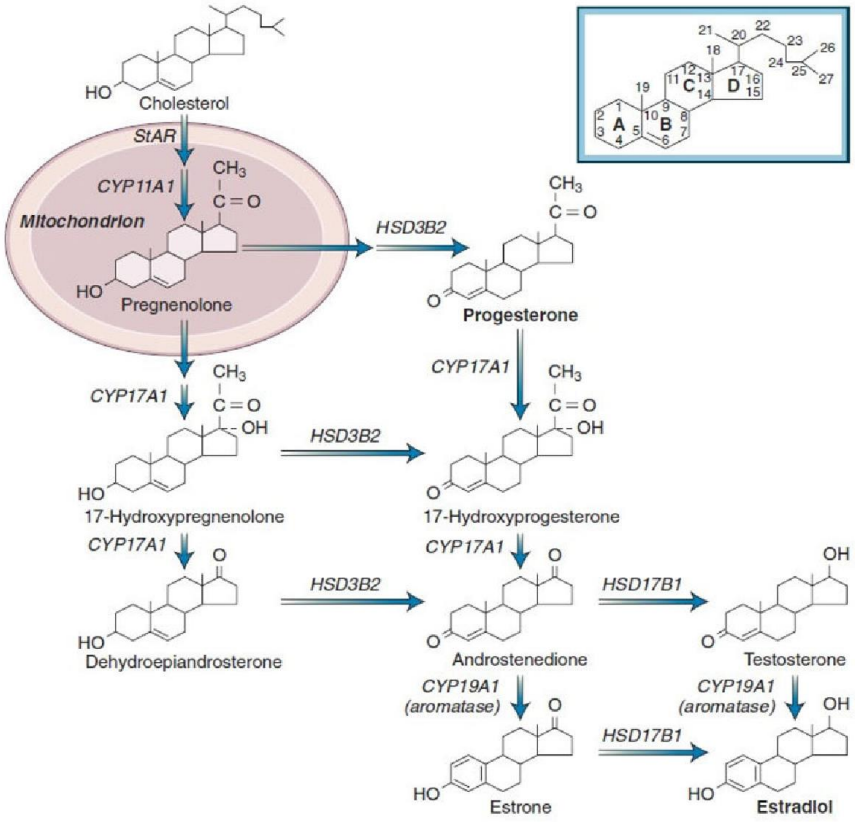

Figure 6. The biosynthesis of estrogens. Illustration of the pathway for estrogen synthesis in humans. Abbreviations: steroidogenic acute regulatory protein (StAR) [72].

Estrogen metabolism is a strictly regulated process that is essential for maintaining hormonal balance. The liver is crucial in metabolizing estrogens into various metabolites such as 2-hydroxyestrone (2-OHE1) and 16-hydroxyestrone (16-OHE1), which have unique biological functions. These metabolites are conjugated and excreted through feces and urine. Estrogens circulate in the bloodstream, largely bound to sex hormone-binding globulin (SHBG) and albumin, influencing their availability to target tissues. The physiological effects of bound and free estrogens are shaped by their equilibrium, with alterations contributing to cancer risk [73].

Estrogen diffuses across cell membranes and binds to receptors, subsequently regulating multiple physiological processes. Estrogens, via the ER, play a critical role in ER-positive breast cancer [74]. The physiological actions of estrogens are mediated by their natural receptor, of which there are two isoforms (ERα and ERβ). Furthermore, a protein from the G protein-coupled receptor (GPCR) family, known as G protein-coupled estrogen receptor (GPER), exhibits a high affinity for binding exclusively to E2. Positioned within the endoplasmic reticulum, GPER contributes to E2's rapid actions through non-genomic mechanisms (Section 2.2.1.1.3.) [75].

2.2. Estrogen receptor

Estrogen receptors (ERs) belong to the nuclear receptor superfamily, participating in various developmental and physiological processes [74]. For example, ERs have an impact not just on the female reproductive system, but also on other body systems such as the skeletal, cardiovascular, neurological and immune systems [76]. ERs can move between the nucleus and the cytoplasm, although the majority of them are found in the nucleus. With only around 5% of ERs are found in the cytoplasm [77].

ERs encompass two main isoforms: estrogen receptor alpha (ERα) and estrogen receptor beta (ERβ), encoded respectively by ESR1 on chromosome 6 (locus 6q25.1) and ESR2 on chromosome 14 (locus 14q23.2) [69]. ERα, with a molecular weight of 66 kDa and 595 amino acids, holds a more prominent role, particularly in promoting tumorigenesis in several cancers, including breast cancer. Whereas the precise function of ERβ (54 kDa and 530 amino acids) remains unclear [78].

ERα is predominantly found in the mammary gland, hypothalamus, uterus, male reproductive organs and ovary (thecal cells), while ERβ is highly concentrated in the ovary (granulosa cells), the prostate and, to a lesser extent, in the lung, heart, intestine, brain and bone. Both, however, are expressed in subcutaneous fatty tissues and the vascular system [79]. Studies have shown that the ERα subtype is upregulated during the development of breast cancer, whereas the ERβ subtype is often downregulated. The ratio between ERα and ERβ might shift during breast carcinogenesis, although the exact implications of this transformation remain unclear. The ER, activated by its ligand, forms dimers, which may be homodimers ER (αα or ββ) or heterodimers (αβ) [80].

The structural makeup of ERs involves five distinct domains including the N-terminal (A/B domain), the DNA-binding domain (DBD or C-domain), the hinge region (D-domain) and the ligand-binding domain (LBD or E-domain) (Figure 7) [81].

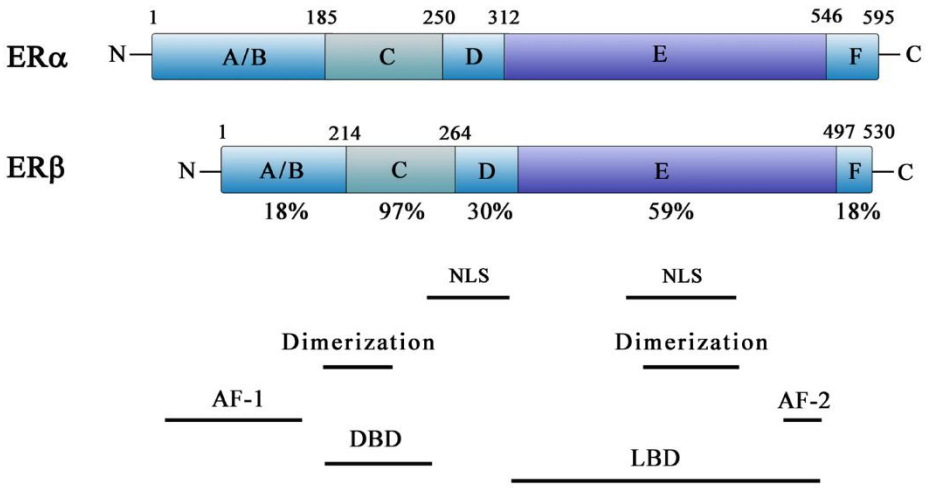

Figure 7. Schematic representation of the functional regions of human ERα and ERβ. The N-terminal A/B domain contains the AF-1 site. The C domain encompasses the DNA-binding domain (DBD) and a dimerization site. The D domain carries a nuclear localization signal [81].

The N-terminal (A/B domain) contributes to hormone-independent transcriptional activation, with the Activating Factor 1 (AF-1) region acting without the need for ligands. The transcriptional activity of target genes is regulated by AF-1, which binds to transcription activators and co-activators. However, this activation is milder and more selective than that associated with the E domain. The DBD binds ER to estrogen response elements (EREs), enabling ER interaction with the DNA. The DBD interacts directly with the DNA double helix regulating the expression of target genes and facilitating receptor dimerization via two zinc finger-like structures. The hinge region or D domain, acts as a separator between the C domain and the E domain, enabling nuclear transportation. The ERE domain, also known as LBD, has a dimerization (homo- and heterodimerization) interface and encodes ligand-dependent transcription activation through Activating Factor 2 (AF-2). This domain also acts as a site where co-repressors and co-activators can interact. AF-2, in collaboration with AF-1, regulates ER transcriptional activity and facilitates interactions with co-activators or co-repressors [82]. The ER has a fifth domain in the carboxyl-terminal known as F-domain. It has been reported that F-domain changes its conformation when ER binds to the hormones and allows the binding of co-activators. Mutations in this domain enhance binding of co-activators regardless of the presence of hormones and leads to resistance [83]. ERα and ERβ have a high homology specially in the DBD and the LBD regions, with a 97% and 59% similarity in amino acid sequence, respectively. However, the amino-terminal (18%), hinge region (30%), and carboxyl-terminal (18%) domains are divergent [64].

2.2.1. Mechanism of action of Estrogen-ER pathway

As previously mentioned, the ER signaling pathway is critical in the pathogenesis of breast cancer, as it regulates processes like cell cycle progression, apoptosis, and angiogenesis [84]. This section delves into the various activation mechanisms of ER signaling pathways in breast cancer.

Depending on how ER pathway is regulated in response to estrogen stimulation, the ER signaling pathway can be divided into two mechanisms: ER (estrogen or ligand)-dependent and ER (estrogen or ligand)-independent gene transcription. In ligand-dependent pathway, estrogen binding to ER induces a structural change that triggers various co-regulators to activate the transcription of ER-targeted genes. This ligand-dependent activation pathway is further classified as direct genomic or classical, indirect genomic or non-classical, and non-genomic activation mechanisms. The ER ligand-independent mechanism involves the activation of ERs without the presence of E2. Instead, extracellular signaling pathways like growth factor signaling initiate the process, leading to dimerization, DNA binding, and ultimately, gene regulation [64] (Figure 8).

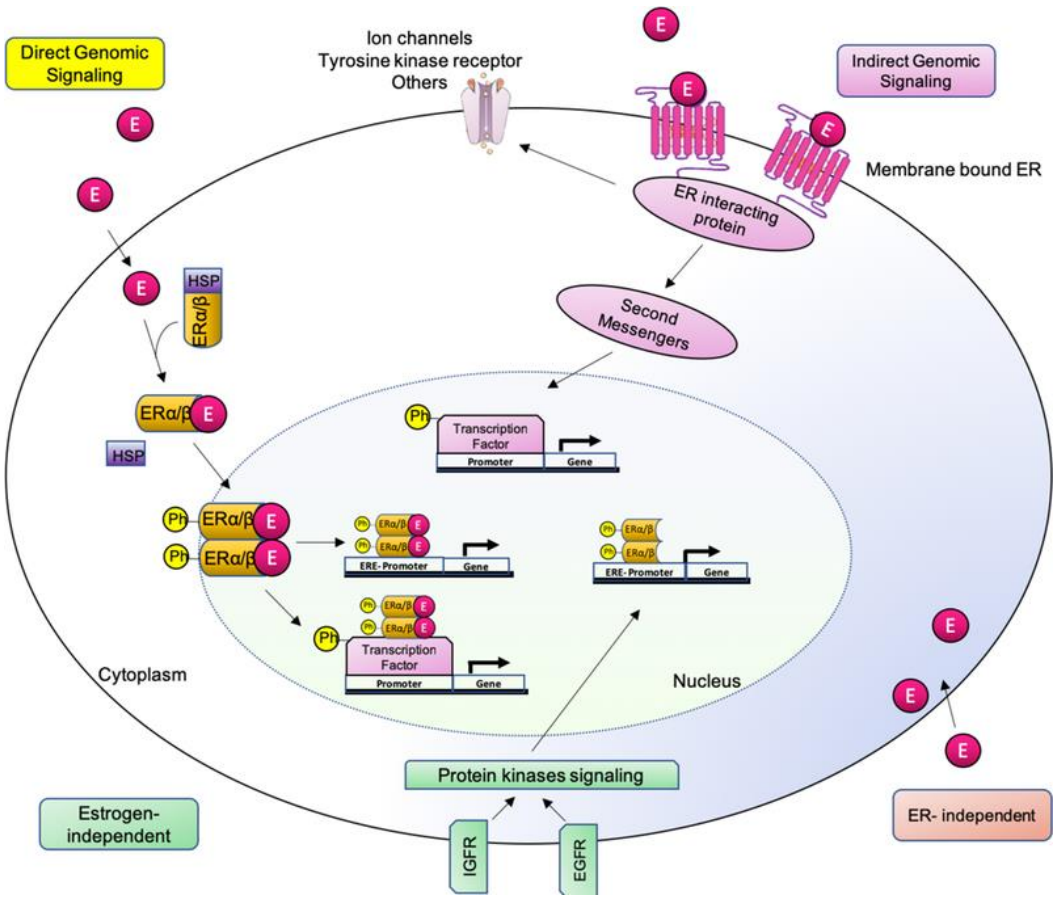

Figure 8. Estrogen-ER signaling pathway. The direct genomic signaling: estrogen binds to ERs, leading to the formation of a complex that translocates into the cell nucleus. This results in the modulation of transcriptional activity, affecting estrogen-responsive genes, both with and without EREs. The indirect genomic signaling: membrane-bound receptors initiate cytoplasmic events, including the modulation of ion channels, activation of second-messenger cascades, and transcription factor regulation. These events contribute to the genomic effects of estrogen. The ER-independent: estrogen can exert antioxidant effects independently of ERs, highlighting alternative pathways through which estrogen influences cellular responses. Estrogen-independent signaling: genomic events can be initiated by estrogen in a ligand-independent manner, expanding the complexity of estrogen-mediated actions [85].

2.2.1.1. ER (estrogen or ligand)-dependent pathway

2.2.1.1.1. Genomic, nuclear or classical pathway

The genomic pathway is a relatively slow response, as it involves changes in gene expression and protein synthesis, which take longer to manifest, usually over hours to days. The genomic pathway initiates with estrogen entering the plasma membrane and interacting with cytoplasmic ERα and ERβ. This binding leads to the detachment of heat shock proteins (HSP) 70 and 90, prompting a conformational change that triggers the dimerization of ER in the cytosol [86]. This estrogen-ER dimer is then translocated into the nucleus. Once inside, it acts as a transcription factor, directly binding to the chromatin at specific sequences (ERE) in the promoter regions of target genes. Binding of the ER-ligand complex to EREs makes a conformational change enabling helix 12 in the AF-2 region within the F-domain to accept co-activator or co-repressor proteins which, in turn, modulate gene expression [87].

Co-activator proteins possess histone acetyltransferase activity, facilitating gene transcription by opening chromatin. In contrast, co-repressor proteins are deacetylases that act on histones to promote chromatin compaction [88]. Several co-regulators have been linked to cancer, for example, the co-activator Amplified in Breast 1 (AIB1) is amplified in a small fraction of breast tumors but overexpressed in two-thirds [65]. Another example is the co-repressor Paired Box gene 2 (PAX2) which plays a role in tamoxifen efficacy [89].

2.2.1.1.2. Indirect genomic, non-classical or transcriptional cross-talk pathway

The estrogen-ER complex can also regulate gene expression through indirect mechanisms, without directly binding to DNA. Only about 75% of genes affected by estrogen rely on ERα binding to EREs for their activation [90]. This ERE-independent genomic signaling is accomplished by protein-protein interactions rather than direct binding of ERs to DNA. Instead, the estrogen-ER complex interacts with other transcription factors and response elements, influencing the expression (activation or suppression) of the target

genes. ER complexes work as a co-regulator by interacting with transcription factors such as Activator Protein 1 (AP1) or Specificity Protein 1 (Sp1) at their specific sites on DNA, hence, influencing cell processes such as proliferation and survival [91].

The presence of ER enhances transcription factor Sp1 binding to GC-rich promoter regions regulating expression of the following genes: low-density lipoprotein (LDL) receptor, progesterone receptor B (PR-B), endothelial nitric oxide synthase (eNOS), GATA binding protein 1 (GATA1), signal transducer and activator of transcription 5 (STAT5), and retinoic acid receptor-1α (RAR-1α). Another key mediator is AP1, a transcription factor that controls cell processes such as cell differentiation, proliferation, and apoptosis. Some examples of genes induced by ERα via the AP1 mechanism are insulin-like growth factor-1 (IGF-1), collagenase, Insulin-like Growth Factor 1 receptor (IGF-1R), ovalbumin, and cyclin D1.

ER, in addition to Sp1 and AP1, can interact with additional transcription modulators such as nuclear factor-κB (NF-κB) complex, activating transcription factor (ATF)-2, c-Jun, c-Fos, ATF-1/cAMP response element binding protein (ATF-1/CREB), and nuclear transcription factor-Y (NF-Y) [85].

2.2.1.1.3. Non-genomic pathway

The non-genomic pathway involves rapid cellular responses through membrane-associated receptors. Indeed, some ERs are associated with the cell membrane and can be rapidly activated by estrogens circulating in the bloodstream. Additionally, some ERs are located in the inner part of the cell membrane forming complexes with other molecules, like caveolin-1, G proteins (GPER1), receptor tyrosine kinases (RTKs) such as Epidermal Growth Factor Receptor (EGFR) and IGF-1, and proteins with kinase activity like SRC. When estrogen binds to these receptors, it triggers the activation of Phosphoinositide 3-Kinase (PI3K)/Akt signaling pathway and the Mitogen-Activated Protein Kinase (MAPK/ERK) pathway delivering proliferative signals to the nucleus [92]. These signaling cascades leads to rapid cellular responses, such as changes in intracellular calcium levels, activation of protein kinases, and alterations in cell metabolism, migration, or survival [93].

The non-genomic pathway produces very rapid responses, frequently within seconds to minutes after estrogen exposure. The non-genomic pathway, unlike the genomic pathway, does not directly involve changes in gene expression or protein synthesis. Instead, it modulates existing proteins and cellular processes [94].

2.2.1.2. ER (estrogen or ligand)-independent pathway

ERs can also be activated without the presence of estrogens or other receptor agonists [95]. This ligand-independent ER activation is primarily triggered by phosphorylation on specific serine (Ser118, Ser104 and Ser167) residues in the receptors themselves. This mechanism requires the action of regulatory molecules necessary for phosphorylation, such as protein kinase A (PKA), protein kinase C (PKC), MAPK phosphorylation cascade components, inflammatory cytokines (interleukin-2), cell adhesion molecules (heregulin), cell cycle regulators (RAS, p21, protein activator cyclins A and D1) and transforming growth factor beta (TGF-β).

This ligand-independent ER activation by phosphorylation of ER has consequences in breast cancer. It can enhance transcriptional activity even in the absence of estrogen, leading to the expression of genes involved in cell proliferation and survival. Additionally, phosphorylation can affect ER stability and localization. Certain phosphorylation stabilizes ER, preventing its degradation and promoting its translocation to the nucleus, where it exerts its transcriptional activities. Moreover, phosphorylation can create, or modulate, cross-talk between signaling pathways enhancing its activity and promoting cellular responses. Altogether this phosphorylation can, ultimately, lead to resistance to hormonal therapies (by allowing ER to function independently of estrogen), rendering these therapies less effective [96].

3. Breast cancer treatment in luminal patients

Breast cancer treatment strategies consist of endocrine therapy as neoadjuvant and adjuvant therapy. Indeed, endocrine therapy is the main treatment approach for hormone receptor (HR)-positive breast cancer, inhibiting estrogen-driven tumor growth. Standard endocrine regime consists of taking oral antiestrogen drugs daily for, at least, 5 years with different endocrine treatment alternatives according to the menopausal state (pre- or post-menopausal) [97].

3.1. Therapeutic implications of targeting ER in luminal patients

As indicated in Section 1.3.4. (Introduction), luminal tumors, which are classified as ER-positive breast cancer, contain more ER than normal mammary cells, indicating that ER is involved in cell proliferation [98]. Overactivation of ER, often triggered by estrogen, contributes to breast cancer progression. Consequently, since ERs mediate estrogen's effect, a potential treatment strategy to treat hormone-dependent breast cancer is to suppress estrogen production. In order to treat hormone-dependent breast cancer, antiestrogens to inhibit estrogen synthesis and their action on the ER have been developed [99]. Indeed, the development of ER ligands (natural and synthetic estrogens) is a focus in therapeutic research and antiestrogen therapies like Selective Estrogen Receptor Modulators (SERMs), Selective Estrogen Receptor Degraders (SERDs) and Aromatase Inhibitors (AIs) have been shown to be effective in the treatment of breast cancer (Figure 9). However, the main issue with these antiestrogens is the emergence of resistance [100].

Antiestrogens, or also known as endocrine therapy, are categorized into steroidal and non-steroidal drugs based on their chemical structure. Among them, steroidal antiestrogens cause a complete loss of estrogenic activity in all tissues, which is undesirable as estrogen is involved in crucial physiological processes in all tissues. Non-steroidal antiestrogens, on the other hand, exhibits partial antagonist activity [101].

Within the endocrine therapy, there are several inhibitors available that block the ER pathway in breast cancer. They are categorized according to their mechanism of action. The first category includes drugs that directly antagonize ERs (for example, SERMs and SERDs. The other group are compounds that lower estrogen levels by decreasing endogenous estrogen production (for example, AI and gonadotropin-releasing hormone agonists

(GnRH)). However, the therapeutic usage of each antiestrogen in breast cancer treatment is guided by specific criteria that takes into account numerous factors such as age, tumor stage and past treatment history [102].

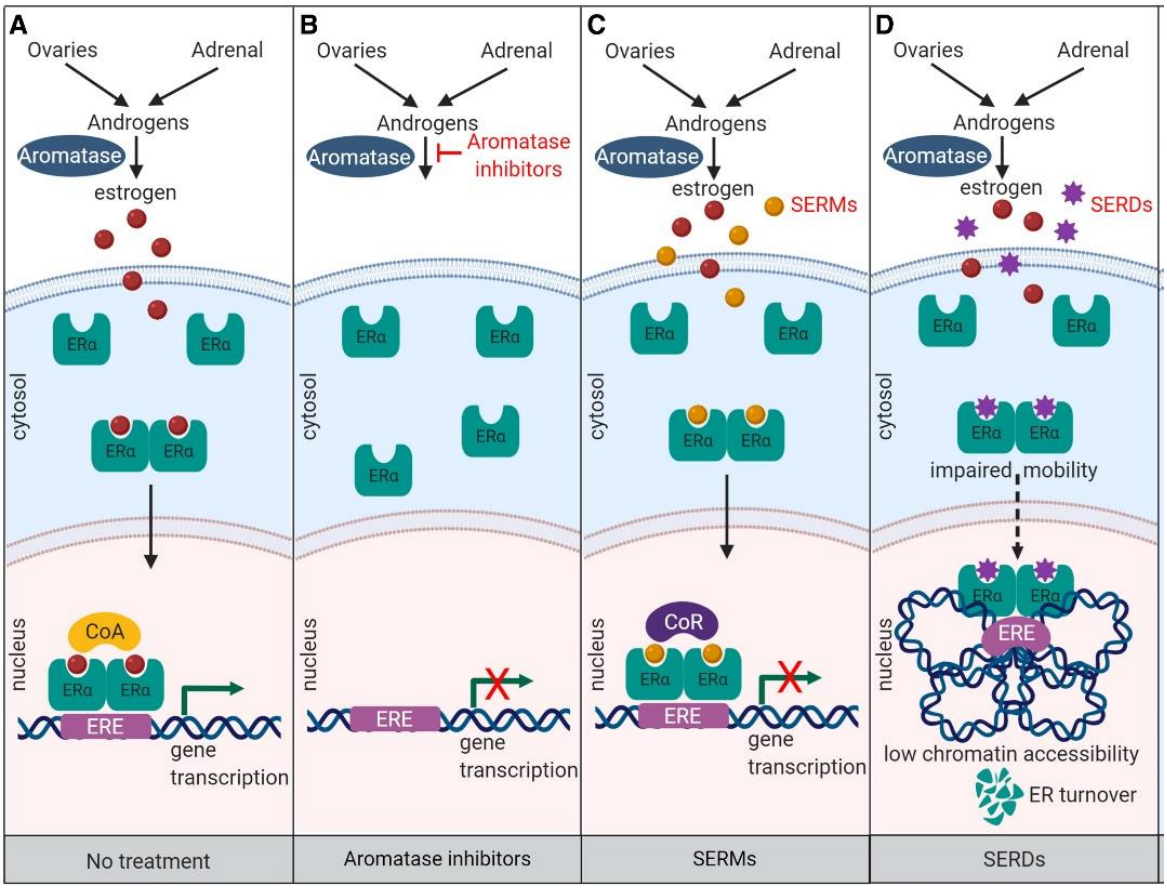

Figure 9. Mechanism of action of endocrine therapies overview. **(A)** When estrogen binds to the ER, it forms dimers and moves into the cell nucleus. Within the nucleus, ER dimers bind to co-activators, forming an active ER complex, activating transcription. **(B)** AIs block the production of estrogen by inhibiting the aromatization process, where androgens are converted into estrogens. **(C)** SERMs, like tamoxifen, competitively inhibit estrogen binding to the ER. When bound to SERMs, ER dimers interact with chromatin at ERE. However, this interaction with SERMs leads to the recruitment of co-repressors, which inhibits ER's transcriptional activity in breast tissue. SERDs, like fulvestrant, inhibit ER's ability to move into the nucleus effectively. **(D)** The ER-SERD complex fails to establish an open chromatin conformation necessary for the transcription of ER-regulated genes. Due to these impairments, SERD-bound ER undergoes degradation [103].

Different endocrine drugs are given based on the menopausal state. Tamoxifen, for example, is beneficial in both, pre- and postmenopausal women, whereas aromatase inhibitors are mainly effective in postmenopausal women. Patients with HR-positive breast cancer, treated with endocrine therapy, are at the risk of recurrence, even multiple decades after primary diagnosis [104]. However, prolongated endocrine therapy provides slight benefits, but adds toxicity. Therefore, it is essential to consider extending endocrine therapy for high-risk patients. In the early stages of metastatic HR-positive breast cancer, treatment should be centered around endocrine therapy, often combined with a cyclin-dependent

kinase (CDK) 4/6 inhibitor like abemaciclib, palbociclib, or ribociclib, either as a first-line or second-line treatment. Chemotherapy becomes a viable option when patients develop resistance to current hormonal therapies. Clinicians must decide when to add chemotherapy to endocrine therapy for HR-positive breast cancer patients, based on the assessment of clinicopathologic features like stage, tumor grade, risk and chemosensitivity [105].

In recent years, novel anti-ER approaches have emerged. One such innovation is proteolysis-targeting chimerics (PROTACs), which consists of two ligands: one binding to ER and the other to an E3 ubiquitin ligase. This dual interaction triggers ER degradation via the ubiquitin-proteasome complex. Another mechanism, known as complete estrogen receptor antagonists (CERANs), blocks ER's transcriptional activation domains (AF1 and AF2). These antagonists recruit nuclear receptor co-repressors to deactivate AF1 and directly impede AF2, effectively ceasing ER activity. Lastly, selective estrogen receptor covalent antagonists (SERCAs) function by covalently bonding to a specific cysteine residue (C530) on the ER, leading to ER inactivation and subsequent gene transcription inhibition [106].

3.2. Neoadjuvant and adjuvant endocrine therapy

The use of systemic therapy before surgery to reduce tumor size is referred to as neoadjuvant therapy. This allows less invasive surgery, improving the likelihood of breast-conserving surgery, or making initially inoperable tumors, of locally advanced breast cancer or inflammatory breast cancer, operable [107]. In general, postmenopausal women with HR-positive breast cancer may benefit from neoadjuvant endocrine therapy usually with an aromatase inhibitor. Premenopausal patients, with HR-positive breast cancer, on the other hand, are generally not indicated for neoadjuvant endocrine therapy unless they are included in a clinical study. The recommended period of neoadjuvant endocrine therapy varies, although it is typically given for 3-6 months, or until maximal response or breast-conserving surgery is achievable [108]. Tumor characteristics such as histology, grade, stage and hormone receptor status play a role in determining whether, or not, neoadjuvant chemotherapy should be used instead of endocrine therapy [59].

Adjuvant endocrine therapy is crucial for the treatment of luminal breast cancers. The expression of hormone receptors (ER and PR) and the patient's menopausal status guides the choice to provide adjuvant endocrine therapy. In premenopausal women, the suggested adjuvant treatment would be ovarian suppression or ablation combined with tamoxifen or an

AI [109]. In postmenopausal women, AIs are the standard choice, either as initial therapy or as a follow-up to tamoxifen [110]. Recent advancements showed that the addition of cyclin-dependent kinase 4/6 (CDK4/6) inhibitors, such as palbociclib and ribociclib, into adjuvant therapy regimens has resulted in enhanced disease-free survival [111].

Adjuvant chemotherapy decisions in luminal breast cancer are influenced by characteristics such as tumor size, nodal involvement and proliferation rate. Indeed, combinations of chemotherapy and targeted therapies, such as CDK4/6 inhibitors, have shown promise in achieving pathological complete responses (pCR) in some luminal breast cancer patients. The term pCR refers to the absence of any residual invasive cancer cells in the tissue sample obtained from the site where the tumor initially existed after the course of treatment [112]. However, selecting the right patients suitable for chemotherapy is crucial to avoid overtreatment. Therefore, tailored chemotherapy selection approaches based on multigene assays such as Oncotype DX and MammaPrint aid in identifying patients who are more likely to benefit from adjuvant chemotherapy (Section 1.3.1. in Introduction).

In the following sections, the use of endocrine therapy, both as neoadjuvant and adjuvant therapies, have been extensively explored, focusing on Selective Estrogen Receptor Modulators (SERMs), Selective Estrogen Receptor Degraders (SERDs), and Aromatase Inhibitors (AIs). These sections delve into understanding the mechanisms and clinical applications associated with these specific classes of endocrine therapy.

3.2.1. Selective estrogen receptor modulators (SERMs)

Selective Estrogen Receptor Modulators (SERMs) are a group of compounds used to successfully treat diverse clinical conditions including breast cancer, osteoporosis and serum lipid profiles in postmenopausal women. SERMs are antiestrogenic drugs developed to compete with estrogen and precisely modulate the activity of ER. Thus, they have a high specificity and strong affinity solely for ER and no affinity for any other steroid hormone receptor. Depending on the tissue, SERMs can act as agonists or antagonists. This versatility is beneficial for pharmacological applications as it allows for precise targeting of specific tissues while minimizing off target effects. The tissues in which SERMs have estrogenic activities (ER agonist) are bone, liver and cardiovascular system, while the tissues in which SERMs operate as ER antagonist, preventing ER action, are the breast and the uterus [113].

The mechanism of action of SERMs consists on inhibiting ER by competing with estrogens for its interaction. SERMs cans bind to both ERα and ERβ resulting in a high level of target sites and tissues specificity. This agonistic, or antagonistic, activity induces diverse structural changes in the receptors, particularly in the helix 12 (H12) region, resulting in either activation or repression of estrogen target genes. In general, when SERMs bind to the ER, they prevent H12 from capping and cause H12 to occlude the co-activator recognition. This inhibits co-activator proteins from binding and recruits co-repressors, leading to effectively suppressing estrogen-driven gene transcription like cell proliferation and survival [106].

SERMs can be classified based on their chemical structure including triphenylethylenes (tamoxifen and similar), benzothiophenes (raloxifene, arzoxifene), phenylindoles (bazedoxifene, pipindoxifene), and tetrahydronaphthalenes (lasofoxifene). However, SERMs can also be categorized into three generations according to their developmental stages: first-generation (tamoxifen), second-generation (raloxifene), and third generation (arzoxifene hydrochloride). Each class of SERMs exerts a distinct effect on its target tissue, significantly broadening the scope of applications in treating estrogen-related diseases such as osteoporosis. These new structures have overcome some adverse effects experienced with first-generation SERMs, like thromboembolic or uterine carcinogenesis.

Tamoxifen given to HR-positive breast cancer patients for the first 5 years after the diagnosis reduces breast cancer recurrence by approximately 50% when compared to non-endocrine therapy [114]. However, it is important to note that despite these advancements, these new-generation SERMs have still faced challenges like cross-resistance to tamoxifen and the inability to show superiority over tamoxifen in clinical trials. Prompting the need to explore novel-generation SERMs with different structures [115].

3.2.1.1. Tamoxifen

Tamoxifen is the most used SERM and it was the first one to reach clinical practice as an alternative to hormonal replacement therapy (HRT), and it quickly became the gold standard in breast cancer treatment. Tamoxifen is a non-steroidal first-generation SERM that was developed in the 1960s by ICI (AstraZeneca) under the brand name Nolvadex. Initially it was used for birth control but, it surprisingly revealed antitumor effects. It was launched in 1973 and authorized by the Food and Drugs Administration (FDA) in 1977, for the treatment and prevention of breast cancer, becoming the primary drug choice. Moreover, it

is also used to treat osteoporosis and to maintain bone density in postmenopausal women [64].

Tamoxifen and its metabolites, such as 4-hydroxytamoxifen and endoxifen, easily traverse from the bloodstream to the cellular cytoplasm where they work in two ways. On the one hand, they competitively block the attachment of estradiol to its native receptor, the ER, and, on the other, they simultaneously cause a conformational change in the receptor's structure. This structural alteration results in fewer co-activators and more co-repressors, such as nuclear receptor co-repressor (NCoR) 1 and 2, attaching to the formed complex of ER and tamoxifen. This complex ultimately blocks the transcription of critical genes involved in cell replication [116].

Tamoxifen is the preferred treatment for pre-menopausal women. Tamoxifen has been shown to reduce mortality by 31% in HR-positive women over a 5-year period, leading to the survival of over 500000 women [102]. Tamoxifen is metabolized by the hepatic enzyme CYP2D6, and genotypic variation in CYP2D6 has not been shown to affect the benefit of tamoxifen therapy. However, ER expression levels significantly influence the effectiveness of endocrine therapy, as it is not advantageous for patients that lack both ER and PR expression [109]. Despite its efficacy, tamoxifen resistance has been a focus for researchers, particularly in the metastatic setting, occurring within the first 5 years of treatment. This resistance appears to be the result of a shift in tamoxifen's biocharacter, involving its switching from being recognized as an antagonist to an agonist. Although tamoxifen has become the "gold standard" for breast cancer treatment, there is still a need to develop new drugs with less adverse effects and resistance, while preserving therapeutic efficacy [113].

3.2.2. Selective estrogen receptor degraders or down regulators

SERDs are another type of endocrine therapy that is crucial in the treatment of ER-positive breast cancer. SERMs and aromatase inhibitors (AIs) are commonly used as the first line of treatment for this type of cancer. However, a major challenge is that some patients do not respond to this treatment or that they develop resistance after several years of therapy. SERDs are a viable treatment option for ER-positive breast cancer patients, particularly in cases of treatment resistance, as they can inhibit both ligand-dependent and independent ER signaling. Thus, SERDs have been used as a therapeutic strategy in early, advanced and resistant ER-positive breast cancers [117, 118].

SERDs compete with estrogen for binding to the ER and inhibit its dimerization. When SERDs are bound to the ER, they destabilize the helix 12 of ER preventing the receptor translocation into the nucleus. This destabilization leads to the subsequent degradation of the ER protein via proteosome and, consequently, inhibits ER transcriptional activity [119]. One of the most well-known SERDs is fulvestrant, which is a pure ER antagonist that prevents transcription of ER-regulated genes, and it also downregulates ER via degradation. Fulvestrant binds to the ER with a greater affinity than tamoxifen, limiting the creation of an open chromatin conformation required for the transcription of ER-regulated genes [14]. Additionally, the ER-fulvestrant forms an unstable complex, which leads to ER protein degradation via the ubiquitin-proteasome system.

Despite major advances made with endocrine treatment, resistance to these treatments remains an issue. Fulvestrant, on the other hand, has showed efficacy against breast cancer cells with ER mutations in helix 12. This has spurred development into a new generation of SERDs with higher potency that can be orally administrated [120]. In addition, to overcome endocrine resistance in breast cancer, one strategy involves combining endocrine therapy with targeted approaches. In early-phase trials, the combination of CDK4/6 inhibitors with either, an aromatase inhibitor (AI) or fulvestrant, has emerged as a significant breakthrough in treating ER-positive breast cancer and it has become the standard first-line of treatment for advanced-stage disease. The combination of fulvestrant plus CDK4/6 inhibitors has demonstrated ability to prolong progression-free survival (PFS) by approximately 8-12 months [121].

3.2.3. Aromatase inhibitors

Aromatase inhibitors (AIs) reduce estrogen levels by inhibiting the conversion of androgens into estrogen, a process catalyzed by the aromatase enzyme. Aromatase, also known as CYP19, is a cytochrome P450 enzyme produced by the CYP19A1 gene located on chromosome 15. It is necessary for estrogen synthesis, as it facilitates the conversion of androgens, including androstenedione and testosterone, into estrone and estradiol [122]. Indeed, aromatase inhibition represents a specific approach to suppressing estrogen biosynthesis, ensuring that the biosynthesis of other steroids remains unaffected. Another advantage of suppressing aromatase is that the cytochrome P450 subunit, expressed by the aromatase CYP19 gene, has only 30% homology with the other steroidogenic P450 enzymes, which provides specificity to the inhibitors [123].

The development of AIs arose from the need to address the side effects associated with SERMs, such as endometrial cancer or thromboembolic disorders. However, they have now become the preferred therapy for neoadjuvant or adjuvant treatment in postmenopausal women with early-stage ER-positive breast cancer. This is related to the fact that aromatase is typically overexpressed in postmenopausal woman with ER-positive breast cancer, making it the primary source of local estrogen production in cancerous tissues. Therefore, by interfering with aromatase activity, a reduction of estrogen levels in tumor tissue could potentially slow the progression of breast cancer. Notably, while AIs are most commonly used in postmenopausal women, they have also been demonstrated to be effective in premenopausal women [124].

Historically, steroidal inhibitors like testololactone, an androstenedione analogue, were the first AIs to be studied. They competed with the substrate for enzyme binding but could be displaced in the presence of high substrate concentrations. Subsequent structural modifications of androgenic analogues led to the development of clinically used steroidal AIs, formestane and exemestane. Currently, several AIs are in clinical use, with each generation exhibiting greater selectivity and potency. AIs are classified as either non-steroidal inhibitors (e.g., aminoglutethimide, anastrozole, and letrozole) or steroidal (e.g., formestane and exemestane). Non-steroidal AIs bind reversibly to the aromatase enzyme through non-covalent interactions. On the other hand, steroidal AIs, derived from the substrate androstenedione, interact with the aromatase enzyme through irreversible binding. This type of inhibition, referred to as suicide inhibition, is time-dependent, but its effects are

long-term and specific. Consequently, unlike with non-steroidal inhibitors, the effects of steroidal AIs persist even after discontinuation of the drug, and the duration of inhibitory effects primarily depends on the rate of *de novo* synthesis of aromatase [125].

The third generation of AIs, including exemestane, anastrozole, and letrozole, has been approved by the FDA as first-line therapy for adjuvant postmenopausal women with HR-positive breast cancer. These AIs have proven to be more effective than tamoxifen. They also significantly inhibit peripheral aromatase activity, resulting in undetectable estrogen levels in many patients. Letrozole, in particular, has demonstrated the highest potency in inhibiting peripheral aromatase activity and reducing estrogen levels [126].

A meta-analysis of 31920 women confirmed the superiority of AIs over tamoxifen in terms of recurrence risk (19% vs 22%, respectively), clinical response rates, as well as breast conservation rates. In this regard, there has been a switch in strategy, consisting on taking tamoxifen for the first 2-3 years followed by an AI, instead of taking an AI for 5 years, showing equivalent results [127]. Some trials have explored the use of fulvestrant or anastrozole in the neoadjuvant setting, with anastrozole showing slightly better efficacy and tolerability. In premenopausal settings, AIs showed superiority over tamoxifen in response rates. In the ACOSOG-Z1031 trial, three different AIs were evaluated and exhibited equally effectiveness. The results suggest that individuals with less proliferative tumors, particularly older women with low-grade, HR-positive luminal A breast cancers, tended to have a more favorable response to AIs [128]. In these following sections, two different types of aromatase inhibitors (exemestane and letrozole) and their lack of cross-resistance will be explained.

3.2.3.1. Exemestane

Exemestane (6-methylenandrosta-1,4-diene-3,17-dione), clinically known as Aromasin, is an orally active AI used in breast cancer treatment. Exemestane is rapidly absorbed after oral administration, with 90% binding to plasma proteins. A 25 mg daily dose is clinically effective, reducing estrogen levels by 85–95% within 2–3 days. It has a long-term effect on estrogen suppression, up to 5 days after a single dose. The drug is mainly excreted through urine and feces, with an average elimination half-life of 24 h, although this can vary among individuals. Exemestane specifically targets aromatase, significantly reducing its levels without affecting other steroidogenic enzymes [129]. The most common adverse effects of exemestane include hot flashes, nausea, fatigue, dizziness, increased sweating, headache and changes in body weight. Despite the adverse effects, exemestane has shown efficacy in

treating metastatic breast cancer, particularly in patients who were previously exposed to tamoxifen and other treatments. It has been found to be superior in terms of relapse-free survival (60.1 vs 49.1 weeks) in various clinical studies [130].

After binding to aromatase, exemestane undergoes biotransformation mediated by enzymes, such as P450-cytochrome enzymes and aldoketoreductases, leading to the formation of active metabolites. These enzymes include CYP1A1/2, CYP4A11, CYP3A4/5, CYP2B6, CYP2A6, CYP2C8, CYP2C9, and CYP2C19. Variability in exemestane metabolism by these enzymes may contribute to differences in the clinical response to the drug [131]. The primary active metabolite is 17β-hydroexemestane accounting for, approximately, 20% of plasma exemestane [132] (Figure 10). 17β-hydroexemestane has a high affinity for the androgen receptor (AR) [133]. Another significant metabolite is 6-hydroxymethylexemestane, primarily detected in urine. In addition to these major metabolites, several others have been identified, although their biological effects remain unknown. Exemestane metabolites are now recognized as important molecules in the mechanism of action of exemestane [134].

Exemestane has demonstrated significant therapeutic effects both *in vitro* and *in vivo*. Studies have shown that it can lead to substantial reductions in tumor volume (around 83%). However, its toxicity can vary among patients, possibly due to genetic factors. At low concentrations (1 µM), exemestane exhibits weak estrogen-like activity, which can induce proliferation in aromatase-overexpressing breast cancer cells. This effect might be linked to ER activation and the transcription of estrogen-responsive genes. Interestingly, the androgenic effects observed with exemestane and its main metabolite, 17β-hydroexemestane, might contribute to its relatively lower adverse effects on bones compared to non-steroidal aromatase inhibitors. Higher concentrations (10 µM) of exemestane have shown antiproliferative effects on ER-positive breast cancer cells. They induce cell cycle arrest in G0/G1 and, for longer treatment periods, in G2/M phase, which is associated with apoptotic processes. Autophagy is also implicated and seems to act as a survival mechanism against apoptosis. Moreover, exemestane metabolites, like 17β-hydroexemestane, induce cell cycle arrest and cell death through apoptosis and autophagy, potentially contributing to exemestane's clinical efficacy [135].

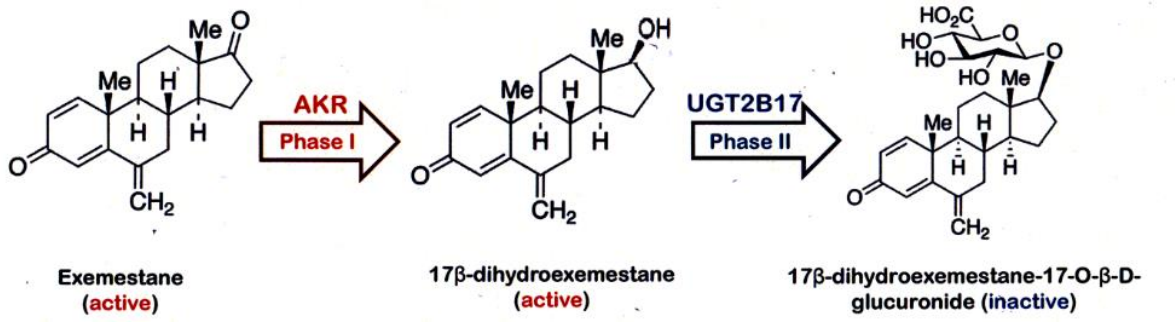

Figure 10. Exemestane major metabolism pathway. Scheme illustrating the metabolism pathway for exemestane [132].

3.2.3.2. Letrozole

Letrozole, also known as Femara, is a potent third-generation AI used in breast cancer treatment. It effectively inhibits the aromatization process, blocking the conversion of steroidal androgens to estrogens. Letrozole, in particular, is highly potent among AIs due to its structure, which can bind to the heme group of the aromatase enzyme, resembling androstenedione. Unlike earlier-generation inhibitors, letrozole has a high degree of selectivity, potency and significantly reduces serum estrogen levels in post-menopausal women. Indeed, studies like BIG 1-98, have shown that anastrozole and letrozole are superior to tamoxifen in terms of preventing cancer relapse (Hazard Ratio (HR), 95% CI, 0.81 to 1.01, respectively). Additionally, letrozole appears to be more effective in suppressing estrogen levels compared to anastrozole [136].

Letrozole is rapidly and completely absorbed orally with nearly 100% bioavailability. It has moderate protein binding and a large distribution volume. The recommended daily dose is 2.5 mg, and it is primarily metabolized as glucuronide in urine with an elimination half-life of 48 h. However, letrozole can have side effects in up to 30% of patients, including gastrointestinal disturbances like nausea, vomiting and diarrhea. Other side effects may include heartburn, headache, peripheral edema, hot flushes and fatigue. Severe adverse effects include hepatitis and autoimmune features in post-menopausal women with breast cancer. Prolonged exposure to high doses can cause bone resorption and increased cholesterol levels [137].

3.2.3.3. Lack of cross-resistance

Cross-resistance does not occur between the two types of AIs. This means that some patients, who are resistant to one AI type, may respond to the other AI type [138]. For example, approximately one in four patients have benefited from exemestane therapy after failing non-steroidal compounds and vice versa. As mentioned in Section 3.2.3.1. (Introduction), exemestane, a steroidal aromatase inhibitor, has distinct properties compared to non-steroidal aromatase inhibitors like letrozole and anastrozole. While both types of AIs can induce apoptosis and cell cycle arrest, exemestane exhibits unique characteristics, including weak estrogen-like activity and androgenic effects. Indeed, androgens have been shown to inhibit breast cancer growth both *in vitro* and *in vivo* and most breast cancers express AR. Exemestane, with its moderate androgenic activity as a steroidal compound, might impact AR activity, potentially affecting breast cancer cell growth and therapy sensitivity. This lack of cross-resistance could be related to exemestane's stronger aromatase inhibition, differences in direct aromatase protein interactions (binding sites), and potential genetic factors influencing therapy response [139]. However, the clinically observed lack of cross-resistance among AIs is not fully understood. Therefore, there is a need to comprehend the mechanisms behind endocrine resistance to each AI and develop strategies to overcome it. In fact, these differences between steroidal and non-steroidal AIs have prompted clinical trials such as NeoLetExe to explore their impact on clinical outcomes [140].

4. Resistance to endocrine therapy

Resistance to endocrine therapy can raise a major challenge, as it can hinder cancer treatment. In the following sections, the resistance to tamoxifen, fulvestrant and aromatase inhibitors will be elucidated.

4.1. Resistance to tamoxifen

Despite tamoxifen's efficacy in treating breast cancer, approximately 20-30% of tumors remain resistant to this therapy, representing a significant clinical challenge. This resistance can be *de novo* or acquired. *De novo* resistance refers to tamoxifen's inherent resistance, in which cancer cells do not respond to the treatment even when it is administered in the beginning. This could be caused by pre-existing genetic alterations or the activation of signaling pathways that are not altered by the mechanism of action of tamoxifen. Acquired resistance, occurs when previously responsive cancer cells adapt and develop mechanisms to counteract the effects of tamoxifen, which frequently involves genetic mutations, microenvironment changes or the development of alternative signaling pathways that bypass the need for ER. This section delves into the underlaying mechanisms that contribute to tamoxifen resistance in breast cancer (Figure 11).

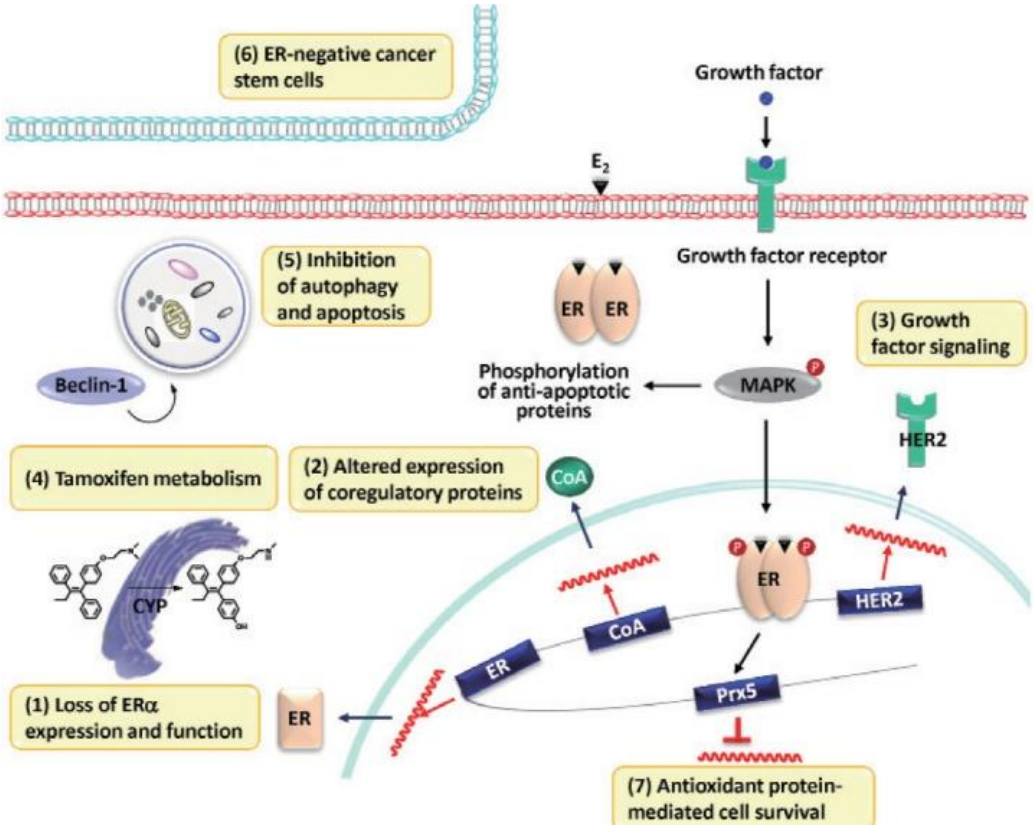

Figure 11. Mechanism of resistance to tamoxifen. **(1)** Loss of ER expression: results in the absence of the molecular target for tamoxifen. **(2)** Altered expression of co-activators or co-regulators: changes in the levels of proteins that are crucial for ER-mediated gene transcription. **(3)** Ligand-independent growth factor signaling cascades: activation of kinase pathways and phosphorylation of ER, triggered by growth factor signaling pathways, even in the absence of estrogen. **(4)** Altered availability of active tamoxifen metabolites: modulation of the levels of active tamoxifen metabolites, often influenced by drug-metabolizing enzymes like CYP2D6. **(5)** Regulation of autophagy and apoptosis: influences the balance between cell survival and cell death mechanisms. **(6)** ER-negative cancer stem cells: differentiation of ER-negative cancer stem cells that evade growth inhibition by antiestrogen treatments, unlike ER-positive cancer cells. **(7)** Antioxidant protein-mediated cell survival: tamoxifen's prevention of the repression of antioxidant proteins, such as Prx5, which leads to cell survival and resistance to tamoxifen therapy [141].

4.1.1. *De novo* or intrinsic resistance

De novo resistance accounts for 30% of the ER-positive tumors resistant to tamoxifen therapy [102]. This intrinsic resistance is primarily attributed to the lack of ER expression, but it can also be caused by inactive cytochrome P450/2D6 (CYP2D6) alleles, which prevents the conversion of tamoxifen into its active metabolite, endoxifen. Clinical studies have revealed that particular single nucleotide polymorphisms (SNPs) in CYP2D6 can lead to no, or reduced, enzyme activity, resulting in poorer outcomes for patients treated with tamoxifen [142].

4.1.2. Acquired resistance

Acquired resistance, as previously mentioned, occurs when a previously responsive cancer cells develop mechanism to counteract the effects of tamoxifen. This adaptation can be caused by a variety of reasons, which will be explained in the following sections.

4.1.2.1. Loss of ER expression

Over time, around 20% of breast cancer patients receiving endocrine therapy show a loss of ER expression [143]. This involves a shift from an ER-positive to an ER-negative phenotype, rendering the tumor resistant to ER-targeting therapy. Various mechanisms could explain the loss of ER expression, including epigenetic changes, such as aberrant CpG island methylation of the ER promoter or to ER chromatin binding sites and histone deacetylation, which compacts the nucleosome structure and limits transcription [144, 145].

4.1.2.2. Mutation in ER

ER gene mutations are commonly observed in resistant breast cancer cells. Mutations frequently occur in the ER's LBD domain, altering the conformational dynamics of the loop connecting Helix 11 and Helix 12. The most prevalent hot spot mutations take place at the following residues: Leu536Arg, Tyr537Ser, Tyr537Asn, Tyr537Cys and Asp538Gly. These mutations are commonly observed in resistant breast cancer cells. They cause alterations in the way that ER responds to estrogen or other ligands, impacting the receptor's ability to bind to estrogen and subsequently regulate gene expression. Moreover, these mutations can lead to constitutive activation of the ER, meaning the receptor becomes active even in the absence of estrogen [146].

4.1.2.3. Altered expression patterns of co-regulatory proteins

Altered expression patterns of co-regulatory proteins, which influence ER-driven transcription, have been recognized as contributors to endocrine resistance, particularly in tamoxifen therapy.

When an antagonist, like tamoxifen, binds to ER, co-repressors are normally recruited, resulting in the suppression of target gene transcription. However, in certain conditions, where ERBB2/HER2 activity is elevated, the tamoxifen-ER complex may attract co-activators resulting in agonistic outcomes. Indeed, tamoxifen's agonistic activity is enhanced by co-activator proteins such as AIB1, PGC-1β, and SRC family. High levels of AIB1 alone, or in combination with high levels of HER2, are linked with shorter disease-free survival in women receiving adjuvant tamoxifen therapy. Regarding the SRC family, co-activator SRC-1, SRC-2, and SRC-3 facilitate ER-mediated transcription. SRC-1, for example, is capable of initiating the transcription of endocrine-resistant genes independently of ER and the overexpression of SRC-3 has been linked to tamoxifen resistance [147].

Several transcriptional co-repressors are implicated in breast cancer, but it has been demonstrated that lower activity of co-repressors may contribute to tamoxifen resistance. Among these co-repressors, NCoR 1 and 2, and nuclear receptor subfamily 2, group F member 2 (NR2F2) have been linked to tamoxifen resistance. For example, low levels of NCoR1 predict poor response to tamoxifen, because they relieve the inhibition of MYC, CCND1 and SDF1 gene transcription. Additionally, NCoR1 modulates chromatin accessibility by recruiting histone deacetylase (HDAC) 3, which causes histone deacetylation, chromatin condensation, and RNA polymerase II loss. As a result of NCoR1

downregulation, tamoxifen behaves as a partial agonist for cell cycle progression. Similarly, low expression of NCoR2 is associated with tamoxifen resistance, owing to its direct binding to the ER and subsequent recruitment of additional corepressors, which leads to the suppression of proliferative pathways. Like other co-repressors, the expression of NR2F2 is also reduced in tamoxifen resistance [102].

4.1.2.4. Alteration of transcription factors

Tamoxifen resistance in ER-positive breast cancer has been linked to increased levels of the transcription factors Sp1, AP1, and NF-κB, which are involved in the indirect, or non-classical, pathway that regulates transcription of genes lacking EREs [148].

4.1.2.5. Tyrosine kinase receptors

Another origin for acquired tamoxifen resistance is the activity of receptor tyrosine kinase. In the following sections, the three main tyrosine kinase receptors will be explained.

Human Epidermal growth Factor 2 (HER2)

Tamoxifen's effectiveness depends on various signals, including those originating from membrane growth factors like receptor tyrosine kinases. The presence of epidermal growth factor receptor (EGFR) and HER2 have been shown to induce tamoxifen resistance through non-genomic mechanisms, without altering the genomic suppression of ER. Increased cross-talk between ER and HER2, particularly when there are high levels of the co-activator steroid receptor co-activator 3 (SRC3), is known as one of the mechanisms behind resistance to endocrine drugs. Overexpression of EGFR or ERBB2/HER2 has been linked to resistance to endocrine therapy. Specifically, in breast cancer cells with elevated HER2 expression, tamoxifen mimics the effects of estrogen. In addition, overexpression of HER-2 results in higher levels of anti-apoptotic proteins Bcl-2 and BclxL, diminishing tamoxifen’s ability to induce apoptosis and, thus, promoting resistance. The increased presence of HER2 and its downstream MAPK pathway may also contribute to the loss of ER, a factor directly associated with resistance to endocrine therapies [149].

Furthermore, it has been demonstrated that for tamoxifen to achieve its full potential, it requires the inhibition of HER2. This process involves the collaborative efforts of the PAX2 protein. When PAX2 is present, the tamoxifen/ER complex can suppress HER2 expression. Conversely, if the co-activator protein AIB-1 is more abundant than PAX2, the

tamoxifen/ER complex stimulates the upregulation of HER2, leading to increased cell proliferation [89].

Insulin-Like Growth Factor-1 Receptor (IGF-1R)

The IGF-1R signaling pathway regulates energy metabolism, cell proliferation, and apoptosis. IGF-1R, a receptor tyrosine kinase, exerts its effects by binding to the ligands IGF-I and IGF-II. After ligand binding and receptor activation, adaptor molecules are recruited, leading to the activation of downstream pathways. When IGF-1R interacts with ER in breast cancer cells, it induces the translocation of ER from the nucleus to extranuclear areas and increases the ligand-independent activation of ER, which results in acquired endocrine resistance. This, in turn, activates the Ras/MAPK and PI3K/AKT pathways, resulting in the development, progression and metastasis of breast cancer. Tamoxifen generally decreases the transcription of IGF-IR, which is an estrogen-dependent gene. However, when breast cancer cell lines develop resistance, the levels of phosphorylated IGF-IR (p-IGF-IR), the active form, rise significantly [150].

Fibroblast growth factor receptor (FGFR)

The FGFR family of receptor tyrosine kinase has been linked to the development and progression of breast cancer. High levels of FGFR3 are linked to tamoxifen-resistant breast tumors, as it also activates the Ras/MAPK and PI3K/AKT signaling pathways. In ER-positive breast cancer, FGFR1 amplification also increases cyclin D1 expression, contributing to resistance to antiestrogen therapies. Additionally, FGFR2 has been identified as a mediator of FGF7 action and is associated with tamoxifen resistance [151].

4.1.2.6. Cell cycle regulators

Cell cycle progression is meticulously regulated by various proteins, including cyclins and cyclin-dependent kinases (CDKs). Cyclin D1, for example, is essential for cell cycle regulation, specifically promoting progression from G1 to S phase. Cyclin D1 interacts with CDK4/6 to regulate cell cycle progression during the G1 phase and is a known downstream target of the PI3K/AKT/mTOR pathway. Additionally, CDK4/6 is known to interact with the ER signaling pathway. Cyclin D1 inhibits the retinoblastoma (Rb) protein early in the G1 phase, allowing the transcription factor E2F to induce cyclin E expression. Cyclin E then pairs with CDK2, forming an active complex that facilitates entry into the S phase [152] (Figure 12).

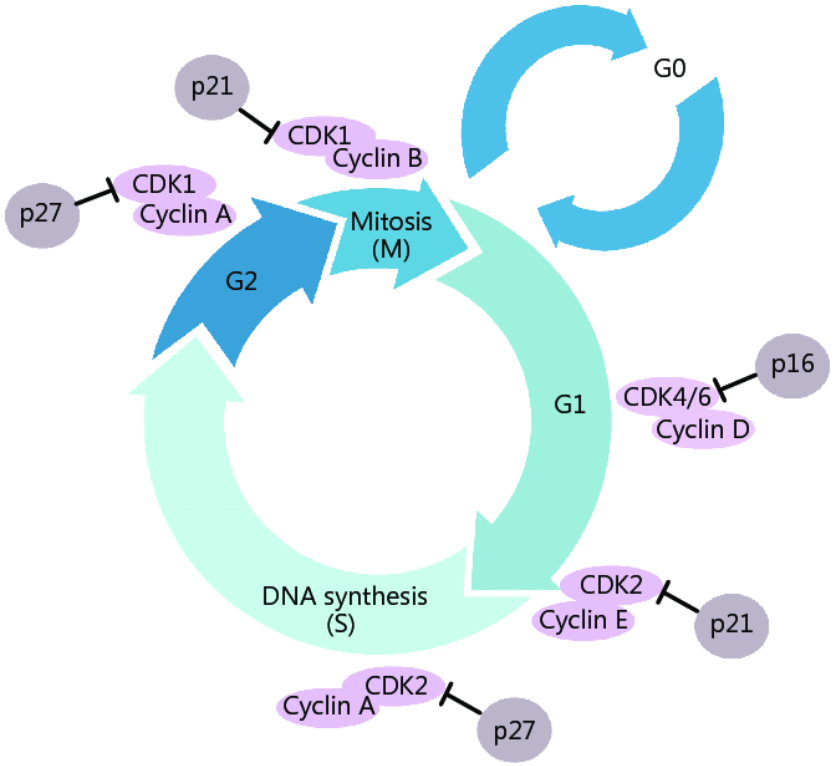

Figure 12. Cell cycle representation. Progression through each phase of the cell cycle is under the control of cyclin-dependent kinases (CDKs) in conjunction with their regulatory companions, the cyclins [153].

Tamoxifen suppresses cell cycle progression, whereas estrogen increases progression from G1 to S phase. As a result, the expression and activity of these cell cycle regulators has a substantial impact on the efficacy of tamoxifen and the development of resistance. Tamoxifen resistance has been linked to overexpression of positive regulators of cell cycle. Overexpression of c-MYC (a cell cycle regulator and oncogene) and cyclins E1 and D1, are all implicated in endocrine resistance by activating CDKs. Notably, elevated cyclin E2 expression has been associated to worse outcomes in patients with ER-positive breast cancers. Combining cell cycle inhibitors and hormone therapy could be a potential therapeutic approach.

Conversely, tamoxifen resistance is associated with lower expression of negative regulators of cell cycle progression, which are CDK inhibitors that prevent cell cycle progression, such as p21 and p27. For example, loss of p21 function is considered as a possible cause of tamoxifen resistance, because in the absence of p21, cyclin-CDK complexes aberrantly phosphorylate ER, resulting in a growth-stimulatory phenotype. Similarly, p27 inhibition has been linked to tamoxifen resistance [102].

4.1.2.7. Extracellular vesicles

Another method of tamoxifen resistance is extracellular vesicles (EVs), which are small particles secreted by cells carrying DNA, RNA, and proteins that can transfer information and affect receptive cells. EVs have been associated to hormone therapy resistance via the activation of PI3K/AKT pathway, as well as AP-1 and NF-κB. In addition, EVs transport P-glycoprotein, a protein responsible for pumping drugs from the cytoplasm of the cell to the extracellular surface, which is a major mechanism of endocrine resistance. EVs also carry miR-221/222, which have been linked to endocrine resistance [154].

4.1.2.8. The immune system

The immune system is involved in tamoxifen resistance. High levels of tumor-associated macrophages (TAM), soluble mediators such inteleukin-1B (IL-1B), and tumor necrosis factor α (TNFα) are associated with a poor prognosis in breast cancer. For example, the chemokine CCL2, released by TAM, promotes the PI3K/AKT/mTOR signaling pathway in the tumor microenvironment. This activation results in a feedback loop, which contributes to endocrine resistance. Additionally, TNFα and IL-1B activate a key transcription factor known as NF-κB, which is also involved in the development of endocrine resistance [155]. Indeed, the cytokine IL-1B causes epithelial-mesenchymal transition (EMT) by upregulating TWIST1, resulting in the methylation of ER gene promoter. This epigenetic modification decreases ER levels and promotes tamoxifen resistance [156].

4.1.2.9. MicroRNAs

MicroRNAs (miRNAs) are non-coding RNA molecules that regulate gene expression by degrading mRNA or impeding translation. There are oncogenic and tumor suppressor miRNAs, which either stimulate or inhibit cancer cell growth and invasion, respectively. The primary mechanism behind endocrine treatment resistance involves miRNAs interacting and modifying ER and, finally, culminating in ER loss. For example, miR-221/222 affect p27 and ER, allowing tumor development in an ER-independent way leading to tamoxifen resistance [157]. Another example is miR-21, which enhances tamoxifen resistance by targeting PTEN, whereas miR-148a and miR-152 have been shown to reduce tamoxifen resistance in ER-positive breast cancer [158].

4.2. Fulvestrant resistance

Resistance to fulvestrant in breast cancer can occur through various mechanisms. In the following subsections, the main ones will be explained. A summary of some of the primary mechanisms associated with fulvestrant resistance is displayed in Table 3.

Table 3. Summary of some mechanisms associated with fulvestrant resistance [159].

Mechanism of resistance	Molecular aberration
ER	ER suppression by stromal cells ER loss by TWIST1 ER methylation
ER-associated Transcription factors	NF-κB activation
Grow factor receptor signaling	EGFR and HER2 amplification ERBB3 upregulation ERBB4 upregulation/downregulation IGF-1R overexpression
PI3K signaling	AKT overexpression and activation PTEN loss
Cell cycle	CDK6 overexpression Rb inactivation
MicroRNA	MiR-221/222 overexpression
Microenvironment	HIF-1α VEGF upregulation TIGAR overexpression Stromal microvesicle IL6-STAT3-Notche3 mediation

4.2.1. PI3K/AKT and MAPK pathways

Both preclinical and clinical studies have demonstrated that signaling pathways involving growth factor receptors converge on PI3K and MAPK/ERK, contributing to resistance to antiestrogen therapy. Indeed, overexpression of AKT in breast tumors has been linked to poor responses to antiestrogen therapy. Inhibiting AKT with drugs like wortmannin, which is a PI3K inhibitor, can effectively suppress the proliferation of fulvestrant-resistant cells [160]. Furthermore, highly active AKT has been identified as a contributor to fulvestrant resistance, and this resistance can be reversed by using the mTOR inhibitor (everolimus). The silencing of PTEN has been shown to enhance sensitivity to fulvestrant in ER-positive breast cancer cells. This enhanced sensitivity is achieved by increasing autophagic cell death. Conversely, overexpression of the growth factor ERBB2

can confer resistance to both tamoxifen and fulvestrant via the activation of the PI3K pathway [161].

4.2.2. PIK3CA gene mutation

Mutations in the PIK3CA gene, which encodes the p110 catalytic subunit of PI3K, play a role in fulvestrant resistance. These mutations activate the PI3K/AKT pathway, promoting cellular transformation and tumor growth. Clinical trials have demonstrated that combining PI3K inhibitors like everolimus, buparlisib, or taselisib with fulvestrant can improve progression-free survival (PFS), particularly in patients with PIK3CA mutations [162].

4.2.3. Cell cycle regulators

Fulvestrant resistance can also occur due to changes in cell cycle regulatory proteins. In ER-positive breast cancer, ER signaling leads to cyclin D1 overexpression, forming the cyclin D1-CDK4/6 complex, which phosphorylates and inactivates Rb, facilitating cell cycle progression. Even when ER signaling is downregulated, Rb phosphorylation persists. However, this persistent phosphorylation can be countered by palbociclib, a selective CDK4/6 inhibitor. In advanced breast cancer, ESR1 mutations are frequently observed, indicating that cancer cells continue to stimulate cell cycle progression through the cyclin D1-CDK4/6 pathway. In ESR1 mutant patients, fulvestrant may only partially inhibit ER signaling, because fulvestrant works by binding to the ER and inducing its degradation, effectively blocking estrogen signaling. However, in cases where there are mutations in the ligand-binding domain of ER, these alterations can impact how fulvestrant interacts with the mutated ER. Nevertheless, the combination of palbociclib with fulvestrant effectively overcomes this resistance. However, combining CDK4/6 inhibitors and fulvestrant does not benefit patients with high CDK expression [163]. By contrast, acquired resistance to fulvestrant due to CDK6 overexpression can be reversed with TSA, a histone deacetylase inhibitor, suggesting a role for nucleosome acetylation in resistance development [164].

4.2.4. Growth factor receptor signaling

The activation of the ERBB family of receptors, particularly EGFR and ERBB2, has been linked to fulvestrant resistance. ERBB3 is associated with poor patient survival and contributes to fulvestrant resistance. The downstream PI3K/AKT and MAPK pathways are stimulated upon ERBB activation. In breast cancer, which are resistant to fulvestrant and

where the ERBB system and PI3K/AKT and MAPK pathways are activated, dual inhibitors targeting both pathways may be a more potent therapeutic approach.

Moreover, in ER-positive breast cancer, IGF-1R and ER are often co-expressed and respond to the synergistic action of IGF-1 signaling and estrogen, but the interaction between IGF-1R and ER contributes to the development of endocrine resistance. Importantly, stimulation by IGF-1 ligands leads to activation of IGF-1R, as well as MAPK and PI3K signaling pathways, resulting in irreversible resistance to antiestrogen treatments, independent of ER [165].

4.2.5. ER-associated transcription factors

Another mechanism of fulvestrant resistance is through the NF-κB pathway, which regulates transcription of several genes, including cytokines, cell adhesion molecules, Cyclin D1, c-MYC and numerous apoptosis inhibitors. Constitutive NF-κB activity is observed in breast cancer, and its overexpression can lead to fulvestrant resistance [166].

4.2.6. MicroRNAs

Aberrant expression of particular microRNAs (small noncoding RNA molecules that restrict transcription or promote degradation), such as miR-221/222, can contribute to fulvestrant resistance by boosting cell cycle progression and tumor invasion [167].

4.2.7. Microenvironment

Tumor microenvironment and epigenetic alterations contribute to fulvestrant resistance. The tumor microenvironment, including factors like hypoxia-inducible factor 1α (HIF-1α), vascular endothelial growth factor (VEGF) and cancer-associated fibroblasts (CAFs) can promote resistance to fulvestrant. Epigenetic alterations are of great importance in promoting tumor initiation, progression and endocrine therapy resistance. Both DNA methylation and histone modifications serve as important sources of fulvestrant resistance [168].

4.3. Resistance to aromatase inhibitors

Despite the widespread use of AIs, challenges such as non-responsiveness in some patients, resistance to AI treatment, and inhibition of other CYP450 enzymes have emerged. While antiestrogens and AIs have improved overall survival rates, over half of ER-positive breast tumors eventually develop resistance to one or more of these endocrine therapies. Aromatase inhibitors, similar to tamoxifen and fulvestrant, also have multiple mechanisms of acquired resistance for the treatment of ER-positive breast cancer [169]. Some resistance mechanisms are widespread in endocrine resistance, whereas others are particular to letrozole or exemestane. In this section, the most common resistance mechanisms to AIs will be explained.

4.3.1. Estrogen receptor-related mutations

Estrogen-related mutations occur under the treatment of AIs. For example, mutations in the estrogen receptor 1 (ESR1) gene, which encodes ERα, have been linked to AI resistance. Particularly, being more common (ranging from 11% to 55%) in metastatic tumors which have progressed despite AI treatment, as these mutations can lead to estrogen-independent ER activation and cell proliferation. In addition, chromosomal translocations involving ESR1 can result in a fusion between different genes, such as YAP1, POLH, AKAP12 and CCDC170. These fusions may lead to estrogen-independent growth and, thus, resistance to AIs. Some cases of AI resistance involve the amplification of ESR1 and CYP19A1 genes, although their prevalence and clinical relevance remains uncertain [170].

4.3.2. Aberrant growth factor receptor activation

Another mechanism of AI resistance is the aberrant growth factor receptor activation due to prolonged estrogen deprivation and ER signaling disruption. Indeed, dysregulated activation of growth factor receptors (GFRs), along with downstream signaling pathways like MAPK and PI3K, has been associated with AI resistance. Therefore, cross-talk between GFRs and ER can bypass estrogen deprivation. Additionally, it has been shown that tumors retaining ER expression can escape the limitations of estrogen deprivation, by increasing their hypersensitivity to residual levels of estrogens [171].

4.3.3. Androgen receptor expression

The AR is a steroid receptor, similar to ER, involved in several physiological processes. Roughly 60-85% of breast cancers that are ER-positive, and around 77% of invasive breast cancers, express the AR [172].

In cells which are sensitive to AIs, ER promotes cell growth, while AR induces cell death. In such cases, having higher levels of AR (AR overexpression) is associated with better disease-free survival (DFS) compared to cancers lacking AR. Conversely, the absence of AR expression predicts earlier treatment failure when AIs are used. In cells resistant to AIs, AR overexpression can occur in response to reduced ER activity, potentially contributing to resistance. While AR is generally seen as a favorable prognostic marker, its precise role and the impact of targeting AR in AI acquired resistance is not clearly established and more research is needed. Nonetheless, recent findings highlighting the importance of AR in breast cancer and its dual role in both AR-sensitive and AR-resistant cells, suggest that it could be a promising therapeutic target worth deeper exploration [173].

4.3.4. Cell cycle regulators

Aberrant expression and activation of cell cycle regulators, such as cyclin D1, CDK4/6 and Aurora kinases, has been associated with AI resistance. Several survival pathways, such as MAPK, NF-κB or ER, promote the expression of cyclin D1. Cyclin D1 is responsible for the progression of G1-to-S phases, by forming a complex with cyclin-dependent kinase 4/6 (CDK4/6), inactivating the Rb protein and inducing the synthesis of cyclin E. The joint action of cyclin D1-CDK4/6 and cyclin E-CDK2 contributes to the progression of cell cycle. Thus, inhibitors of CDK4/6 have shown promising results in clinical trials. Resistance can also involve upregulation of anti-apoptotic proteins and pro-survival autophagy. Finally, other mechanisms of AI resistance involve deregulation of miRNAs like miR-125b, miR-205, and miR-424 affecting the PI3K/AKT pathway and promoting resistance [174].

4.4. Resistance to exemestane

Unlike non-steroidal AI-resistant cells, cancer cells that have developed resistance to exemestane still exhibit hormone-dependent behavior [175]. In recent years, various mechanisms have been linked to the development of resistance to exemestane (Table 4). Some of these mechanisms are shared with non-steroidal AIs, while others seem to be unique to this particular steroidal AI (Figure 13).

Table 4. Mechanisms of resistance to exemestane [174].

Mechanism of resistance	Molecular aberration
Increase MAPK pathway activity	AREG overexpression
Decrease expression of ER	PI3K/AKT/mTOR overexpression
Promotion of cell cycle progression	Aurora kinase A/B upregulation
NF-κB expression	HDAC aberrant activity
Increased IGF-1R and PI3K/AKT/mTOR signaling	AR overexpression
Pro-survival cellular mechanism	Autophagy

4.4.1. MAPK pathway

At some point, a large part of breast tumors undergoes complex molecular alterations that may result in *de novo*, or acquired, resistance to endocrine therapy. Exemestane resistance may arise from its weak estrogen-like activity, which can drive tumor proliferation through several pathways. The amphiregulin (AREG) protein, which binds to the epidermal growth factor receptor (EGFR) when activated by estrogens, is upregulated in exemestane-resistant cells [176]. Exemestane's weak estrogen-like activity might induce AREG upregulation in an ER-dependent manner, activating the EGFR pathway and downstream MAPK pathway, creating an autocrine loop that promotes cell proliferation. Inhibition of AREG, ER, EGFR and MAPK can suppress the proliferation of exemestane-resistant cells, indicating a cross-talk between these pathways. Cross-talk between ER and growth factor pathways involving EGFR, HER2 and IGF-1R is a well-established mechanism of endocrine resistance, including resistance to exemestane. This cross-talk leads to the activation of MAPK, PI3K, AKT, mTOR and other signals crucial for cell proliferation and survival [177]. Targeting mTOR with everolimus in combination with exemestane is being explored in clinical trials (BOLERO-2) to overcome resistance [178].

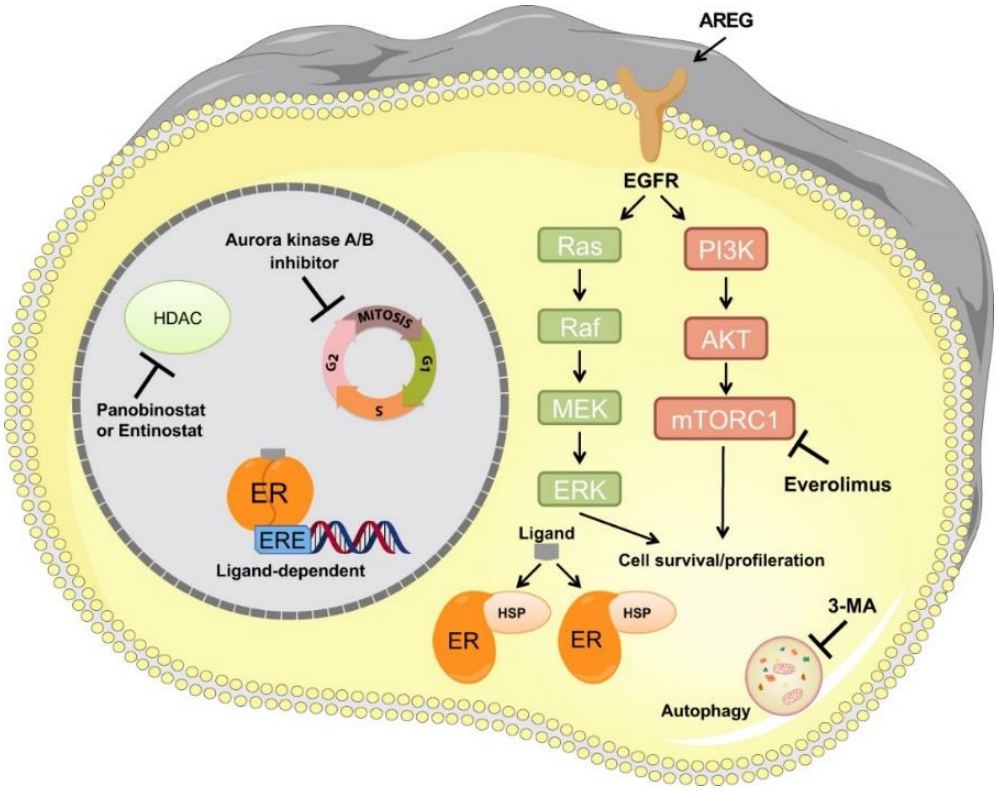

Figure 13. Mechanisms of acquired resistance to exemestane. Exemestane resistance often involves estrogen-dependent pathways and the upregulation of survival and proliferation signaling pathways, including PI3K/AKT and MAPK/ERK. Several investigational strategies are under exploration to overcome this resistance, including the inhibition of histone deacetylases (HDACs) using compounds like panobinostat or entinostat, inhibition of the mTORC1 pathway with everolimus, suppression of autophagy with 3-methyladenine (3-MA), and regulation of the cell cycle through the inhibition of Aurora kinase A/B. Key molecular players in these pathways include AKT (serine/threonine-specific protein kinase family), AREG, EGFR, ER, ERE, HDAC, HSP, MAPK, mammalian target of rapamycin complex 1 (mTORC1), and PI3K [174].

4.4.2. Cell cycle regulators

Recent research has identified the role of other kinases in AI-resistant breast cancer models, including Aurora kinase A and B. These kinases control cell cycle progression and were found to be upregulated in AI-resistant cells, making them potential therapeutic targets [179]. Genetic and epigenetic alterations can deregulate these pathways and contribute to AI resistance. Additionally, downregulation of INrf2 led to Nrf2 upregulation, promoting cytoprotective signaling and reducing drug efficacy. Inhibiting Nrf2 re-sensitizes exemestane-resistant cells, suggesting that this is another mechanism involved in endocrine resistance [180].

4.4.3. NF-κB expression

Genetic and epigenetic alterations are also known to be implicated in AI-resistance and can even be responsible for deregulation of the previously referred pathways. Indeed, histone deacetylase inhibitors (HDACi) have shown promise in suppressing the proliferation of exemestane-resistant cells by inducing cell cycle arrest and apoptosis. NF-κB transcription factor, overexpressed in AI-resistant cells, is also implicated in resistance [181].

4.4.4. AR overexpression

Exemestane, in addition to causing estrogen deprivation, leads to increased levels of androgens within tumors [182]. Currently, clinical trials (NCT02007512) are underway to investigate the potential benefits of combining the AR antagonist enzalutamide with exemestane. However, in postmenopausal patients, who were previously treated with non-steroidal AIs, the inhibition of androgen production using abiraterone acetate (AA) and prednisone, alongside exemestane, did not result in improved progression-free survival compared to exemestane treatment alone [183, 184].

4.4.5. Pro-survival cellular mechanisms

Autophagy inhibition in the presence of the drug caused a reduction in the viability of AI-resistant breast cancer cells. This indicates that the pro-survival role of autophagy might be one of the mechanisms involved in acquired resistance to exemestane. Therefore, autophagy is another potential mechanism of exemestane resistance, and inhibiting autophagy can re-sensitize resistant cells to the drug. Intermittent treatment with exemestane has shown potential in delaying resistance development.

Other mechanisms of exemestane resistance include changes in ER status, cell cycle deregulation, apoptosis inhibition, high Ki67 expression, somatic mutations in genes like TP53 and RB1, tumor microenvironment interactions, and a recently discovered factor, programmed cell death 4 (PDCD4), which is downregulated in AI-resistant cells [135].

4.5. Resistance to letrozole

Several mechanisms are associated with acquired resistance to letrozole (Table 5). These mechanisms involve the MAPK and PI3K pathways, as well as cell cycle regulators.

Table 5. Mechanisms of resistance to letrozole [174].

Mechanism of resistance	Molecular aberration
Decrease expression and ligand-independent activation of ER	HER2 overexpression PI3K/AKT/mTOR overexpression
Promotion of cell cycle progression	CDK4/6 activity Cyclin E overexpression Aurora kinase A/B upregulation
HER2 modulation	HDCA aberrant activity

4.5.1. Decrease expression and ligand-independent activation of ER

Letrozole-resistant cells often depend on MAPK pathways, particularly through overexpression of HER2 and EGFR, leading to ligand-independent activation of ER. Co-targeting HER2 and ER signaling has shown promise in restoring letrozole sensitivity and inducing tumor regression in resistant cells. Furthermore, the PI3K/AKT/mTOR pathway is frequently upregulated in letrozole-resistant cells [185]. Clinical trials have explored the use of PI3K inhibitors like buparlisib in combination with letrozole, showing potential anti-tumor efficacy (Figure 14) [186].

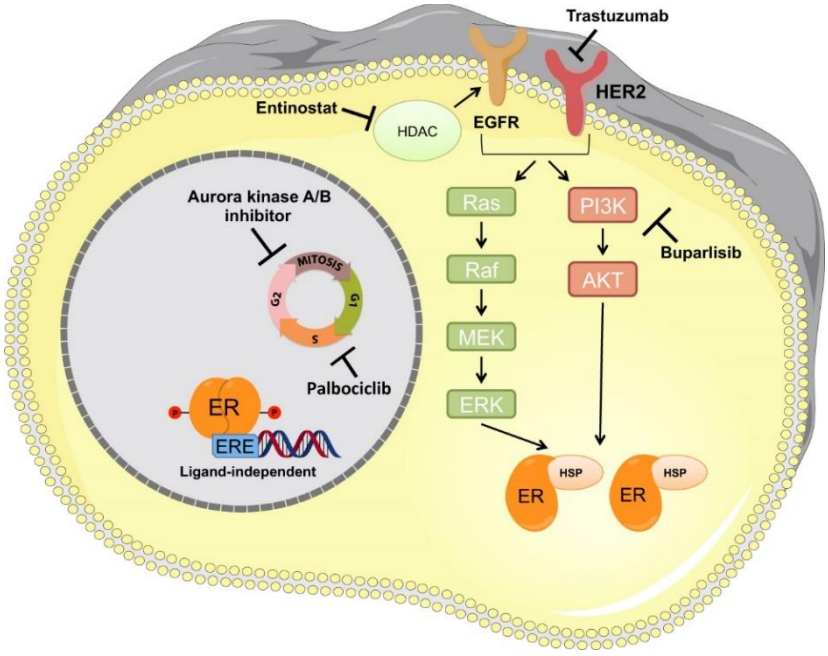

Figure 14. Mechanisms of acquired resistance to letrozole. Letrozole resistance can arise independently of estrogen signaling, driven by the upregulation of survival and proliferation pathways. These include PI3K/AKT and MAPK/ERK pathways. Potential strategies to overcome resistance involve HDAC inhibitors, HER2 blockade using trastuzumab, PI3K inhibition with buparlisib, and cell cycle regulation via Aurora kinase A/B inhibitors or palbociclib. Key molecular players include AKT, EGFR, ER, ERE, ERK, HDAC, HER2, HSP, MAPK, and PI3K [174].

4.5.2. Cell cycle regulators

Cell cycle regulation plays a role in letrozole resistance. The inhibition of CDK 4/6 with drugs like palbociclib and ribociclib, in combination with letrozole, has demonstrated effectiveness in preventing resistance and extending progression-free survival in clinical trials [187]. Aurora kinase A and B upregulation are implicated in letrozole resistance, and inhibiting these kinases has shown promise as a therapeutic approach [179]. Studies involving HDAC inhibitor, entinostat, have suggested a beneficial effect on letrozole-resistant cells, potentially through modulation of HER2 [188].

5. Epigenetics, chromatin and histone modification

DNA is packed into chromatin, a highly structured and dynamic protein-DNA complex that serves as the transcriptional regulatory platform. Chromatin, which is the combination of DNA and histone proteins, can take 2 distinct states: open (euchromatin) or closed (heterochromatin). These distinct states of chromatin, whether it is open or closed, are influenced by histone modifications. Histones are essential regulatory proteins responsible for maintaining the 3-dimensional structure of chromatin and also play a crucial role in gene regulation [189]. Chromatin, in its most basic form, comprises nucleosomes, each consisting of 146 base pairs (bp) of DNA, wrapped around an octamer composed of four core histones: H2A, H2B, H3, and H4 (Figure 15) [190]. The structure of chromatin is significantly influenced by modifications on histone tails.

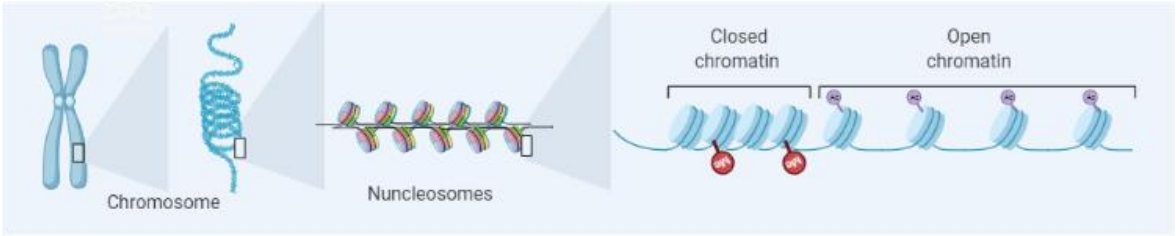

Figure 15. Chromatin structure. The nucleus stores genetic information, organized into chromosomes. Chromosomes consist of nucleosomes, the fundamental units, composed of double-stranded DNA wrapped around a histone octamer. Linker histone H1 connects octamers, and various histone tails undergo modifications to control chromatin accessibility. Illustration created using BioRender.com.

Additionally, there are regulatory proteins called transcription factors (TFs) that influence gene expression by binding to specific DNA sequences. TFs regulate various biological processes, including gene transcription, DNA replication, recombination, repair, chromosomal stability, cell cycle progression and epigenetic silencing [189]. Chromatin conformation can either directly regulate transcription by allowing, or preventing, DNA-binding proteins from accessing DNA, or it can modify the nucleosome surface to promote or inhibit TF recruitment [191]. When transcription factors bind to DNA, histone-modifying enzymes are attracted, then, they control histone tail modification and, thus, gene expression [192]. Interactions between TFs and their genomic targets are of particular importance, as some TFs are encoded by oncogenes linked to cancer and drug resistance.

The study of changes that take place in the chromatin is known as epigenetics. Epigenetic modifications involve chemical modifications to DNA or histones and affect gene expression. Indeed, epigenetic modifications are critical in regulating when and how genes are turned on or off. They operate as "marks" on DNA or histones, altering gene accessibility

to the transcription machinery in the cell. Unlike mutations in the DNA sequence, epigenetic changes are usually reversible and occur without alterations to the underlying DNA sequence. Aberrant epigenetic changes can contribute to the development, progression and drug resistance in breast cancer. On early carcinogenesis, epigenetic modifications have a significant impact on influencing cellular plasticity and promoting oncogenic reprogramming contributing to the heterogeneity of breast tumors. In later stages, additional epigenetic changes further modulate cancer cell behavior, including metastasis [193].

Common epigenetic mechanisms encompass DNA methylation (the addition of methyl groups to DNA) and histone modifications (post-translational modifications of histones). These changes can either promote gene expression (activation) or repress it (silencing). Post-translational modifications occur at histone tails and include methylation, acetylation, phosphorylation, ubiquitination, sumoylation and ADP ribosylation. To date, about 60 distinct modification sites have been identified on histones [194]. These modifications result in a "histone code" that influences the transcriptional potential of specific genes or genomic areas. In fact, each histone modification acts as a unique marker indicating the state of chromatin structure. Thus, these modifications impact chromatin structure and, consequently, gene expression that can either facilitate or impede access of TFs to gene promoters. In general, histone acetylation activates genes, while histone methylation can either activate or repress them, depending on the specific modification site [195].

For instance, histone acetylation diminishes histone-DNA interactions, increasing DNA accessibility and promoting transcription. Conversely, histone deacetylation eradicates this mark, leading to transcriptional repression and the formation of heterochromatin. The balance between histone acetylation and deacetylation is crucial in regulating gene expression. Elevated levels of histone acetylation (hyperacetylation) are usually associated with higher transcriptional activity, whereas reduced levels (hypoacetylation) are linked to gene repression [196]. Various enzymes, including histone acetyltransferases (HATs) and histone deacetylases (HDACs), regulate histone acetylation. HATs add acetyl groups to histones, facilitating transcription factor binding, while HDACs remove these groups, resulting in tightly coiled chromatin structures that are less accessible to TFs. Given its relevance, HDAC inhibitors are being explored as potential anticancer therapies, especially in combination with other treatments like antiestrogens [197].

Regarding histone methylation, it involves the transfer of a methyl group to a lysine or arginine residue by histone methyltransferases (HMTs), with histone demethylases (HDMs) removing these methyl groups. Histone methylation can lead to either the opening or closure of chromatin regions. Transcription depends on the position and number of methyl groups attached, thus, either activating or repressing transcription [198]. Dysregulated HMTs and HDMs are associated with breast cancer resistance, making them potential therapeutic targets. Epigenetic therapies, such as DNA methyltransferase inhibitors (DNMTi) offer promise in breast cancer treatment by reversing abnormal DNA methylation and histone modifications.

Apart from histone post-translational modifications, DNA can be methylated. DNA methylation at CpG sites can lead to gene reactivation, chromosomal instability, increased mutation rates or gene repression, genomic instability and suppression of tumor suppressor genes [199].

To study protein-DNA interactions, histone modifications, and TFs binding sites on a genome-wide scale, there is a powerful technique called Chromatin Immunoprecipitation (ChIP) that can be coupled to sequencing, thus, called ChIP-Seq [200]. ChIP-seq identifies enriched regions within a genome by using an antibody against a specific TF or histone modification mark. The strength of ChIP-seq lies in its ability to capture a snapshot of a particular protein-DNA interaction happening within a system [201]. With the increasing affordability and efficiency of sequencing technology [202], ChIP-sequencing has emerged as a potent tool for gaining insights into the fundamental processes behind the development and progression of diseases and the investigation of modifications in epigenetics [203]. The utilization of ChIP-seq has facilitated advancements in the field of medical genetics, making it easier to unravel the mechanisms underlying human diseases and identify therapeutic targets, particularly in cancer [204].

OBJECTIVES

OBJECTIVES

This Ph.D. thesis was dedicated to study the mechanisms of response of aromatases inhibitors and had two primary objectives, each explored in individual chapters. The main goals were the following:

1. Uncover novel response mechanisms to aromatase inhibitors within luminal breast cancer patients. The main goal is to identify a subgroup of patients who exhibit a preferential response to a particular aromatase inhibitor and to understand the cross-resistance between two different aromatase inhibitors.

2. Elucidate the factors responsible behind the cessation of response to treatment, development of resistance and subsequent development of metastasis, following the administration of aromatase inhibitors in luminal breast cancer patients.

CHAPTER I

STUDYING RESPONSE MECHANISMS TO AROMATASE INHIBITORS IN LUMINAL BREAST CANCER

INTRODUCTION I

1. Precision medicine: addressing therapy failure

Breast cancer is a complex and heterogeneous disease, both clinically and molecularly. This heterogeneity has become evident in the fact that patients of the same type, respond differently to treatments and are more susceptible to side effects. This leads to the development of therapeutic resistance [205]. Indeed, breast cancer resistance is a major issue which is not being effectively addressed, since rather than focusing on studying the molecular pathways in depth to understand the cause of the resistance; the strategy of utilizing a different treatment is widely used. The one-dose-fits-all model has been ineffectual, as it often is associated with the risks of drug toxicities and treatment failures. Furthermore, adverse drug reactions, affecting 16% of patients in the United States and causing over 100000 deaths annually, emphasize the need for more precise and individualized medicine [206]. Therefore, to tackle breast cancer treatment complications, a deep understanding of the molecular mechanisms underlying breast cancer and its response to drugs is needed [207].

One approach to tackle these challenges is through the integration and analysis of various data points using multiomics, offering hope for more informed therapeutic decisions [208]. Recent technological advances, particularly in gene expression profiling, have enhanced the knowledge of the molecular basis of tumor progression and treatment responses. Prognostic markers have emerged as valuable tools to help clinicians predict the aggressiveness of tumors, leading to improved treatment choices [209]. By identifying molecular biomarkers that can serve as prognostic and predictive indicators, clinicians are empowered to make more individualized and precise treatment decisions, ultimately optimizing therapy and minimizing cases of under or overtreatment. Indeed, recent advances in molecular research have improved the understanding of tumor features, leading to the development of individualized patient therapy [210].

To summarize, omics technologies are enabling a more precise approach to breast cancer treatment, allowing for tailored solutions [211]. Precision medicine, based on individual variations, genetics, and lifestyle, aims to deliver more personalized and effective disease prevention and treatment. This development holds great promise for enhancing breast cancer management [212].

2. NeoLetExe clinical trial: understanding AIs

Aromatase inhibitors (AIs), as mentioned in Section 4.2.3. (Introduction), are the main endocrine therapy that is as nearly as effective as standard neoadjuvant chemotherapy [213]. Moreover, neoadjuvant endocrine treatment, using the third generation of aromatase inhibitors (letrozole, anastrozole, and exemestane), is currently the preferred treatment in postmenopausal women. As highlighted in Section 4.2.3.3. (Introduction), AIs exhibit a lack of cross-resistance between steroidal inactivators and non-steroidal AIs, a phenomenon substantiated by multiple clinical trials [214, 215]. These evidences provide the rationale for the sequential and interchangeable use of steroidal and non-steroidal AIs [216]. Despite extensive previous research, the mechanism underlying the reported absence of cross-resistance remains unexplained. Additionally, it has been suggested that a thorough study of this clinical occurrence could lead to a novel approach to treating hormone-sensitive breast cancer [217].

To explore the underlying mechanism for the lack of cross-resistance, Dr. Jürgen Geisler initiated a clinical study named NeoLetExe. NeoLetExe constitutes a neoadjuvant, randomized, open-label and single-center clinical trial with intrapatient cross-over design. This study is focused on unraveling the intratumoral mechanisms of adaptation to letrozole and exemestane, specifically examining how these two compounds directly impact tumor biology. Both drugs were administered as neoadjuvant endocrine therapy to postmenopausal patients with locally advanced breast cancer in a randomized and cross-over design sequence [140].

NeoLetExe clinical trial was conducted exclusively among postmenopausal women with locally advanced breast cancer, characterized by ER-positivity in at least 10% of cancer cells. The eligibility criteria are delineated in Table 10 in Annex. Locally advanced breast cancer (T3-T4 and/or N2-3) is generally considered to be inoperable in its primary state and presurgical therapy is required. This presurgical therapy, also known as neoadjuvant therapy, establishes local tumor control transforming an initially inoperable situation into an operable one and minimizing long-term complications like bleeding, wound complications, and exudation. In addition, neoadjuvant therapy is acknowledged as one of the best model systems for predicting responses in clinical settings, allowing adjustments at a relatively early stage [218].

The NeoLetExe clinical trial was designed as an intrapatient cross-over study, due to the considerable hormonal interpatient variation. This approach enables the examination of letrozole (Let) and exemestane (Exe) impact within a single patient. Thus, each patient serves as their own control to make comparisons (Figure 16). This methodology has previously demonstrated success in comparing anastrozole and letrozole for breast cancer [219]. Upon the completion of neoadjuvant endocrine therapy, all patients underwent an evaluation by a breast surgeon to determine the most appropriate local surgical treatment (breast-conserving surgery or mastectomy, among others).

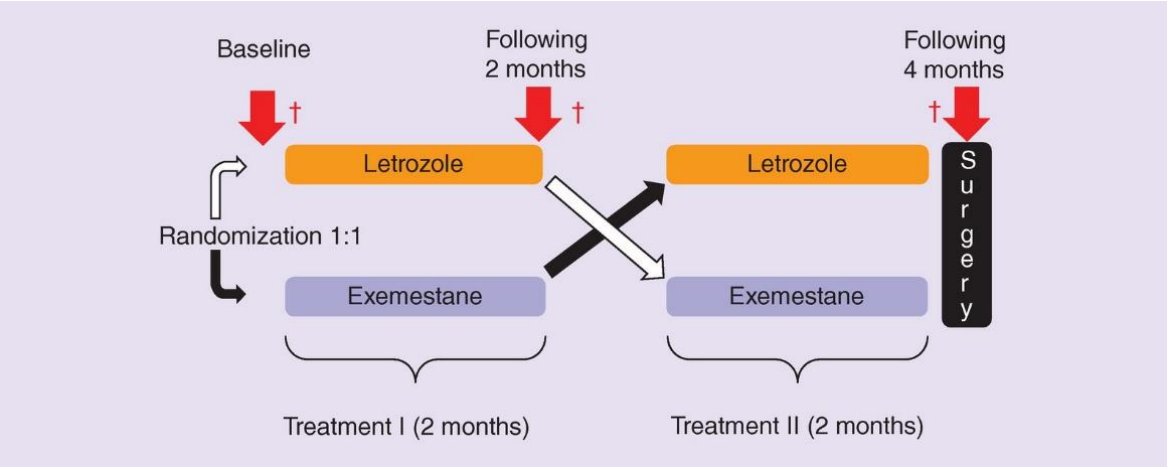

Figure 16. Design of NeoLetExe clinical trial. The first arm-initiated treatment with letrozole (2.5 mg) for a minimum of 8 weeks, followed by a subsequent 8-week course of exemestane (25 mg) before surgery. The second arm began with exemestane (25 mg) for at least 8 weeks, followed by letrozole (2.5 mg) for 8 weeks before surgery [140].

OBJECTIVES I

The first project of this Ph.D. thesis was dedicated to uncovering novel response mechanisms and cross-resistance to aromatase inhibitors within luminal breast cancer patients. The main objectives of this study were the following:

1. To elucidate the mechanisms of response to aromatase inhibitors within the NeoLetExe clinical trial.

2. To identify a specific patient subgroup exhibiting a potential predilection for favorable responses to aromatase inhibitors.

3. To explore the lack of response, or cross-resistance, to aromatase inhibitors.

RESULTS I

1. Clinical data exploration shows better clinical outcome in patients receiving exemestane followed by letrozole treatment

1.1. Sequential administration of exemestane followed by letrozole treatment yields remarkable Ki67 reduction, highlighting exemestane's efficacy in lowering Ki67 levels in the whole NeoLetExe cohort

To meet the specified objectives and identify a subgroup of patients exhibiting a preferential response to a particular aromatase inhibitor, we examined the data derived from the NeoLetExe clinical trial. We conducted an exploratory data analysis on clinical data provided by Prof. Jürgen Geisler to explore potential relationships between variables related to the treatment response. To protect patient identities, Geisler anonymized them by assigning unique numerical identifiers from 1 to 100. Additionally, they ensured random treatment allocation. The clinical data variables assessed in our study encompassed parameters such as age, body mass index (BMI), breast cancer type, tumor grade, ER status, HER2 status, residual tumor, treatment sequence, relapse, presence of metastasis at diagnosis, decease, and decease related to breast cancer. In these cases, we only looked for overview tendencies, without performing any significance tests.

We initially thought of comparing all these mentioned variables with the response variable, which was categorized into 3 main groups: partial response (PR), stable disease (SD), and complete response (CR) (Experimental models in Methods). Among the 83 analyzed patients, 91% were classified as PR, 7% as SD, and 1% as CR. This distribution, with the majority of samples falling into one category, rendered the analysis non-viable since there were no significant differences discernible. Consequently, we decided to use the Ki67-fold change (the ratio between the levels of Ki67 at surgery vs. baseline) as a proxy for measuring treatment response. The Ki67-fold change can vary from 0 to very high values. A value below 1 indicates that the Ki67 levels at baseline were higher than at surgery, meaning a successful treatment. Conversely, a value greater than 1 suggests that the Ki67 levels at surgery were higher than at baseline, indicating treatment ineffectiveness. Out of the initial 100 enrolled patients, 82 of them had non-null values in the Ki67-fold change and 18 of them had a null in either the Ki67 levels at baseline or at surgery. Additionally, each variable had some patient with null values, consequently, these patients were not plotted and, thus, each plot could have a different number of samples.

To evaluate Ki67-fold change as a marker of treatment response, we plotted the Ki67-fold change against the 3 response categories. In this graph, there are 2 Y-axis, one corresponding to the Ki67-fold change, as a measurement of response to the treatment, and the other one corresponds to the percentage that each group represents among total population for the assessed variable. In the X-axis, the different response categories are stated (Figure 17). The results showed that patients with a PR response had an average Ki67-fold change of 0.4, while the SD group had a Ki67-fold change of 0.6, and the CR group had a fold change of 0. These findings strongly suggest that the Ki67-fold change could serve as a valuable metric for more precisely assessing patient responses to the treatment.

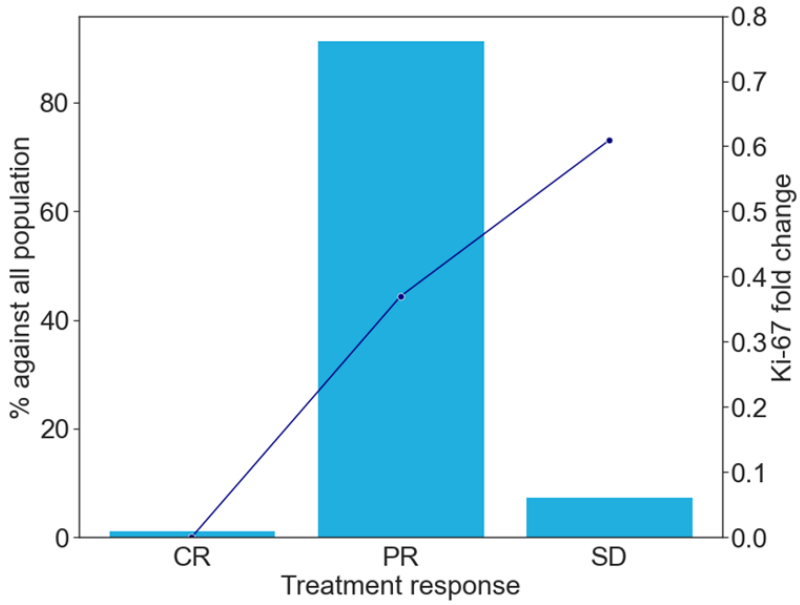

Figure 17. NeoLetExe classification of treatment response in comparison to Ki67-fold change. Bar plot of treatment response categorized in partial response (PR), stable disease (SD), and complete response (CR) plotted with Ki67-fold change as a line plot. A correlation between the Ki67-fold change and the treatment response can be observed. The total number of plotted patients is 81.

Subsequently, we continued the analysis focusing on assessing several patient characteristics. When looking at age, as it was a continuous variable, we categorized it. Indeed, age was divided into 4 categories: patients under 60 years old, those between 60 and 80 years old, between 80 and 90 years old, and over 90 years old. The relationship between Ki67-fold change and age showed a relatively constant fold change for patients under 90 years old, with a notable increase for those older than 90. However, it is essential to note that the number of patients over 90 was reduced, and this increase may not be statistically representative (Figure 18 A). BMI, originally a continuous variable, was categorized into 3 groups: patients with a BMI below 25, between 25 and 30, and those with a BMI above 30. Ki67-fold change exhibited a clear downward tendency, with highest levels corresponding

to patients with lower BMI (0.5-fold change) and lower Ki67-fold change for those patients who had a BMI equal or higher than 30 (0.2-fold change). This could suggest that patients with a higher weight-to-height ratio tend to respond better to the treatment (Figure 18 B).

Regarding tumor grade, the majority of patients (55%) had a grade II tumor. Ki67-fold change did not show remarkable differences between grade I and grade II-III patients; in all cases, the fold change was below 0.5, indicating treatment effectiveness. However, grade III patients exhibited a poorer response to the treatment with a Ki67-fold change of 0.75 (Figure 18 C). Concerning breast cancer type, 70% of patients had non-special type (NST), with an average Ki67-fold change of 0.4. Infiltrating lobular carcinoma (ILC) patients accounted for 25% of the total and had a Ki67-fold change of 0.36. The treatment appeared to be effective in all breast cancer types, with Ki67-fold change consistently below 0.5. Nevertheless, the "other" category, which included underrepresented cancer types like mucinous carcinoma (MUC-CA) and neuroendocrine carcinoma (SNEC), represented only 5% of the patients, and its apparent effectiveness may not be representative due to the small number of patients (Figure 18 D).

Regarding the estrogen receptor (ER) status, most patients (73%) expressed between 90-100% of ER, indicating that breast cancer patients were ER-positive. There was a slight decrease in Ki67-fold change levels between patient with 50%-90% of ER and 100% of ER, but it may not be enough to state that there is an influence in treatment effectiveness. Additionally, it can be appreciated how patients with less than 50% ER expression had a much higher Ki67-fold change level. Yet, due to the small number of patients, this trend may not be representative (Figure 18 E). For HER2 immunohistochemistry (IHC) staining status, all patients were considered HER2-negative, categorized into 3 main groups based on IHC results: 0, 1+, or 2+. Ki67-fold change was consistently below one in all cases. However, patients with higher levels of IHC HER2 (2+) appeared to exhibit a more significant reduction in Ki67 than those with lower levels of IHC HER2 (0) (Figure 18 F).

The variable of metastasis at diagnosis revealed that 93% of patients did not have metastasis at the time of breast cancer diagnosis, while 7% were already diagnosed with metastasis. Patients without metastasis responded better, showing a lower Ki67-fold change compared to the group with metastasis. Nonetheless, in both cases, Ki67-fold change remained below 1, indicating treatment effectiveness (Figure 18 G). Finally, the treatment sequence was assessed to determine if patients receiving one sequence of aromatase inhibitor

or the other could have any impact on the effectiveness of the treatment. Surprisingly, the results suggested that patients in the Exe-Let branch exhibited a better response, as indicated by a lower Ki67-fold change. Despite in both branches Ki67-fold change remained below 1, for the Exe-Let branch the Ki67-fold change was equal to 0.38 and for the Let-Exe branch was equal to 0.54 (Figure 18 H). Of the patients, 51% belonged to the Let-Exe branch, and 49% to the Exe-Let branch of the clinical trial. Overall, these findings shed light on the relationship between these patient characteristics and the Ki67-fold change in response to the treatment.

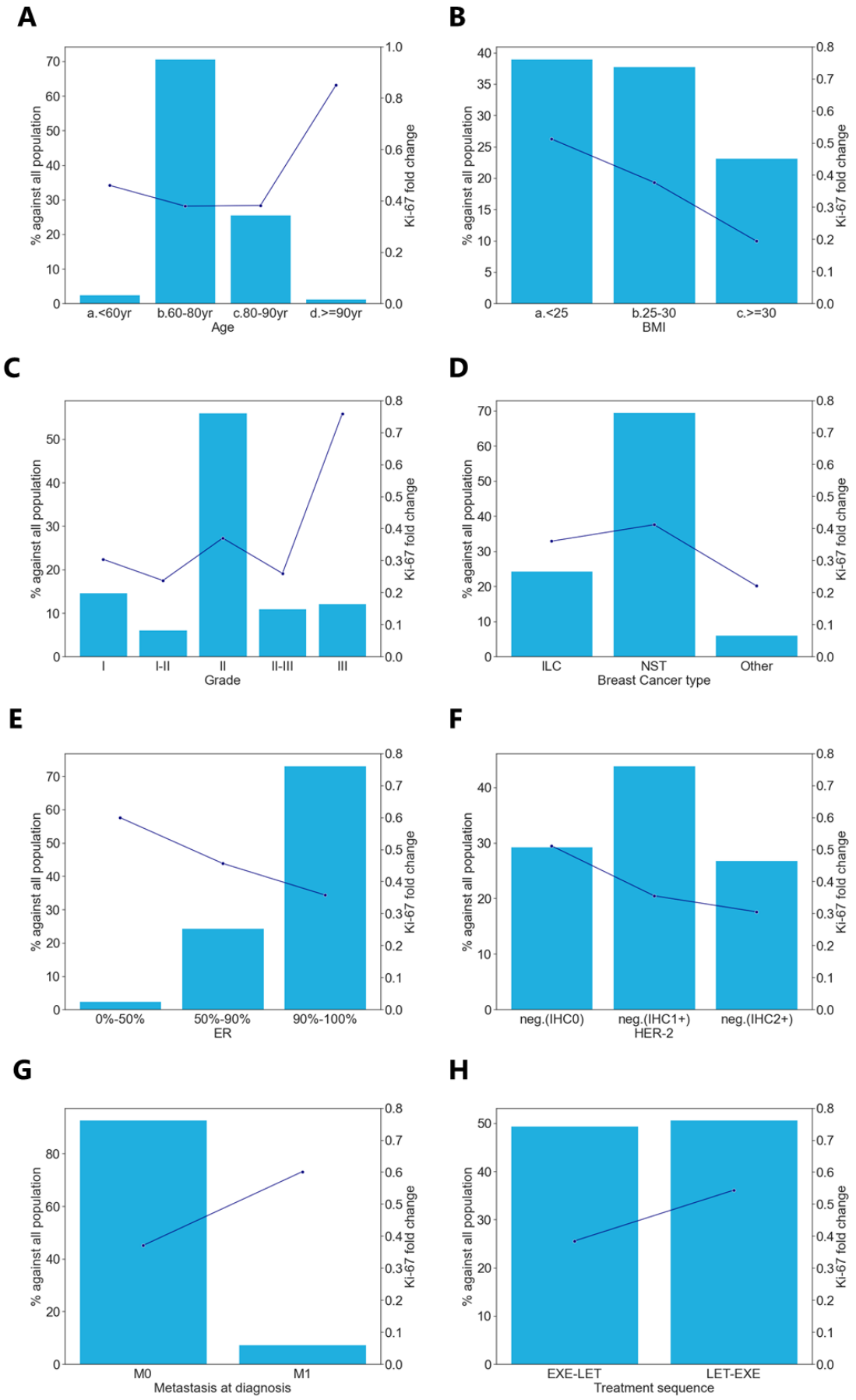
A
% against all population
Ki-67 fold change
a.<60yr
b.60-80yr
c.80-90yr
d.>=90yr
Age
B
a.<25
b.25-30
c.>=30
BMI
C
I
I-II
II
II-III
III
Grade
D
ILC
NST
Other
Breast Cancer type
E
0%-50%
50%-90%
90%-100%
ER
F
neg.(IHC0)
neg.(IHC1+)
neg.(IHC2+)
HER-2
G
M0
M1
Metastasis at diagnosis
H
EXE-LET
LET-EXE
Treatment sequence

Figure 18. Features of the NeoLetExe clinical trial plotted in correlation with Ki67-fold change. **(A)** Bar plot of patient age distribution reveals a relatively consistent fold change in individuals under 90 years old, but a noticeable increase in patients older than 90 (82 plotted patients). **(B)** BMI in relation to Ki67-fold change demonstrates a constant downward tendency for Ki67-fold change with highest values corresponding to patients with lower BMI (82 plotted patients). **(C)** Tumor grade bar plot with Ki67-fold change line plot shows no remarkable change between grade I and grade II-III patients (0.3-0.4), while grade III patients exhibit a poorer response to treatment with a Ki67-fold change of 0.75 (82 patients plotted). **(D)** Tumor type bar plot with Ki67-fold change line plot indicates a lower Ki67-fold change for infiltrating lobular carcinoma (ILC) patients compared to non-special type (NST) patients. The other category may not be representative due to the small number of patients (82 patients plotted). **(E)** ER status bar plot with Ki67-fold change line plot suggests a lower fold change in patients with more than 50% ER expression compared to those with less than 50% ER (82 patients plotted). **(F)** HER2 status bar plot with Ki67-fold change line plot indicates that all patients were classified as HER2 negative and exhibited a fold change ranging from 0.3 to 0.5 (82 patients plotted). **(G)** Patients with metastasis at the time of diagnosis bar plot with Ki67-fold change line plot reveals that patients without metastasis showed a lower Ki67-fold change compared to the group with metastasis (82 patients plotted). **(H)** Treatment sequence bar plot with Ki67-fold change line plot shows that patients in the Exe-Let branch exhibited a lower Ki67-fold change (0.38) compared to the Let-Exe branch (0.54) (82 patients plotted).

In this initial data exploratory analysis, we have delved into the general patient characteristics. Subsequently, our investigation was centered on factors associated with treatment effectiveness and patient response. When we examined cases where patients had deceased and, their causes of death, it was evident that 81% of patients remained alive during the evaluation period, while 19% passed away. Notably, an analysis of the Ki67-fold change revealed that patients who were alive had lower Ki67-fold change (0.38) whereas deceased patients exhibited slightly higher Ki67-fold change values (0.43), suggesting that the treatment had been less effective in these cases (Figure 19 A). Among the deceased patients, we categorized them based on whether their cause of death was related to breast cancer or not. Among those who passed away for reasons unrelated to breast cancer (85% among deceased patients), they had relatively low Ki67-fold change values, with an average of 0.32. This indicated that the treatment had proven effective in these patients. Conversely, in patients whose cause of death was directly tied to breast cancer, the Ki67-fold change exhibited a higher average of 0.9, highlighting the ineffectiveness of the treatment in these cases. These findings underscore the efficacy of Ki67-fold change as a precise metric for monitoring patient response to treatment (Figure 19 B).

Moving on to the assessment of residual tumors following the NeoLetExe clinical trial, we observed that over 80% of patients exhibited either small (10-50%) or large (>50%) residual tumors. It seems that there is an increase in Ki67-fold change levels as the fraction of residual tumor increases. These results suggest a direct correlation between the Ki67-fold change and the effectiveness of the treatment, evaluated as % of residual tumor (Figure 19 C).

Finally, our analysis extended to breast cancer relapse. Among the patients assessed, 90% did not experience breast cancer relapse within the assessment period, while 10% did. Examining the Ki67-fold change, a clear distinction emerged. Patients without relapse had an average Ki67-fold change of 0.33. Conversely, patients who experienced relapses exhibited a markedly higher average Ki67-fold change of 0.85 (Figure 19 D). These findings further underscore the role of Ki67-fold change as a precise and reliable measure for monitoring patient responses to treatment.

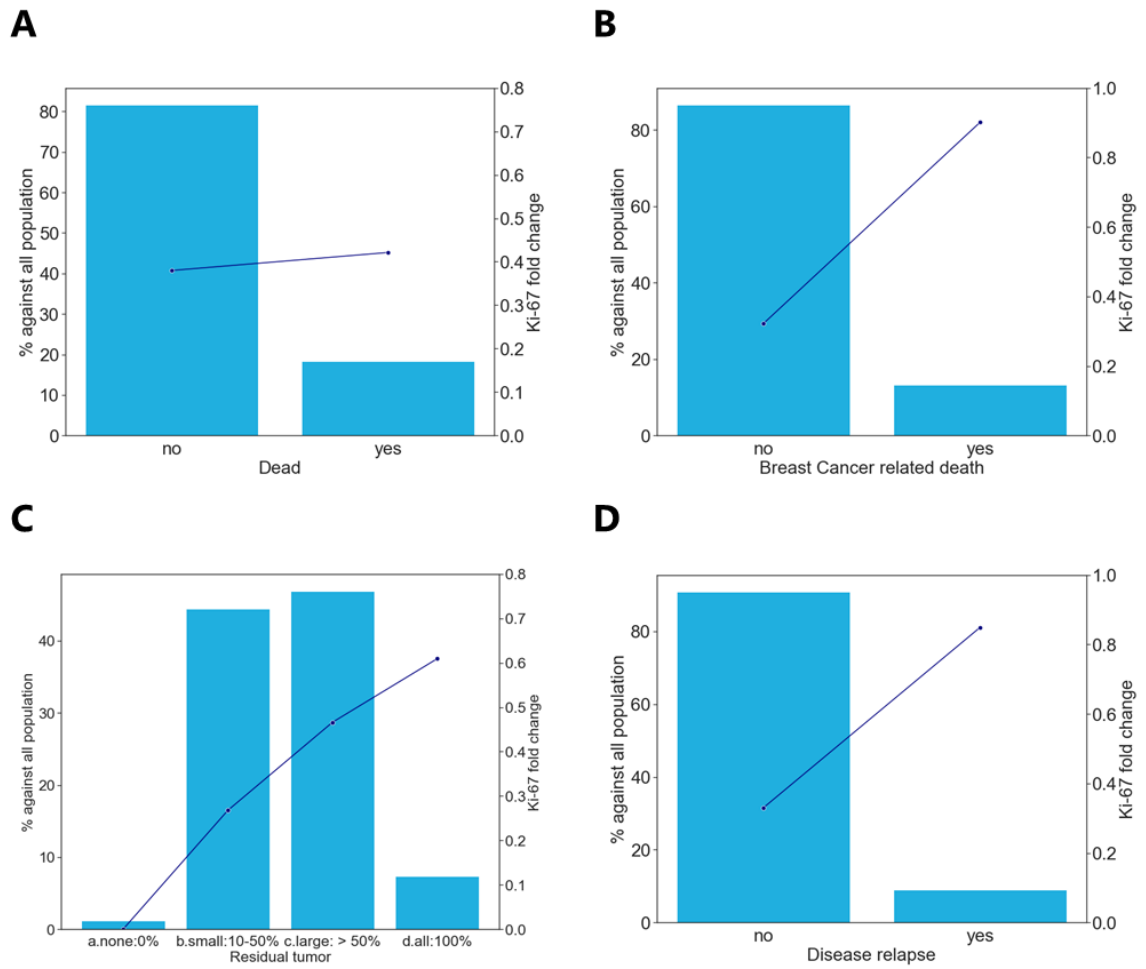

Figure 19. NeoLetExe patients' response to the treatment in correlation with Ki67-fold change. **(A)** The comparison of survival outcomes against Ki67-fold change reveals a lower Ki67-fold change (0.38) in surviving patients and higher values (0.43) in deceased patients (82 plotted patients). **(B)** Bar plot of patients with breast cancer-related deaths have a higher Ki67-fold change (0.9) compared to those who passed away due to unrelated causes, showing a Ki67-fold change of 0.32 (15 plotted patients). **(C)** Bar plot of the percentage of residual tumor with Ki67-fold change line plot, demonstrating a direct correlation between lower % of residual tumors and lower Ki67-fold change values. Higher residual tumor percentages correlate with higher Ki67-fold change values (81 patients plotted). **(D)** Bar plot and line plot illustrating the association between patient relapse and Ki67-fold change. Patients without relapse exhibit a lower Ki67-fold change (0.33), whereas those experiencing relapses show higher Ki67-fold change values (0.85) (77 plotted patients).

These findings suggest that the Ki67-fold change serves as a valuable metric for evaluating patients' response to treatment. Notably, a low Ki67-fold change, which suggest treatment effectiveness, is associated with patients in the age group of 80-90 years. Additionally, patients with a BMI over 30, patients with low-grade tumors, and patients diagnosed with ILC breast cancer tend to exhibit a lower Ki67-fold change. Furthermore, patients displaying high expression of ER and negative expression of HER2 (IHC2+) also show a favorable correlation with low Ki67-fold change. Importantly, patients without metastasis exhibit similar characteristics in their response.

Remarkably, the data exploration highlights that the sequential administration of exemestane followed by letrozole treatment (Exe-Let) yields superior clinical outcomes in the NeoLetExe patients' cohort compared to the letrozole-exemestane regimen (Let-Exe). This enhanced response, validated by a substantial reduction in Ki67 levels, underscores the efficacy of Exe-Let sequence in reducing Ki67 compared to Let-Exe sequence. Furthermore, a low Ki67-fold change is consistently observed in patients with minimal, or no, residual tumors. Patients who do not experience disease relapse also demonstrate a low Ki67-fold change.

1.2. The first 30 patients from the NeoLetExe cohort are a representative subset of the overall NeoLetExe clinical trial cohort

Our initial analysis included all patients for whom we had data in the NeoLetExe clinical trial. However, for the subsequent *in vitro* experiments, we exclusively used samples obtained from the first 30 patients. Thus, our first step involved reevaluating the characteristics of these 30 patients to confirm that the trends observed in the larger patient cohort were similar in this subset. This was undertaken to ensure the representativeness of our patient subset from the NeoLetExe clinical trial. It is worth noting that out of these 30 patients, data analysis was conducted on 25 due to missing data in the Ki67 levels or patient withdrawal.

In terms of patient age, these patients were categorized into 2 primary groups: the 60-80 age group (65%) and the 80-90 age group (35%). Notably, the analysis revealed that Ki67-fold change slightly diminished as age increases. (Figure 20 A). Importantly, this decreasing trend was also evident in the overall cohort. Regarding BMI, patients in this subset spanned into 3 categories: <25, between 25-30 and >30. The overall trend is steady going downwards

with patients with a BMI exceeding 30, having the lowest fold change (Figure 20 B). This same pattern was also observed in the full cohort.

When considering tumor grade in this cohort, we had patients with grade I (23%) and grade II (77%). Ki67-fold change increased with higher tumor grades (Figure 20 C). Once again, the same pattern observed in the entire NeoLetExe cohort was reflected in this subset of patients. Regarding breast cancer type, patients in this subset encompassed all three types: ILC (25%), NST (70%), and other (5%). Patients with NST exhibited a higher Ki67-fold change compared to those with ILC breast cancer type (Figure 20 D). The same trend observed in the complete cohort remained consistent in this smaller group.

For the ER status, all 30 patients had ER expression levels ranging between 50-90% or between 90-100%. Notably, Ki67-fold change showed no variance between these groups, suggesting that ER status did not substantially affect the Ki67-fold change following AI treatment (Figure 20 E). In the overall cohort, there was a slight decrease in Ki67-fold change levels for the patients with 90-100% ER expression levels, which is not visible in this subgroup. In terms of HER2 status, all patients in this subset were categorized as HER2-negative but exhibited varying levels of HER2 staining via IHC. The analysis indicated that patients with higher HER2 staining seemed to respond more favorably to treatment, with lower Ki67-fold changes (Figure 20 F). This trend was also consistent with observations from the complete cohort.

In the context of the metastasis at diagnosis, patients with metastasis displayed higher Ki67-fold changes, exceeding 1 (Figure 20 G). These results go in line with the results observed in the whole cohort. Finally, patients treated with exemestane followed by letrozole exhibited an average Ki67-fold change of 0.32, while patients treated with letrozole followed by exemestane had an average Ki67-fold change of 0.84 (Figure 20 H). This pattern was also observed in the entire NeoLetExe cohort, reinforcing the notion that the Exe-Let treatment regimen had the most significant impact in reducing Ki67-fold change, suggesting a more effective treatment approach.

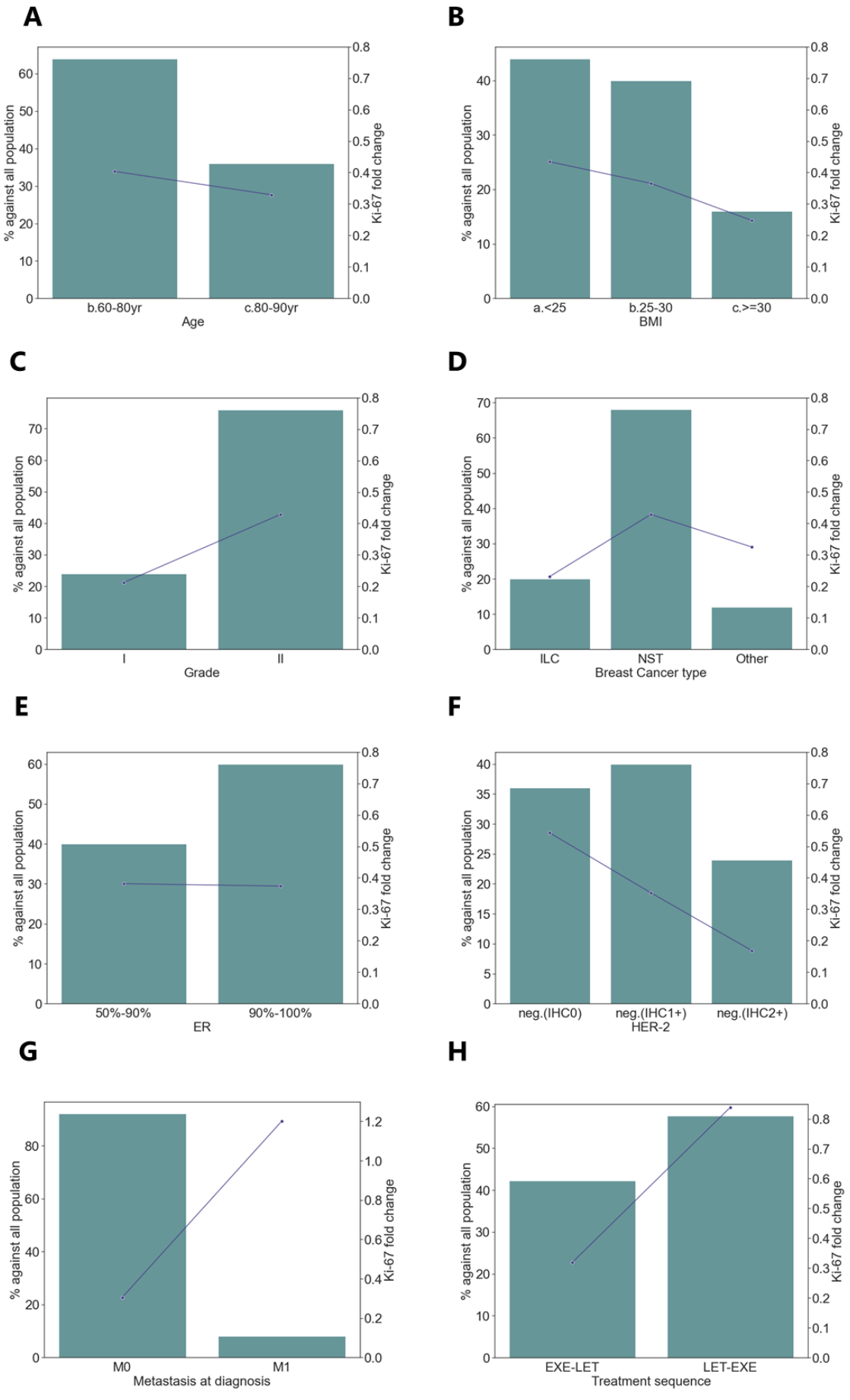
A
% against all population
Ki-67 fold change
b.60-80yr
c.80-90yr
Age
B
% against all population
Ki-67 fold change
a.<25
b.25-30
c.>=30
BMI
C
% against all population
Ki-67 fold change
I
II
Grade
D
% against all population
Ki-67 fold change
ILC
NST
Other
Breast Cancer type
E
% against all population
Ki-67 fold change
50%-90%
90%-100%
ER
F
% against all population
Ki-67 fold change
neg.(IHC0)
neg.(IHC1+)
neg.(IHC2+)
HER-2
G
% against all population
Ki-67 fold change
M0
M1
Metastasis at diagnosis
H
% against all population
Ki-67 fold change
EXE-LET
LET-EXE
Treatment sequence

Figure 20. Features of the NeoLetExe 30 patient cohort plotted in correlation with Ki67-fold change. (A) Bar plot of patient age distribution reveals Ki67-fold change slightly diminished in the 80-90 years-old cohort with respect to the 60-80 years-old group (25 patients plotted). **(B)** BMI in relation to Ki67-fold change demonstrates a downward tendency, with patients with a BMI over 30 having the lowest Ki67-fold change at 0.25 (25 patients plotted). **(C)** Tumor grade bar plot with Ki67-fold change line plot show that patients with grade I tumors have a lower Ki67-fold change level (0.2) than those with grade II tumors (0.43) (25 patients plotted). **(D)** Tumor type bar plot with Ki67-fold change line plot indicates a lower Ki67-fold change for infiltrating lobular carcinoma (ILC) patients compared to non-special type (NST) patients (25 patients plotted). **(E)** ER status bar plot with Ki67-fold change line plot suggests a similar Ki67-fold change level for patients with 50-90% ER expression than those with 90-100% (25 patients plotted). **(F)** HER2 status bar plot with Ki67-fold change line plot exhibits a steady downward trend, with patients with higher HER2 (IHC2+) having the lowest fold change (25 patients plotted). **(G)** Patients with metastasis at the time of diagnosis plotted against Ki67-fold change reveals that patients without metastasis showed a lower Ki67-fold change compared to the group with metastasis (25 patients plotted). **(H)** Treatment sequence plotted against Ki67-fold change suggests that patients in the Exe-Let branch exhibited a lower Ki67-fold change (0.32) compared to the Let-Exe branch (0.84) (25 patients plotted).

In this cohort, deceased patients had higher Ki67-fold changes. Notably, among those who died due to breast cancer, the average Ki67-fold change was approximately 1.4. These findings suggest that the treatment may not have been effective in those patients. Additionally, these results show the potential of Ki67-fold change as a valuable parameter for evaluating patient response (Figure 21 A and B). This trend was consistent with the whole NeoLetExe cohort. Regarding the residual tumor parameter, the 30 patients in this cohort were primarily categorized into 3 groups: small, large and 100% of residual tumor. Results showed that patients with small (10-50%) and large (>50%) residual tumors exhibited similar Ki67-fold changes, with the large category having slightly higher values (Figure 21 C). However, the 100% of residual tumor group showed a considerably lower Ki67-fold change; opposed to the whole patient cohort. This might be due to the fact that this group is only composed by 2 patients and its values could not be representative. Lastly, when assessing patient's relapse, it becomes evident that patients who experienced a relapse had notably higher Ki67-fold changes, averaging around 1.4 (Figure 21 D). These results align with the patterns observed in the complete NeoLetExe cohort of patients.

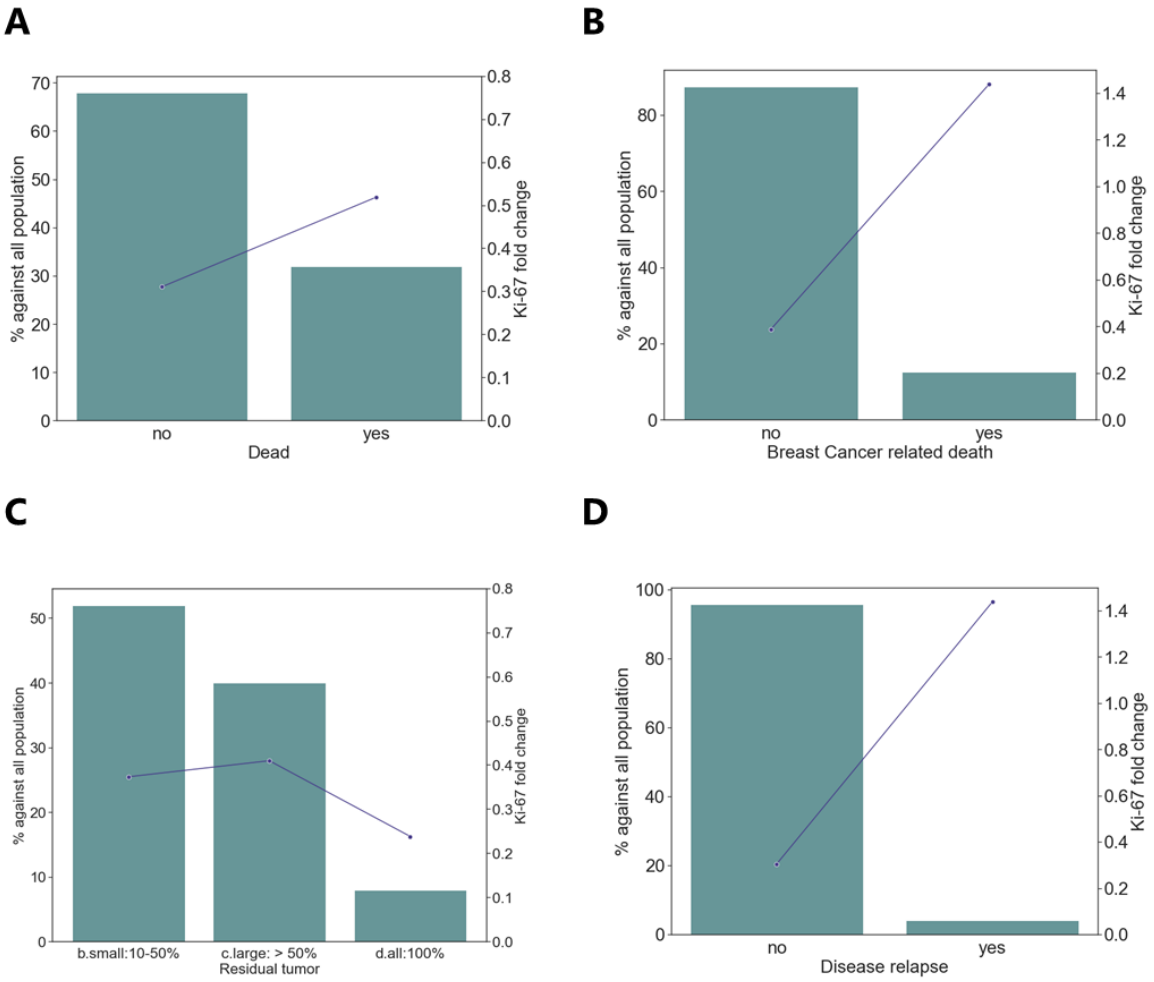

Figure 21. NeoLetExe 30 patient cohort response to the treatment in correlation with Ki67-fold change. **(A)** The comparison of survival outcomes against Ki67-fold change reveals a lower Ki67-fold change (0.33) in surviving patients and higher values (0.53) in deceased patients (25 plotted patients). **(B)** Bar plot of patients with breast cancer-related deaths have a higher Ki67-fold change (1.4) compared to those who passed away due to unrelated causes, showing a Ki67-fold change of 0.40 (8 plotted patients). **(C)** Bar plot of the percentage of residual tumor with Ki67-fold change line plot showing a stable trend between the small and large group and a fall in the full tumor group. However, this group is only composed by two patients (25 patients plotted). **(D)** Bar plot and line plot illustrating the association between patient relapse and Ki67-fold change. Patients without relapse exhibit a lower Ki67-fold change (0.35), whereas those experiencing relapse show higher Ki67-fold change values (1.4) (24 plotted patients).

These findings suggest that the initial 30 patients can serve as a representative sample cohort for the NeoLetExe clinical trial, potentially functioning as a pilot group.

1.3. Biochemical data analysis confirmed that exemestane exhibits aromatase inhibition by lowering estrogen levels similarly to letrozole

In order to understand why patients who received exemestane as their initial treatment responded better to the therapy, we explored the possibility that exemestane might be more effective due to its ability of inhibiting aromatase activity. To investigate this, we analyzed the estrogen (E2) levels in these patients. We had access to biochemical data derived from serum samples collected at 3 timepoints: baseline, 2 months, and 4 months. Our initial aim was to evaluate how well exemestane reduced the levels of circulating estrogen in these patients compared to letrozole over time. To accomplish this, we plotted the average estrogen levels in the bloodstream over the 3 timepoints for the 2 treatment groups (Exe-Let and Let-Exe) (Figure 22). The results revealed a reduction in estrogen levels between the baseline and the 2-month timepoints and this trend was observed in both treatment groups. At 4-month, after the treatment switch, estrogen levels remained relatively stable and low. Interestingly, although patients assigned to the Let-Exe group seemed to initially have higher E2 levels at baseline, they achieved similar levels to those in the Exe-Let group at both, the 2-month and 4-month, timepoints. These results strongly indicate that both letrozole and exemestane are highly efficient in inhibiting aromatase activity within this patient cohort.

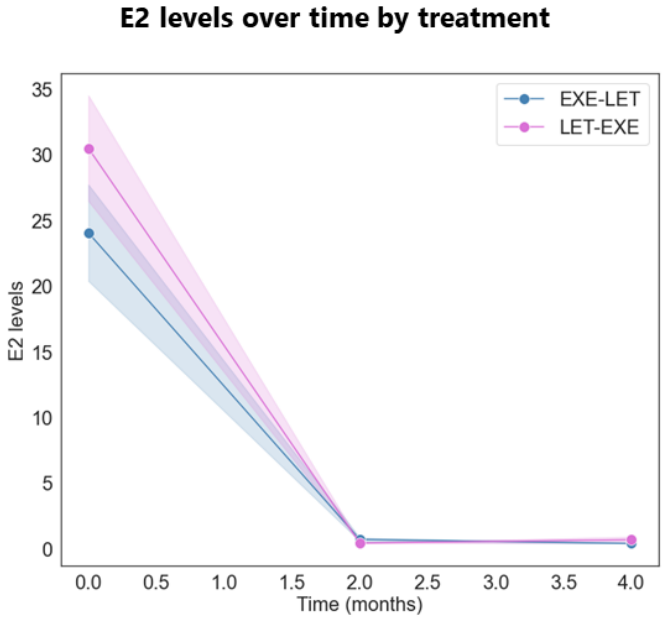

Figure 22. Comparable aromatase inhibition between exemestane and letrozole, resulting in decreased estrogen levels. E2 levels are presented as the mean ± standard error (SE) (Let-Exe n=48 patients; Exe-Let n=42 patients). The Exe-Let treatment sequence is depicted in blue, while the Let-Exe treatment sequence is represented in pink. The findings demonstrate a consistent reduction in E2 levels at both 2 months and 4 months for both treatment sequences.

Interestingly, these results also challenge our initial hypothesis that the distinction between these 2 drugs lays in their aromatase inhibitory activity. This suggests that exemestane may be operating through an alternative mechanism, distinct from aromatase inhibition, to achieve superior clinical outcomes compared to letrozole.

1.4. The exemestane and the 17-HEXE bloodstream levels are not identical in all patients

After realizing that clinical variances between the two treatment sequences were not attributable to their capacity to inhibit aromatase, we formulated a new hypothesis based on previous literature findings. These studies suggested that the primary mechanism of action of exemestane may be due to its active metabolite, 17β-hydroxyexemestane (17-HEXE), through AR activation [220]. To prove this hypothesis, we proceeded to analyze the NeoLetExe biochemical data provided by our collaborator Prof. Geisler. Our aim was to examine the presence of exemestane and its metabolite, 17-HEXE, in the bloodstream of these patients to check if exemestane was being metabolized. We explored the levels of Exe and 17-HEXE at 2 months for patients treated with Exe-Let sequence and at 4 months for those on Let-Exe sequence. Patients numbered from 6 to 40 were included in this analysis, but if any patient was omitted, it was due to either missing data or patient withdrawal.

For Exe-Let patients, we created a graphical representation showing the levels of both Exe and 17-HEXE in the bloodstream at 2 months of treatment for a total of 14 patients (Figure 23 A). When examining the levels of exemestane, we observed variability, ranging from 2000 to 37000, indicating notable differences in drug levels among patients. These results underscore the potential variations in exemestane metabolism. In terms of 17-HEXE, we also noticed some variability, with levels ranging from nearly 350 to almost 4000. These results also suggest that exemestane is being metabolized into 17-HEXE, to a different extent.

Additionally, we graphically represented the levels of both, exemestane and 17-HEXE, in the blood samples of Let-Exe patients after 4 months of treatment, involving a total of 16 patients (Figure 23 B). An examination of the exemestane levels revealed substantial variability, ranging from 2000 to 91000. These findings emphasize the presence of significant interpatient differences in exemestane metabolism. Furthermore, when analyzing the levels of 17-HEXE, we also observed variability, with levels spanning from nearly 400

to almost 7000. These observations indicate varying degrees of exemestane metabolism into 17-HEXE among the patients.

Our results confirmed that exemestane undergoes metabolism to produce 17-HEXE in patients. However, they also highlight that the levels of exemestane in the bloodstream exhibit considerable variation among patients, irrespectively of whether they received the Exe-Let or Let-Exe treatment sequence.

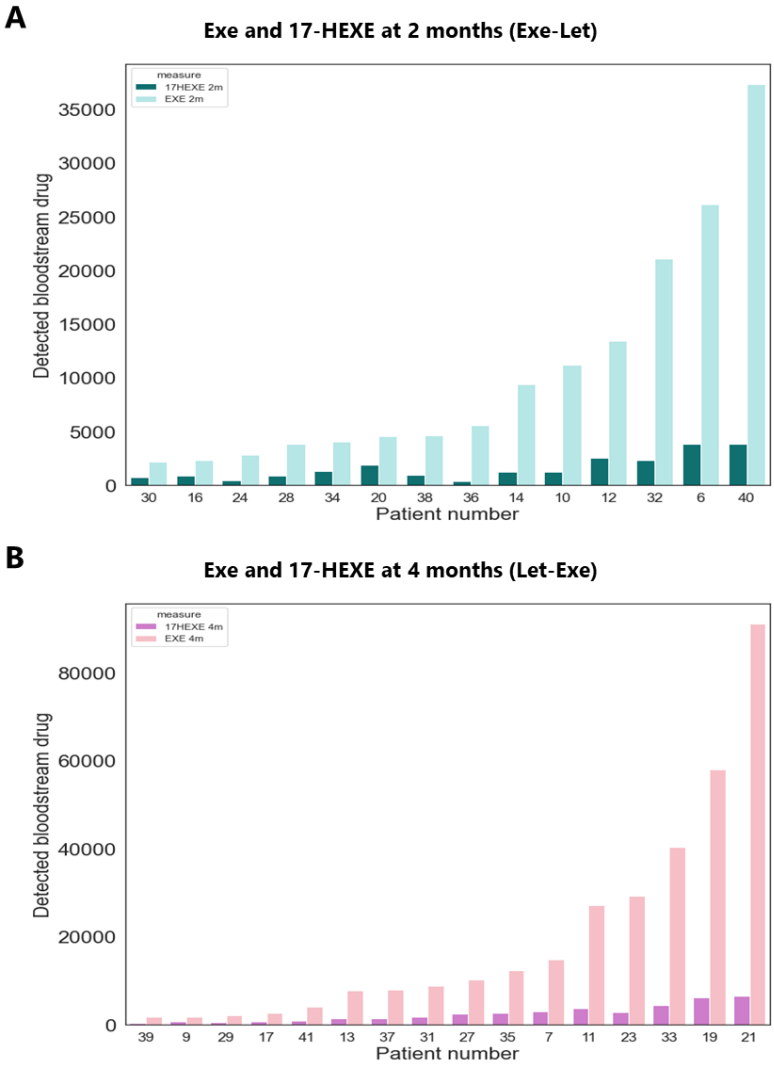

Figure 23. Diverse metabolism of exemestane into 17-HEXE among NeoLetExe patients. **(A)** Bar plot sorted in ascending order of the levels of exemestane (light blue). Levels of 17-HEXE also plotted for each patient (dark blue). Both magnitudes were assessed at the 2-month mark of treatment for 14 patients (Exe-Let). Exemestane levels exhibited a broad range from 2000 to 37000, underscoring interpatient differences. Similarly, 17-HEXE levels ranged from 350 to almost 4000, suggesting substantial heterogeneity in metabolism. **(B)** Bar plot sorted in ascending order of the levels of exemestane (light pink). Levels of 17-HEXE also plotted for each patient (dark pink). Both magnitudes were assessed in Let-Exe patients' blood after 4 months of treatment, involving 16 patients. Exemestane levels at 4-months varied notably, ranging from 2000 to 91000. The levels of 17-HEXE also displayed variability, ranging from nearly 400 to almost 7000. These findings underscore the varying extent of exemestane metabolism into 17-HEXE among patients, regardless of the treatment sequence.

2. Exemestane and 17-HEXE interact with AR and might be responsible for the enhanced clinical response to exemestane in certain patients

2.1. Our cellular model efficacy in emitting bioluminescence upon nuclear receptor activation was validated

In our study, we aimed to determine whether 17-HEXE or exemestane, both present in patients' serum, could interact with the androgen receptor (AR). Our research encompassed patients from both treatment branches: Exe-Let and Let-Exe. We employed serum samples collected at different timepoints, which included the baseline, as well as at 2 months and 4 months after treatment initiation. To assess the potential binding of exemestane or 17-HEXE to AR, we utilized a previously established cellular model developed in our laboratory and performed a luciferase assay with the serum samples [221].

The cellular model consists of MCF7 cells that were previously modified with a reporter cassette, which contains the TFF1 promoter positioned upstream of the luciferase expression. From now on, this cell line will be referred to as MCF7-Luc. Previous research established that, certain nuclear receptors including the ER and AR, exhibited affinity for this reporter cassette and could bind to it. In this cellular model, the presence of steroids like estrogen leads to the activation of the nuclear receptor, resulting in its binding to the reporter cassette (TFF1 promoter). As a consequence, this activation is translated into the emission of bioluminescence through luciferase activity (Figure 24 A). Conversely, if steroids are reduced, for example, by AIs, fewer nuclear receptors could activate and bound to the reporter cassette (promoter), leading to a subsequent decrease in bioluminescence (Figure 24 B).

We first aimed to confirm the proper functionality of the cellular model. For that, we initially examined the protein levels of AR and ER within these cells (Figure 24 C and D). Simultaneously, we evaluated the effect of fulvestrant (ER degrader) and bicalutamide (a competitive antagonist of the AR), on the MCF7-Luc cell line compared to the vehicle (DMSO). The protein analysis, carried out by western blot at 24 and 48 h, demonstrated that MCF7-Luc cells express both ER and AR. Our findings also indicated that while fulvestrant led to a reduction in ER protein levels, bicalutamide did not result in a decrease in AR protein levels.

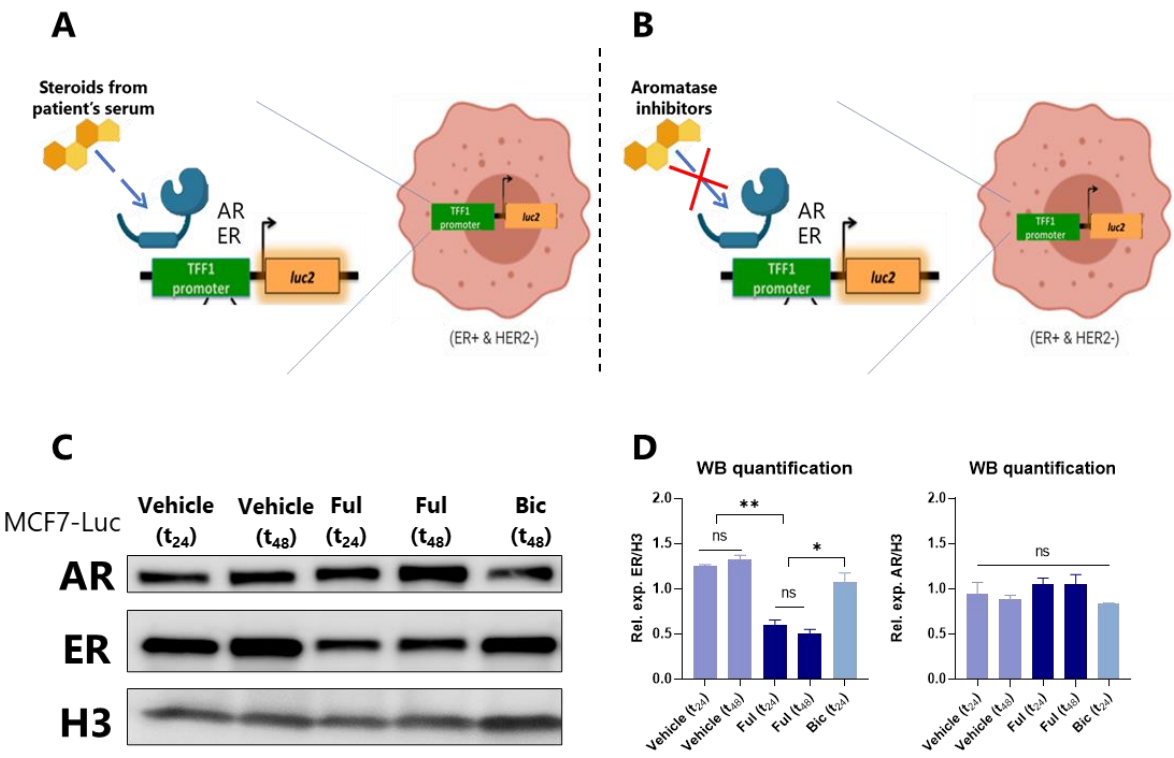

Figure 24. *In vitro* validation of the cellular model for detecting nuclear receptor activation via luciferase bioluminescence. **(A)** Schematic representation of our cellular model in the presence of steroids, leading to nuclear receptor activation and subsequent bioluminescence emission through luciferase activity. **(B)** Schematic representation of our cellular model with reduced steroids, resulting in a subsequent decrease in bioluminescence. **(C)** Confirmation of the impact of the vehicle (DMSO), fulvestrant (Ful), and bicalutamide (Bic) on AR and ER protein expression at 24 and 48 h post-treatment. Histone 3 (H3) served as a loading control. While fulvestrant reduced ER expression, bicalutamide did not lead to a decrease in AR expression. **(D)** Quantitative analysis of the western blot results presented in (C) (n=3). Data is presented as the mean ± standard error mean (SEM). Statistical significance was evaluated using a One-Way ANOVA multiple comparison test (Tukey's).

To evaluate the response of our cells to serum from patients, a luciferase assay was conducted. MCF7-Luc cells were cultured in DMEM medium supplemented with charcoal-stripped FBS (medium without hormones) for 3 days to eliminate all hormones from the medium and to ensure that the bioluminescence came exclusively from the serum of the patients. Subsequently, cells were exposed to serum collected at three different timepoints: baseline, after 2 months of treatment and after 4 months of treatment. The patient's serum was added at a concentration of 20%, and it was left for 48 h before measuring luciferase activity. After measuring the luciferase signal (luminometer), this was normalized to the absorbance of bovine serum albumin (BSA) (an indirect measurement of protein concentration). The selection of adding patient's serum at 20% was based on a dose-concentration optimization process (Figure 25). It was demonstrated that it existed a correlation between the percentage of serum and the luciferase signal. This analysis

concluded that 20% was an adequate serum concentration to observe an increase in the luciferase signal, because going from 20% to 50% of serum reported no notable differences in luciferase activity.

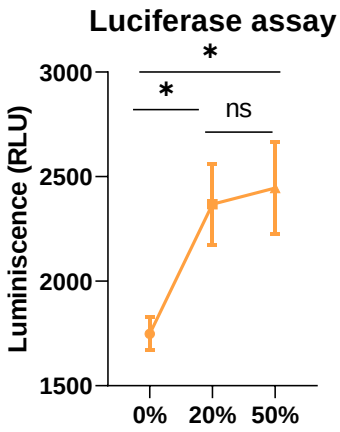

Figure 25. A dose-concentration optimization process to select patients % of serum. Comparative analysis of the luminescence in RLU (normalized with BSA) involved MCF7-Luc cells treated with baseline serum from 3 different patients at different %: 0, 20 and 50%. This revealed that a serum concentration of 20% was sufficient to notice an increase in the luciferase signal, because no significant variations in luciferase activity were observed when the serum concentration was increased to 50%. Data is presented as the mean ± SEM Statistical significance was evaluated using a One-Way ANOVA multiple comparison test (Tukey's)(3 patients and 3 replicates each).

2.2. Fulvestrant validated the MCF7-Luc cellular model by reducing the luciferase bioluminescence emission of patient serum upon fulvestrant administration

To further validate our cellular model, we conducted luciferase experiments using MCF7-Luc cells exposed to patient's serum collected at baseline point, and we simultaneously, treated the cells with either the drug vehicle (DMSO) or with 1µM of fulvestrant (an ER degrader). The results were visualized using a box plot comparing the normalized luminescence of the vehicle and fulvestrant-treated cells (Figure 26 A). Our findings revealed a significant reduction in the luciferase signal after fulvestrant treatment. The luciferase assay conducted on MCF7-Luc cells, clearly demonstrated reduced signal emission when exposed to fulvestrant, confirming the effectiveness of our cellular model. This reduction in the luciferase signal suggests the inhibitory effect of fulvestrant on ER levels.

In addition, we generated a heatmap to visualize the fold change in luminescence of baseline patient serum treated with fulvestrant compared to the luminescence of the control (vehicle condition). Patients who exhibited a substantial reduction in luminescence fold change when treated with fulvestrant compared to the control (vehicle) were colored in darker red. Conversely, patients with insignificant changes in their response to fulvestrant were depicted in lighter blue (P1). The fold change of the normalized vehicle against itself, which is consistently 1, is shown in blue (Figure 26 B). These findings highlight that in the majority of patients the luciferase signal experienced a remarkable decrease when fulvestrant was administered to the MCF7-Luc cells in conjunction with patient serum at baseline.

A

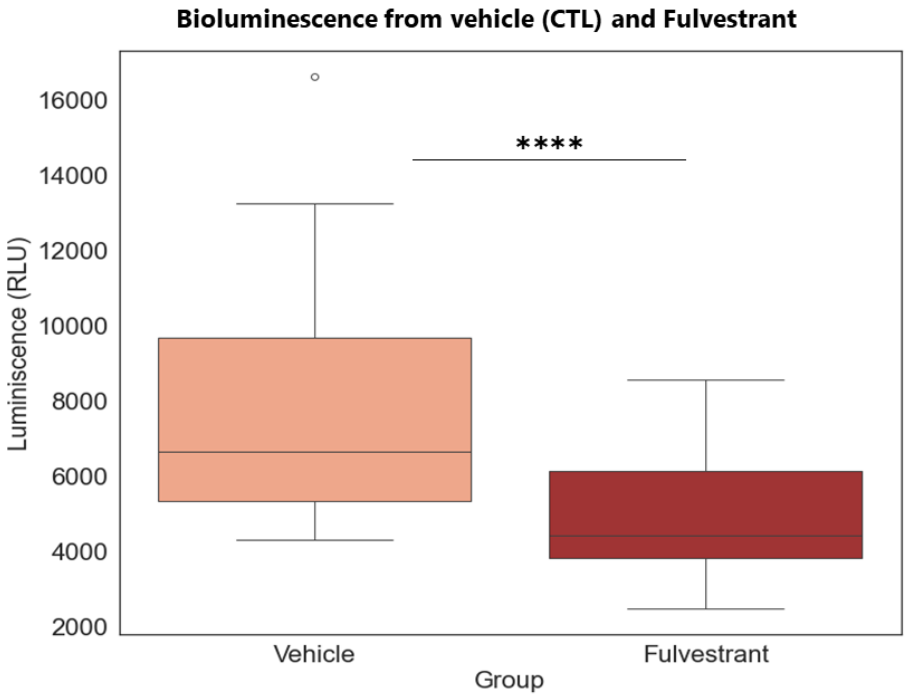

B

	P1	P2	P5	P6	P7	P8	P9	P10	P11	P12	P13	P14	P15	P16	P17	P18	P19	P20	P21	P23	P24	P27	P28	P29	P30
Vehicle	1,00	1,00	1,00	1,00	1,00	1,00	1,00	1,00	1,00	1,00	1,00	1,00	1,00	1,00	1,00	1,00	1,00	1,00	1,00	1,00	1,00	1,00	1,00	1,00	1,00
Fulvestrant	0,92	0,64	0,83	0,71	0,52	0,52	0,58	0,52	0,71	0,58	0,75	0,66	0,80	0,66	0,83	0,83	0,83	0,67	0,70	0,52	0,57	0,75	0,60	0,71	0,59

Figure 26. Validation of cellular model through reduction in luciferase bioluminescence emission upon fulvestrant administration. (A) Comparative box plot analysis of average luminescence in RLU (normalized with BSA) involved MCF7-Luc cells treated with baseline serum from patients along with, either the vehicle (DMSO) or fulvestrant at 1 µM. The box plot reveals a significant reduction in the luciferase signal following fulvestrant treatment. Statistical significance was assessed using a Student t-test (25 patients with 3 replicates for each one). **(B)** Heatmap representing fold change in luminescence of patient serum under fulvestrant treatment visually depicts the fold change in luminescence in comparison to the luminescence of the control (vehicle condition). Patients (P) with a substantial reduction in luminescence fold change are shown in darker red, while those with insignificant changes in response to fulvestrant are depicted in lighter blue. The fold change of the normalized vehicle against itself, consistently 1, is represented in blue.

2.3. Our cellular model validated that 17-HEXE from serum patients might be binding to AR

After validating our cellular model, we conducted an experiment using serum samples collected from patients when treated with exemestane, either at 2 or 4 months. In this study, we introduced bicalutamide (1 µM), which acts as a competitive antagonist of the AR. This assay was performed to indirectly explore the activation of AR by either exemestane or its metabolite, 17-HEXE, both present in the serum of patients and both having affinity to the AR. If the AR interacts with the reporter cassette located upstream of the luciferase reporter, it emits bioluminescence. If the addition of bicalutamide results in a more significant reduction, or increment, in the luciferase signal, compared to the control, it would imply that either exemestane or 17-HEXE had activated the AR. However, if no differences are observed after the administration of the bicalutamide, it suggests that neither exemestane nor 17-HEXE are binding to the AR.

We seeded MCF7-Luc cells and exposed them to patients' serum, and we also treated the cells with either the vehicle (DMSO) or bicalutamide at each timepoint. For every even patient ID, we examined the impact of exemestane at 2 months, while for odd patient IDs, we assessed it at 4 months. Subsequently, we calculated the fold change of the normalized luminescence when cells were treated with bicalutamide in conjunction with the serum, compared to luminescence when cells were treated with the control (vehicle) at each timepoint. Using these fold changes, we generated a heatmap to illustrate the effect of bicalutamide for each patient (Figure 27 A). In this heatmap, the fold changes that remarkably affected luciferase bioluminescence, either increasing it or decreasing it, were shown in darker red. Whereas patients that did not exhibit differences in their bioluminescence response when bicalutamide was introduced were depicted in lighter blue. Additionally, the fold change of the normalized vehicle control against itself, consistently equal to 1, is represented in blue.

These results revealed that among the 25 patients we analyzed, the patients with remarkable changes in the luciferase signal were: 2, 5, 9, 10, 12, 16, 17, 20, 21, 27, 28 and 30. The patents for whom their luciferase signal did not experience any remarkable change with the bicalutamide were: 1, 6, 7, 8, 11, 13, 14, 15, 18, 19, 23, 24 and 29. These results allowed us to categorize these patients into 2 groups based on if there is an effect when bicalutamide was added or not.

Subsequently, we evaluated if there was a correlation between bicalutamide's effect classification with the sequential treatment followed (Exe-Let vs Let-Exe). Our results revealed that, in the group of 12 patients who showed a response to bicalutamide, 7 of them were part of the Exe-Let treatment sequence, while 5 of them were part of the Let-Exe sequence. This suggests that the effectiveness of exemestane may not be related to the treatment sequence.

After these results, we decided to correlate the 2 identified group of patients according to bicalutamide's effect with the clinical outcome determined by magnetic resonance imaging (MRI) and other parameters (Methods section) provided by our collaborator Prof. Geisler (Figure 27 B). This assessment was conducted at various timepoints, including baseline, 2 months into the treatment, and 4 months. Following surgery, this data was classified to determine the overall response which was categorized into 3 primary groups: a reduction in tumor size within the range of 25% to 50%, a reduction of 50% to 90%, and a complete response. The reason for using this variable as a measure of the clinical response rather than the Ki67-fold change is because the Ki67-fold change is a continuous variable, and, for this experiment, we needed a categorical variable.

The results after correlating the clinical outcome with the effect of bicalutamide showed that, among the 12 patients who responded to bicalutamide, 7 showed an intermediate response (a 50-90% reduction in tumor size), 4 had a complete response, and 1 had a 25-50% reduction. In contrast, among the 13 patients classified as having no response to bicalutamide, 6 exhibited an intermediate response, 1 had a complete response, and 6 had a 25-50% reduction. These results revealed that a higher percentage of patients who exhibited a complete clinical response fell into the category of those showing an effect when bicalutamide was added. Conversely, patients classified as having no effect with bicalutamide, demonstrated a significant percentage of the individuals with poor clinical outcomes, characterized by only a 25-50% reduction. This suggests that patients classified as having a bicalutamide effect had a better response to the treatment.

Altogether, these findings led us to think that the differences between Exe-Let and Let-Exe might have been due to the exemestane itself rather than the sequence treatment. Additionally, these findings suggest that the activation of the AR, by 17-HEXE, or exemestane, could be associated with better clinical outcomes.

With this premise, we sought to study the correlation between the levels of exemestane or 17-HEXE and the effect of bicalutamide treatment. To do this, we plotted the levels of exemestane and 17-HEXE for each patient in ascending order of exemestane levels. The patients with light and dark red bars are those who responded to bicalutamide, indicated with "w/ Bicalutamide effect". The patients colored with light and dark blue are those who were categorized as no effect with the bicalutamide and are indicated as "w/o Bicalutamide effect" (Figure 27 C). Out of the 10 patients with the highest exemestane levels, 4 showed an effect with bicalutamide, while 6 did not. It appears that there is no clear correlation between high levels of exemestane, or 17-HEXE, and the effect of bicalutamide.

In the subsequent analysis, we aimed to investigate whether a correlation existed between the fold change in 17-HEXE and exemestane levels. We sought to determine if the ratio of exemestane metabolization into 17-HEXE was linked to the activation of the AR. For this purpose, we performed the 17-HEXE/EXE ratio for all patients and classified them according to the bicalutamide's effect. To do this, we plotted the ratio of 17-HEXE/EXE for each patient in descending order and colored the patients with bicalutamide effect in gold and the ones without an effect were colored in beige (Figure 27 D).

Interestingly, this examination revealed that, among the top 10 patients with a higher proportion of 17-HEXE relative to exemestane (ranging from 50% to 20%), 8 of them (80%) exhibited an effect when bicalutamide was added. In contrast, among the bottom 9 patients with a higher fraction of 17-HEXE (less than 20%), 7 of them (78%) did not respond to bicalutamide. These results suggest that patients with a higher fraction of 17-HEXE relative to exemestane, experienced a luminescence change upon bicalutamide administration. This seems to imply that either exemestane or 17-HEXE, from the serum of patients, could potentially bind to the AR. These findings also serve to further validate our cellular model, highlighting the luciferase assay's capability to detect the indirect activation of the AR. Furthermore, these results suggest the existence of a threshold, of approximately 20%, beyond which patients tend to exhibit a more favorable clinical response.

A

	P1	P2	P5	P6	P7	P8	P9	P10	P11	P12	P13	P14	P15	P16	P17	P18	P19	P20	P21	P23	P24	P27	P28	P29	P30
Vehicle	1,00	1,00	1,00	1,00	1,00	1,00	1,00	1,00	1,00	1,00	1,00	1,00	1,00	1,00	1,00	1,00	1,00	1,00	1,00	1,00	1,00	1,00	1,00	1,00	1,00
Bicalutamide	0,94	0,79	1,32	1,08	1,14	1,15	0,77	1,55	1,13	0,77	1,13	1,00	0,99	1,53	0,78	1,03	1,14	1,31	1,35	1,07	0,98	0,80	0,79	1,15	0,79

B

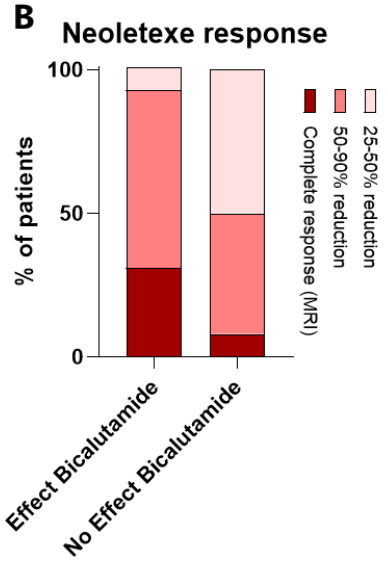

C

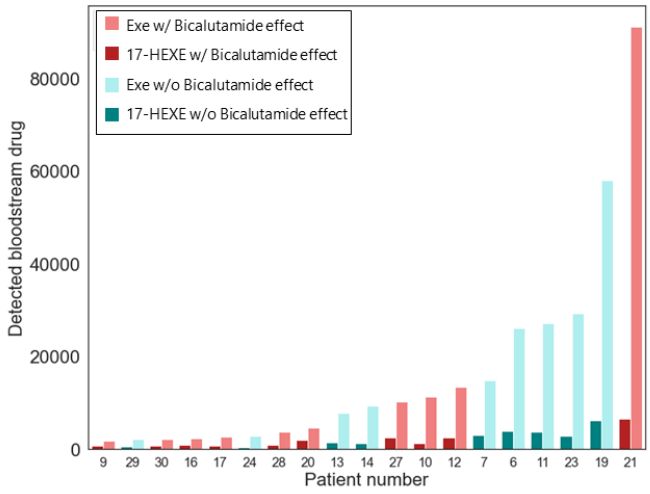

D

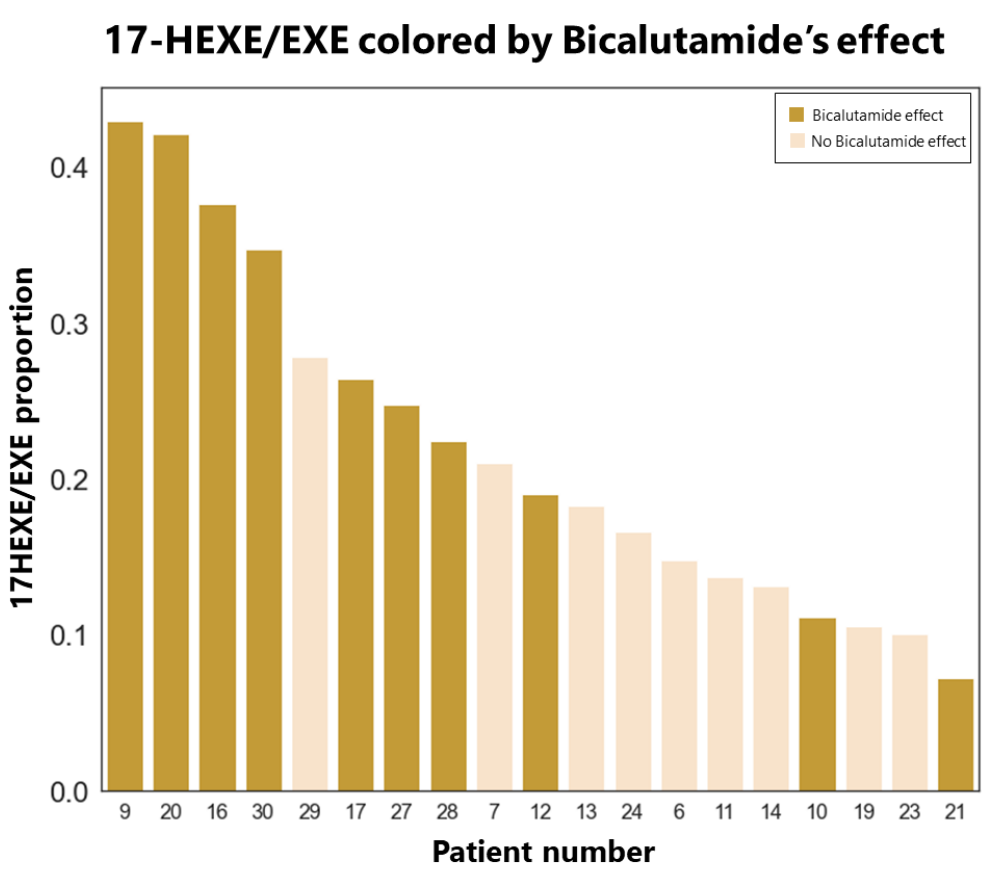

Figure 27. Changes in luciferase bioluminescence emission following the administration of bicalutamide indicates a potential binding of 17-HEXE from patients' serum to AR. **(A)** A heatmap depicting the fold change of normalized luminescence from patient's serum treated with bicalutamide compared to the control (vehicle condition). Patients exhibiting a substantial change are highlighted in darker red, while those with insignificant changes are shown in lighter blue. The fold change of the normalized vehicle against itself, consistently 1, is represented in blue. **(B)** Correlation analysis between bicalutamide's effect classification and treatment response indicates a higher percentage of patients with a complete clinical response in the category showing an effect with bicalutamide. Conversely, patients with no effect demonstrated a significant percentage with poor clinical outcomes. **(C)** The levels of Exe and 17-HEXE for each patient in ascending order of exemestane levels were plotted. The patients with light and dark red bars are those who responded to bicalutamide, indicated with "w/ Bicalutamide effect". The patients colored with light and dark blue are those who were categorized as no effect with the bicalutamide, and it is indicated as "w/o Bicalutamide effect". No correlation was found between the levels of Exe or 17-HEXE and the effect of bicalutamide treatment. **(D)** The 17-HEXE/EXE ratio for all patients was performed and patients were classified according to the bicalutamide's effect. The ratio was plotted in descending order and patients with bicalutamide effect were colored in gold and the ones without an effect were colored in beige. A correlation exists between the fold change in 17-HEXE/EXE and the effect of bicalutamide.

2.4. 17-HEXE induces stronger binding of AR to chromatin compared to exemestane

Our previous experiments suggested that 17-HEXE and exemestane, present in patients' serum, may have an affinity for the AR and are able to bind to it. To evaluate whether the actions of exemestane and 17-HEXE were mediated by AR, we performed an *in vitro* assay called chromatin pellet. This technique consists of identifying the chromatin-associated proteins by isolating the chromatin and detecting the proteins.

In this experiment, MCF7 cells were subjected to different treatments, including the administration of the drug's vehicle (DMSO) as a negative control, dihydrotestosterone (DHT) at 100 nM as a positive control, and the application of exemestane at 15 µM and 17-HEXE at 5 µM under medium with hormones. Samples were collected at the baseline (before the treatment) and at 2, 4 and 24 h after the drug administration (Figure 28 A).

The western blot from the chromatin pellet revealed that the addition of the vehicle led to little, or no, AR binding to the chromatin. In contrast, the results from the DHT treatment displayed the highest AR binding to the chromatin at the 24-hour timepoint. Exemestane exhibited noticeable AR binding to the chromatin at 2, 4, and 24 h after the drug administration, compared to the baseline (0 h). Strikingly, 17-HEXE exhibited higher significant AR binding at 2, 4, and 24 h compared to the condition in which cells were treated with exemestane. However, 17-HEXE exhibited the same affinity as the DHT. Chromatin pellet western blot was normalized to the protein levels with the relative protein expression of histone 3 (Figure 28 B).

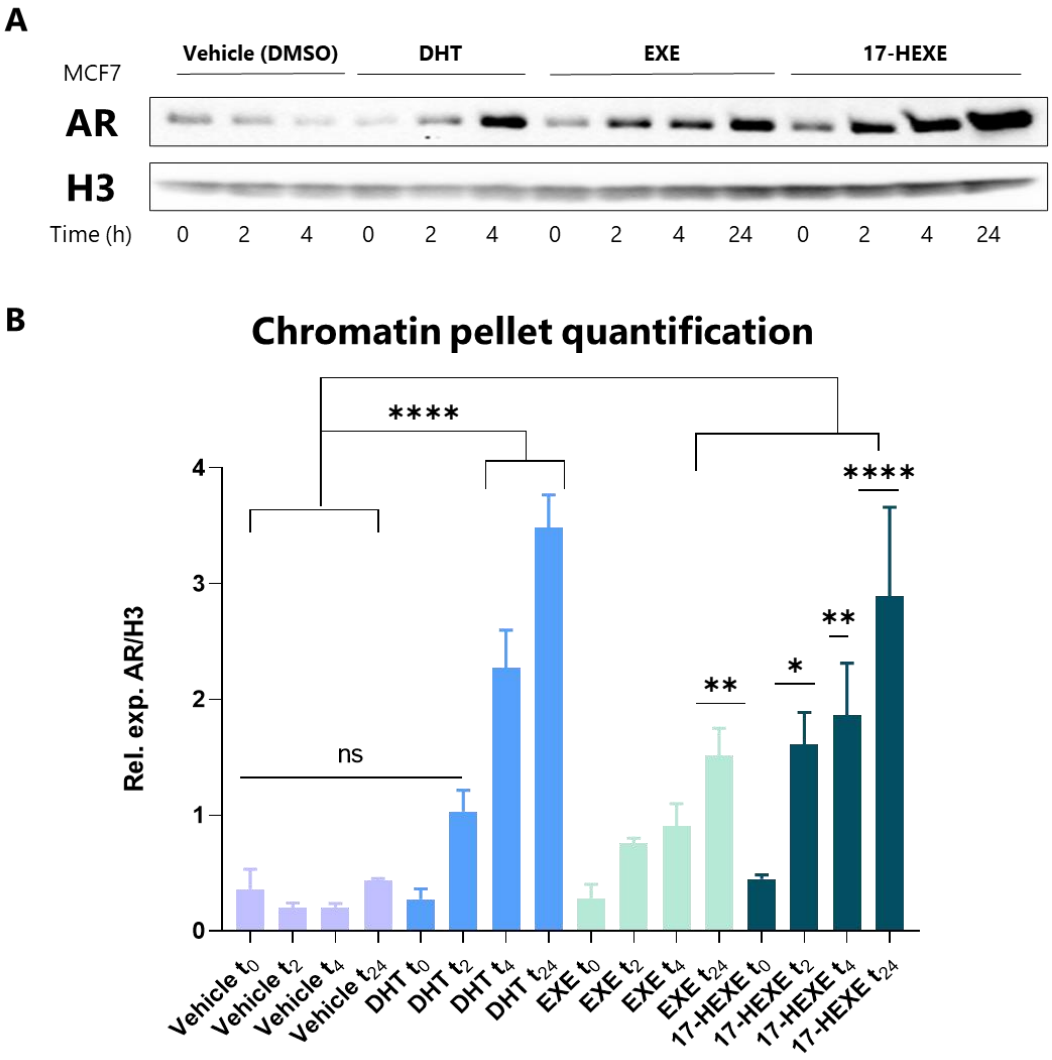

Figure 28. Chromatin pellet assay demonstrate that 17-HEXE induces stronger and earlier binding to AR on chromatin, compared to exemestane. **(A)** The western blot (WB) from the chromatin pellet assay performed on MCF7 cells depicts minimal AR binding with the vehicle, while dihydrotestosterone (DHT) exhibits the highest binding at 4 h. Exemestane shows noticeable AR binding at 2, 4, and 24 h post-administration compared to the baseline (0 h). Notably, 17-HEXE demonstrates significantly higher AR binding at 2, 4, and 24 h compared to exemestane (n=3). Histone 3 (H3) serves as a loading control. **(B)** Quantitative analysis of the western blot results presented in (A) show, via One-Way ANOVA significance test, that 17-HEXE exhibits higher affinity for AR than Exe and its affinity is comparable to that of DHT (n=3). Data is presented as the mean ± SEM.

The findings from these experiments provided evidence that 17-HEXE induces the binding of the AR to the chromatin in MCF7 cells at 2, 4, and 24 h after treatment. Moreover, 17-HEXE seems to have a strong affinity to the AR, reaching similar affinity levels as DHT. It has also been proved that 17-HEXE induces stronger and earlier AR binding than exemestane.

3. High percentage of AR-positive cells are associated with a more favorable response to exemestane treatment by reorganizing AR binding to chromatin and by upregulating apoptosis pathways

3.1. NeoLetExe patients exhibiting low Ki67-fold change, when treated with exemestane, correlate with high levels of AR at baseline

In this work, we have identified that the variation in NeoLetExe patient's responses to treatment seemed to be related with the levels of 17-HEXE relative to exemestane (17-HEXE/EXE ratio). Subsequently, we validated whether 17-HEXE and exemestane could bind and activate the AR in patients. However, we sought to investigate the mechanisms behind the clinical outcome between patients, as the 17-HEXE/EXE ratio might not solely be the responsible for the variation in patient responses to treatment. Therefore, we expanded our inquiry to explore whether treatment efficacy could also be influenced by the % of AR-positive cells.

To address this, we conducted IHC analyses from formalin-fixed paraffin-embedded (FFPE) tissue. Samples were serially cut and stained with hematoxylin eosin (H&E), AR and Ki67 (Figure 29 A). For the AR-positive cells, we assessed them at baseline whereas the Ki67 levels, were assessed at baseline and after 2 months of exemestane treatment for the Exe-Let cohort and after 4 months of exemestane treatment for the Let-Exe cohort. Utilizing QuPath, we quantified the percentage of stained cells and calculated the Ki67-fold change (2 months of Exemestane/Baseline for Exe-Let patients and 4 months of Exemestane/Baseline for Let-Exe patients).

The Ki67-fold change was subsequently correlated with AR-positive cells at baseline (Figure 29 B). The X-axis represents % of AR-positive cells determined by IHC at baseline, while the Y-axis represents the Ki67-fold change. Each data point signifies one patient. This plot suggests a negative correlation between Ki67-fold change and the % of AR-positive cells, meaning that patients with higher % of AR-positive cells, upon exemestane treatment, exhibited lower levels of Ki67-fold change. This was validated performing a Spearman rank-order correlation, which indicated a correlation of -0.714 with a p-value of 0.047.

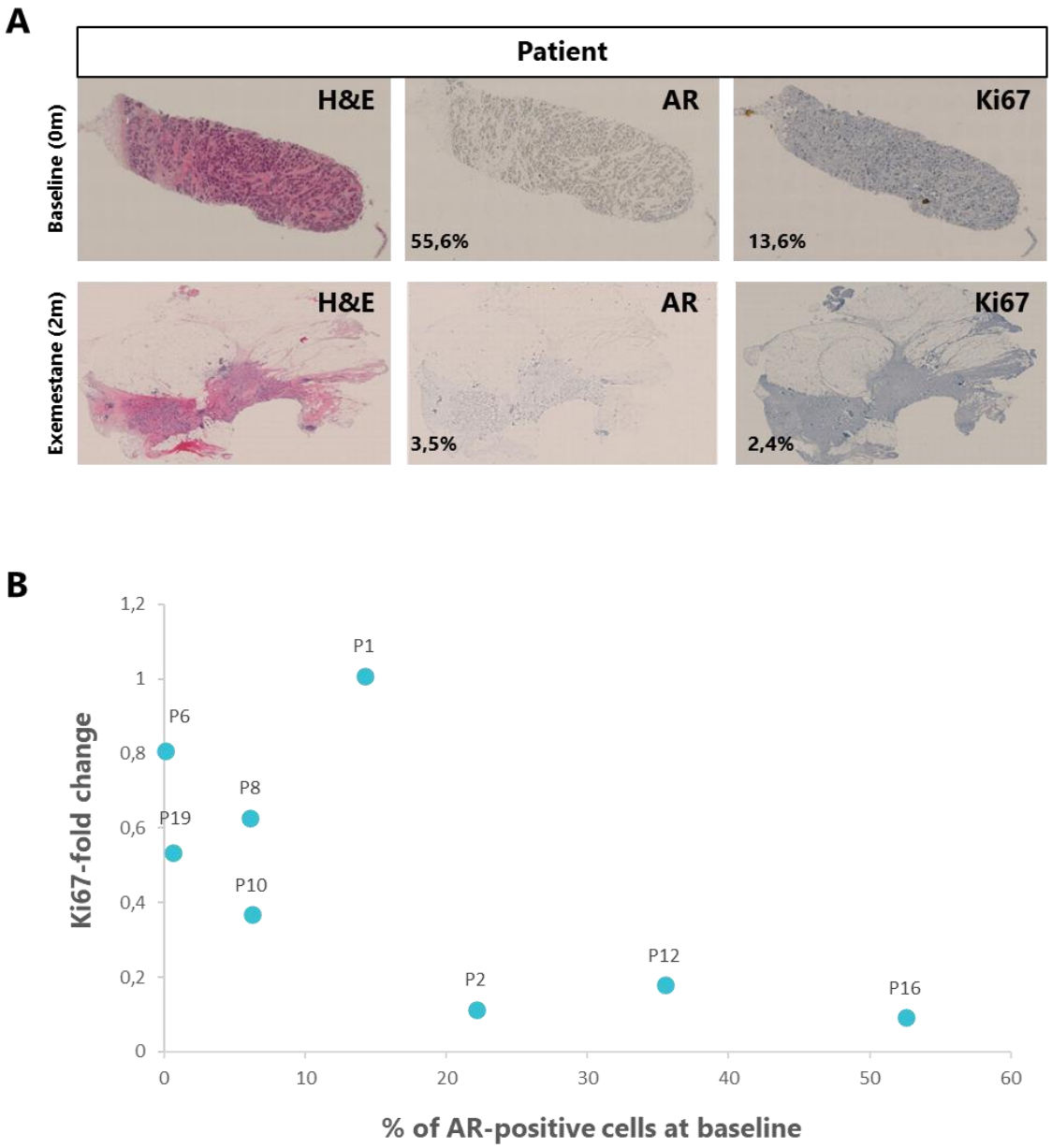

Figure 29. Indirect correlation between Ki67-fold change and AR positive cells in NeoLetExe patients. **(A)** IHC results for hematoxylin eosin (H&E), AR and Ki67 in serial cuts of patient 16 at baseline and after 2 months of exemestane treatment. Positive cell percentages for AR and Ki67 were determined using QuPath software. Patient 16 has been shown as an example to elucidate a general behavior, but these quantifications were performed in all analyzed patients (n=8). **(B)** Graphical representation of the correlation between Ki67-fold change and the % of AR-positive cells at baseline. The X-axis represents the % of AR-positive cells quantified by IHC, and the Y-axis represents the Ki67-fold change. Each data point signifies one patient (n=8).

These results suggest that a higher % of AR-positive cells is associated with a more favorable response to exemestane treatment, proved by lower Ki67-fold change. Therefore, these results complement the hypothesis that the efficacy of treatment in patients is also associated with the fraction of positive cells expressing AR.

3.2. Exemestane treatment in patients reorganizes AR binding to chromatin

In this study, we elucidated that NeoLetExe patients with a higher percentage of AR-positive cells, undergoing exemestane treatment, experienced a more significant reduction in Ki67 and, consequently, had a more favorable response to the treatment. Therefore, we aimed to investigate, by ChIP-Seq, which genes, or binding sites, were regulated by AR in patients treated with exemestane.

For this assay, we first assessed the percentage of AR-positive cells in the tumors of the patients. To address this, we conducted IHC analyses, staining serial cuts with AR at baseline. Utilizing QuPath, we quantified the percentage of stained cells (Table 6). For the ChIP-Seq analysis we selected patients belonging to the Exe-Let treatment sequence with high and intermediate % of AR-positive cells.

Table 6. Quantification of the percentage of stained AR-positive cells at baseline from NeoLetExe patients. This table only show the % of AR-positive cells for the Exe-Let branch and the categorization of the % of AR-positive cells in 3 categories.

Patient number	% of AR-positive cells	Categorization
P6	0.096	Low
P28	0.269	Low
P14	1.19	Low
P18	4.26	Intermediate
P24	5.48	Intermediate
P8	6.10	Intermediate
P10	6.23	Intermediate
P20	15.21	High
P2	22.12	High
P30	29.23	High
P12	35.52	High
P16	52.56	High

To perform the ChIP-Seq of AR, we used fresh-frozen (FF) tissue at baseline and after 2 months of treatment with exemestane from patients of the Exe-Let sequence. To perform the ChIP-Seq, tissue was pulverized, dounced, and lysated. Subsequently, chromatin was sonicated, followed by immunoprecipitation using AR antibody (Methods section) (Figure 30).

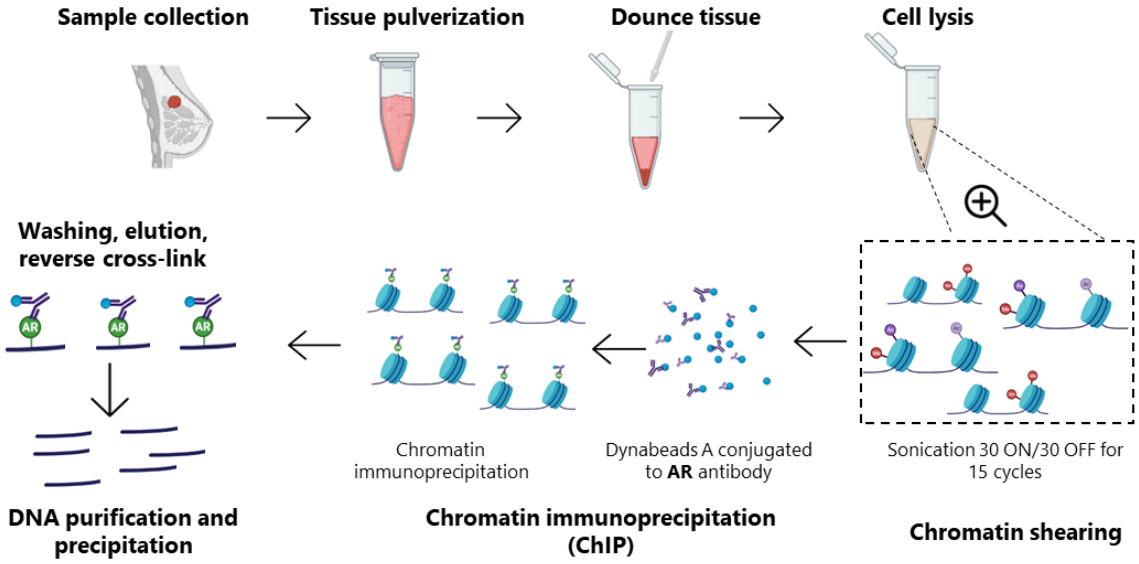

Figure 30. Schematic illustration of ChIP-sequencing process from fresh-frozen (FF) tissue.

Next, samples were sequenced and underwent a quality assessment to ensure the reliability of the data (data not shown in the thesis). Subsequently, we proceeded to conduct the bioinformatic analysis of the ChIP-Seq data. To identify the AR binding sites in the genome with enriched aligned reads, we conducted a peak calling (SICER) of the ChIP-Seq data at baseline and after 2 months of treatment. This identified binding sites were annotated to the human genome (hg19) with a 3 kb distance from the transcription start site (TSS) for each patient and timepoint (Table 7).

Table 7. Summary of number of peaks identified by SICER and the number of genes annotated from these peaks. Each patient is represented by its patient number and timepoint.

Patient number	Timepoint	SICER peaks	Annotated genes
P2	Baseline	5751	3708
P2	2 months	14301	6951
P10	Baseline	6851	3192
P10	2 months	2245	1233
P16	Baseline	7591	2412
P16	2 months	11394	4833
P18	Baseline	32176	12261
P18	2 months	15824	7705
P20	Baseline	1918	876
P20	2 months	4756	3060
P24	Baseline	8154	3858
P24	2 months	3687	2126
P30	Baseline	10284	5750
P30	2 months	6808	4127

Subsequently, we conducted a Principal Component Analysis (PCA) of this AR ChIP-Seq data (Figure 31 A). In this representation, each patient was plotted at baseline and after exemestane treatment (after 2 months of treatment). The representation of the two dimensions that explain the highest degree of variance suggests that three clusters are formed. The two small clusters, labelled as Cluster 2 and 3, are formed by patients with a high % of AR-positive cells according to Table 6. For the upcoming analysis, these two clusters will be treated as one, named Cluster 2-3, which includes both timepoints for patients: 2, 16, 20 and 30. The remaining cluster, Cluster 1, is composed by both timepoints of patients who have an intermediate % AR-positive cells (patients 10, 18 and 24).

Subsequently, we combined the peak calling data from all patients belonging to Cluster 1 and compared, by performing a Venn Diagram, the baseline versus 2 months of treatment with exemestane. The same representation was carried out for patients in Cluster 2-3 (Figure 31 B). For Cluster 2-3, there was a total of 57108 peaks, from those, only 5090 (9%) were shared between the 2 timepoints. In contrast, Cluster 1, there was a total of 56644 peaks, with 10742 of them (19%) being common between timepoints. Upon exemestane treatment, for Cluster 2-3, 31681 (55%) peaks were gained whereas for the Cluster 1, 10289 (18%) new peaks were identified. These comparisons revealed a reorganization of chromatin binding sites upon the treatment with exemestane.

To further investigate this, we annotated the genes identified through AR-ChIP and compared the ones annotated at baseline with those at 2 months, specifically comparing between clusters (Figure 31 C). Over the course of the treatment, for Cluster 2-3, 4598 (36%) genes were annotated at 2 months while for Cluster 1, 1257 (8%) genes were annotated after exemestane treatment. These comparisons again revealed the AR-mediated differences between clusters.

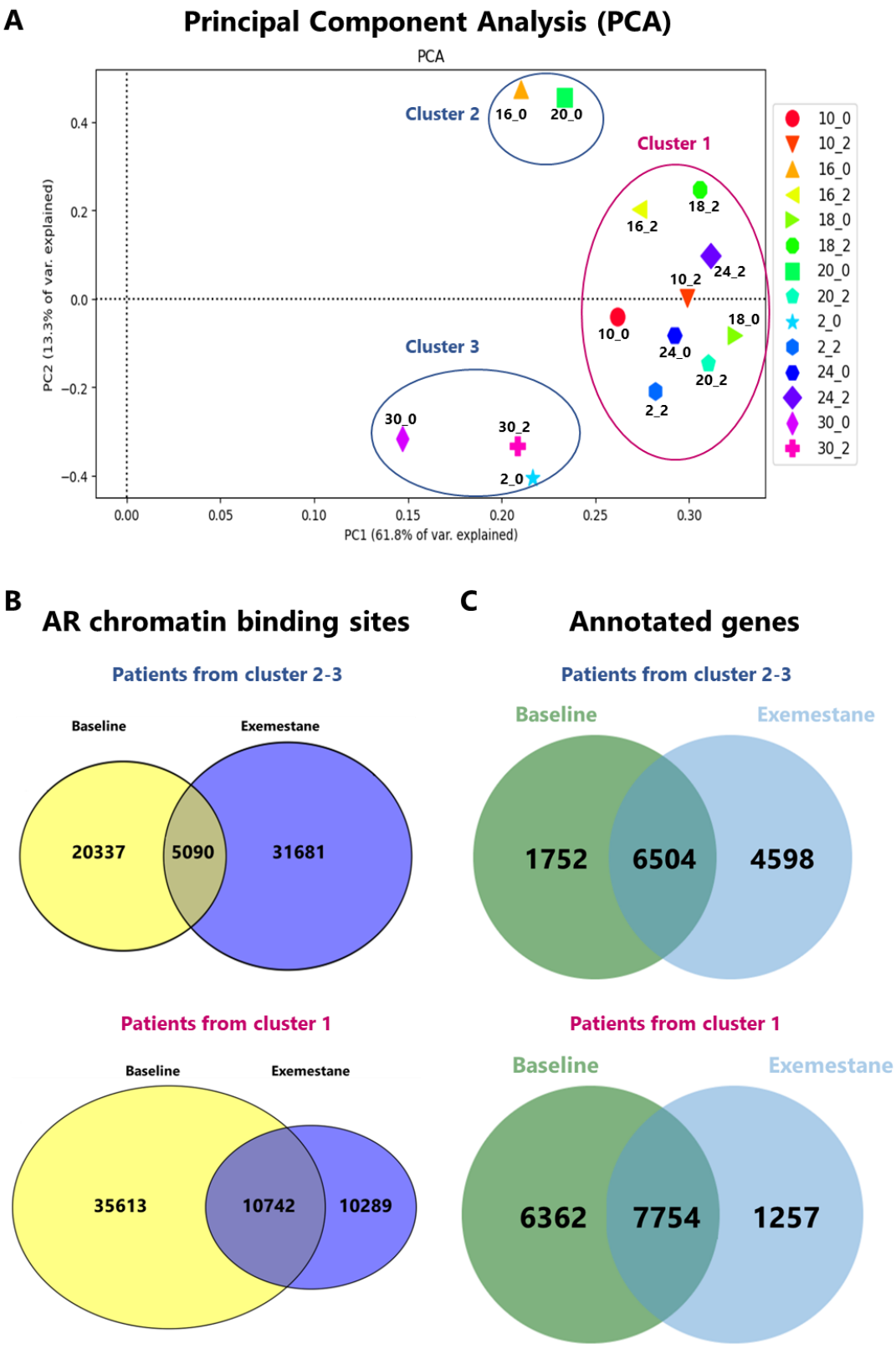

Figure 31. Exemestane treatment in patients reorganizes AR binding to chromatin. **(A)** Principal Component Analysis for Exe-Let patients for datapoints at baseline (0 months) and after treatment with exemestane (2 months). Three cluster can be identified. **(B)** Venn diagram of SICER peak calling of Cluster 1 and Cluster 2-3. It can be observed a redistribution of the AR chromatin binding sites throughout the treatment. **(C)** Two Venn diagrams comparing the annotated genes at baseline and after treatment with exemestane between the clusters.

3.3. Apoptosis related pathways seem to be upregulated in patients with high variance upon exemestane treatment

To gain some insights on the mechanism by which exemestane activates AR, we performed a Gene Set Enrichment Analysis (GSEA) on the unique annotated genes at 2 months. After conducting a GSEA on these annotated genes from Cluster 1 and Cluster 2-3, we plotted the pathways with the highest sorted Net Enrichment Score (NES). NES is a measure of the degree of upregulation of a pathway. The higher the NES, the more upregulated, all the represented pathways have a p-value lower than 0.05 meaning that they are all significative.

The most notable difference between the two clusters, is that pathways related to cell death (apoptosis) and a negative regulation of Ras signaling appeared highly upregulated in patients belonging to Cluster 2-3, thus, the ones that had higher % of AR-positive cells (Figure 32 A). In contrast, these pathways did not appear among the ones with higher NES for patients in Cluster 1 (Figure 32 B). This data suggests that the binding of AR to chromatin, upon exemestane treatment, might play a crucial role in promoting favorable responses by influencing specific pathways related to cell growth inhibition (apoptosis).

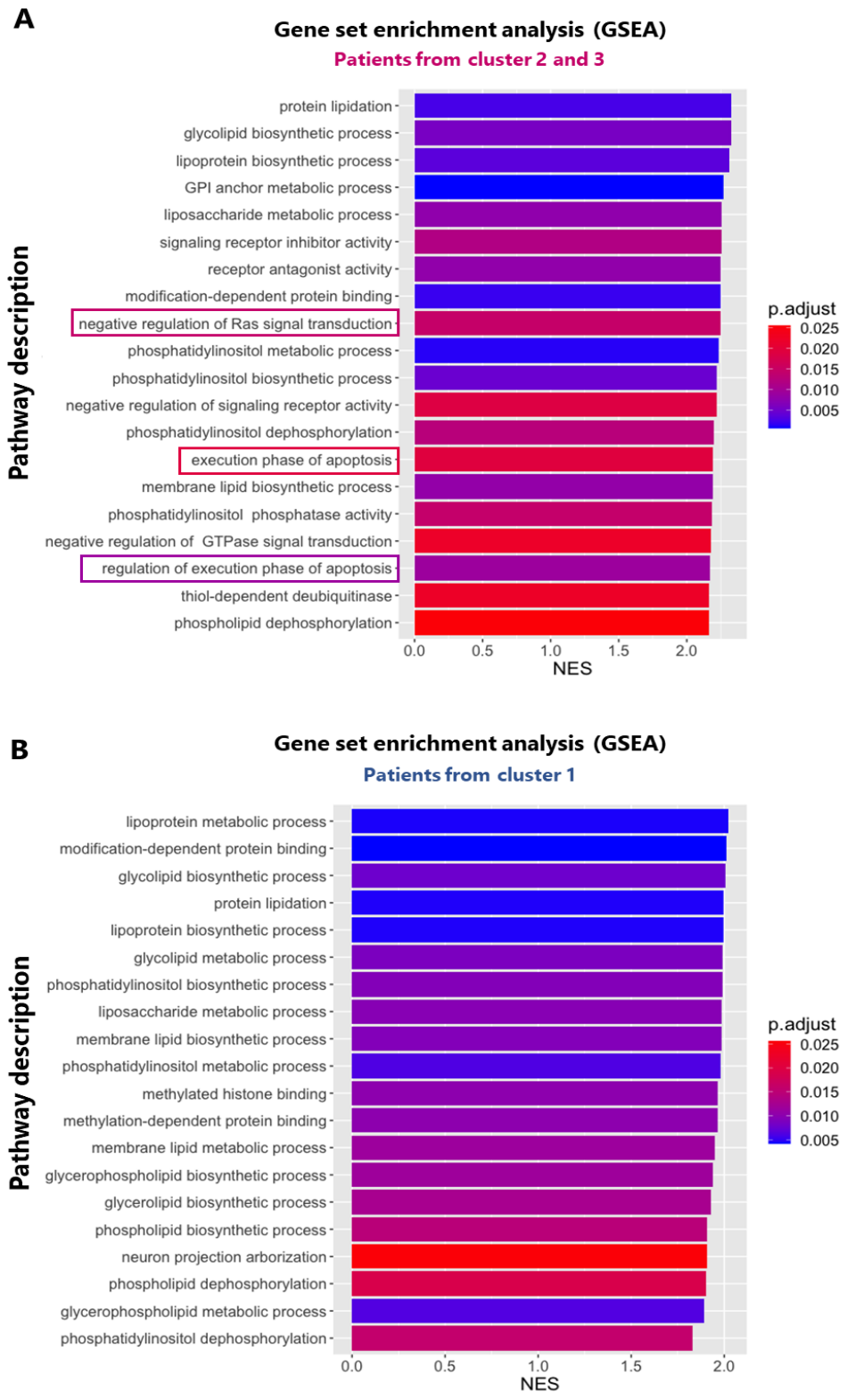

Figure 32. Patients from Cluster 2-3 exhibit upregulated pathways related to apoptosis after being treated with exemestane. **(A)** Gene Set Enrichment Analysis (GSEA) performed for Cluster 2-3 (patients 2, 16, 20 and 30) at 2 months. The bar plot represents the Net Enrichment Score (NES) on the X-axis and the pathway in decreasing order of NES on the Y-axis, each pathway is colored according to its adjusted p-value. Top 20 pathways have been plotted. Pathways related to apoptosis and downregulation of Ras signaling pathway appeared among the top ones. **(B)** GSEA performed for the Cluster 1 (patients 10, 18 and 24) at 2 months. The bar plot represents the NES on the X- axis and the pathway in decreasing order of NES on the Y-axis, each pathway is colored according to its adjusted p-value.

4. Synergistic effect and enhanced cytotoxicity of 17-HEXE combined with exemestane through AR by enhancing apoptotic pathways

4.1. Enhanced cytotoxicity and synergistic effect of 17-HEXE and exemestane combination in AR-overexpressing breast cancer cells

After elucidating an enrichment of apoptotic pathways in patients with a high % of AR-positive cells, we hypothesized that 17-HEXE, and/or exemestane, might contribute to improved clinical outcomes observed in those patients. To investigate this, we evaluated, *in vitro*, the impact of 17-HEXE and exemestane on cell proliferation. To ensure that any observed effect was attributed to the AR, we engineered an MCF7 cell line with constitutive AR overexpression, referred as MCF7-AR. The AR expression in these cells was validated using western blot analysis, assessing AR protein levels normalized to GAPDH expression (Figure 33 A and B).

The effect of 17-HEXE in proliferation was assessed in regular MCF7 cells and in MCF7-AR, by performing a crystal violet proliferation assay, carried out for 72 h in standard DMEM medium with 5% of serum. This assay involved treating cells with DMSO (vehicle), DHT (100 nM), exemestane at 15 µM (IC50 data not shown), and 17-HEXE at 5 µM (IC50 data not shown) with treatments applied every 24 h (Figure 33 C). At 72 h, no significant differences were observed in proliferation between MCF7, and MCF7-AR cells treated with the vehicle. Administration of DHT resulted in a significant increase in cell growth in MCF7 compared to MCF7-AR. Additionally, this significant difference was also observed when comparing MCF7 cells treated with the DHT vs the vehicle. Additionally, MCF7 cells treated with exemestane exhibited higher growth compared to MCF7-AR cells under the same conditions, but no significant differences were observed with the control (MCF7-vehicle). Notably, this experiment revealed that MCF7 cells treated with 17-HEXE for 72 h exhibited significantly more cell growth compared to MCF7-AR cells, but no significant differences were observed with the control (MCF7-vehicle). Overall, these findings suggest that 17-HEXE is more effective in inhibiting cell growth, and its action appears to be mediated through the AR. While exemestane also induces cell growth inhibition, this effect is more pronounced in MCF7 cells overexpressing AR.

Subsequently, we sought to investigate the combined impact of 17-HEXE and exemestane on cell growth inhibition. This examination was conducted in both MCF7 and MCF7-AR cells, with cells treated using vehicle (DMSO and chloroform), a fixed concentration of 5 µM of 17-HEXE and different concentration of exemestane: 15 µM, 5 µM to 1 µM. Cell proliferation was evaluated under DMEM 5% serum through a 72-h crystal violet assay (Figure 33 D). The results indicated no significant difference between MCF7 and MCF7-AR when treated with the vehicles. However, high concentrations of exemestane (15 µM) in combination with 17-HEXE exhibited some efficacy in impeding cell proliferation in MCF7-AR. Interestingly, a similar trend was observed when MCF7-AR cells were treated with 17-HEXE and the same concentration of exemestane (5 µM). Surprisingly, the most pronounced effect was observed when MCF7-AR cells were treated with 17-HEXE in combination with a lower concentration of exemestane (1 µM). These findings suggest that the combination of 17-HEXE (5 µM) with exemestane (1 µM) had the most significant impact on cell proliferation in MCF7-AR.

After having elucidated that combination of 17-HEXE (5 µM) with exemestane (1 µM) in MCF7-AR was the treatment exhibiting the most optimal effect on cell proliferation at 72 h, we compared it against individual treatments (exemestane alone at 15 µM and 17-HEXE alone at 5 µM). This assay was performed in MCF7-AR using the Incucyte system over an extended period of 180 h (7.5 days). Cells were cultures under DMEM medium with 5% of serum and were re-treated every 48 h. Cell confluence was monitored at each timepoint using artificial intelligence analysis, plotting the average phase object area against time in hours (Figure 33 E). Results indicated that cell confluence steady decreased over time in MCF7-AR cells treated with the combination of 17-HEXE and Exe. Although, the individual treatments of 17-HEXE and Exe also affected cell confluence compared to the control (vehicle), the combined treatment exhibited the most substantial impact on cell growth.

This Incucyte software also allowed us to assess the percentage of dead cells (Figure 33 F). This analysis indicated that the highest percentage of cell death was attributed to MCF7-AR cells treated with the combination of 17-HEXE (5 µM) with exemestane (1 µM), showing a consistent increase in cell death (%) over time. Regarding the individual treatments, cells treated with 17-HEXE (5 µM) showed a higher percentage of cell death compared to the control group (vehicle) after 78 h. However, exemestane (15 µM) alone did not exhibit any noticeable difference in cell death compared to the vehicle. These results

strongly suggest that MCF7-AR treated with the combination of 17-HEXE (5 µM) with exemestane (1 µM) exhibited a significant effect on cell confluence and in cell death compared to the vehicle and to the single treatments.

From this assay performed over time, it seemed that the enhanced effect observed with the combination of 17-HEXE (5 µM) with exemestane (1 µM) happened sooner than the effect observed with the single treatment. Therefore, we conducted a detailed assessment of the effects of these drugs at shorter timepoint (at 24 h). We performed an identical experiment treating MCF7-AR cells, with the vehicle, exemestane, 17-HEXE, and the combination of both drugs. This assay was performed using the Incucyte system assessing the cell confluency (Figure 33 G) and the % of cell death (Figure 33 H) at 24 h. The results obtained after assessing the cell confluency at 24 h indicate a substantial reduction in cell confluency when MCF7-AR cells were treated with 17-HEXE (5 µM) and exemestane (1 µM). However, no significant differences were observed between the exemestane and the 17-HEXE alone, but they exhibited significant differences in cell confluency compared to the vehicle and the combined treatments. The analysis of the fraction (%) of cell death assessed after 24 h, reveals that the combination of 17-HEXE (5 µM) with exemestane (1 µM) significantly induced higher cell death compared to the vehicle (DMSO and chloroform) and to the individual treatments in MCF7-AR cells. However, no significant differences were observed between the exemestane and the 17-HEXE alone, neither compared to the vehicle.

Overall, these findings suggest that 17-HEXE is more efficient in inducing cell death in cells with higher levels of AR. Notably, this effect is also evident when cells are treated, *in vitro*, with a combination of 17-HEXE and Exe at a 5:1 ratio. Furthermore, the combination demonstrates more pronounced effects on MCF7-AR in terms of both cell confluency and cell death from 24 h up to the assessed time, which was 7.5 days. Hence, it suggests that there is a synergistic effect, enhancing cytotoxicity when 17-HEXE and Exe are combined at a 5:1 ratio.

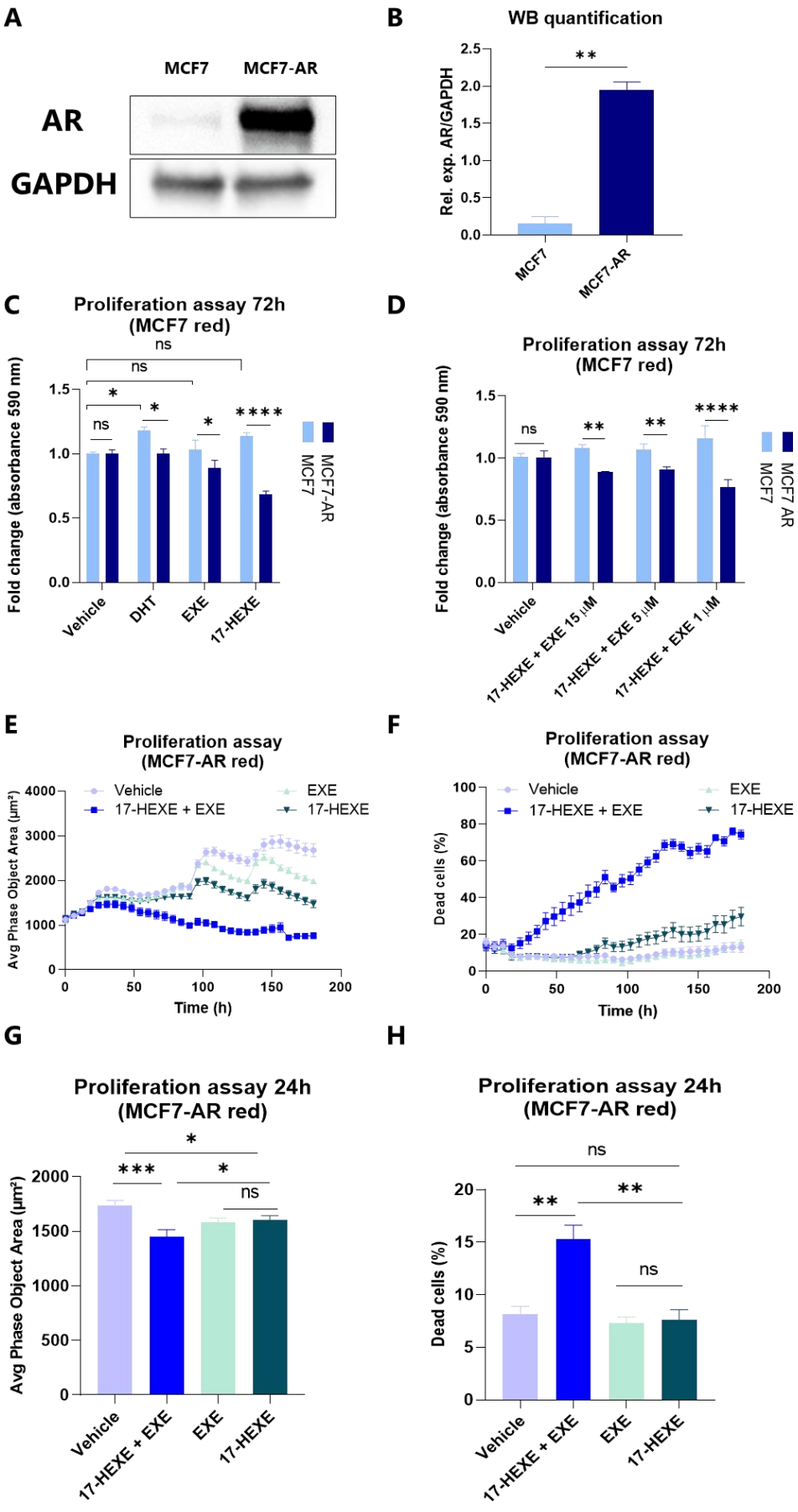
A
MCF7
MCF7-AR
AR
GAPDH
B
WB quantification
Rel. exp. AR/GAPDH
MCF7
MCF7-AR
C
Proliferation assay 72h
(MCF7 red)
Fold change (absorbance 590 nm)
MCF7
MCF7-AR
Vehicle
DHT
EXE
17-HEXE
D
Proliferation assay 72h
(MCF7 red)
Fold change (absorbance 590 nm)
MCF7
MCF7 AR
Vehicle
17-HEXE + EXE 15 µM
17-HEXE + EXE 5 µM
17-HEXE + EXE 1 µM
E
Proliferation assay
(MCF7-AR red)
Avg Phase Object Area (µm²)
Vehicle
17-HEXE + EXE
EXE
17-HEXE
Time (h)
F
Proliferation assay
(MCF7-AR red)
Dead cells (%)
Vehicle
17-HEXE + EXE
EXE
17-HEXE
Time (h)
G
Proliferation assay 24h
(MCF7-AR red)
Avg Phase Object Area (µm²)
Vehicle
17-HEXE + EXE
EXE
17-HEXE
H
Proliferation assay 24h
(MCF7-AR red)
Dead cells (%)
Vehicle
17-HEXE + EXE
EXE
17-HEXE

Figure 33. Enhanced cytotoxicity and synergistic effects have been observed in AR-overexpressing breast cancer cells when treated with a combination of 17-HEXE (5 µM) and exemestane (1 µM). (A) The generation of an MCF7 cell line with constitutive AR overexpression (MCF7-AR) was confirmed through western blot analysis, with GAPDH as a loading control. **(B)** Quantitative analysis of AR expression of panel (A) with statistical significance determined by a T-test (n=3). Data is presented as the mean ± SEM. **(C)** Proliferation effects were evaluated in standard MCF7 cells and in MCF7-AR cells over 72 h by performing a crystal violet. While no notable differences were observed in vehicle-treated MCF7 and MCF7-AR cells, treatment with 17-HEXE for 72 h resulted in significantly higher cell growth inhibition in MCF7-AR cells. DHT significantly increased cell growth in MCF7 but not in MCF7-AR. Exemestane treatment led to higher growth in MCF7 compared to MCF7-AR. Statistical significance was assessed by a Two-Way ANOVA multiple comparison test (Tukey's) (n=3). Data is presented as the mean ± SEM. **(D)** Crystal violet cell proliferation assay performed at 72 h in DMEM 5% showed the most significant impact on cell growth inhibition when MCF7-AR cells were treated with 17-HEXE and a lower concentration of EXE (1 µM). Statistical significance was determined by a Two-Way ANOVA multiple comparison test (Tukey's) (n=3). Data is presented as the mean ± SEM. **(E)** Cell confluence was monitored over 180 h using the Incucyte system in DMEM 5% FBS. The combination of 17-HEXE (5 µM) with EXE (1 µM) in MCF7-AR exhibited the most significant impact on cell confluency, as evaluated by artificial intelligence analysis. Statistical significance was assessed by a One-Way ANOVA multiple comparison test (Tukey's) (n=3). Data is presented as the mean ± SEM. **(F)** The percentage of cell death was monitored over time (180 h) with the Incucyte in DMEM 5% FBS. The combination of 17-HEXE (5 µM) with EXE (1 µM) in MCF7-AR significantly enhanced cell death, as evaluated by artificial intelligence analysis. Statistical significance was determined by a One-Way ANOVA multiple comparison test (Tukey's) (n=3). Data is presented as the mean ± SEM. **(G)** Cell confluency at 24 h evaluated by the Incucyte system in DMEM 5% FBS conditions in MCF7-AR cells, showed a substantial reduction when 17-HEXE (5 µM) was combined with EXE (1 µM). Statistical significance was assessed by a One-Way ANOVA multiple comparison test (Tukey's) (n=3). Data is presented as the mean ± SEM. **(H)** The percentage of cell death at 24 h, employing the Incucyte system in DMEM 5% FBS conditions, showed higher cell death induced by the combination of 17-HEXE (5 µM) with EXE (1 µM) when compared to the vehicle (DMSO and chloroform) in MCF7-AR cells. Statistical significance was assessed by a One-Way ANOVA multiple comparison test (Tukey's) (n=3). Data is presented as the mean ± SEM.

4.2. RNA-Seq validated synergistic effect of 17-HEXE and exemestane via activation of pathways related to apoptosis

Lastly, we decided to perform an RNA-Seq of MCF7-AR cells treated with the drug vehicle as a control, individual treatments and the combination of 17-HEXE (5 µM) and exemestane (1 µM). We aimed to compare the RNA expression of the different conditions compared to the control group (vehicle) to gain some insights on the individual and synergistic impact that these drugs have in MCF7-AR cells. These comparisons were represented as a volcano plot with the log2 of the fold change against the negative log10 of the p-value (Figure 34 A).

The significant genes are the ones that exhibited a log2 fold change bigger than 1, or smaller than -1, and that had a negative log10 of the p-value bigger than 5 (which equals to a raw p-value of 0.00001), comparing them with the 62656 genes in the ENSEMBL database. The number of upregulated and downregulated genes varied between the conditions and is displayed in Table 8.

Table 8. Summary of the significantly upregulated and downregulated genes in the different conditions.

Condition	Genes significantly up	Genes significantly Down
Exe vs Vehicle	88	35
17-HEXE vs Vehicle	182	33
17-HEXE&Exe vs Vehicle	177	44

Subsequently, we performed a GSEA for the upregulated and another one for the downregulated genes belonging to the cancer hallmark database. However, as these sets have a reduced number of genes to perform a successful GSEA, we selected the genes that had a p-value equal or smaller than 0.05 (which corresponds to 1.30 in the -log10 scale). The selected subset for the Exe vs Vehicle condition was composed of 537 upregulated genes and 1364 downregulated ones. For the 17-HEXE vs Vehicle condition, there were 1510 upregulated and 862 downregulated genes. Finally, for the 17-HEXE&Exe vs Vehicle condition there were 874 upregulated and 987 downregulated genes. We plotted the top 10 pathways from the combined treatment for the upregulated and downregulated genes sorted by the -log10 of the adjusted p-value calculated in the GSEA (Figure 34 B).

The GSEA for the upregulated genes indicated a significant increase in the hypoxia pathway when 17-HEXE was combined with exemestane. Comparing this pathway across different conditions revealed that, while both 17-HEXE and exemestane individually upregulated this pathway, the combination showed a more pronounced effect. Moreover, the combination significantly upregulated the TNF-α signaling pathway, via NF-κB, and the apoptosis pathway, which were only significantly affected in the combined treatment. Surprisingly, the Exe alone significantly upregulated genes associated with the androgen response pathway. This upregulation was even more pronounced than in the combination treatment and the 17-HEXE alone condition. Additionally, the mTOR signaling pathway showed significant upregulation in the combination treatment, whereas it was slightly upregulated with 17-HEXE alone and not significantly altered in the Exe alone condition. Once again, among the significantly upregulated pathways, the KRAS signaling emerged.

Regarding the downregulated pathways, the combined treatment showed significant downregulation of estrogen-response and KRAS signaling. The first was also significantly downregulated for the 17-HEXE alongside the epithelial-mesenchymal transition (EMT). For the Exe treatment, the interferon α and γ response pathways were significantly downregulated. Detail of all genes in each pathway is in Table 23 (Annex).

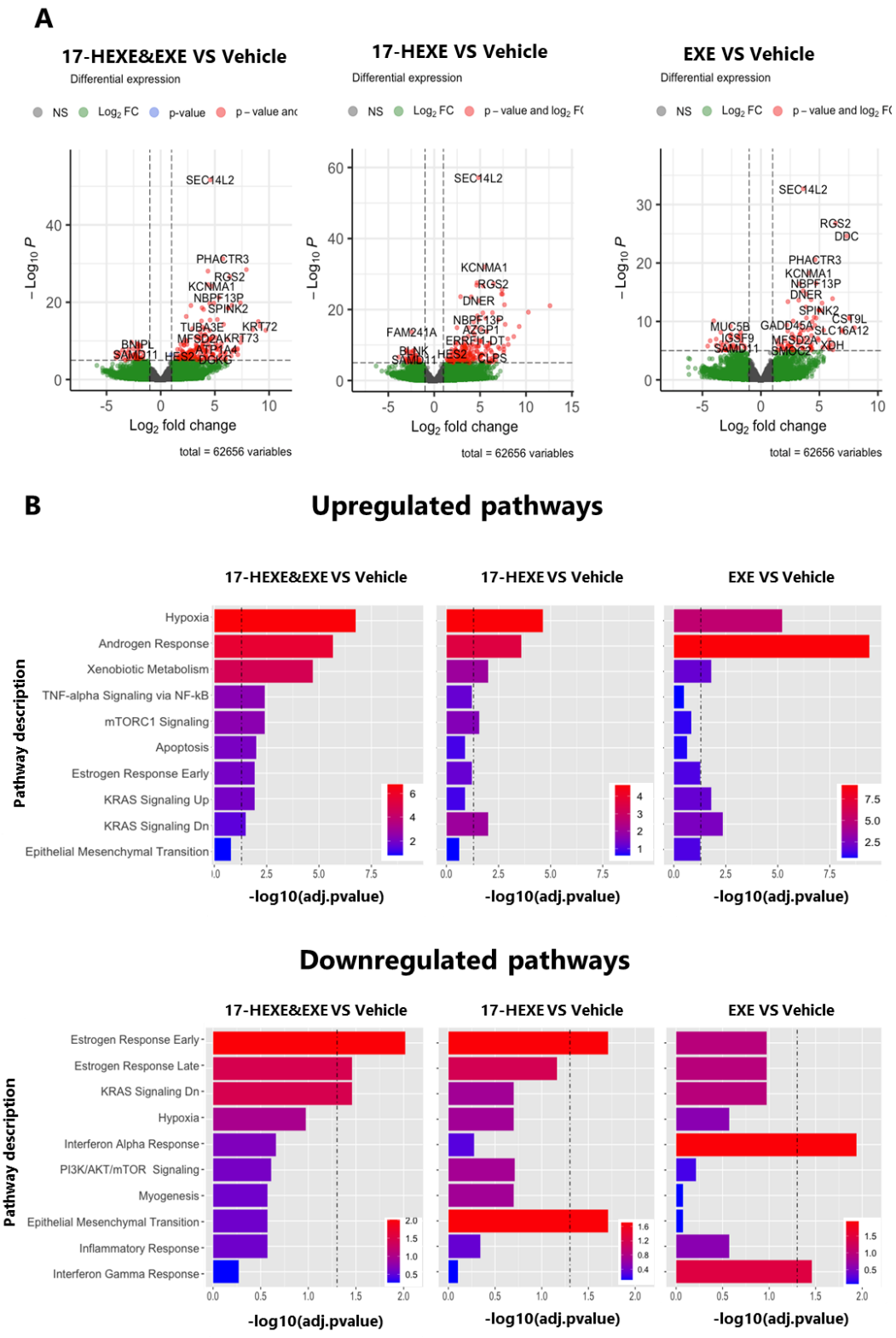

Figure 34. RNA-Seq data validated synergistic effect of 17-HEXE and exemestane in MCF7-AR compared to single treatments. **(A)** Volcano plot showing the log2 fold change against the -log10 p-value when comparing 17-HEXE&Exe vs vehicle, 17-HEXE vs vehicle and Exe vs vehicle expression. The genes with a log2 fold-change greater than 1, or smaller than -1, and a -log10 p-value bigger than 5 are highlighted. **(B)** Barplot showing the cancer related pathways identified via GSEA for the upregulated and downregulated genes of the 17-HEXE&Exe vs vehicle, 17-HEXE vs vehicle and Exe vs vehicle expression. Bars are sorted in descending order of the -log10 of the adjusted p-value calculated by the GSEA. The vertical dotted line indicates a -log10 p-value of 1.30 which corresponds to a p-value of 0.05.

DISCUSSION I

The complexity of breast cancer, both clinically and molecularly, underscores the variability in treatment responses among patients, even though they belong to the same subtype [205]. Nevertheless, novel technological advances, particularly in gene expression profiling, have contributed substantially to comprehending tumor progression and treatment response. Indeed, prognostic markers have emerged as crucial tools, aiding clinicians in predicting tumor aggressiveness, thereby developing personalized treatments [209].

Despite extensive research of aromatase inhibitors (AIs), the underlying mechanism governing this lack of cross-resistance remains elusive. In order to better understand breast cancer response to two aromatase inhibitors: letrozole and exemestane, the NeoLetExe clinical trial was designed. This comprehensive approach not only aimed to understand resistance mechanisms to AIs, but also aimed to pave the way for developing novel therapeutic strategies, encouraging precision medicine in breast cancer treatment [214].

This work aimed to identify a specific patient subgroup exhibiting a potential favorable response to AIs while elucidating the mechanism of response to these treatments. To achieve this goal, we first explored patients' features correlated with treatment response. Regarding the treatment response, it was evaluated and graded into 3 categories. However, the majority of patients were graded into the same category, rendering the analysis nonviable since there were no significant differences. Therefore, Ki67-Fold change, defined as the variation of Ki67 score at baseline versus post-surgery (after both treatments), was as used instead. Ki67-fold change offered a way to assess response in a quantitative and a more precise manner.

Nevertheless, we first tested whether the Ki67-fold change was, in fact, a reliable metric for evaluating patient responses to AI therapy. The provided categorical treatment response variable was correlated with Ki67-fold change, exhibiting a clear correlation between high levels of Ki67-fold change and worse response (Figure 17). This finding suggests that Ki67-fold change could be used as a more precise proxy for assessing treatment response compared to the provided treatment response. Indeed, the Ki67 expression has also been used as a proliferation marker to assess the antiproliferative action of the AIs in MCF7 cells [222].

The results after correlating the Ki67-fold change with patient's features revealed interesting insights on treatment efficacy and it allowed us to hypothesize the relationship between variables. For example, the relationship between Ki67-fold change and age showed a relatively constant fold change for patients under 90 years old. It seems that post-

menopausal women age does not correlate with patient's response. Similarly, no differences were observed regarding patient's tumor subtype, as 70% of the patients were categorized as non-special type and the Ki67-fold change value was very similar to the infiltrating lobular carcinoma (ILC) cohort, which represented 25% of the patients.

When correlating the Ki67-fold change with the BMI, patients who had a BMI higher than 30, exhibited a lower Ki67-fold change, thus had a more favorable response. One possible explanation of such positive correlation might be due to the expression of leptin in patients with higher BMI. Leptin is an adipokine secreted by adipose tissue, which is typically elevated in obesity, and contributes to breast cancer progression by increasing estrogen levels. It has been reported that leptin levels decrease exclusively upon exemestane treatment [223]. Therefore, patients with high BMI might benefit from exemestane treatment by reducing their leptin levels.

Correlating the Ki67-fold change with the tumor grade exhibited direct correlation, meaning that lower grades correlated with lower Ki67-fold change. Additionally, the association between Ki67-fold change and the presence of metastasis at the time of diagnosis, revealed that no metastasis at diagnosis correlated with lower Ki67-fold change, thus, a more favorable response. These two correlations further support the importance of early breast cancer detection to increase survival probability [224].

Additionally, we correlated the Ki67-fold change with features related to patients' survival (dead, residual tumor and relapse). When correlating the patient's deaths and, their causes, with the Ki67-fld change, breast cancer-related deaths exhibited higher Ki67-fold change, supporting the potential association between higher Ki67 levels and a less effective treatment response. Moreover, examining residual tumors and relapse, revealed that patients with higher % of residual tumor, or those experiencing relapse, displayed significantly higher Ki67-fold change (Figure 19). This is a clear indicator of potential treatment ineffectiveness in these subsets. These results further emphasize the utility of Ki67-fold change in predicting treatment response and reinforces the choice of Ki67-fold change as a treatment response marker.

Furthermore, the examination of patient's response to sequential administration of exemestane followed by letrozole (Exe-Let) or letrozole-exemestane (Let-Exe) revealed interesting insights into treatment efficacy. This correlation was the most relevant finding from this exploratory patient's data analysis. There was a notable reduction in Ki67-fold

change levels in patients from the Exe-Let cohort compared to the Let-Exe sequence (Figure 18 H and Figure 20 H). This surprising observation was further studied in this work to uncover the mechanisms that led to this behavior.

This exploratory data analysis included all patients enrolled in the NeoLetExe clinical trial. However, for the subsequent *in vitro* experiments, we exclusively had access to materials derived from the first 30 patients. Thus, our first step involved reevaluating the characteristics of these 30 patients to confirm that the trends observed in the larger patient cohort were similar on this subset. This was undertaken to ensure the continued representativeness of our patient subset from the NeoLetExe clinical trial. This study confirmed the consistency of trends observed in the larger cohort (Figures 20 and 21). Despite the smaller sample size, this subset remained representative, underlining the potential of these patients as a pilot group for further studies.

After discovering that the Exe-Let sequence was correlated with lower Ki67-fold change, suggesting a better clinical outcome, we hypothesized that this effect might have been due to differences between these drugs to inhibit aromatase enzyme effectively. This hypothesis was assessed by comparing the estrogen levels between Exe-Let and Let-Exe patients (Figure 22). The results suggested a comparable efficacy of letrozole and exemestane in inhibiting aromatase activity, as evidenced by the consistent reduction in estrogen levels in both groups at 2 and 4 months. Therefore, our initial hypothesis postulating differences in efficiency in inhibiting aromatase enzyme was challenged by our data. This suggests an alternative mechanism behind the observed better clinical outcomes from Exe-Let sequence patients. Bearing this idea in mind, we based our new hypothesis on previous literature findings to help us explain why Exe-Let sequence exhibited a more favorable clinical outcome demonstrated by lowering Ki67-fold change.

Following an extensive literature review search, we found that exemestane undergoes metabolic processes producing various metabolites. These metabolites have been associated with potent aromatase inhibition activity suggesting that, exemestane efficacy in treating breast cancer, may also be attributed to the active metabolites [225]. Among these metabolites, the 17-hydroxy-6-methylenandrosta-1,4-dien-3-one, known as 17β-hydroxyexemestane, or 17-HEXE, stood out due to its strong affinity for the androgen receptor (AR), its weak binding to ER and its potent anti-aromatase activity, similar to exemestane [226].

However, a discrepancy exists in the literature regarding the precise role that 17-HEXE plays *in vitro*. Certain studies suggest that 17-HEXE hampers breast cancer cell survival through mechanisms that differ from those of exemestane and that 17-HEXE stimulates cell proliferation by acting as an AR agonist [227]. Conversely, other studies argue that 17-HEXE reduces the viability of ER-positive breast cancer cells by inducing apoptosis and autophagy [228, 229]. Based on these literature findings, we decided to explore whether 17-HEXE was playing a role in making Exe-Let sequence exhibit a more favorable clinical outcome demonstrated by lowering Ki67-fold change.

To prove this hypothesis, we first examined if there were circulating levels of 17-HEXE, meaning that exemestane was being metabolized. Regarding the hepatic metabolism of exemestane into 17-HEXE, it involves the reduction of exemestane by enzymes such as aldoketoreductases (AKR) and CYP4A and CYP1A11 to give rise to 17-HEXE. Subsequently, 17-HEXE undergoes inactivation through glucuronidation, which is facilitated by enzymes like CYP3A and UGT2B17 [230].The examination of the exemestane and 17-HEXE levels validated that exemestane was metabolized into 17-HEXE across all patients, but at different rates (Figure 23). Therefore, our analysis underscores considerable variability in exemestane metabolism among individuals. This finding goes in line with the previously reported polymorphism in the enzymes (AKR, CYP1A and CYP4A11) responsible for exemestane conversion to 17-HEXE leading to a wide interindividual variability in the plasma concentrations of 17-HEXE [226]. However, the expression of these enzymes in NeoLetExe patients could not be evaluated.

Additionally, this variation existed regardless of whether these patients belonged to the Exe-Let or Let-Exe cohorts. Therefore, this finding suggests that, in Let-Exe patients, previous metabolization of letrozole seems to not affect the exemestane metabolism. This finding also suggests that the more favorable clinical outcome, demonstrated by lower Ki67-fold change in Exe-Let patients, seems not to be related with the treatment sequence. Instead, it seems to be related to exemestane, or its metabolite 17-HEXE, via AR.

Once it was confirmed that exemestane was metabolized into 17-HEXE, we explored whether 17-HEXE, or exemestane, both present in the patients' serum, could interact and activate the AR. This interaction was evaluated, *in vitro*, by performing a luciferase assay using MCF7 cells that have a promoter cassette upstream of the luciferase reporter (MCF7-Luc). After validating the MCF7-Luc protein levels of ER and AR (Figure 24), a luciferase

assay experiment, to further validate the cellular model using fulvestrant (ER degrader), was performed (Figure 26). These findings highlighted that in the majority of the evaluated patients the luciferase signal experienced a significant decrease when fulvestrant was administered. This implied that, as ER was degraded, less estrogen could bind to the ER and activate the luciferase reporter, thus, less bioluminescence was emitted.

MCF7-Luc cells have been demonstrated as a valid model to determine the capacity of estrogenic compounds to activate ER in patient's serum [231]. Consequently, we also explored whether exemestane and, its metabolite 17-HEXE, might interact with AR, and then, affect the luciferase signal. For that, we used the competitive AR antagonist bicalutamide (Figure 27 A). In this experiment, the detected luciferase signal was solely attributed to the presence of exemestane, or 17-HEXE, at either the 2 or 4-month timepoints. It is crucial to emphasize that the luciferase signal observed did not come from estrogens, as its absence in the patients' bloodstream, at both the 2 and 4-month, was confirmed in Figure 22. After performing these luciferase assay on 25 patients, results revealed that, half of the patients exhibited alterations in bioluminescence upon the addition of bicalutamide. This enabled us to categorize the patients based on bicalutamide's effects, identifying two distinct trends.

In patients where the luciferase signal remained unchanged, following the administration of bicalutamide, it could imply that the AR was not activated. Nevertheless, if there was a change in the luciferase signal upon administration of bicalutamide, it might mean that the AR, in those patients, was being activated. Specifically, if there was an increase in the luciferase signal following the administration of bicalutamide, this might suggest that the remaining portion, that was previously interacting with the AR, is now bound to the ER. Conversely, a decrease in the luciferase signal upon bicalutamide administration might suggest that some of the remaining 17-HEXE, and/or Exe, are now unbound and do not activate the ER. Nonetheless, in both scenarios, it indicates that the AR in these patients was being activated by the presence of exemestane, and/or 17-HEXE, in the serum of patients.

After categorizing the patients depending on the bicalutamide's effect, we aimed to correlated them with the clinical outcome. However, for that purpose we could not use the Ki67-fold change as it was a continuous variable, and we needed a categorical variable. Moreover, we neither could use the first provided categorization of patient's response as most of the patients felt into the same category making it unable to perform meaningful

analysis. Therefore, we asked our collaborator, Prof. Geisler, for a categorical variable of the clinical outcome. He provided us the NeoLetExe clinical outcome determined by magnetic resonance imaging (MRI) and other clinical parameters (Methods section). Following surgery, this data was classified to determine the overall response, which was categorized into 3 primary groups: a reduction in tumor size within the range of 25% to 50%, a reduction of 50% to 90%, and a complete response (100%). The results after correlating the two identified group of patients according to bicalutamide's effect with the clinical outcome, revealed that patients classified as bicalutamide effect exhibited better clinical responses (Figure 27 B). These results suggest a potential association between the activation of the AR by either 17-HEXE or exemestane and improved clinical outcomes.

An interesting aspect of our analysis involved evaluating the relationship between the levels of EXE and 17-HEXE with the bicalutamide's effect categorization determined by the luciferase assay. Surprisingly, there was not a clear association between the individual levels of EXE, or 17-HEXE, and the effect of bicalutamide (Figure 27 C). However, there was an observed correlation between the ratio of 17-HEXE to EXE and the categorization of bicalutamide's effect (Figure 27 D). This analysis indicates that patients with a high rate of 17-HEXE relative to exemestane (more than 20%) tended to be associated with bicalutamide effect. Therefore, it seems to either exemestane or 17-HEXE from the serum of these patients is binding and activating the AR. In contrast, among the patients with a low fraction of 17-HEXE/EXE (less than 20%); the majority were categorized as no bicalutamide effect. Furthermore, these results suggest the existence of a threshold of 17-HEXE/EXE ratio to determine and predict clinical response. It seems that this threshold could be set at 20%, meaning that higher ratios could be linked to more favorable clinical response. Intriguingly, this threshold seems to be in line of what has been observed that circulating levels of 17-HEXE, comprising approximately 10-20% of the original compound in the bloodstream, seem sufficient to regulate AR-dependent activities [232].

After determining that exemestane, and/or 17-HEXE, presents in the serum of patient's, could interact with the AR, we aimed to validate this interaction *in vitro*. To explore the binding capacity of exemestane and 17-HEXE with AR, we conducted a chromatin pellet assay. This assay allowed us to identify chromatin-associated proteins. The results unveiled that 17-HEXE induces the binding of the AR to the chromatin in MCF7 cells at 2, 4, and 24 h after treatment (Figure 28). Moreover, 17-HEXE seems to have a strong affinity to the AR,

reaching similar affinity levels as the DHT, which is the natural agonist of AR [233]. It has also been proved that 17-HEXE induces stronger and earlier AR binding than exemestane. Remarkably, this increased AR binding, induced by 17-HEXE, mirrored the affinity observed with DHT, the positive control, highlighting the potency of 17-HEXE in promoting AR binding to chromatin. Finally, it is worth mentioning that these differences could be over or under represented as treatment concentrations were not homogeneous between DHT, exemestane and 17-HEXE.

The results regarding the affinity of exemestane and 17-HEXE for the AR, went in line with what has been previously reported, that 17-HEXE has strong affinity for the AR and a very weak interaction with ER. In contrast, exemestane does not show a binding capacity with ER and exhibits a weak affinity for AR [220]. Therefore, these findings reinforce the conclusion that both, 17-HEXE and exemestane, induce AR binding to the chromatin. Additionally, the prompt onset of AR binding observed at 2 h after treating with 17-HEXE suggests an earlier and more rapid effect compared to exemestane that could be driven by its higher affinity to AR. Moreover, these results reinforce our previous observations that the increment, or decrease, in the luciferase signal, upon bicalutamide administration, could be dependent on the levels of 17-HEXE and exemestane and their respective affinities for ER and AR.

After these findings, we sought to investigate the mechanisms behind the clinical outcome between patients, as the 17-HEXE/EXE ratio might not solely be the responsible for the variation in patient responses to treatment. Therefore, we expanded our inquiry to explore whether treatment efficacy could also be influenced by AR levels. Therefore, we assessed, by IHC, the % of AR-positive cells in NeoLetExe patients at baseline. Concurrently, we examined the Ki67 levels at baseline and after 2 months of exemestane treatment for the Exe-Let cohort and after 4 months of exemestane treatment for the Let-Exe cohort. Our results demonstrated a significantly strong correlation of -0.714 between the Ki67-fold change and AR expression at baseline. Therefore, patients with higher % of AR-positive cells at baseline exhibited a more favorable treatment response, reflected by a lower Ki67-fold change. In contrast, patients with lower % of AR-positive cells treated with exemestane showed a less effective response, demonstrated by a higher Ki67-fold change (Figure 29 B).

Given the limited number of patients in this study, it is challenging to definitively establish a precise threshold of the percentage of AR-positive cells that could indicate a favorable clinical response to exemestane. However, a pattern is discernible, suggesting a potential threshold between 15-20% of AR-positive cells. It appears that having a percentage of AR-positive cells exceeding 20% might predict a decrease in Ki67-fold change.

Our findings are consistent with prior research, highlighting a correlation between AR expression and positive clinical outcomes in HR-positive breast cancers. These previous studies have suggested that AR expression is linked to favorable clinicopathological characteristics [234]. Moreover, in our work we observed a co-expression of AR in numerous ER-positive tumors, aligning with prior findings [235]. However, our study highlighted a significant variance in the % of AR-positive cells among patients, with a notable portion showing minimal, or almost negligible, AR expression.

The association observed between the % of cells expressing AR and the response to treatment reveals a potential role of AR in influencing the effectiveness of exemestane treatment in ER-positive breast cancers. This suggests that the presence of AR could serve as a marker to decide whether to treat the patient with exemestane or consider alternative treatments such as letrozole. Hence, assessing the % of AR-positive cells within breast cancer tumors, before initiating exemestane therapy, could provide valuable insights for predicting treatment outcomes.

After elucidating the relevance of the fraction (expressed as %) of AR-positive cell within the tumor in the treatment with exemestane, we aimed to investigate, by ChIP-Seq, which genes, or binding sites, were regulated by AR in patients treated with exemestane. For this assay, we first assessed, by IHC, the % of AR-positive cells in the tumors of the NeoLetExe patient's cohort (Table 6). To conduct the ChIP-Seq of AR, our focus was on patients within the Exe-Let treatment sequence, aiming to prevent any potential impact from prior exposure to letrozole. Within this subset, our goal was to classify patients depending on the % of AR-positive cells, ranging from high to intermediate or low. However, we encountered challenges with patients with a low % of AR-positive cells, rendering them unsuitable for AR ChIP-Seq analysis due to inadequate AR expression for successful pull-down. Consequently, the ChIP-Seq analysis was exclusively carried out on patients exhibiting high and intermediate % of AR-positive cells, which were patients number: 2, 10, 16, 18, 20, 24 and 30.

The analysis conducted using PCA on the ChIP-Seq data indicated the presence of three distinct clusters, but we observed that two of these clusters could be merged (Figure 31 A). The first cluster, labeled as Cluster 1, consisted of patients displaying an intermediate % of AR-positive cells, including patients 10, 18, and 24. Similarly, what we identified as Cluster 2-3 comprised patients with a notably high % of AR-positive cells, encompassing patients 2, 16, 20, and 30.

Within the assessed patients, we had the Ki67-fold change data, at 2 months, for some of them (Figure 29 B). Specifically, patients 2 and 16, who exhibited a high % of AR-positive cells, clustered together and displayed a similarly low Ki67-fold change. Conversely, patient 10, demonstrating intermediate % of AR-positive cells, clustered separately and showed a higher Ki67-fold change. Intriguingly, patients categorized within Cluster 2-3 (16, 20, and 30) were also identified as subjects experiencing the effect of bicalutamide and displayed the highest 17-HEXE/EXE ratio (Figure 27 D).

So far, our findings strongly indicate that patients exhibiting a more favorable response to the treatment, as evidenced by a lower Ki67-fold change, tend to have a higher % of AR-positive cells, estimated to be approximately higher than 15-20%. Additionally, it appears that these patients also exhibit a higher ratio of 17-HEXE compared to exemestane in their bloodstream. However, our subsequent focus was on elucidating the precise mechanism by which 17-HEXE or exemestane triggers a more beneficial clinical outcome, through AR activation.

Following with the ChIP-Seq of AR, we delved into chromatin reorganization among patients from Cluster 1 and Cluster 2-3. Comparing chromatin dynamics between the baseline and after 2 months of exemestane treatment using a Venn Diagram approach, we observed notable differences in peak sharing between these timepoints and clusters. Regarding Cluster 2-3, it exhibited a reorganization of chromatin binding upon treatment with exemestane gaining 55% of chromatin binding site which were 36% of the annotated genes. In contrast, Cluster 1, only 18% of chromatin binding sites for AR were gained upon exemestane treatment, which resulted in 8% of the annotated genes (Figure 31 B and C). The variations observed between clusters indicate that there might be a distinct impact of exemestane on the regulation of the chromatin underscoring the divergent AR-mediated effects within these clusters throughout the course of exemestane treatment.

Further investigations via GSEA highlighted that pathways associated with apoptosis and negative regulation of RAS were exclusively enriched in patients from Cluster 2-3 after two months of treatment with exemestane (Figure 32 A). This data suggests that the reprogramming of AR binding to chromatin, upon exemestane treatment, seems to lead to an upregulation of pathways related to cell growth inhibition and downregulation of Ras signaling, suggesting a feasible explanation for the observed more favorable response in these patients. Such insights into the dynamic changes in AR binding to chromatin in response to exemestane enhance our understanding of the mechanisms underlying treatment responses. These findings exhibit potential for giving personalized treatment to breast cancer patients.

Regarding these results, we propose a cellular model to explain why a better response to exemestane is exhibited in tumors with higher % of cells expressing AR. It appears that this phenomenon could be related to tumor heterogeneity. Therefore, our proposed cellular model suggests the following hypothesis.

We propose that, when only a small percentage of cells within a tumor express AR, treating the patient with exemestane, primarily inhibits estrogen (E2) production, which is a well-documented mechanism of action. In this scenario, exemestane's effectiveness is primarily due to its aromatase inhibition effect. As a result, even though a significant amount of free 17-HEXE and exemestane may be present in the bloodstream, it may not have a substantial impact on tumor cells, as only a few of them express AR. Therefore, it seems that the presence of AR-expressing cells in the tumor can trigger apoptotic signals affecting neighbor cells. However, these signals have limited, or no effect, as there is a low number of cells expressing AR in the tumor, resulting in only a few apoptotic signals being sent. Thus, patients do not exhibit enhanced response to the treatment with exemestane (Figure 35, Tumor 1). With this proposed hypothesis, we suggest that the choice between letrozole and exemestane may not significantly impact the outcome in such cases, as both primarily act through their aromatase inhibition effects and they have proven to be identical.

However, in cases where the tumor has a higher % of AR-expressing cells, treating the patient with exemestane could be more effective. If the patient effectively metabolizes exemestane to its active metabolite, 17-HEXE, achieving an effective 17-HEXE/EXE ratio, it can activate the AR-expressing cells within the tumor. Consequently, AR-expressing cells could send apoptotic signals to neighbor cells, resulting in more significant cell death within

the tumor. In this situation, the increased presence of AR-expressing cells in the tumor leads to more apoptotic signals being sent, resulting in a chain reaction of pro-apoptotic factors (Figure 35, Tumor 2). In such cases, we suggest that exemestane may be a more favorable treatment option than letrozole.

These results could explain the observed general lack of cross-resistance between aromatase inhibitors. For example, the treatment efficacy for a patient who has been treated with letrozole might be exclusively due to its aromatase inhibition effect (same scenario as Figure 35, Tumor 1). However, if that patient develops resistance to letrozole, switching to exemestane could be beneficial if the patient has high % of AR-positive cells, as it might also inhibit tumor growth via AR (same scenario as Figure 35, Tumor 2).

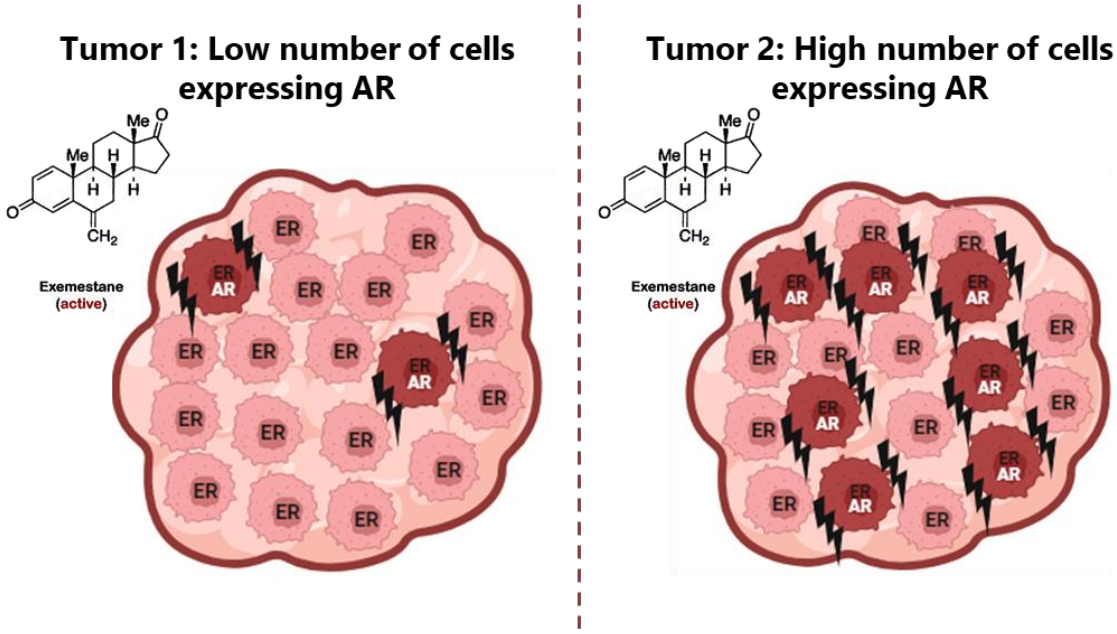

Figure 35. Schematic illustration of our proposed cellular model elucidating the enhanced response to exemestane observed in tumors with a higher % of AR-expressing cells. In the scenario of tumor 1 (depicted on the left), where a breast cancer tumor has a limited percentage of AR-expressing cells, the administration of exemestane might result in a low impact on the tumor. The presence of 17-HEXE in the bloodstream may not significantly affect the tumor since the apoptotic signals initiated by activated AR have restricted efficacy due to the low number of AR-expressing cells. Conversely, in tumor 2 (depicted on the right), characterized by a substantial number of AR-expressing cells, 17-HEXE can activate the AR of these cells. Consequently, AR-expressing cells within the tumor could transmit apoptotic signals to neighboring cells, leading to a more pronounced cell death response. This schematic representation was generated using Biorender.

Bearing this proposed model in mind, we aimed to validate *in vitro*, whether it was 17-HEXE, exemestane or the combination of both drugs what contributes to cell growth inhibition, via AR, resulting in an improved clinical outcome in patients. The observations from our experiments elucidated significant differences of 17-HEXE, exemestane and DHT in cell growth between MCF7 and MCF7-AR cells (Figure 33 C). These findings revealed

that 17-HEXE is more effective in inhibiting cell growth than exemestane and its action appears to be mediated through the AR. Nevertheless, exemestane also induced cell growth inhibition.

Administration of DHT resulted in an increase in cell proliferation in MCF7 cells, compared to MCF7-AR treated with DHT (Figure 33 C). This behavior was reported in previous studies showing that, in MCF7 cells treated with DHT, cell proliferation was enhanced. Conversely, this report also showed that treating cells with high AR expression with DHT inhibited cell growth. These findings could be explained because, in ER-positive cells with low levels of AR, DHT, through its metabolites, binds to ER and exhibits estrogenic activity [236].

Subsequently, we sought to investigate the combined impact of 17-HEXE and exemestane on cell growth inhibition (Figure 33 D). The combination of 17-HEXE with varying concentrations of exemestane, showed a significant reduction in cell proliferation in MCF7-AR cells, compared to individual treatments. Surprisingly, the most pronounced effect on cell proliferation was observed when cells were treated with 17-HEXE (5 µM) in combination with a lower concentration of exemestane (1 µM). Further experiments conducted using this combination over 7.5 days, revealed a significant decrease in cell confluence and a significant increase in cell death (%) in MCF7-AR (Figure 33 E and F). The results after conducting the same experiment at a shorter timepoint (24 h), consistently indicated a significant reduction in cell confluency and a significant increase in cell death (%) when 17-HEXE was combined with exemestane in MCF7-AR cells (Figure 33 G and H).

Overall, these findings strongly suggest a synergistic effect between 17-HEXE and exemestane, particularly in MCF7-AR breast cancer cells. The combination of these compounds, especially at a 5:1 ratio of 17-HEXE to exemestane, demonstrated, *in vitro*, a significant impact on inhibiting cell proliferation and in inducing cell death compared to individual treatments. A priori, the expected proportion of 17-HEXE to exemestane, in order to show effectiveness, was 1:5, as it was previously shown in Figure 27 D. However, this 1:5 ratio was determined by the circulating plasma levels of these compounds and, the 5:1 ratio was observed in *in vitro* assays using cell lines. Consequently, it is no surprise that the proportion between 17-HEXE and exemestane could change, as we do not know how much of the drugs present in the bloodstream finally arrive to the tumor.

Moreover, we suggest that this synergistic effect between 17-HEXE and exemestane might have been due to a possible formation of AR dimer with 17-HEXE and exemestane. Therefore, one AR monomer could bound to 17-HEXE and the other to exemestane, forming an AR dimer. This possible heterodimerization of AR could be influenced by the different affinity of these compounds to AR. In addition, this synergistic effect could reorganize the AR binding, conferring ability to bind to new chromatin sites, allowing the transcription of genes that could be related to improved treatment effectiveness. This last statement could be assessed by performing an AR ChIP-sequencing of cells treated with these drugs.

The RNA-Seq analysis comparing the single treatment with the combination of 17HEXE and Exe in MCF7-AR, revealed a synergistic effect for the combined treatment. This already observed synergistic effect seems to be due to significantly upregulated pathway of TNF-α signaling pathway via NF-κB and the apoptosis. For the TNF-α via NF-κB, the dual-specificity phosphatase 5 (Dusp5) gene stood out (Table 23 in Annex). This gene negatively regulates mitogen-activated protein kinase (MAPK) signaling pathway. It dephosphorylates and inactivates MAP kinases impacting cellular response leading to apoptosis, as demonstrated in renal cancer [237]. Additionally, low expression of Dusp5 has been related to treatment resistance and poor prognosis in breast cancer (basal like cancers) [238]. Additionally, among the upregulated genes belonging to the apoptosis signaling pathway, PMAIP1 (Noxa) stands out (Table 23 in Annex). This gene is a pro-apoptotic gene that inhibits anti-apoptotic proteins from the Bcl-2 family that promote cell death, favoring cell death pathways [239].

In summary, our results seem to indicate that for patients with high % of AR-positive cells (>20%) and also with a metabolization ratio of 17-HEXE/EXE higher than 20%; the single administration of exemestane, or in combination with 17-HEXE, is expected to be effective in reducing Ki67 levels. However, for patients with high % of AR-positive cells, but with a low 17-HEXE/EXE ratio, the double treatment might be a better therapeutic option. Nevertheless, for patients with low levels of AR-positive cells, the administration of either letrozole or exemestane should be equally beneficial.

With our results, we propose that exemestane may have a dual role. On the one hand, it affects ER activation by reducing estrogen levels through its aromatase inhibition effect. On the other, exemestane, especially through its active metabolite, 17-HEXE, may activate apoptotic pathways and intracellular signaling, impacting neighbor cells within the tumor.

This dual mechanism may lead to improved clinical outcomes and response rates. This hypothesis suggests that exemestane's unique combination of aromatase inhibition and pro-apoptotic effects may offer an advantage in specific breast cancer cases where AR-expressing cells are present in higher proportions within the tumor. Nevertheless, further research is needed to explore and validate this hypothesis *in vivo* and its clinical implications.

Further studies to delineate the precise regulatory networks influenced by AR reprogramming following exemestane treatment, could pave the way for the development of more effective therapeutic strategies aimed at harnessing these mechanisms for improved patient outcomes. Altogether, these findings introduce a novel dimension in understanding, and potentially optimizing, AI breast cancer therapy.

CONCLUSIONS I

CONCLUSIONS I

The conclusions of this chapter, dedicated to uncovering the response mechanisms to aromatase inhibitors within luminal breast cancer patients, are the following:

1. Exemestane, followed by letrozole treatment, demonstrated superior clinical outcomes, validated by exhibiting lower Ki67-fold change in the NeoLetExe cohort.

2. Biochemical data analysis confirmed that exemestane exhibits similar aromatase inhibition to letrozole, demonstrated by the reduction of estrogen levels in patients' bloodstream.

3. Both exemestane and 17-HEXE interact with the AR, confirmed through luciferase assays and chromatin pellet.

4. High percentage of AR-positive cells showed a more favorable response, exhibiting low Ki67-fold change, to exemestane treatment by altering AR binding to chromatin and upregulating apoptosis pathways.

5. Synergistic effects and enhanced cytotoxicity of 17-HEXE combined with exemestane in AR-overexpressing breast cancer cells were demonstrated.

CHAPTER II

IDENTFIYING TRANSCRIPTION FACTORS RESPONSIBLE FOR METASTASIS DEVELOPMENT UPON AROMATASE INHIBITORS TREATMENT

INTRODUCTION II

1. Metastatic breast cancer

Breast cancer metastasis occurs in a cascade process starting with local invasion of surrounding tissue spreading into the blood, or lymphatic vessels, and ending with dissemination of tumor cells to distal organs [240]. The different breast cancer subtypes exhibit distinct metastatic patterns, with a preference for specific distant sites. For instance, luminal breast cancer frequently metastasizes to the bone (50-70%), liver (20-30%), lung (15%), and brain (10-30%) [241].

Metastasis is a complex process that consist of the spread of cancer cells from the primary tumor to distant sites. It often leads to treatment failure and patient mortality, significantly impacting cancer prognosis [242]. Approximately, 30% of breast cancer patients eventually develop metastatic disease and in 10-15% of patients, metastasis occur within the first 3 years after diagnosis. Only 6% of breast cancers are metastatic when they are diagnosed [243].

Metastasis involves intricate cellular mechanisms, including the critical process of epithelial-mesenchymal transition (EMT). EMT entails the transformation of epithelial cells into mesenchymal ones, endowing them with migration and invasion capabilities. This transition is a reversible process, as cells can undergo mesenchymal-epithelial transition (MET) at distant sites. Indeed, EMT is associated with alterations in cell behavior, gene expression, and morphology, impacting the invasive potential of breast cancer cells [244].

In EMT, transcription factors (TFs), which are proteins that control gene expression by binding to chromatin, play an essential role in cancer progression and metastasis. Particularly, EMT is regulated by TFs like Snail, Slug, Twist, and zinc finger E-box-binding (ZEB), as well as cytokines such as interleukin-6 (IL-6) [245]. In addition, recent studies have demonstrated that the loss of expression, or dysfunction, of GATA3 promotes breast cancer metastasis by regulating G9A and metastatic tumor antigen (MTA) family proteins recruited by ZEB2 [246]. In breast cancer, ER is connected with EMT by impacting the TFs governing this process. This influence leads to increased cell aggressiveness and proliferation, ultimately causing a transition towards a mesenchymal phenotype and the adoption of an EMT status. For instance, when dealing with endocrine resistance, the

suppression of ER can activate EMT, resulting in alterations in gene expression and cellular behavior [247].

Furthermore, cell migration, particularly during EMT, is characterized by dynamic interactions between cells and their microenvironment. The tumor microenvironment (TME) has an impact on metastatic breast cancer through immune and non-immune cells, including cancer-associated fibroblasts (CAFs), tumor-associated macrophages (TAMs), immune cells, adipocytes, and endothelial cells. These components have the potential to induce tumor growth, invasion, and metastasis, by releasing cytokines, chemokines, and growth factors, among other mechanisms [248]. In addition, epigenetic changes such as DNA methylation and histone modifications are linked to breast cancer metastasis, affecting gene expression and tumor suppressor genes. As a treatment option for metastatic breast cancer, strategies targeting these epigenetic alterations using DNA methyltransferase (DNMT) and histone deacetylase (HDAC) inhibitors are being investigated [249].

2. Study of the development of resistance to AI therapy

To explore the reason why patients who received aromatase inhibitors (AIs) eventually developed metastases and ceased to respond to the therapy, samples of luminal primary tumors were collected. Patients were pre-menopausal women with primary tumors treated with adjuvant hormone therapy. In particular, these patients were closely monitored over, at least, 5 years during which they were administered tamoxifen for the first 2 years and given AIs (mostly letrozole) for the following 3 years. Following this timeframe, certain patients failed to respond to the treatment and experienced the development of metastases. Metastatic samples were collected for an in-depth examination of the molecular mechanisms behind treatment resistance (Experimental models section in Methods).

OBJECTIVES II

The second research project of this Ph.D. was dedicated to investigating the factors responsible for the development of resistance upon treatment with aromatase inhibitors in luminal breast cancer patients. The main objectives of this study were the following:

1. To understand the underlying mechanisms to the loss of responsiveness to aromatase inhibitors.

2. To unveil the existing disparities between primary and metastatic tumors upon aromatase inhibitor treatment.

3. Explore the transcriptional regulators contributing to the emergence of metastasis in patients undergoing aromatase inhibitor therapy.

RESULTS II

1. Epigenetic modifications in paired samples are associated with resistance to endocrine treatment

1.1. Origin of FFPE samples and overview of the Fit-Sequencing technique

To delve into the mechanisms causing the loss of responsiveness to aromatase inhibitors (AIs), we conducted an epigenetic analysis of paired samples (primary and metastatic). This analysis aimed to identify transcriptional regulators that might elucidate the reasons behind the ineffectiveness of the treatment. To accomplish this, we examined samples from pre-menopausal women with primary breast tumors who had received adjuvant hormone therapy for 5 years. Our focus was on patients who failed to respond to the treatment and developed metastases. We utilized formalin-fixed paraffin-embedded (FFPE) samples (n=5) obtained from both the primary and metastatic tumors within the same patient (Experimental models in Methods) (Figure 36 A).

FFPE samples are commonly used in the clinical setting and have an enormous potential for epigenomic analysis. However, traditional chromatin analysis methods struggle with these samples due to excessive cross-linking from formalin. To analyze FFPE samples, we performed experiments as reported by Cejas, P. (2016) and Font-Tello, A. (2019) who designed a protocol to address this challenge and created a new technique called fixed-tissue chromatin immunoprecipitation sequencing (Fit-Seq) [250]. This innovative protocol significantly improves chromatin solubilization without compromising the histone mark's integrity. Fit-Seq has unlocked the potential of FFPE samples for epigenetic analysis. Particularly, it is a valuable method for analyzing histone marks in FFPE clinical tissue samples. It has been used to identify specific chromatin states and enhancers in various tumor types, including colorectal, breast and bladder carcinomas exhibiting robust performance [251].

In our study, we employed Fit-Seq to identify epigenetic changes associated with active transcription that could account for the lack of response to AI treatment. Specifically, we used the H3K27actylation (H3K27ac) histone mark as an epigenetic marker of activated regulatory regions. H3K27ac enabled us to profile transcriptionally activated enhancers, promoters, and proximal, or distal, transcription start site (TSS). This approach allowed us to gain insights into the molecular mechanism of the observed treatment resistance in breast cancer patients.

The Fit-Seq protocol was adapted particularly focusing on refining the sonication step (Figure 36 B). Next, samples were sequenced and underwent a quality assessment to ensure the reliability of the data (data not shown in the thesis). Subsequently, we proceeded to conduct the bioinformatic analysis of the Fit-Seq data.

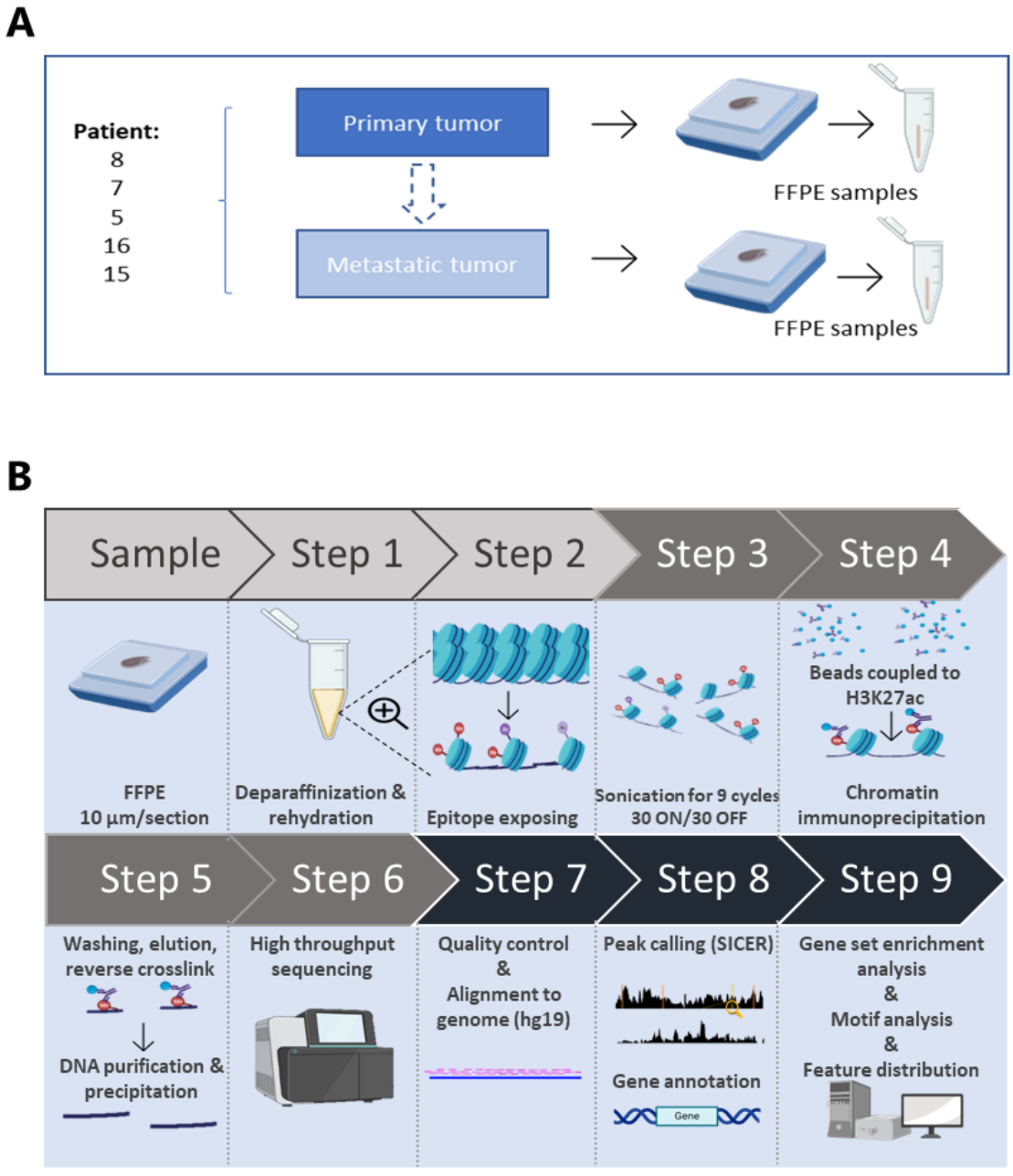

Figure 36. Overview of the paired samples cohort and experimental and bioinformatic workflow. (A) Diagram illustrating a paired sample cohort, consisting of pre-menopausal women who received a 2-year treatment with tamoxifen followed by 3 years of AI therapy. Formalin-fixed, paraffin-embedded (FFPE) samples were acquired from the primary tumor and the metastatic tumor. **(B)** Diagram outlining the experimental process for Fit-Seq, encompassing steps such as deparaffinization, rehydration, epitope exposure, sonication, and ChIP-sequencing. The Fit-Seq data analysis pipeline encompasses various quality control assessments, genome alignment, peak identification, gene annotation, and subsequent downstream analyses.

1.2. Fit-Seq analysis of paired tumor samples identified transcriptional regulators that could explain the lack of response to the treatment

To identify binding sites in the genome with enriched aligned reads, we conducted a peak calling (SICER) of the Fit-Seq data of primary and metastatic tumors for each patient (Table 9). Subsequently, we combined the obtained peaks from all primary and metastatic patients into two datasets and compared their overlapping using a Venn diagram (Figure 37 A). This comparison revealed a reorganization of chromatin binding sites. Indeed, there was a gain and loss in modified chromatin between the primary and metastatic tumors, which entails a gain and a loss of transcriptionally active regions. The identified binding sites were annotated to the human genome (hg19) with a 3 kb distance from the TSS for each patient and timepoint (Table 9). Subsequently, the individual annotated genes for all patients were combined and their overlapping was compared using a Venn diagram (Figure 37 B). These analyses indicated that, over the course of the treatment, transcriptional activity of certain genes in the primary tumors changed in the metastatic setting. Nevertheless, a subset of 1250 genes remained unaltered, while 292 genes, without prior presence in the primary tumor, were activated in the metastatic one. In addition, there were 6157 genes that were lost in the metastatic setting but were present in the primary tumor. This suggests that changes in the assessed transcriptionally active epigenetic markers could be related to a lack of response to AIs and, thus, relapse.

Table 9. Summary of the number of peaks identified by SICER and the number of genes annotated from these peaks. Each patient is represented by its patient number and timepoint (P = primary tumor, M = metastatic tumor).

Patient number	SICER peaks	Annotated genes
5P	12571	7108
5M	22989	11566
7P	13194	7107
7M	11389	7081
8P	9097	4469
8M	5448	4043
15P	37172	11899
15M	10989	5799
16P	3723	2987
16M	15269	7069

Furthermore, our analysis continued by performing a Principal Component Analysis (PCA) to see if it was possible to identify a visual difference between primary and metastatic tumors; and if different patients followed similar trends. This technique exhibited a remarkable shift between primary and metastatic tumors for the majority of patients (Figure 37 C). This difference in distance between the two timepoints means that there is great variance between the primary and metastatic tumors and reinforces the idea that there are epigenetic modifications of transcriptional activity throughout the treatment.

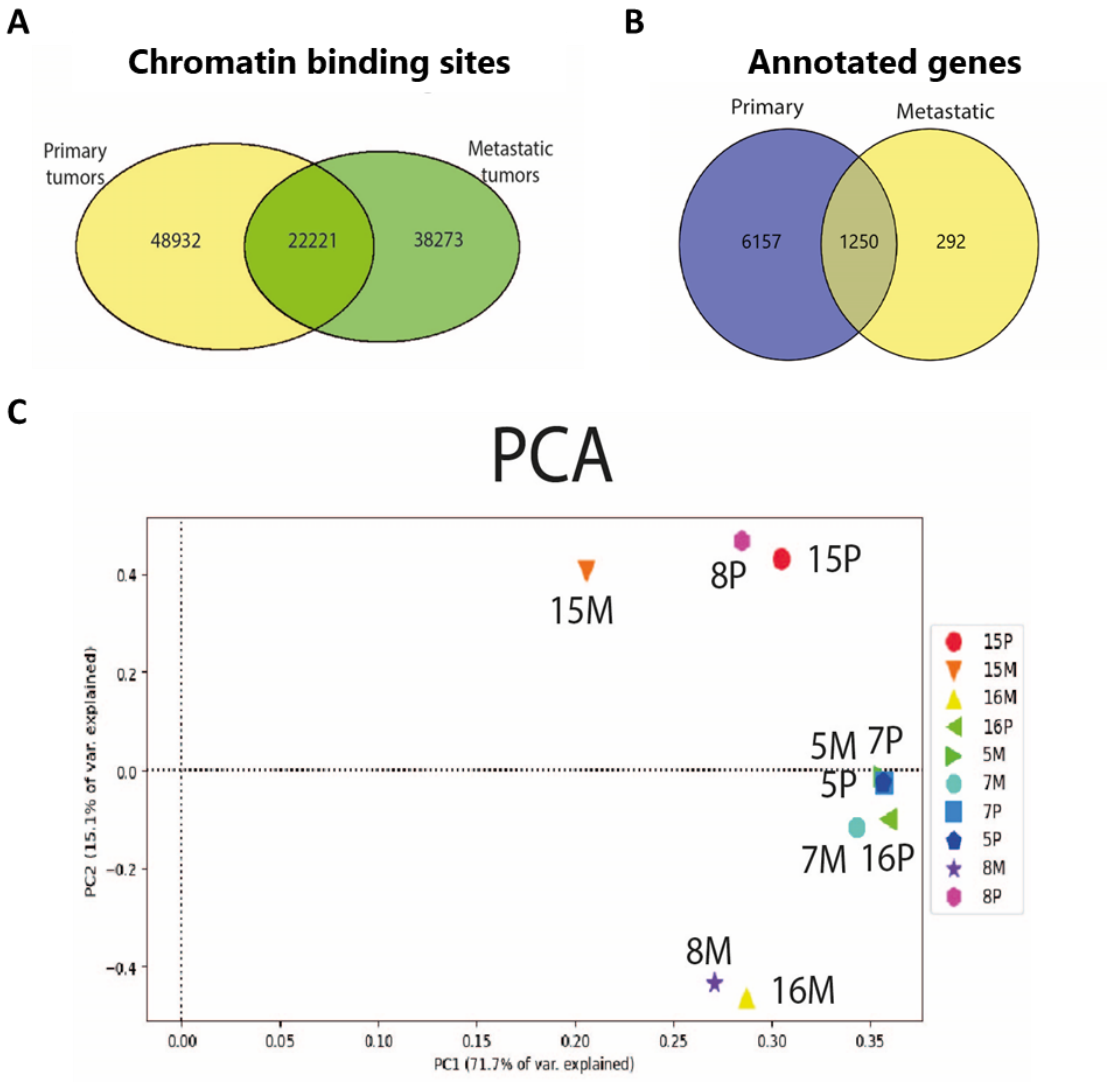

Figure 37. Fit-Seq analysis of paired tumor samples. (A) Venn diagram of SICER peak calling of primary and metastatic tumors. It can be observed a distribution of transcriptionally active chromatin binding sites throughout the treatment. **(B)** Venn diagram comparing primary and metastatic annotated gens from the peak calling. **(C)** Principal Component Analysis (PCA) of primary and metastatic tumors shows a great variance between timepoints for each patient.

From all these annotated genes, it can be observed how, upon metastasis, there is a massive reduction in the number of actively transcriptional genes. Therefore, our focus was on understanding the transcription factors (TF) responsible for this loss in the metastatic tumor. Consequently, we studied the common genes that are present in both settings and assess which ones have significantly changed their expression. Thus, we performed a pathway analysis of the Fit-Seq data to identify in which biological pathways these genes are involved. The first step of this analysis was to remove all the genes that did not belong to the cancer hallmarks gene sets form the Molecular Signatures Database (MSigDB). The Gene Set Enrichment Analysis (GSEA) was performed for the primary and metastatic tumors and the obtained pathways were ranked in descending order of the net enrichment score (NES). Therefore, the most overexpressed pathways were in the first positions and the most under-expressed ones were at the bottom. Then, we merged the two GSEAs to see how each pathway changed its position between primary and metastatic tumors, to find the ones that had the biggest win and loss of positions. Regarding the pathways with the largest positive change in position in the metastatic setting, we can find various pathways related to immune response (Figure 64 in Annex). Regarding the pathways with the biggest negative change in position the metastatic setting, we identified pathways related to histone modification, histone methylation and peptide methylation (Figure 38 A). This suggests that pathways related to methylation and histone modification were altered throughout the therapy. These findings suggest that these genes, despite being present in the primary and in the metastatic tumor, have decreased their expression.

To validate these results, the enrichment plots at both stages (primary and metastatic) were plotted for each of the three pathways (Figure 38 B). In each plot, we can see a red line which represents the enrichment score of the pathway on the point where it crosses the green distribution. As it can be seen, in each pathway, the net enrichment score is higher in the primary tumor than in the metastatic one. For example, for the histone methylation pathway the NES in the primary tumor is equal to 1.74 and in the metastatic tumor is equal to 1.42. This representation elucidates the fact that these pathways are overrepresented in the primary tumor and then they suffer a loss in expression the metastatic setting.

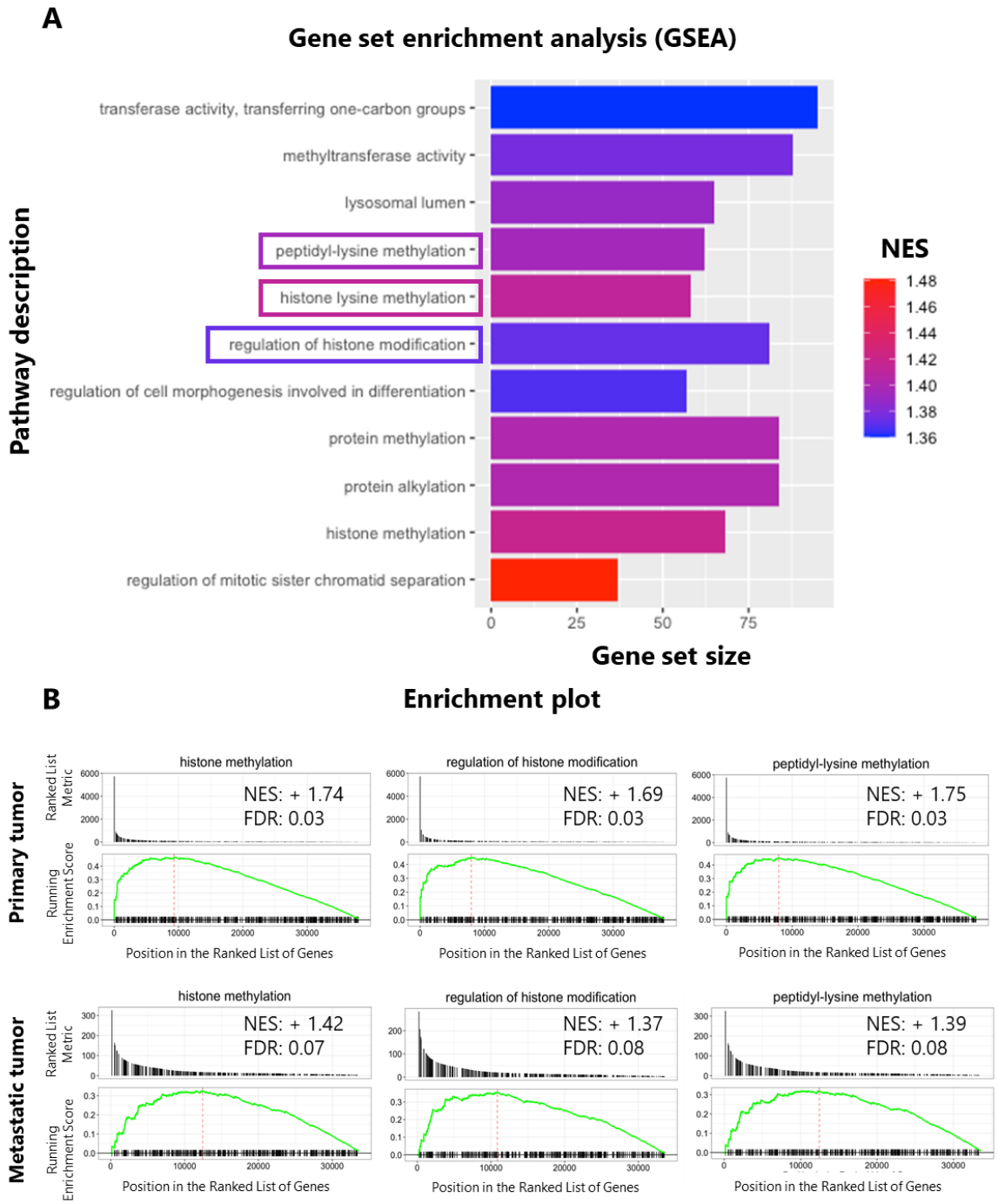

Figure 38. Gene Set Enrichment Analysis of the pathways with a biggest loss in NES ranking between primary and metastatic tumors. (A) Pathways with biggest loss of rank between primary and metastatic tumor for the GSEA of common genes from the cancer hallmark gene set. The length of the bars represents the gene set size of each pathway and the color is the net enrichment score (NES). **(B)** Enrichment plots showing the distribution of the running enrichment score (bottom plot) for each pathway and for primary and metastatic tumors. The point where the red line crosses the green distribution is the net enrichment score (NES) for the pathway. The upper plot is the ranked pathways, and the intersection of the red lines tells where this pathway is in the list of all ranked pathways. The numerical values of the NES and the false discovery ratio (FDR) are displayed on each graph.

Having identified these relevant pathways, we proceed to study the overlapping between the genes from each of the three pathways. This was performed to identify if there was a common gene (or set of genes) that could be responsible for the lack of response to the treatment. These overlaps were calculated using a Venn diagram between the three pathways, which obtained 14 common genes (Figure 39 A). These 14 genes that were possible transcription factors regulators that could be involved in the development of the metastasis were: DNMT1, WDR5, LMNA, DNMT3B, MACROH2A1, SMARCB1, AUTS2, JARID2, GATA3, PRDM12, NSD3, NNMT, EHMT2 and SUPT6H.

To further filter this set of genes, and see which ones could be more closely involved with the lack of response to the treatment, we compared these 14 genes to unpublished Nanostring data from the group, also performed in the analyzed patients [252]. Expression of mRNA was measured by using Nanostring technology with a list of genes associated with poor prognosis in groups of ER-positive patients. From these 14 genes, only GATA3 appeared in the list of poor prognosis markers.

After this surprising finding, we proceeded to assess which was the GATA3 expression for each patient and timepoint in the Nanostring dataset (Figure 39 B). From this plot, no remarkable trend among all patients can be identified as the expression levels of GATA3 drop in two patients and go up in three of them.

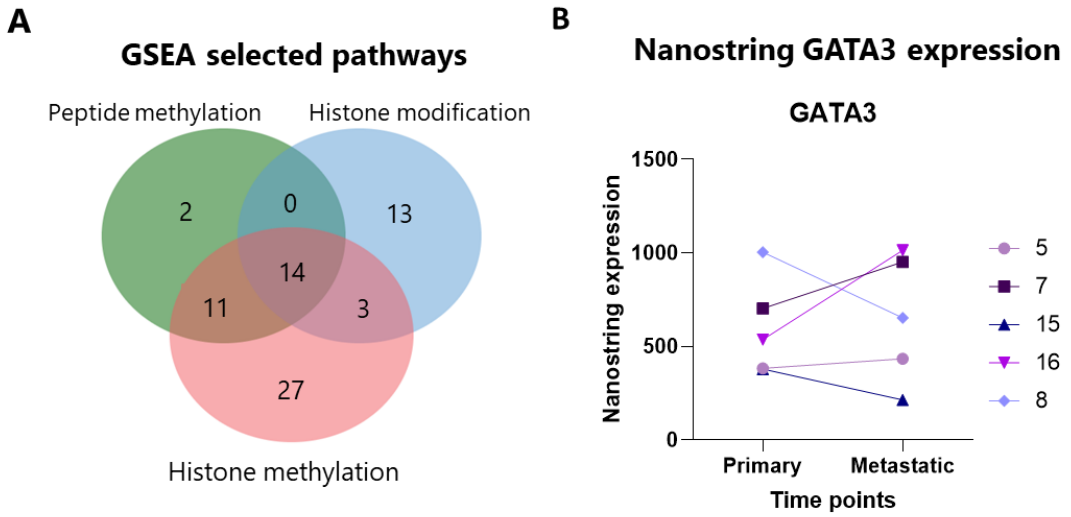

Figure 39. The transcription factor GATA3 could play a role in the development of metastasis. (A) Venn diagram comparing the common genes between primary and metastatic gene sets for the following pathways: peptidyl-lysine methylation, regulation of histone modification and histone methylation. There are 14 genes in common for all three pathways that may be involved in the development of metastasis throughout the treatment. **(B)** Nanostring expression data of GATA3 for 5 patients at primary and metastatic timepoints reveals no remarkable overall trend.

1.3. GATA3 is a key transcription factor in breast cancer

What is known about the implications of GATA3 in the metastasis is that it forms a complex with Metastasis Associated 3 (MTA3), a component of the Nucleosome Remodeling and Deacetylase (NuRD) complex. The NuRD complex plays a critical role in breast cancer progression. This complex consists of various subunits with enzymatic and non-enzymatic functions that regulate chromatin assembly and reorganization.

It has been demonstrated that the specific composition of the NuRD complex, might contribute to cell migration and invasiveness [246]. In this regard, we hypothesized that GATA3/NuRD complex with MTA1 might promote a metastatic phenotype. By contrast, a GATA3/NuRD complex with MTA3 might promote a non-metastatic phenotype. Therefore, tumors that gain expression of MTA1 might be more susceptible to induce metastasis. To test this hypothesis, we compared reads signal intensity for MTA1 and MTA3 identified in the primary and in the metastatic tumors of the same patients. Cumulative signal intensity of the peaks around the TSS (± 500b) was plotted (Figure 40). It can be seen that, for MTA1, the signal in metastatic tumors was consistently higher than in the primary tumors (60%) and for the other 40% of patients, the signal remained constant. In contrast, for MTA3 (80%) the signal in primary tumors was above the signal in metastatic tumors. Therefore, our data seems to indicate that MTA3 expression increased in primary tumors, whereas MTA1 seems to be mainly present in metastatic tumor.

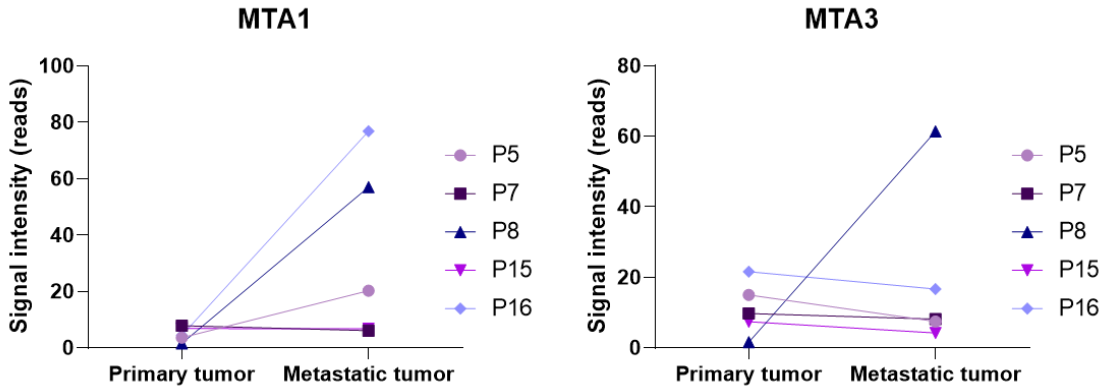

Figure 40. MTA3 was mainly present in primary tumors, whereas MTA1 seems to be mainly present in metastatic tumor. Cumulative signal intensity of the peaks around the TSS (±500b) of the 5 assessed patients at each timepoint showed an imbalance between the MTA1 and MTA3 levels.

These intriguing findings prompted us to question whether variations in the levels of MTA1 or MTA3 proteins could impact the invasive and migratory capabilities of breast cancer cells and whether this was influenced, or dependent, on aromatase inhibitors (AIs).

2. Functional experiments reveal that MTA1 and MTA3 are implicated in cell migration and invasion

2.1. *In vitro* validation of the NuRD complex dynamics was confirmed in non-invasive breast cancer cells

To confirm the previously explained hypothesis, an *in vitro* experiment was conducted using MCF7 cells, which represent non-invasive breast cancer cells. In this experiment, cells were subjected to transient siRNA-mediated silencing of MTA3 or MTA1. Afterwards, the levels of their respective proteins and mRNAs at 48 h were assessed through western blot and RT-qPCR analysis (Figure 41 A). Notably, when MTA1 was depleted, we observed an increase in both MTA3 mRNA levels and protein. Conversely, the depletion of MTA3 led to a slight increase in MTA1 protein levels (Figure 41 C and D), but a significant increase in MTA1 mRNA levels (Figure 41 B). These findings confirmed that MTA1 and MTA3 are influenced by each other in our *in vitro* model, as previously proposed [246].

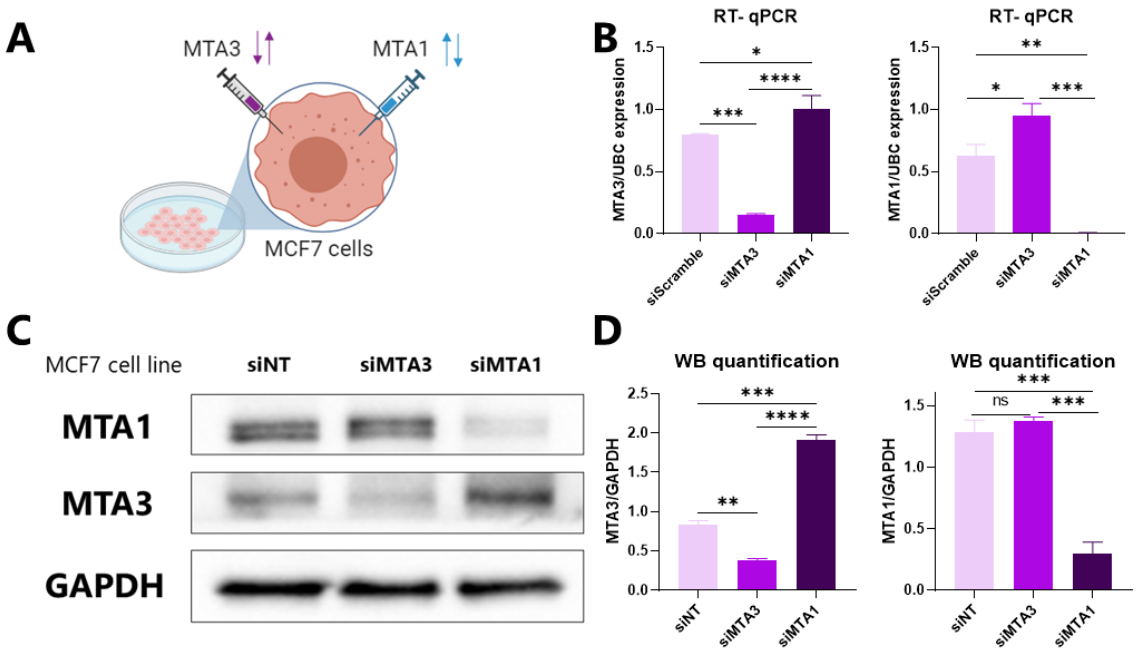

Figure 41. *In vitro* validation of the influence between MTA1 and MTA3 expression within the NuRD complex. **(A)** Illustration representing depletion or overexpression of MTA1 and MTA3. **(B)** Quantification of MTA3 and MTA1 RNA expression normalized against the reference gene UBC using RT-qPCR. Data is presented as the mean ± standard deviation (SD) (n=3). Statistical significance was evaluated using a One-Way ANOVA multiple comparison test (Tukey's). **(C)** Validation of the influence between MTA1 and MTA3 by assessing their protein expression. GAPDH was used as a loading control. **(D)** Quantitative analysis of the western blot results presented in (C) (n=3). Data is presented as the mean ± standard error mean (SEM) Statistical significance was evaluated using a One-Way ANOVA multiple comparison test (Tukey's).

2.2. HDAC1 interacts with ER and GATA3 as part of the NuRD complex regardless of the levels of MTA1 and MAT3

The NuRD complex is composed of various subunits, among them, histone deacetylase (HDAC) 1 and HDAC2 subunits are responsible for histone deacetylation. To further investigate the components of the NuRD complex, we aimed to explore the physical interactions of the NuRD complex involving MTA1 and MTA3. Previous research demonstrated that GATA3 is physically associated with G9A and the NuRD (MTA3) complex and that it only interacts with MTA3. The same report showed that MTA1 and MTA3 both interact with HDAC1 [246]. However, the contribution of GATA3 interacting with MTA1 at NURD complex has not been investigated yet.

Consequently, we conducted immunoprecipitation (IP) experiments of HDAC1. The IP assays were performed under 3 different conditions: in MCF7 control transfected cells (with a non-targeting siNT), silenced MTA3, and silenced MTA1. Our findings revealed that GATA3 interacts with HDAC1 under all 3 conditions (Figure 42). Additionally, it was observed that ER also exhibits a physical interaction with HDAC1 under these same conditions. These results suggest that, in the NuRD complex component, HDAC1 is physically associated with GATA3 in three conditions and indicate that ER may also be engaged in a physical interaction with HDAC1.

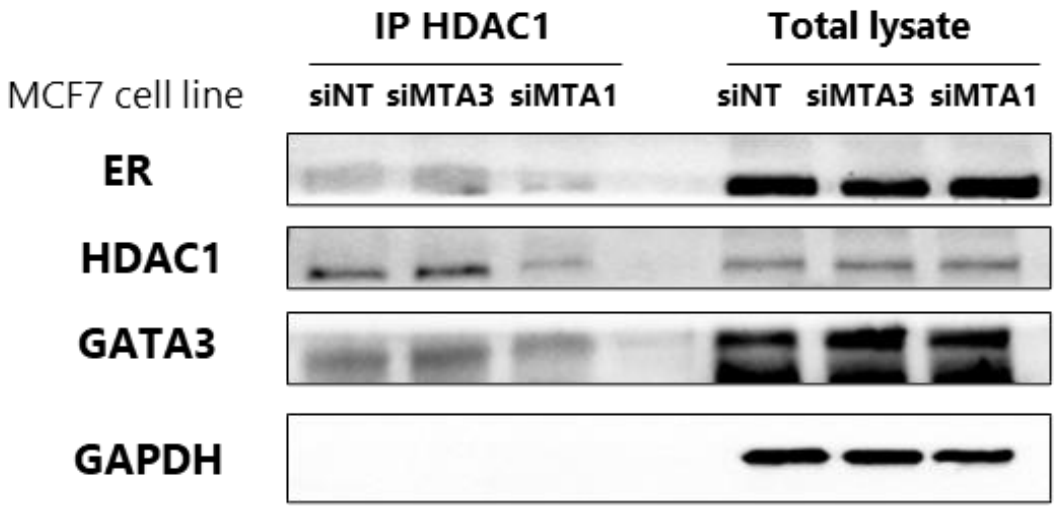

Figure 42. HDAC1 interacts with ER and GATA3 regardless of MTA1 and MTA3 levels. Western blot analysis demonstrates the levels of the specified proteins (on the left) in total cellular lysates and anti-HDAC1 immunoprecipitated (on the right) obtained from MCF7 cells following transfection with the designated siRNAs for 48 h. GAPDH was utilized as a loading control. IP indicates immunoprecipitation.

2.3. Proliferation is not affected by the MTA1 - MTA3 imbalance

After confirming that MTA1 and MTA3 influence each other's expression, and verifying a physical interaction between ER and GATA3 with HDAC1 within the NuRD complex, we sought to investigate the potential impact of the MTA1-MTA3 imbalance on cell proliferation. To explore this, we assessed cell proliferation by conducting a crystal violet assay 48 h after silencing MTA1, or MTA3, in MCF7 cells. This experimentation was carried out under 2 distinct growth conditions. One of them involved using red medium supplemented with fetal bovine serum (FBS) at 5% (red medium) and the other involved using white medium supplemented with 5% charcoal-stripped FBS (white medium). More precisely, white medium does not contain hormones whereas red medium does.

The results from our proliferation analysis demonstrated that there were no significant differences in cell proliferation when either MTA1 or MTA3 were depleted, regardless of whether we employed medium with or without hormones (Figure 43 A and B). This experiment leads us to conclude that the NuRD complex does not play a role in proliferation, irrespective of the levels of MTA1 or MTA3.

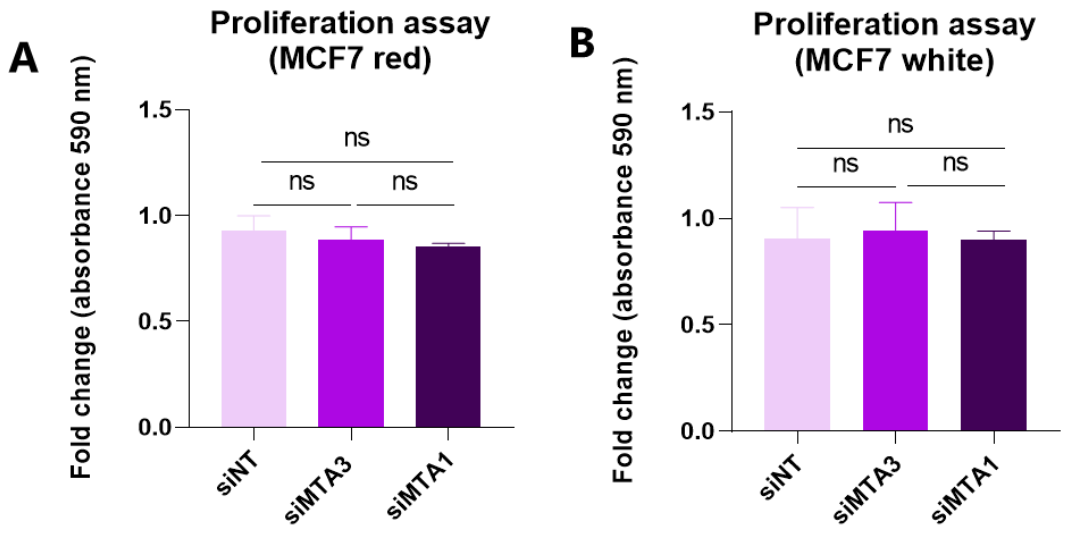

Figure 43. The MTA1 - MTA3 imbalance does not affect proliferation. **(A)** Crystal violet assay results conducted medium with hormones (red) shows no significant difference in the proliferation rate 48 h after silencing either MTA1 or MTA3. The bar chart illustrates the fold change between the absorbance at 590 nm for MTA1 or MTA3 compared to the absorbance of the control (siNT). The data is presented as the mean ± SEM (n=3). Statistical significance was assessed using a One-Way ANOVA multiple comparison test (Tukey's). **(B)** Crytal violet assay results conducted under white medium shows no significant differences in proliferation rate. The data is represented under the same conditions as described in (A).

2.4. *In vitro* validation of the NuRD complex reveals a change in migration when the balance of MTA1 and MTA3 is altered

To determine any impact of MTA1-MTA3 imbalance on cell migration, we depleted the levels of MTA1 and MTA3 in MCF7 (reduced migratory capacity), to assess their impact on cell migration. Migration assays were conducted under medium with and without hormones. We quantified cell migration by carrying out wound healing experiments within IBIDI chambers to create consistent wounds. The results of the migration assays were represented by evaluating the wound closure fold change, calculated as the ratio of the initial length to the length after 24 h. Essentially, when cells migrated extensively, the wound distance decreased, resulting in a smaller fold change value. Conversely, when cell migration was limited, the wound closure distance did not have a great variation, leading to a fold change closer to 1.

In MCF7 cell line, in medium with hormones, the depletion of MTA3 led to a significant increase in cell migration, while depletion of MTA1 resulted in reduced cell migration (Figure 44 A and C). Similar trends were observed in medium without hormones (Figure 44 B and D). These findings strongly suggest that an imbalance between MTA1 and MTA3 has a substantial impact on cell migration. Specifically, when MTA3 levels were depleted, resulting in increased MTA1 levels, it led to a more migratory cell phenotype. Conversely, when MTA1 was depleted, resulting in higher levels of MTA3, MCF7 cells displayed reduced migratory capacity in medium with and without hormones.

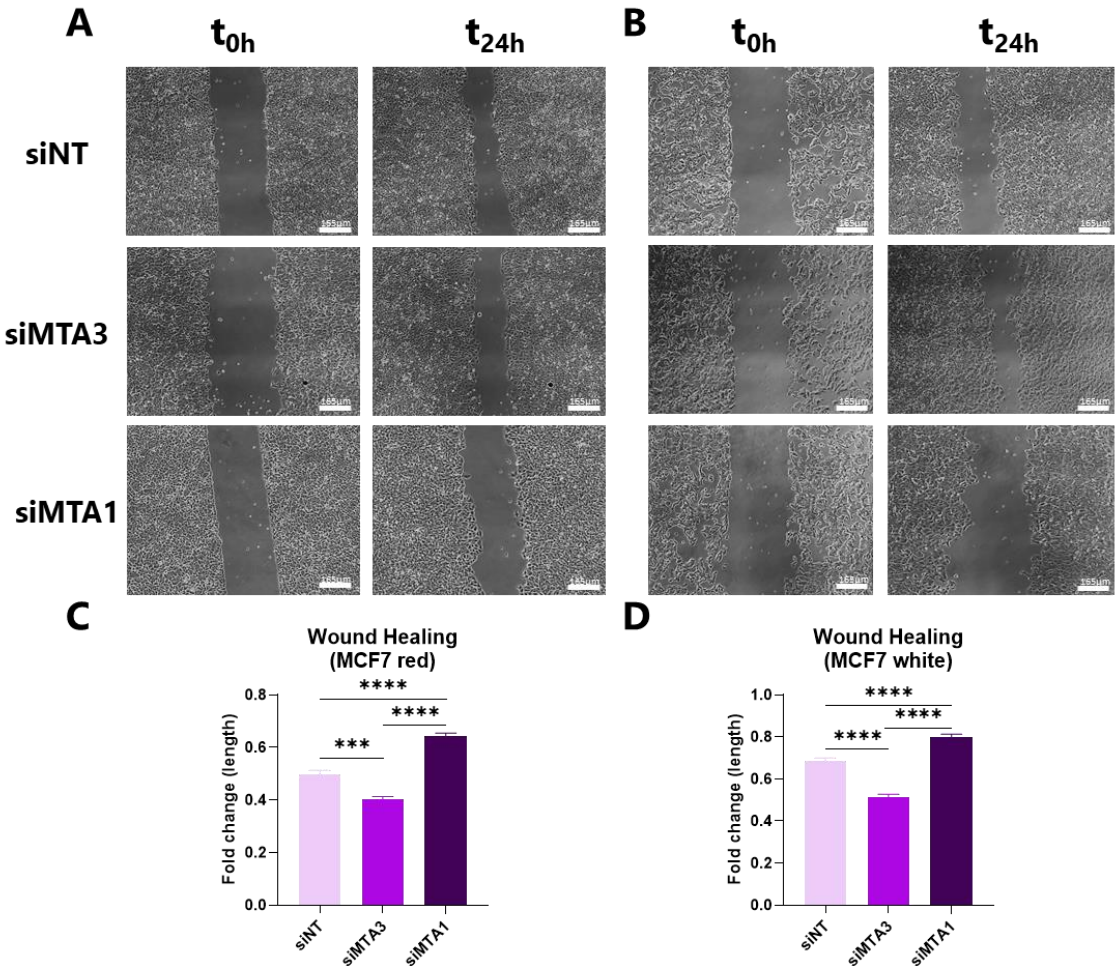

Figure 44. Influence of MTA1 and MTA3 imbalance on MCF7 in cell migration. **(A)** A wound healing assay was conducted in MCF7 cells, demonstrating increased wound closure when MTA3 is silenced under red medium (hormones) conditions. Images were captured at the start and 24 hours after creating the wound. The scale bar is 165 µm. **(C)** The data is presented as the mean ± SEM (n=4). The bar chart illustrates the change in wound length after 24 hours compared to the initial measurement. Statistical significance was assessed using a One-Way ANOVA multiple comparison test (Tukey's). **(B)** Migration assay carried out in MCF7 cells revealed more closure of the wound when MTA3 is depleted in white medium (no hormones). Wound healing imaged were taken under same conditions as in (A). **(D)** The quantification of wound healing results in (B) follows the same parameters as described in (C).

To further validate the impact of an imbalance between MTA1 and MTA3 on cell migration, we conducted additional experiments involving the overexpression of MTA1 and MTA3. We confirmed the overexpression of MTA1 and MTA3 through both western blot (Figure 45 A and B) and RT-qPCR techniques (Figure 45 C). The migration assay was conducted using MCF7 cells under mediums with and without hormones. Migration assay was assessed by quantifying the wound closure fold change as a graphical representation, determined by calculating the ratio of the initial length to the length after 24 h. The results of this experiment showed that in cell growth media, overexpression of MTA3 led to a

notable reduction in cell migration, whereas the overexpression of MTA1 resulted in increased cell migration (Figure 45 D and F). This observed trend persisted in medium without hormones (Figure 45 E and G). These findings strongly indicate that an imbalance between MTA1 and MTA3 significantly impacts cell migration. This implies that in scenarios where MTA1 levels are elevated, the NuRD complex is more likely to associate with MTA1, ultimately enhancing the migratory potential of the cells.

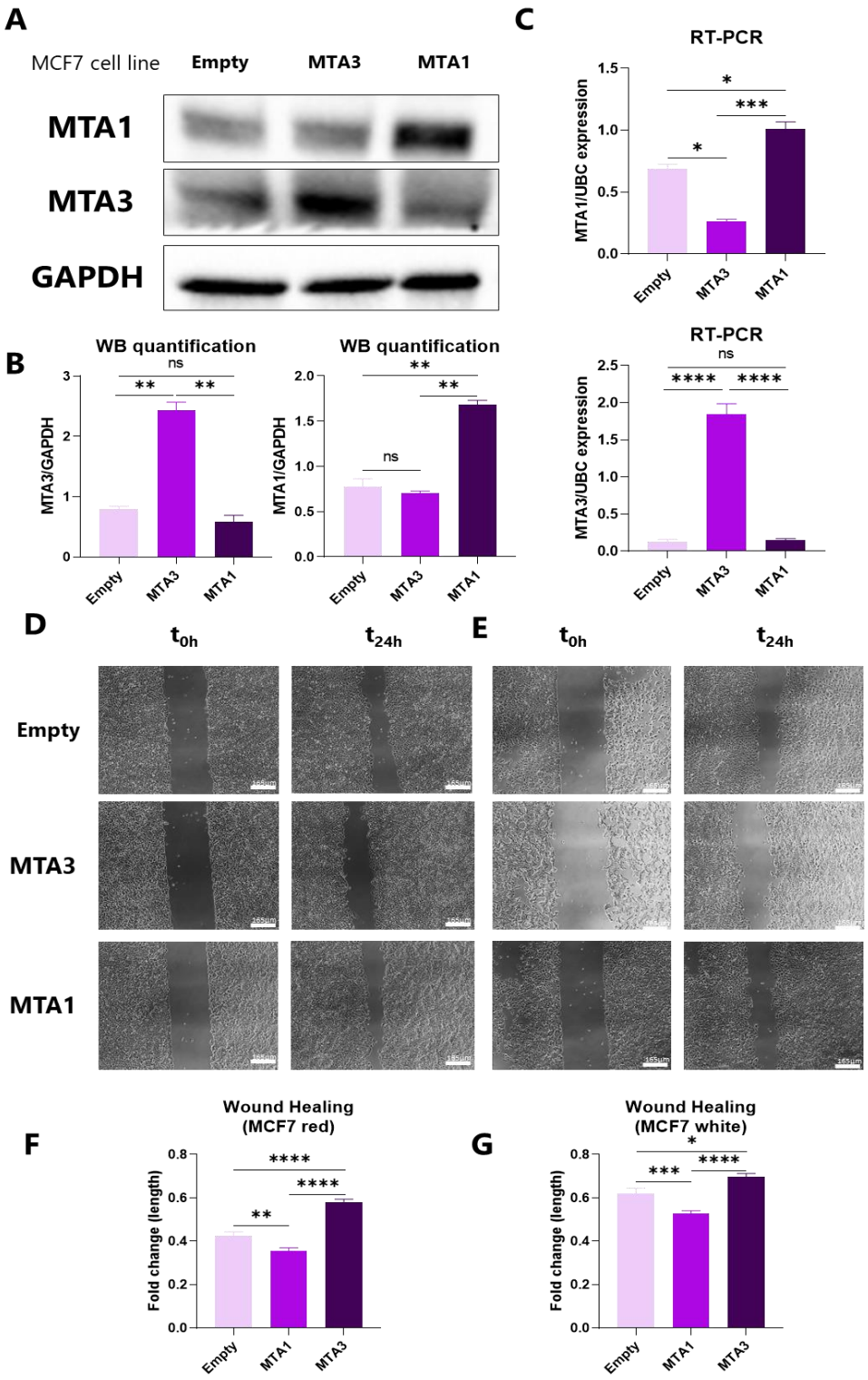

Figure 45. Influence of MTA1 and MTA3 imbalance on MCF7 cell migration. **(A)** Validation of the influence between MTA1 and MTA3 protein overexpression. GAPDH was used as a loading control. **(B)** Quantitative analysis of the western blot results presented in (A) (n=3). Data is presented as the mean ± standard error mean (SEM) Statistical significance was evaluated using a One-Way ANOVA multiple comparison test (Tukey's). **(C)** Quantification of MTA3 and MTA1 RNA expression normalized against the reference gene UBC using RT-qPCR. Data is presented as the mean ± SEM (n=3). Statistical significance was evaluated using a One-Way ANOVA multiple comparison test (Tukey's). **(D)** A wound healing assay was performed in MCF7 cells, demonstrating enhanced wound closure when MTA1 was overexpressed under red medium (hormones) conditions. Images were taken at the beginning and 24 h after creating the wound. The scale bar represents 165 µm. **(F)** The data is represented as the mean ± SEM (n=3). The bar chart illustrates the change in wound length after 24 h compared to the initial measurement. Statistical significance was evaluated using a One-Way ANOVA multiple comparison test (Tukey's). **(E)** Migration assay conducted in MCF7 cells showed increased wound closure when MTA1 was overexpressed in a white medium (no hormones). Wound healing images were captured under the same conditions as in (D). **(G)** The quantification of wound healing results in (E) follows the same criteria as described in (F).

In summary, the results in this section support the validity of the NuRD complex hypothesis, proven in non-invasive cell lines such as MCF7. Additionally, it appears that the ability of cells to migrate is governed by the NuRD complex, influenced on whether it is bound to MTA1 or MTA3.

2.5. *In vitro* validation of NuRD complex hypothesis reveals a change in invasiveness when the balance of MTA1 and MTA3 is altered

Next, we investigated how altering the balance between MTA1 and MTA3 affects cell invasiveness. To accomplish this, we conducted an invasion assay using MCF7 cells, which have a reduced invasion capacity. This assay was performed under 2 different conditions: red medium (with hormones) and white medium (without hormones). In this experimental setup, we generated spheroids composed of cells depleted of either MTA1 or MTA3, which were subsequently embedded in Matrigel. In the invasion assay, we examined the cells' capacity to penetrate the Matrigel matrix and proliferate within it. Microscopic recordings were made at 30-minute intervals over a span of 72 h. Evaluation of invasion outcomes occurred at 4 timepoints: 0, 24, 48, and 72 h post-embedding. To visualize and analyze the data, we graphically presented the invasiveness area of the spheroids. This was achieved by calculating the ratio of the spheroid's initial area (0 h) to its area at each timepoint (24, 48, and 72 h). Essentially, when the cells displayed extensive invasion, the spheroid's area increased, resulting in a higher fold change value. Conversely, when cell invasiveness was limited, the spheroid's area remained smaller, leading to a smaller fold change value (Figure 46 A).

In the medium with hormones, depleting either MTA3 or MTA1 did not lead to any significant differences in invasiveness compared to the control group (Figure 46 B and C). This consistent trend was observed across all 3 assessed time points (24, 48, and 72 h).

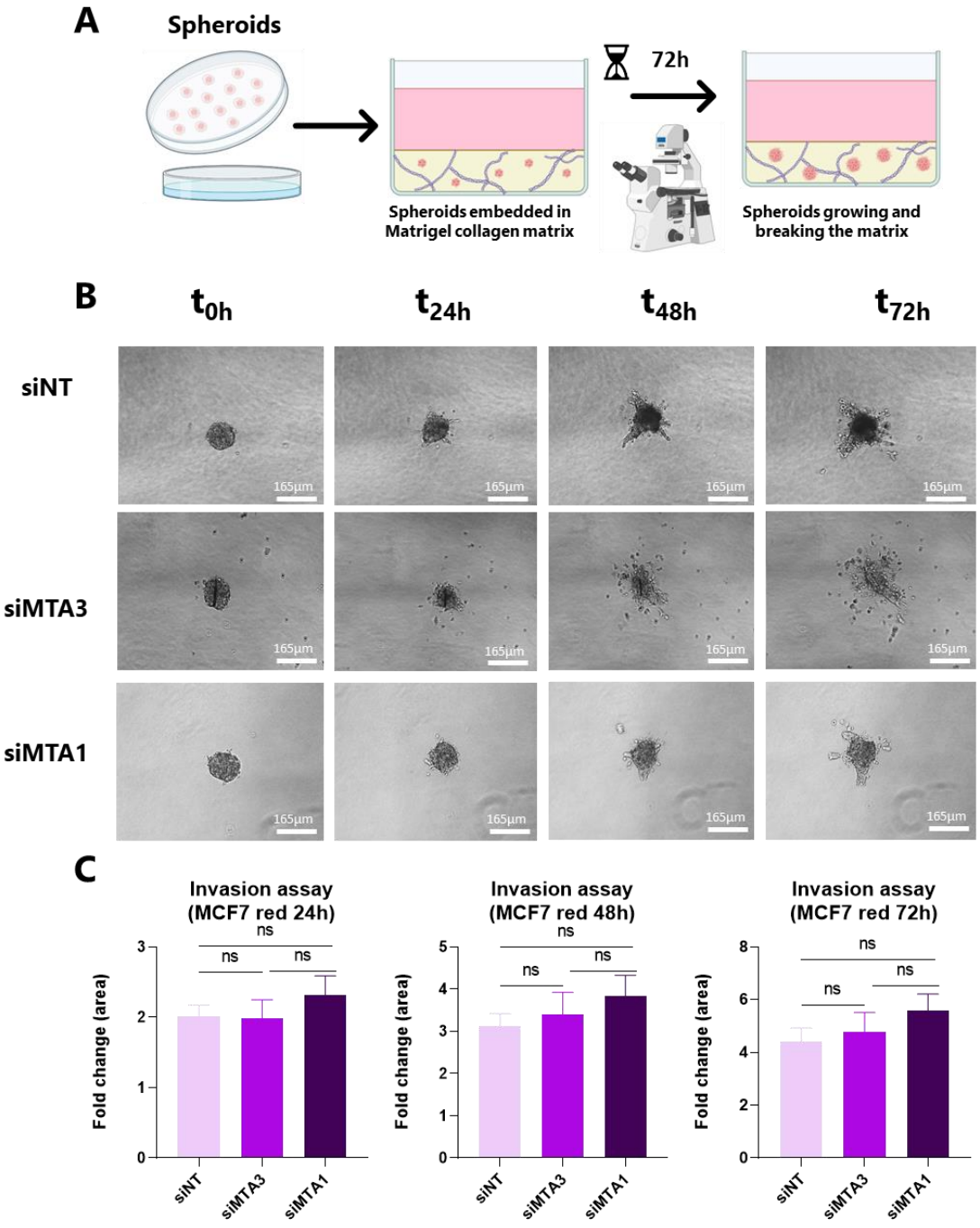

Figure 46. Impact of MTA1 and MTA3 imbalance on MCF7 cell invasion in medium with hormones. **(A)** Diagram depicting the invasion assay methodology, involving the creation of spheroids, embedding them in Matrigel, and monitoring their growth while breaking through the matrix. **(B)** The invasion assay was conducted in MCF7 cells. The results showed no significant invasion rate between the control group (siNT), the group with depleted MTA3, or the one with depleted MTA1 at any of the 3 observed time points (24, 48, and 72 h). The scale bar corresponds to 165 µm. **(C)** The data is presented as the mean ± SEM (n=3). The bar graph illustrates the fold change of spheroid area after 24, 48, or 72 h compared to the initial measurement. Statistical significance was assessed through a One-Way ANOVA multiple comparison test (Tukey's).

In medium without hormones, cells depleted with MTA3 exhibited higher invasiveness compared to the control (siNT) and when MTA1 was depleted. Notably, when MTA1 was silenced, no significant change was observed to the control group. This consistent trend was observed across all 3 time points assessed (24, 48, and 72 h) (Figure 47 B and C).

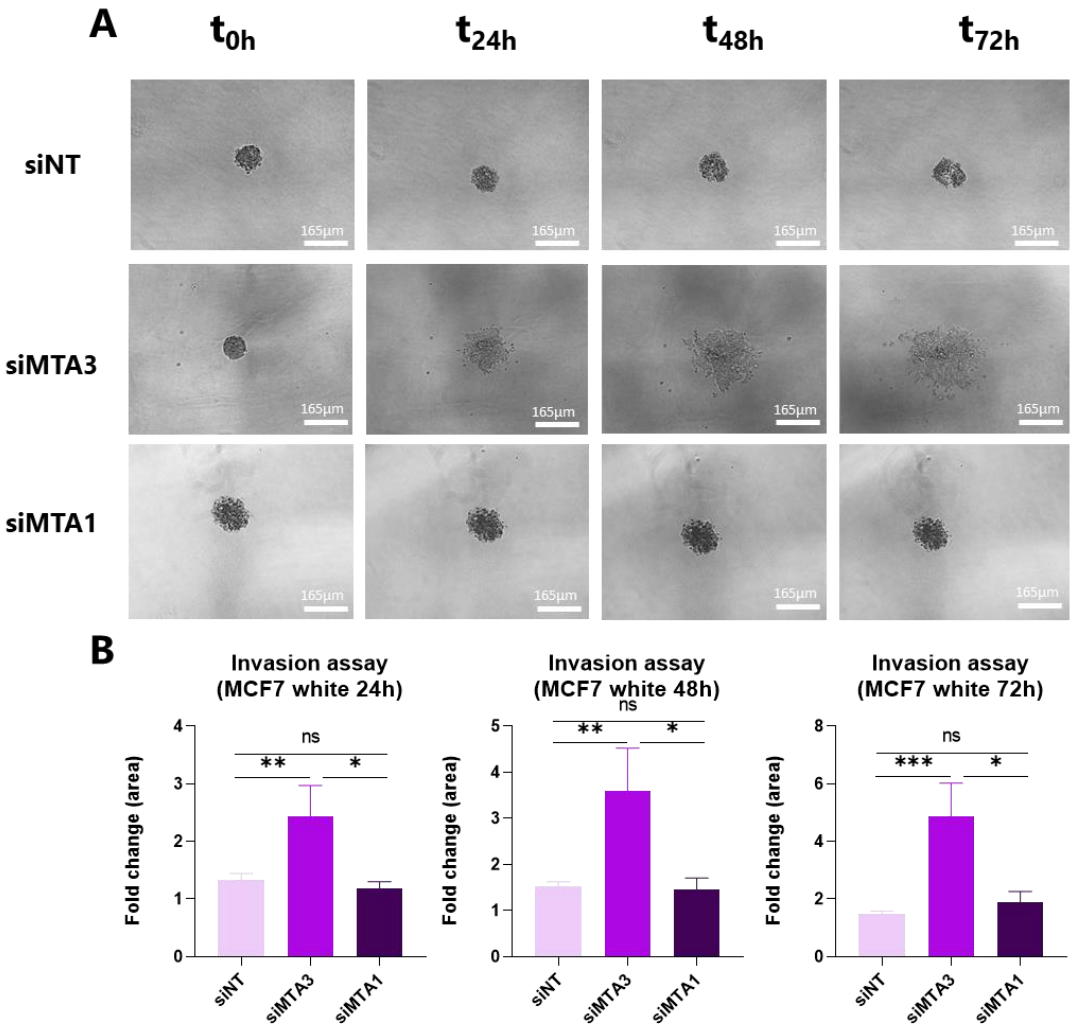

Figure 47. Impact of MTA1 and MTA3 imbalance on MCF7 cell invasion in medium without hormones. **(A)** An invasion assay was performed using MCF7 cells. The results demonstrate a significant difference in the invasion rate between the control group (siNT) and MTA3 depletetion. No notable variance in invasion was observed between siMTA1 and the control in any of the 3 different timepoints: 24, 48, and 72 h. The scale bar represents a distance of 165 µm. **(B)** The data is depicted as the mean ± SEM (n=3). The bar graph illustrates the fold change in spheroid area after 24, 48, or 72 h compared to the initial measurement. Statistical significance was assessed through a One-Way ANOVA multiple comparison test (Tukey's).

To further validate the impact of an imbalance between MTA1 and MTA3 on cell invasion, we conducted additional experiments involving the overexpression of MTA1 and silencing of MTA3, and vice versa. We confirmed the overexpression and silencing of MTA1 and MTA3 through WB (Figure 48 A and B) and RT-qPCR (Figure 48 C).

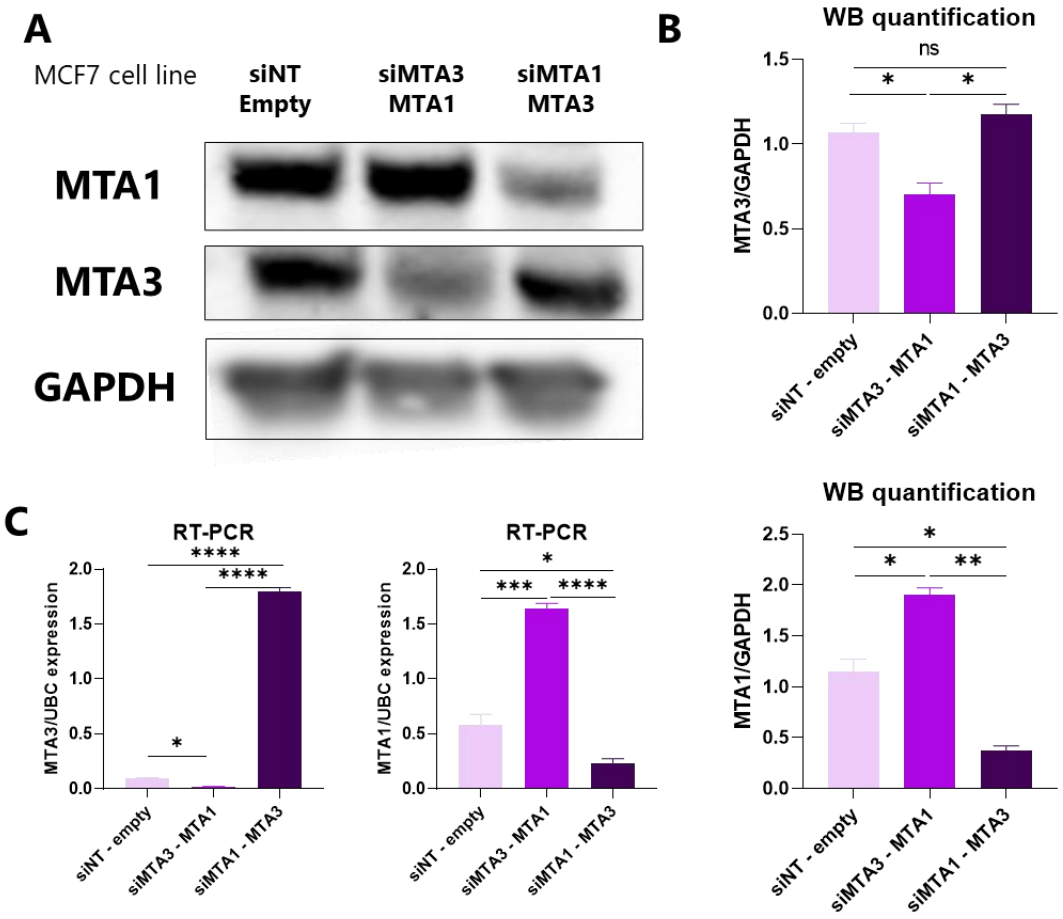

Figure 48. Validation of MTA1 and MTA3 silencing and overexpression. **(A)** Validation of the silencing and overexpression by assessing MTA1 and MTA3 protein levels. GAPDH was used as a loading control. **(B)** Quantitative analysis of the western blot results presented in (A) (n=3). Data is presented as the mean ± standard error mean (SEM) Statistical significance was evaluated using a One-Way ANOVA multiple comparison test (Tukey's). **(C)** Quantification of MTA3 and MTA1 RNA expression normalized against the reference gene UBC using RT-qPCR. Data is presented as the mean ± SEM (n=3). Statistical significance was evaluated using a One-Way ANOVA multiple comparison test (Tukey's).

To further study the consequences of an imbalance between MTA3 and MTA1 on cell invasiveness, we conducted an additional invasion assay. In this experiment, we assessed cell invasiveness after silencing MTA3, while simultaneously overexpressing MTA1, and conversely, we silenced MTA1 while overexpressing MTA3. In medium with hormones, the results of this experiment revealed that enhanced invasiveness was observed when MCF7 cells exhibited elevated levels of MTA1 alongside the depletion of MTA3. Notably, the invasiveness of MCF7 cells in the control group was similar to the invasiveness observed when MCF7 cells had increased levels of MTA3, and MTA1 was silenced (Figure 49 A and B). This trend was consistently observed across the 3 timepoints (24, 48 and 72 h). The results of this experiment provided 2 important insights. Firstly, our suspicion that solely silencing MTA3 or MTA1 was insufficient to induce an invasive phenotype was confirmed.

Secondly, these results suggest that the NuRD complex, through the involvement of MTA1, has a substantial impact on cell invasiveness, enabling non-invasive cell lines like MCF7 to acquire invasive capabilities.

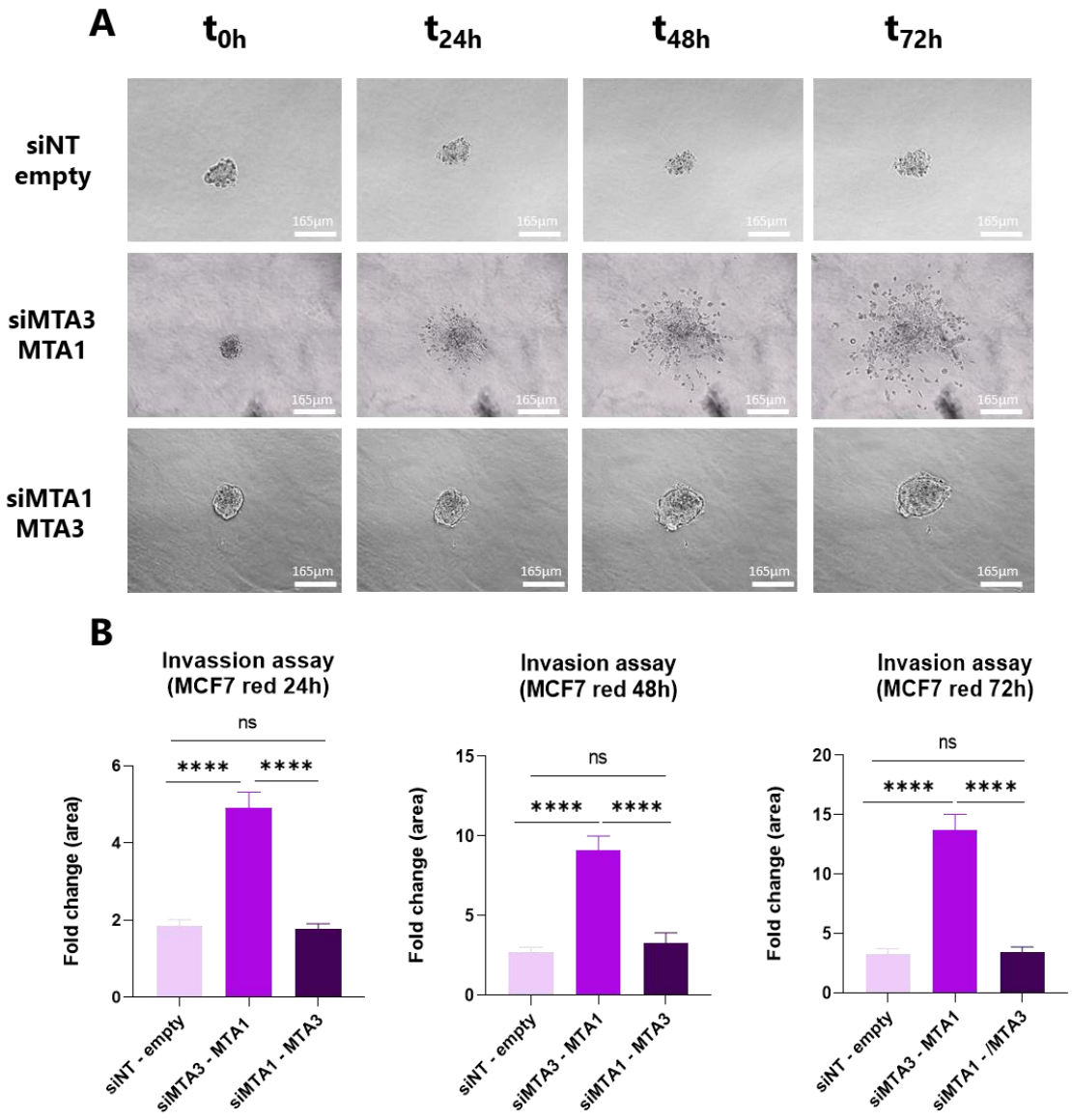

Figure 49. Impact of MTA1 and MTA3 imbalance on MCF7 cell invasion in medium with hormones. **(A)** In medium with hormones, a cell invasion experiment was conducted using MCF7 cells. During this experiment, MTA1 or MTA3 were simultaneously silenced and overexpressed. The outcomes reveal a significant difference in invasion rates when comparing the control group (siNT) with the condition in which MTA3 was depleted and MTA1 was overexpressed. However, no substantial change in invasion was observed when MTA1 was silenced and MTA3 was overexpressed. This assessment was made at 3 different timepoints: 24, 48, and 72 h. The scale bar on the figure represents a distance of 165 µm. **(B)** The data is represented as the mean ± SEM (n=3). The bar chart illustrates the fold change in spheroid area after 24, 48, or 72 h in comparison to the initial measurement. Statistical significance was assessed through a One-Way ANOVA multiple comparison test (Tukey's).

To further explore the impact of an imbalance between MTA3 and MTA1 on cellular invasiveness, we conducted invasion assays by suppressing MTA3 while overexpressing MTA1, and vice versa. Utilizing medium without hormones, our experiments revealed increased invasiveness in MCF7 cells when MTA1 was overexpressed, while MTA3 was concurrently reduced. Interestingly, the invasiveness of the control group mirrored the conditions in which MTA3 levels were elevated and MTA1 was silenced (Figure 50 A and B). This consistent pattern was maintained throughout all 3 timepoints (24, 48, and 72 h).

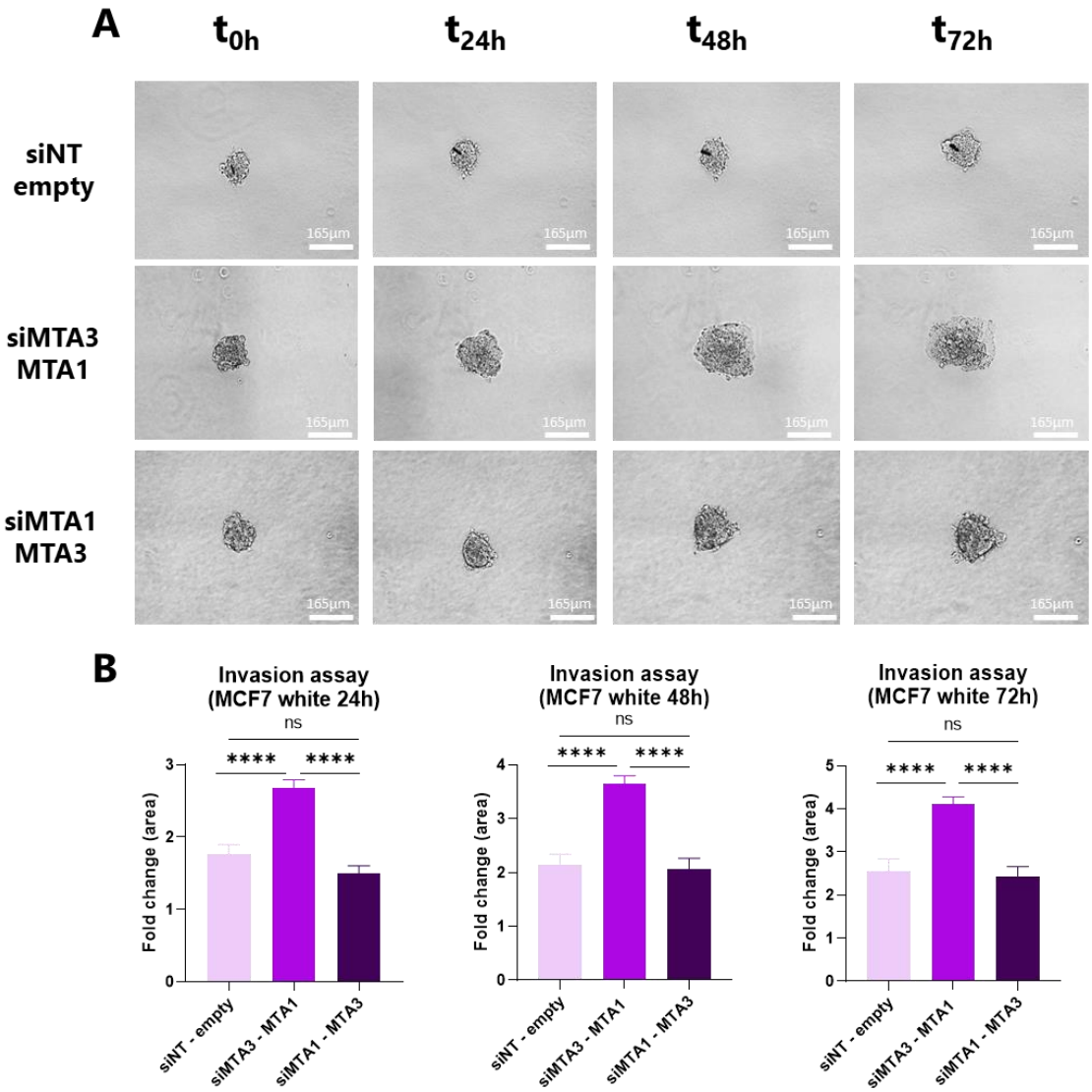

Figure 50. Impact of MTA1 and MTA3 imbalance on MCF7 cell invasion in medium without hormones. **(A)** In medium without hormones, a cell invasion experiment was conducted using MCF7 cells. During this experiment, MTA1 or MTA3 were simultaneously silenced and overexpressed. The outcomes reveal a significant difference in invasion rates when comparing the control group (siNT) with the condition in which MTA3 was depleted and MTA1 was overexpressed. However, no substantial change in invasion was observed when MTA1 was silenced and MTA3 was overexpressed. This assessment was made at 3 different timepoints: 24, 48, and 72 h. The scale bar on the figure represents a distance of 165 µm. **(B)** The data is represented as the mean ± SEM (n=3). The bar chart illustrates the fold change in spheroid area after 24, 48, or 72 h in comparison to the initial measurement. Statistical significance was assessed through a One-Way ANOVA multiple comparison test (Tukey's).

In this section, the obtained results strongly support that an imbalance between MTA1 and MTA3 significantly affects cell invasiveness *in vitro*. This effect is particularly pronounced when cells overexpress MTA1 and MTA3 is silenced, or when only MTA3 is silenced in medium without hormones. These findings indicate that the effect of NuRD complex with MTA1 inducing invasion might be contrasted in cells growing with estradiol. Importantly, our data suggests that the estradiol effect might be avoided in cells with more abundance of MTA1.

2.6. ER decreases the migration and invasion capacity of cells overexpressing MTA1 and decreased levels of MTA3 *in vitro*

After observing the results of HDAC1 IP experiment, which indicated a potential interaction between HDAC1 and ER, our next question was to explore the role of ER within the NuRD complex on cell migration and/or on cell invasion. To perform this investigation, we first determined the ER levels in cells transfected with control oligonucleotides (siNT) or with oligonucleotides silencing ER (siER). Our experiments involved the silencing of MTA3 or MTA1 individually, as well as in combination with ER. To confirm the effectiveness of the silencing, we assessed changes in protein levels through WB analysis conducted 48 h post-transfection (Figure 51 A and B). In this experiment, it was observed that depleting ER alone does not have any effect on MTA1 or MTA3 levels. Likewise, depleting MTA1 or MTA3 individually does not exert any influence on ER protein levels. Interestingly, when both, MTA3 and ER are simultaneously depleted, there is a reduction in MTA1 levels. Furthermore, depleting MTA1 and ER together does not lead to an increase in MTA3 levels, and they remain comparable to the control group (siNT).

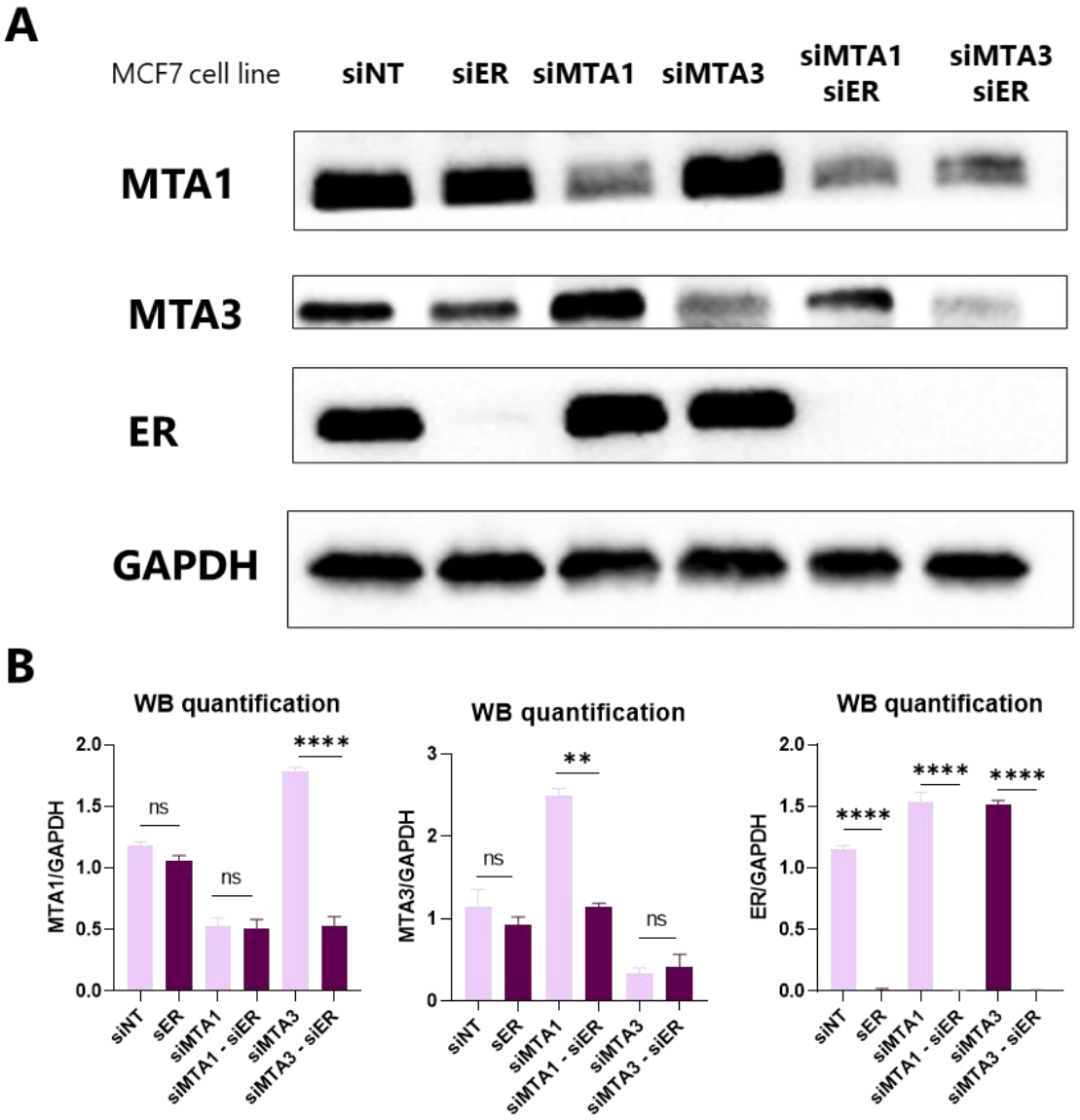

Figure 51. *In vitro* evaluation of ER's role in the NuRD complex. (A) Validation of protein levels of MTA1, MTA3 and ER after being silenced in MCF7 cells alone or in combination. GAPDH was used as a loading control. **(B)** Quantitative analysis of the WB results presented in (A) (n=3). Data is presented as the mean ± SEM. Statistical significance was evaluated using a One-Way ANOVA multiple comparison test (Tukey's).

These findings strongly indicate that the ER has an influence on the NuRD complex. It appears that, when ER is silenced alongside MTA3, MTA1 does not increase, suggesting a dysregulation in the influence in each other's expression. This influence also appears to be disrupted when MTA1 is depleted and ER is absent, causing MTA3 to remain unchanged. These observations support the idea that ER plays a regulatory role in the influence between MTA1 and MTA3 within the NuRD complex.

To assess the impact of ER depletion on cell migration, we performed an *in vitro* experiment of migration using MCF7 cells. Migration was evaluated in medium with and without hormones (red and white, respectively). This data is presented graphically by evaluating the wound closure fold change. This was calculated by determining the ratio of the initial wound length to the wound length after 24 h.

In the MCF7 cell line, under medium with hormones, depletion of ER led to significantly less migration compared to the control. Interestingly, simultaneous depletion of MTA3 and ER reverted this effect, migrating even less than the control group (siNT). However, they migrated more than when ER was silenced alone. Similarly, depletion of MTA1 alone had no discernible effect on cell migration. However, when both MTA1 and ER were depleted concurrently, cell migration decreased compared to MTA1 depletion alone (Figure 52 A and C). These patterns remained consistent when the experiment was conducted under white (hormone-depleted) condition (Figure 52 B and D). The results of this study strongly indicate that ER plays a crucial role in the NuRD complex migration, as the absence of ER is observed to revert the migratory capacity of cells.

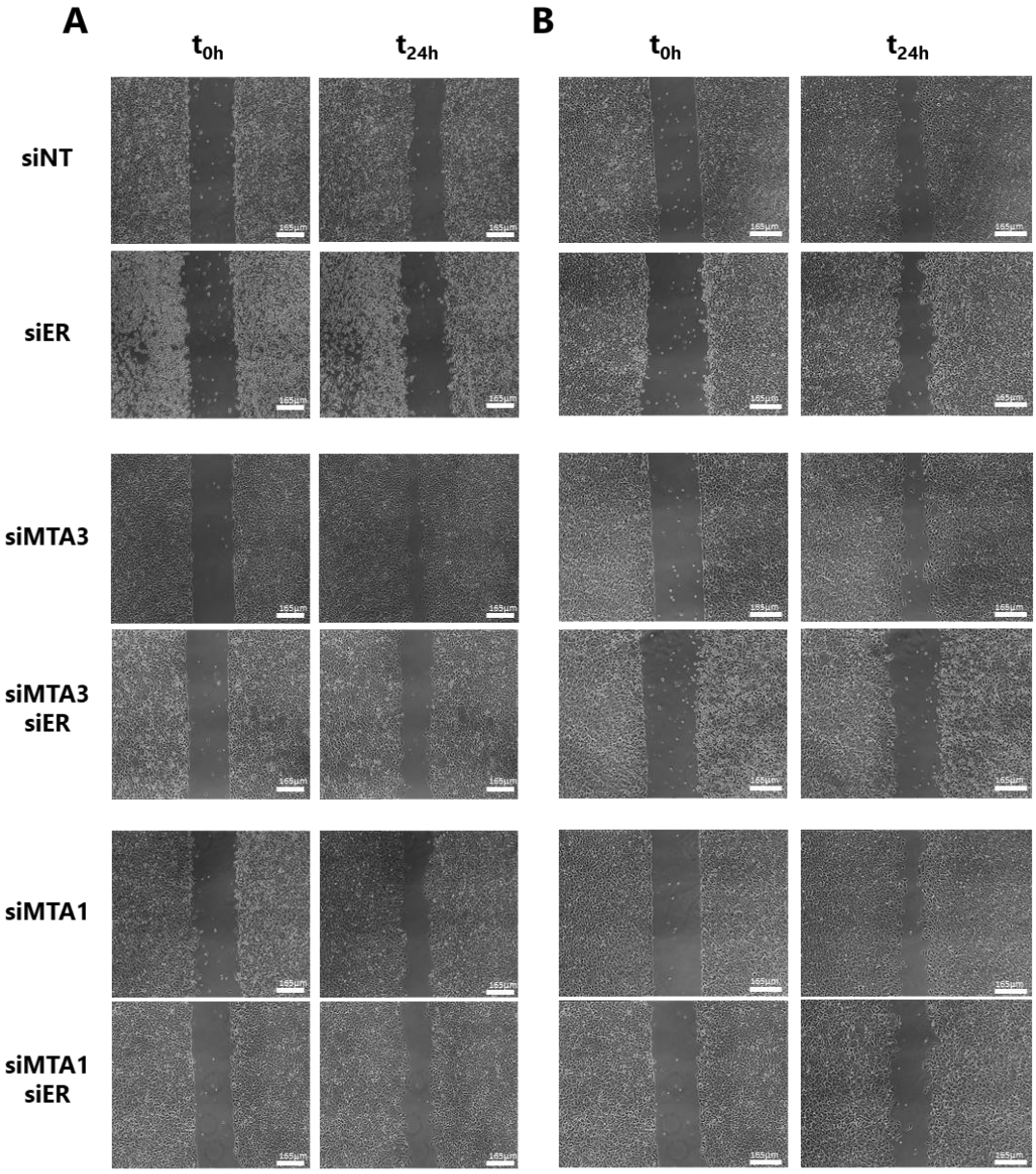
A
B
t_{0h}
t_{24h}
siNT
siER
siMTA3
siMTA3 siER
siMTA1
siMTA1 siER
C
Wound Healing (MCF7 red)
Fold change (length)
1.0
0.8
0.6
0.4
0.2
0.0
****
siNT
siER
siMTA3
siMTA3 - siER
siMTA1
siMTA1 - siER
D
Wound Healing (MCF7 white)

Figure 52. Evaluation of ER's influence on cell migration with MTA1 and MTA3 imbalance. **(A)** A wound healing experiment was conducted in MCF7 cells, showing reduced wound closure when MTA3 was simultaneously silenced with ER in medium with hormones. Images were taken at the beginning of the experiment and 24 h after creating the initial wound. The scale bar represents 165 µm. **(C)** The data is presented as the mean ± SEM (n=3). The bar chart illustrates the change in wound length 24 h after the wound creation compared to the initial measurement. Statistical significance was determined using a One-Way ANOVA multiple comparison test (Tukey's). **(B)** A migration assay was performed in MCF7 cells, demonstrating decreased wound closure when MTA3 is depleted simultaneously with ER in medium without hormones. Wound healing images were captured under the same conditions as in (A). **(D)** The quantification of wound healing results in (B) follows the same parameters as described in (C).

In order to further explore the influence of ER on cellular invasiveness, especially in the context of imbalances between MTA1 and MTA3, we carried out invasion assays under 2 distinct conditions: one using medium with hormones (red) and another using medium without hormones (white). In these experiments, we downregulated MTA3 and ER while simultaneously upregulating MTA1. Subsequently, we assessed the impact on invasiveness. Conversely, we examined the effects of silencing MTA1 and ER while overexpressing MTA3 and compared the invasive potential of these cells.

In medium with hormones, we observed that silencing ER did not significantly impact the invasion capacity of MCF7 cells in comparison to the control group (siNT) (Figure 53 A and B). However, when cells overexpressed MTA1, while simultaneously silencing MTA3 levels, their invasive potential was notably enhanced. However, this invasive capacity was reversed when ER was concurrently silenced. Conversely, when MTA1 was depleted and MTA3 was upregulated, the cells did not exhibit any increase in invasive potential. When ER was simultaneously silenced with MTA1 and MTA3 was overexpressed, the cells retained their baseline invasive capacities similar to the control group (siNT - empty). Importantly, this trend in invasiveness was consistently observed at all 3 assessed timepoints (24, 48, and 72 h).

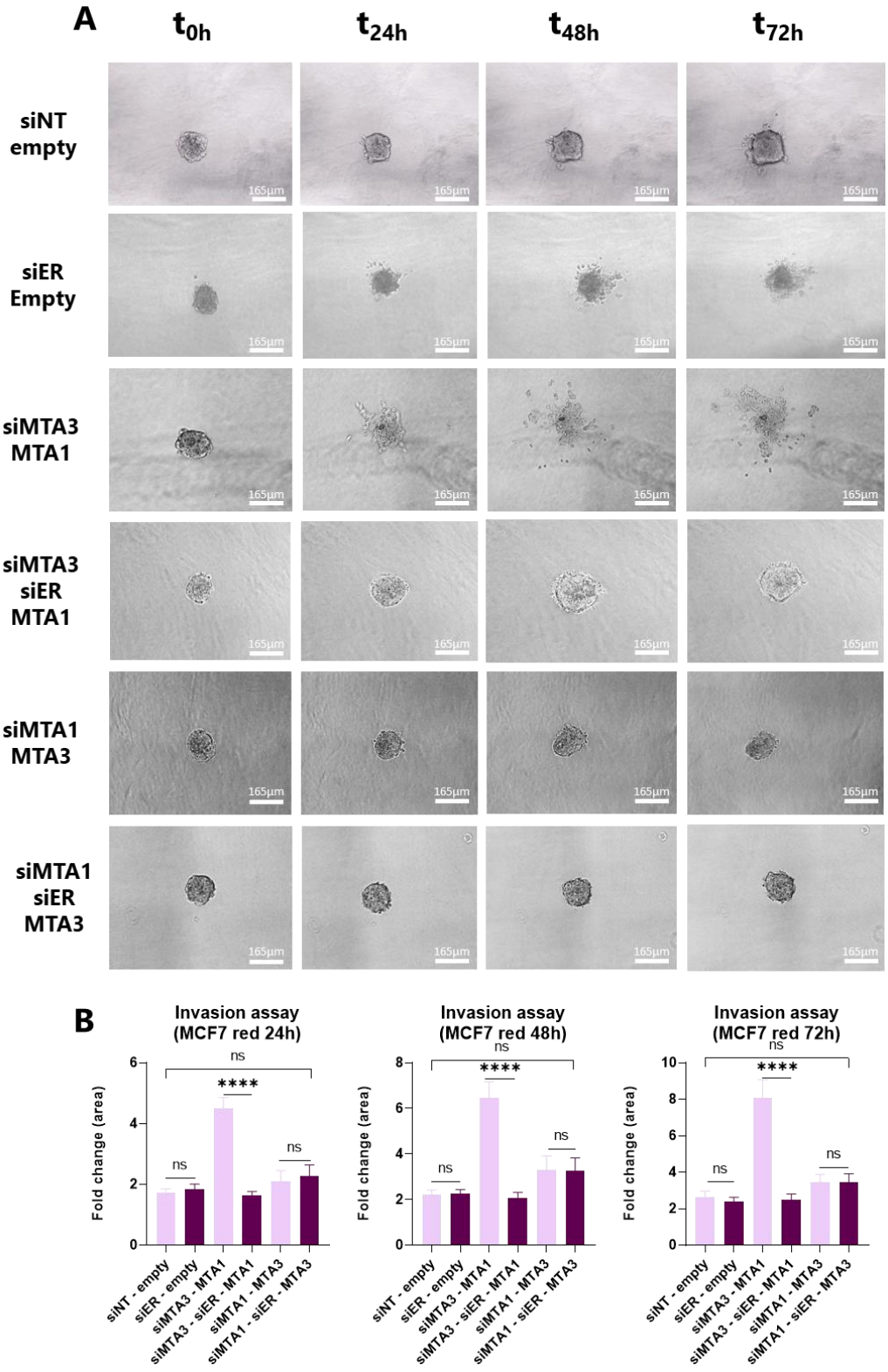

Figure 53. Impact of MTA1 and MTA3 imbalance on MCF7 cell invasion in medium with hormones and silencing of ER. (A) MTA1, or MTA3, were simultaneously silenced and overexpressed in combination with ER silencing. The outcomes reveal that invasion is reverted when MTA3 and ER were depleted and MTA1 was overexpressed. This assessment was made at 3 different time intervals: 24, 48, and 72 h. The scale bar on the figure represents a distance of 165 µm. **(B)** The data is represented as the mean ± SEM (n=3). The bar chart illustrates the fold change in spheroid area after 24, 48, or 72 h in comparison to the initial measurement. Statistical significance was assessed through a One-Way ANOVA multiple comparison test (Tukey's).

In medium without hormones, similar results to the medium with hormones were observed. Silencing ER alone did not substantially affect the invasion capacity of MCF7 cells when compared to the control group (Figure 54 A and B). Cells that were depleted of MTA3, and concurrently overexpressing MTA1, exhibited higher invasiveness. However, this was reversed when ER was simultaneously silenced. Conversely, when MTA1 was depleted, and MTA3 overexpressed, cells did not show any notable increase in invasiveness. Under these conditions, when ER was also silenced, the cells had similar invasiveness as the control. This pattern persisted consistently throughout all 3 timepoints (24, 48, and 72 h).

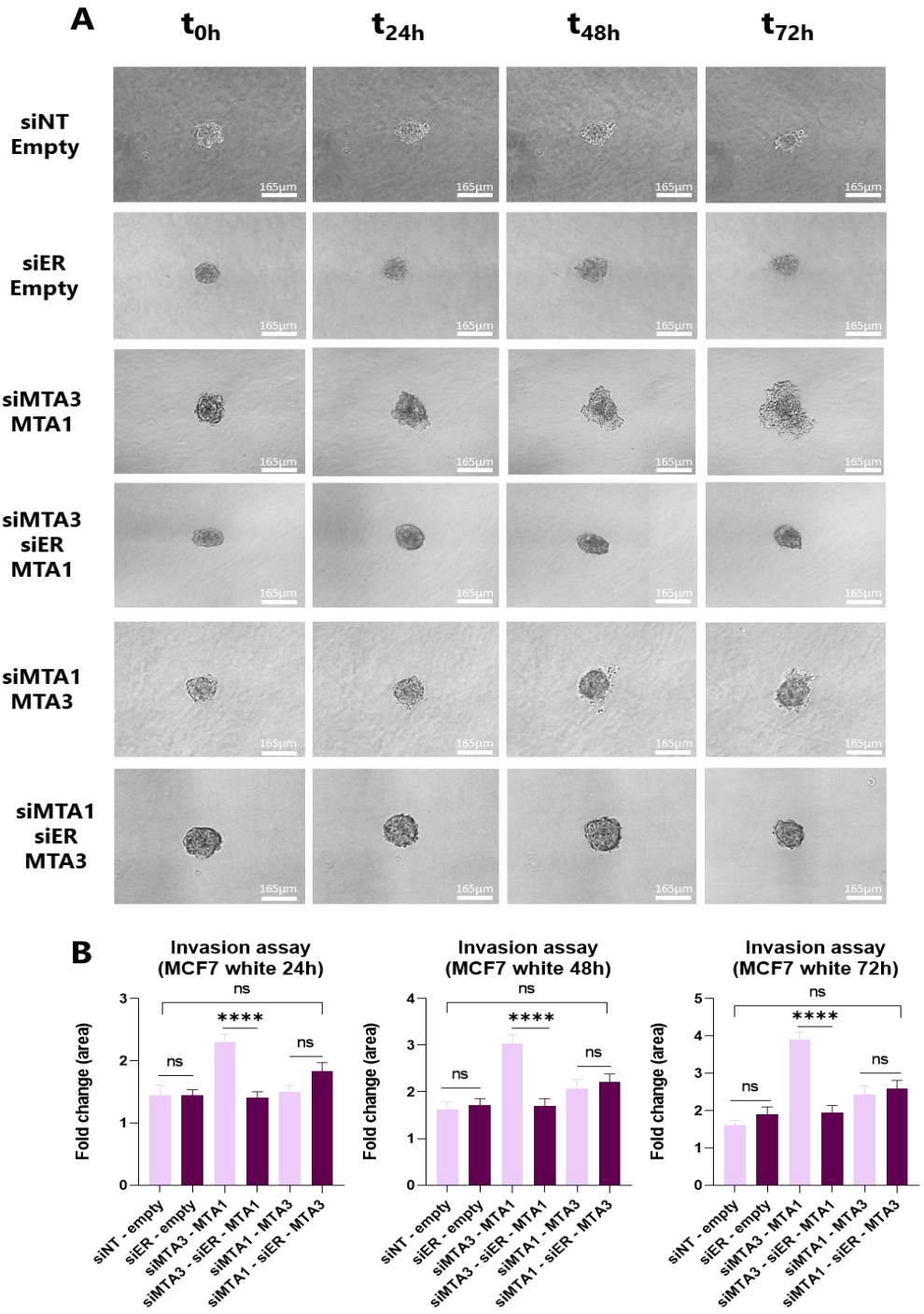

Figure 54. Impact of MTA1 and MTA3 imbalance on MCF7 cell invasion in medium without hormones with silencing of ER. (A) In medium without hormones, cell invasion assay was performed with MCF7 cells concurrently downregulating and overexpressing MTA1 and MTA3 in combination with ER silencing. The results demonstrate that invasion is reversed when MTA3 and ER are suppressed, and MTA1 is overexpressed. This evaluation was conducted at 3 different timepoints: 24, 48, and 72 h. The scale bar in the figure corresponds to a length of 165 µm. **(B)** The data is presented as the mean ± SEM (n=3). The bar chart illustrates the change in spheroid area relative to the initial measurement after 24, 48, or 72 h. Statistical significance was determined using a One-Way ANOVA multiple comparison test (Tukey's).

In summary, these findings indicate that the ER might mediate the effect of NuRD (MTA1) complex, consequently impacting the expression levels of MTA1 and MTA3 and their associated migratory and invasive capabilities. These results underscore the intricate interplay between MTA1, MTA3, and ER in the regulation of breast cancer cell invasiveness.

2.7. GATA3 decreases the migration and invasion capacity of cells overexpressing MTA1 and silencing MTA3 *in vitro*

To further validate the action of GATA3 within the NuRD complex, we decided to evaluate its implications on migration. We performed a migration assay in medium with and without hormones. We silenced MTA3, or MTA1, individually and in combination with GATA3. First, the effectiveness of the silencing process was confirmed by evaluating protein levels via WB at 48 h post-silencing.

The results of this experiment revealed that depleting GATA3 alone decreased slightly MTA1 and MTA3 protein levels compared to the control (siNT) (Figure 55 A and B). Conversely, depletion of MTA1 increased the levels of GATA3 and slightly increased the levels of MTA3. Moreover, when MTA3 was silenced, it increased levels of MTA1, but it decreased the levels of GATA3. Additionally, when MTA1 and GATA3 were both depleted, MTA3 levels slightly increased. Intriguingly, when both MTA3 and GATA3 were depleted, MTA1 levels also decreased. These findings strongly suggest that perturbations in MTA3 and MTA1 levels lead to corresponding changes in GATA3 levels. These results support the hypothesis that GATA3 might influence MTA1 and MTA3 expression.

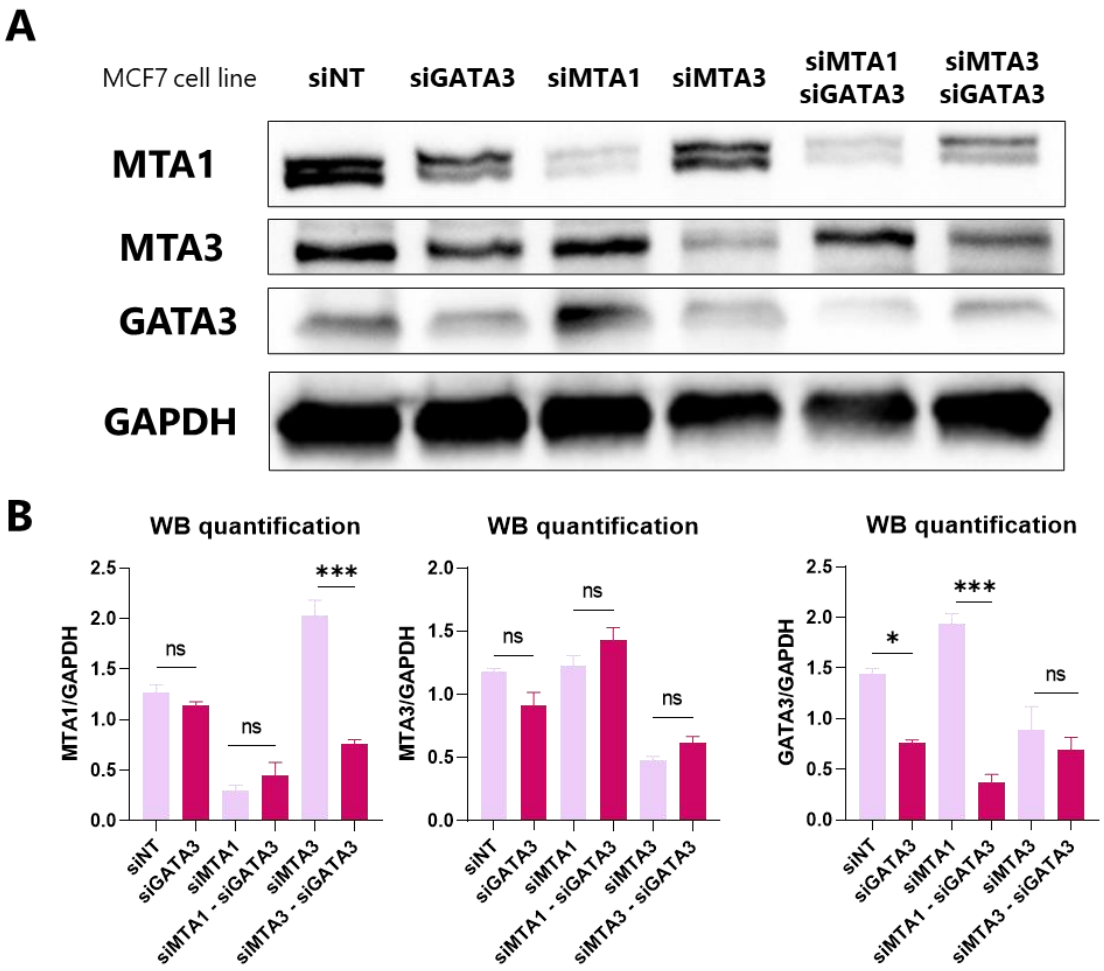

Figure 55. Experimental confirmation of GATA3 role within the NuRD complex under conditions of MTA1 and MTA3 imbalance. **(A)** Validation of protein levels of MTA1, MTA3 and GATA3 after being silenced in MCF7 cells alone or in combination. GAPDH was used as a loading control. **(B)** Quantitative analysis of the WB results presented in (A) (n=3). Data is presented as the mean ± SEM. Statistical significance was evaluated using a One-Way ANOVA multiple comparison test (Tukey's).

To assess the impact of GATA3 within the NuRD complex, an *in vitro* experiment of migration was conducted using MCF7 cells. Migration was evaluated both in medium with and without hormones. This data is presented by evaluating the wound closure fold change. This was calculated by determining the ratio of the initial length to the length after 24 h.

In the MCF7 cell line, in medium with hormones, the silencing of GATA3 resulted in a significant decrease in cell migration when compared to the control group (siNT). Cells depleted of MTA3 showed higher migration, reinforcing the action of NuRD (MTA1). Intriguingly, when MTA3 was depleted along with GATA3, cell migration decreased, and cells migrated even less than the control group. However, it is worth noting that this combined depletion of MTA3 and GATA3 still led to less migration compared to when GATA3 was silenced alone. In a similar way, when MTA1 was depleted, cell migration

remained at the same level as the control group. Nonetheless, when both MTA1 and GATA3 were concurrently depleted, cell migration decreased even further compared to when only MTA1 was silenced (Figure 56 A and C). These trends were consistently observed when the experiment was conducted in hormone-depleted circumstances (Figure 56 B and D).

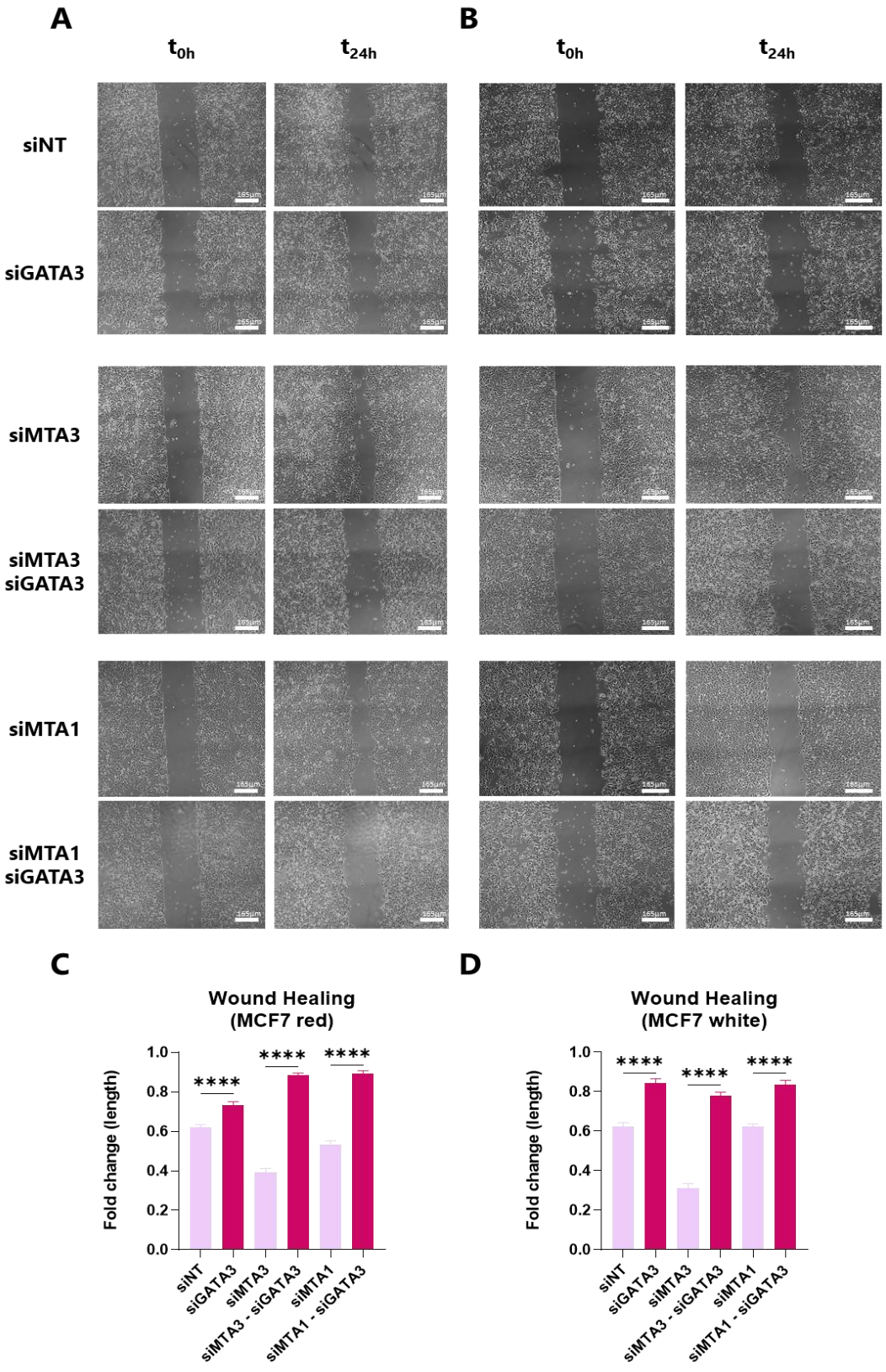

Figure 56. Assessment of GATA3 impact on cell migration under MTA1 and MTA3 imbalance conditions. **(A)** We conducted a wound healing experiment in MCF7 cells, and the results indicated reduced wound closure when both GATA3 and MTA3 were simultaneously suppressed in medium with hormones. Images were captured at the beginning of the experiment and 24 h after creating the wound. The scale bar in the images represents a distance of 165 µm. **(C)** The data is presented as the mean ± SEM (n=3). The bar chart visually represents the change in wound length 24 h after the initial wound creation compared to the initial measurement. We assessed statistical significance using a One-Way ANOVA multiple comparison test (Tukey's). **(B)** In MCF7 cells, we conducted a migration assay, which revealed diminished wound closure when both GATA3 and MTA3 were concurrently suppressed in medium with hormones. The wound healing images were captured under the same conditions as described in (A). **(D)** The quantification of wound healing results in (B) follows the same parameters as described in (C).

The findings from this study provide strong evidence that GATA3 plays a crucial role in counteracting cell migratory potential when an imbalance exists between MTA1 and MTA3 within the NuRD complex. It seems, that when GATA3 is depleted simultaneously with MTA3, MTA1 levels do not increase. Consequently, this dysregulation in the influence between MTA1 and MTA3 has implications for cell migration. Remarkably, it seems that GATA3 levels are influenced by the presence of MTA1, as their depletion leads to increased levels of MTA3, and simultaneously, GATA3 levels also rise. This suggests a complex interplay among these 3 proteins. Notably, the observed trends in medium with and without hormones indicate that GATA3 may not operate through the same pathway or may not be directly involved in estrogen-related activities.

In order to further explore the influence of GATA3 on cellular invasiveness, especially in the context of imbalances between MTA1 and MTA3 expression, we carried out invasion assays under 2 distinct conditions: one using medium with hormones and another using medium without hormones. In these experiments, we downregulated MTA3 and GATA3, while simultaneously upregulating MTA1. Subsequently, we assessed the impact on invasiveness. Conversely, we examined the effects of silencing MTA1 and GATA3, while overexpressing MTA3, and compared the invasive potential of these cells.

In medium with hormones, we observed that silencing GATA3 significantly decreased the invasion capacity of MCF7 cells in comparison to the control group (siNT) (Figure 57 A and B). However, when cells overexpressed MTA1, while simultaneously silencing MTA3 levels, their invasive potential was notably enhanced. However, this invasive capacity was reversed when GATA3 was concurrently silenced. Conversely, when MTA1 was depleted and MTA3 was upregulated, the cells did not exhibit any increase in invasive potential. When GATA3 was simultaneously silenced with MTA1, and MTA3 overexpressed, the cells retained their baseline invasive capacities. This trend in invasiveness was consistently observed at all 3 timepoints (24, 48, and 72 h).

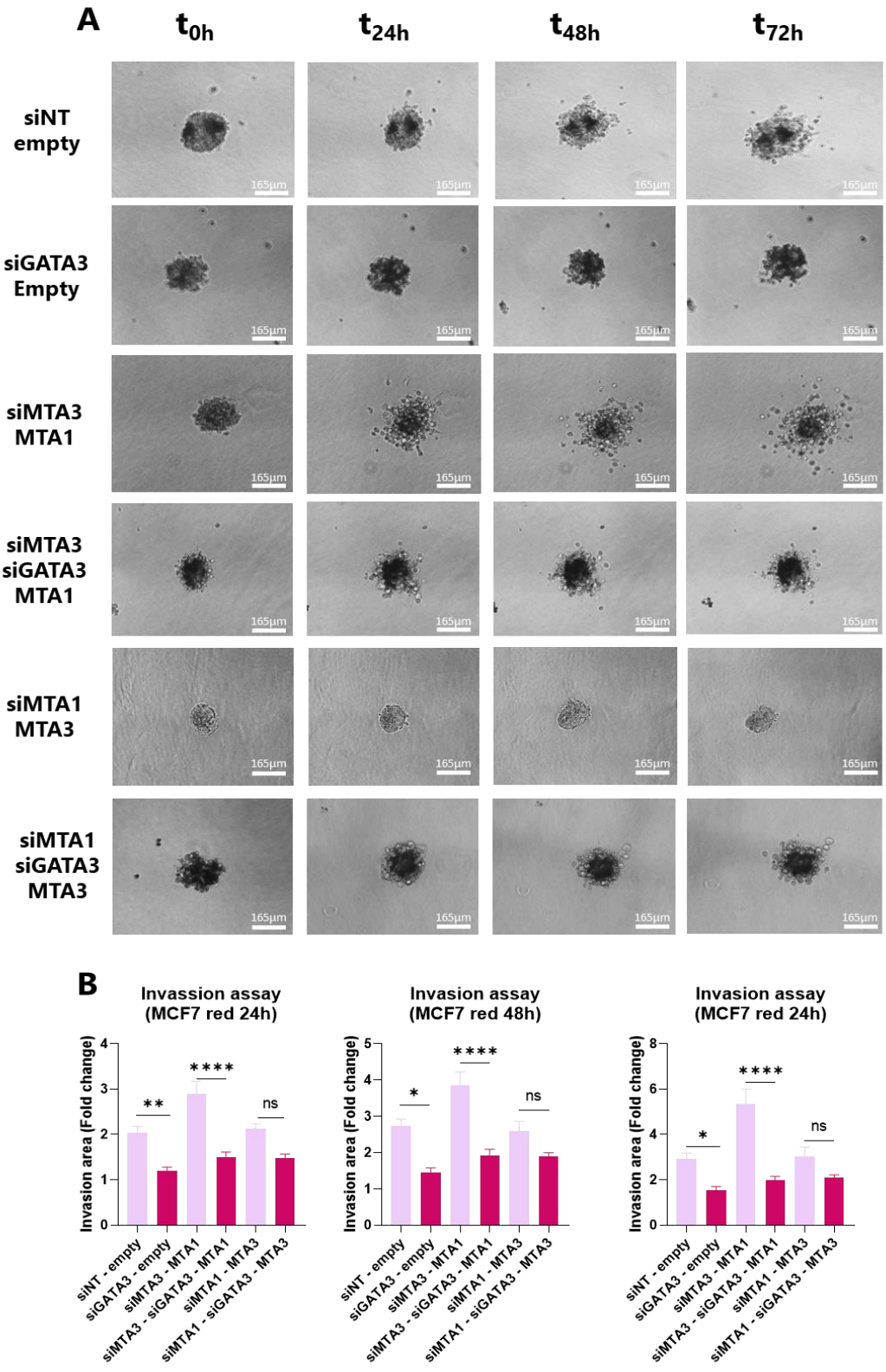

Figure 57. Impact of MTA1 and MTA3 imbalance on MCF7 cell invasion in medium with hormones and silencing of GATA3. **(A)** MTA1 or MTA3 were simultaneously silenced and overexpressed in combination with GATA3 silencing. The outcomes reveal that invasion was reverted when MTA3 and GATA3 were depleted and MTA1 was overexpressed. This assessment was made at 24, 48, and 72 h. The scale bar on the figure represents a distance of 165 µm. **(B)** The data is represented as the mean ± SEM (n=3). The bar chart illustrates the fold change in spheroid area after 24, 48, or 72 h in comparison to the initial measurement. Statistical significance was assessed through a One-Way ANOVA multiple comparison test (Tukey's).

In medium without hormones, silencing GATA3 alone significantly affected the invasion capacity of MCF7 cells compared to the control group (Figure 58 A and B). Cells that were depleted of MTA3 and overexpressed MTA1, exhibited higher invasiveness. However, this was reversed when GATA3 was simultaneously silenced. Conversely, when MTA1 was depleted and MTA3 overexpressed, cells did not show any notable increase in invasive capacities. Under these conditions, when GATA3 was also silenced, cells had reduced invasive capacities compared with silenced MTA1 and overexpressed MTA3. This pattern persisted throughout all 3 timepoints (24, 48, and 72 h) evaluated.

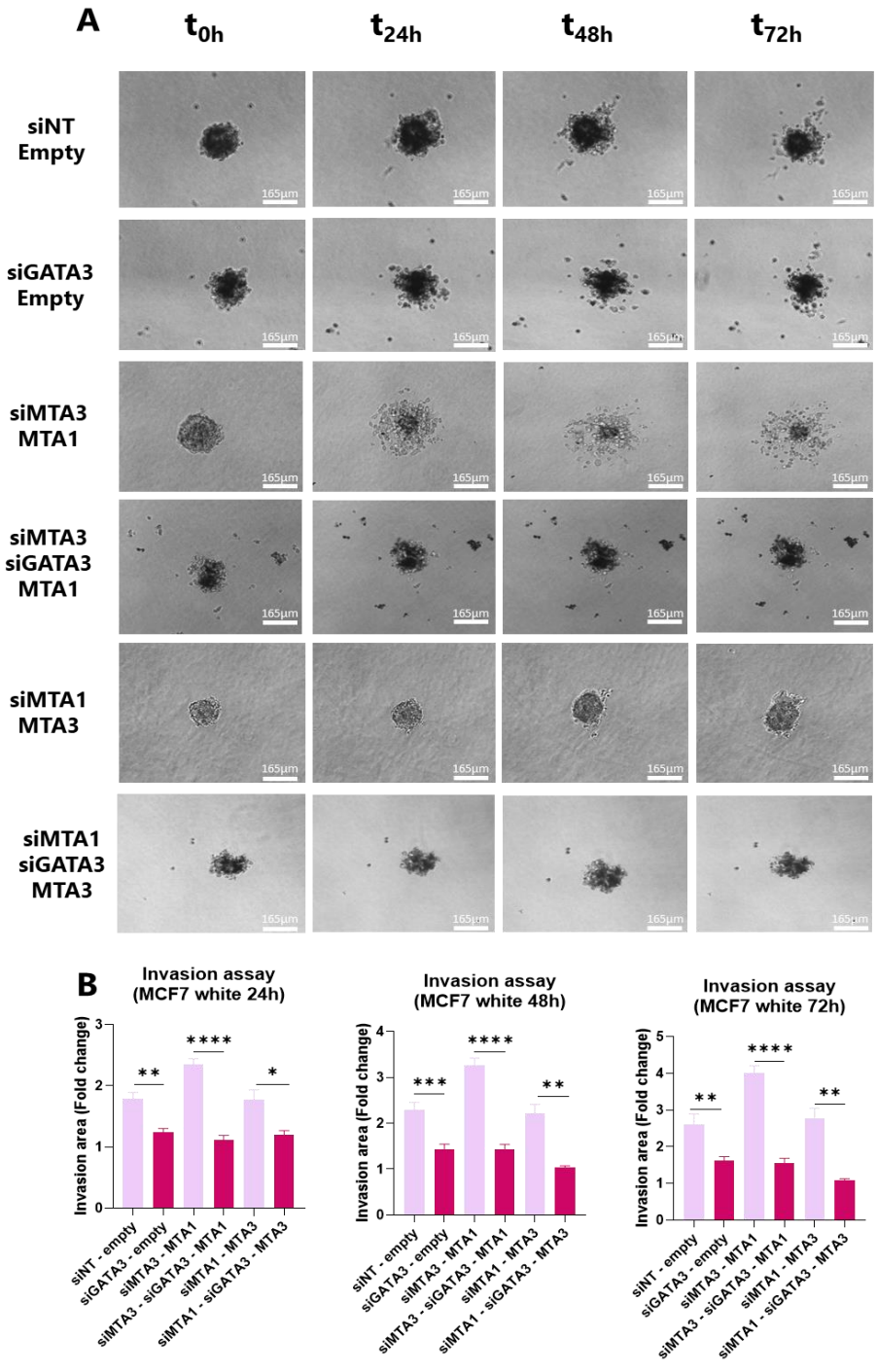

Figure 58. Impact of MTA1 and MTA3 imbalance on MCF7 cell invasion in medium without hormones with silencing of GATA3. **(A)** In medium without hormones cell invasion assay was performed with MCF7 cells concurrently downregulating and overexpressing MTA1 and MTA3 in combination with GATA3 silencing. The results demonstrated that invasion was reversed when MTA3 and GATA3 were suppressed, and MTA1 was overexpressed. This evaluation was conducted at 3 different timepoints: 24, 48, and 72 h. The scale bar in the figure corresponds to a length of 165 µm. **(B)** The data is presented as the mean ± SEM (n=3). The bar chart illustrates the change in spheroid area relative to the initial measurement after 24, 48, or 72 h. Statistical significance was determined using a One-Way ANOVA multiple comparison test (Tukey's).

In summary, these findings indicate that the GATA3 might mediate the effect of NuRD (MTA1) and NuRD (MTA3) complexes, consequently impacting the expression levels of MTA1 and MTA3 and their associated migratory and invasive capabilities. These results underscore the intricate interplay between MTA1, MTA3, and GATA3 in the regulation of breast cancer cell invasiveness.

2.8. *In vitro* validation of NuRD complex in MDA-MB-231 cells revealed that the imbalance of MTA1 and MTA3 depend on ER and GATA3 expression

To determine if the imbalance between MTA1 and MTA3 within the NuRD complex was exclusively dependent on cells that express both ER and GATA3 (like MCF7 cells), we used MDA-MB-231, a cell line that does not express neither ER nor GATA3 and has a high migratory capacity [253]. We assessed their migratory capacity upon depletion of MTA1 and MTA3. Migration assays were conducted under medium with and without hormones. This data is presented graphically by evaluating the wound closure fold change. This was calculated by determining the ratio of the initial wound length to the wound length after 24 h.

In medium with hormones, depletion of MTA3 led to reduced cell migration compared to the control (siNT), whereas downregulation of MTA1 resulted in increased cell migration, relative to the siMTA3 condition, although it remained less than the control (Figure 59 A and C). Conversely, in medium without hormones, depletion of MTA3 in MDA-MB-231 cells resulted in cell migration similar to the control, whereas depletion of MTA1 led to enhanced cell migration (Figure 59 B and D).

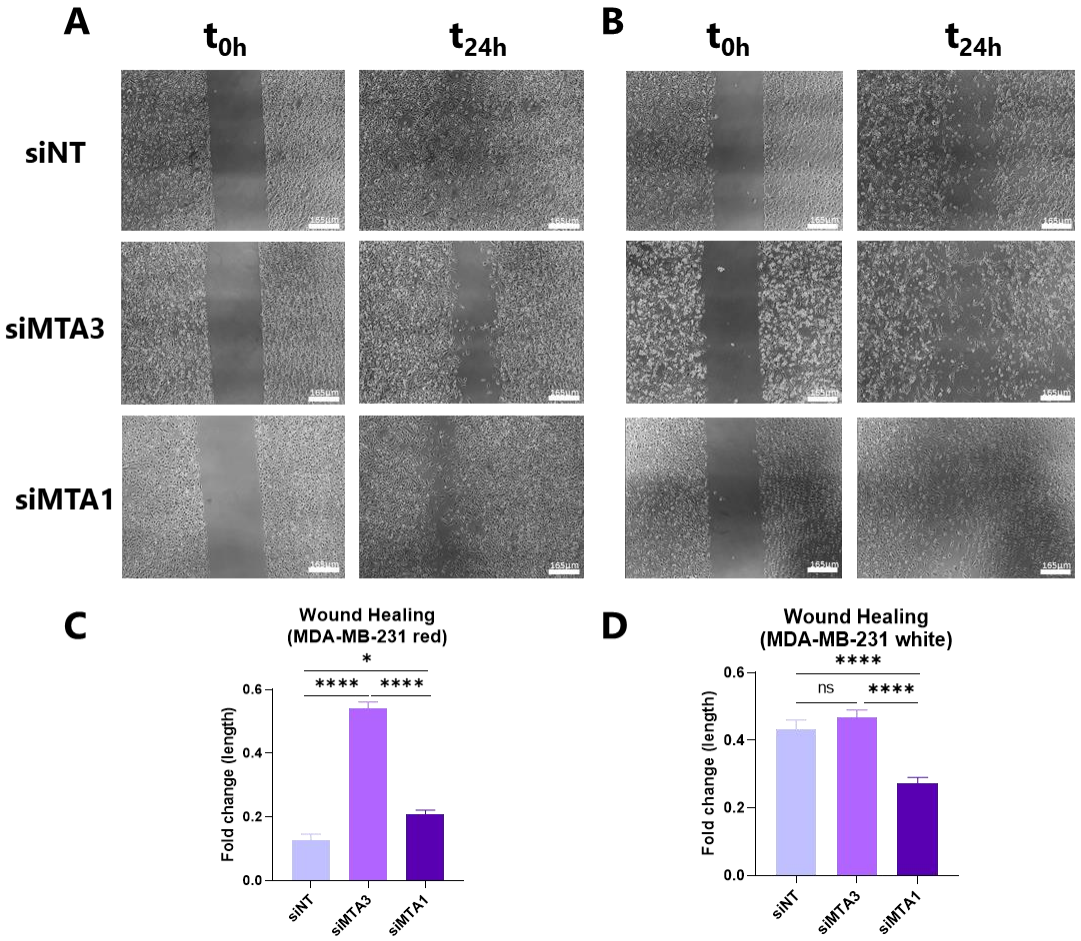

Figure 59. Influence of MTA1 and MTA3 imbalance on MDA-MB-231 in cell migration. **(A)** A wound healing assay conducted in MDA-MB-231 cells showed reduced wound closure when both MTA3 and MTA1 were depleted in medium with hormones. Images were taken at the start and 24 h after creating the wound, with a scale bar of 165 µm. **(C)** The quantification of wound healing results in (A) is presented as the mean ± SEM (n=3). The bar chart illustrates the change in wound length after 24 h compared to the initial measurement. Statistical significance was assessed using a One-Way ANOVA multiple comparison test (Tukey's). **(B)** A wound healing assay in MDA-MB-231 cells revealed increased wound closure when MTA1 was silenced in white medium (without hormones), and images were taken under the same conditions as in (A). **(D)** The quantification of wound healing results in (B) follows the same criteria as described in (C).

These results suggest that the NuRD complex hypothesis may not hold true when the balance between MTA1 and MTA3 is altered in cells that are already invasive, resembling a triple-negative breast cancer phenotype. These results also suggest that the promoting migratory effect of NuRD (MTA1) complex, achieved when silencing MTA3, would depend on the expression of ER and GATA3, as this has not been observed in Figure 59. However, in ER-negative cells the NuRD (MTA3) complex, achieved when silencing MTA1, would lead to enhanced migratory capabilities. Nevertheless, in ER-positive cells, the behavior of the NuRD (MTA3) complex is the opposite, as it represses migration.

3. The NuRD (MTA1) complex phenotype is due to the promotion of the epithelial-mesenchymal transition

3.1. The interaction between MTA1, within the NuRD complex, seems to repress the activity of the ER while promoting the process of EMT

To further investigate the reason of the NuRD complex observed phenotype, we conducted RNA-Sequencing (RNA-Seq) on cells depleted of either MTA1 or MTA3. Additionally, we included a control condition to serve as a reference (siNT). We compared the RNA expression of siMTA3 MCF7 against the expression of the control group. This comparison was represented as a volcano plot with the log2 of the fold change against the negative log10 of the p-value (Figure 60 A). The significant genes are the ones that exhibited a log2 fold change bigger than 1, or smaller than -1, and that had a negative log10 of the p value bigger than 5 (which equals to a raw p-value of 0.00001).

The complete list of these upregulated or downregulated genes upon depletion of MTA3 is reported in Table 24 (Annex). Comparing these genes with the 62618 genes in the ENSEMBL database, 68 were significantly upregulated (0.1% from the total) and 64 genes were downregulated (0.1% from the total). Subsequently, we performed a GSEA for the upregulated and another one for the downregulated genes belonging to the cancer hallmark database. However, as these gene sets have a reduced number of genes to perform a successful GSEA, we selected the genes that had a p-value equal or smaller than 0.05 (which corresponds to 1.30 in the -log10 scale). The selected subset is composed of 407 upregulated genes and 175 downregulated ones. We plotted the resulting pathways for the upregulated and downregulated genes sorted by the -log10 of the adjusted p-value calculated in the GSEA (Figure 60 B). Regarding the upregulated pathways, the only significant one (the one with a -log10 adjusted p-value bigger than 1.30) was the epithelial-mesenchymal transition (EMT). For the downregulated pathways, the three significant ones were: Estrogen Response (Early and Late) and KRAS Signaling Downregulation.

Similarly, when comparing the RNA expression of siMTA1 MCF7 against the expression of the control group (siNT), 48 genes were significantly upregulated (0.1% from the total) and 57 genes were downregulated (0.1% from the total). This comparison was represented as a volcano plot with the log2 of the fold change against the negative log10 of the p-value (Figure 60 C). The complete list of these upregulated or downregulated genes upon depletion of MTA1 is reported in Table 24 (Annex). Subsequently, we performed a

GSEA for the upregulated and another one for the downregulated genes belonging to the cancer hallmark database. We applied the same p-value threshold for the GSEA as in the siMTA3 analysis. The selected subset is composed of 256 upregulated genes and 124 downregulated ones. We plotted the resulting pathways for the upregulated and downregulated genes sorted by the -log10 of the adjusted p-value calculated in the GSEA (Figure 60 D). Regarding the upregulated pathways, there were 5 significant ones, among those, the Late Estrogen Response and EMT, were also significative as in the MTA3 analysis. This finding reinforces the idea that the MTA1 and MTA3 imbalance could be context dependent. For the downregulated pathway, there were no significant pathways.

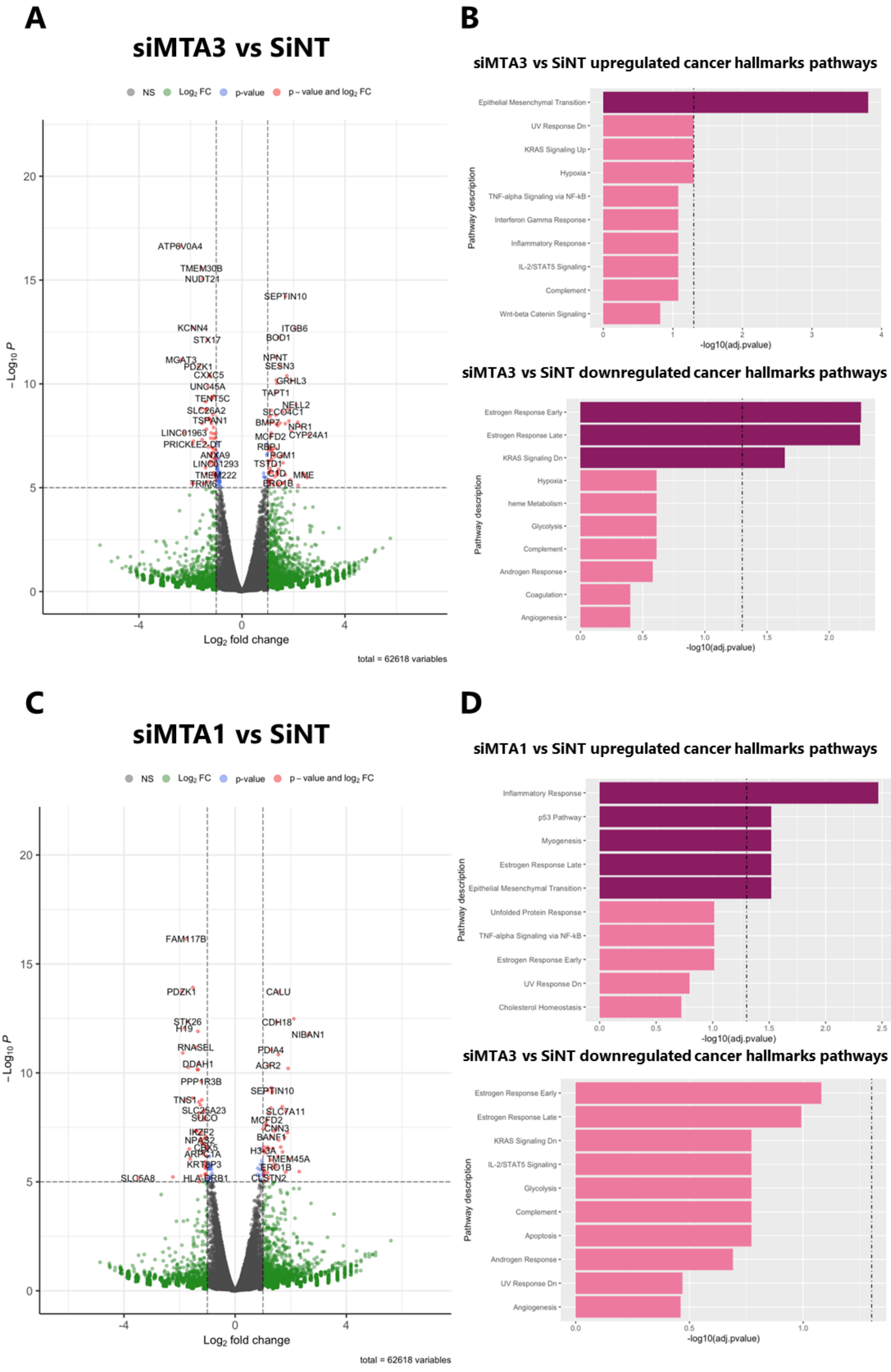
A
siMTA3 vs SiNT
NS
Log2 FC
p-value
p – value and log2 FC
−Log10 P
Log2 fold change
total = 62618 variables
ATP6V0A4
TMEM30B
NUDT21
SEPTIN10
KCNN4
ITGB6
STX17
BOD1
MGAT3
PDZK1
NPNT
SESN3
CXXC5
GRHL3
UNC45A
TAPT1
TENT5C
NELL2
SLC26A2
SLCO4C1
TSPAN1
BMP7
NPR1
LINC01963
MCFD2
CYP24A1
PRICKLE2-DT
RBPJ
ANXA9
PGM1
LINC01293
TSTD1
TMEM222
C1D
MME
TRIM6
ERO1B
B
siMTA3 vs SiNT upregulated cancer hallmarks pathways
Pathway description
Epithelial Mesenchymal Transition
UV Response Dn
KRAS Signaling Up
Hypoxia
TNF-alpha Signaling via NF-kB
Interferon Gamma Response
Inflammatory Response
IL-2/STAT5 Signaling
Complement
Wnt-beta Catenin Signaling
-log10(adj.pvalue)
siMTA3 vs SiNT downregulated cancer hallmarks pathways
Estrogen Response Early
Estrogen Response Late
KRAS Signaling Dn
Hypoxia
heme Metabolism
Glycolysis
Complement
Androgen Response
Coagulation
Angiogenesis
-log10(adj.pvalue)
C
siMTA1 vs SiNT
NS
Log2 FC
p-value
p – value and log2 FC
−Log10 P
Log2 fold change
total = 62618 variables
FAM117B
PDZK1
CALU
STK26
H19
CDH18
NIBAN1
RNASEL
PDIA4
DDAH1
AGR2
PPP1R3B
SEPTIN10
TNS1
SLC25A23
SLC7A11
SUCO
MCFD2
IKZF2
CNN3
NPAS2
BANE1
CBX5
H3-3A
ARPC1A
TMEM45A
KRT8P3
ERO1B
SLC5A8
HLA-DRB1
CLSTN2
D
siMTA1 vs SiNT upregulated cancer hallmarks pathways
Pathway description
Inflammatory Response
p53 Pathway
Myogenesis
Estrogen Response Late
Epithelial Mesenchymal Transition
Unfolded Protein Response
TNF-alpha Signaling via NF-kB
Estrogen Response Early
UV Response Dn
Cholesterol Homeostasis
-log10(adj.pvalue)
siMTA3 vs SiNT downregulated cancer hallmarks pathways
Estrogen Response Early
Estrogen Response Late
KRAS Signaling Dn
IL-2/STAT5 Signaling
Glycolysis
Complement
Apoptosis
Androgen Response
UV Response Dn
Angiogenesis
-log10(adj.pvalue)

Figure 60. Depletion of MTA1, or MTA3, shows significant alterations in gene expression in RNA-Seq analysis. **(A)** Volcano plot showing the log2 fold change against the -log10 p-value when comparing siMTA3 vs control expression. The genes with a log2 fold-change greater than 1, or smaller than -1, and a -log10 p-value bigger than 5 are highlighted. **(B)** Barplot showing the cancer related pathways identified via GSEA for the upregulated and downregulated genes of the siMTA3 vs siNT comparison. Bars are ordered in descending order according to the -log10 of the adjusted p-value calculated by the GSEA and the ones with a -log10 adjusted p-value higher than 1.30 (0.05 adjusted p-value) are highlighted in purple. **(C)** Same analysis conditions as in (A) for the siMTA1 vs control. **(D)** Same representation as in (B) for the siMTA1 vs control.

3.2. RNA-Seq analysis revealed genes mediating EMT, like BMP7 and RBPJ, are upregulated when MTA3 is silenced

From these RNA-Seq analysis we focused on the genes upregulated on the siMTA3 vs siNT condition. More precisely, we focused to study the EMT pathway as it could elucidate which genes are responsible for the observed phenotype when MTA3 was depleted, thus, when the NuRD complex is bound to MTA1. Among the genes implicated in the EMT pathway, we selected RBPJ and BMP7 to perform an *in vitro* validation by RT-qPCR.

To further validate the expression of these genes in MCF7 cells when there is an imbalance between MTA1 and MTA3, we simultaneously treated these cells with a HDAC inhibitor, as HDACs (1 and 2) are subunits of the NuRD complex. We depleted MCF7 cells with MTA1 or MTA3 and we treated them for 24 h with Romidepsin (20 nM) in medium with hormones. We observed that both RBPJ and BMP7 levels were higher in the conditions were MTA3 was depleted, but for the depletion of MTA1, same levels as the control were observed. However, cells treated with Romidepsin showed a homogeneous decreased of the levels of these genes for all 3 conditions with respect to siNT alone (Figure 61 A and B).

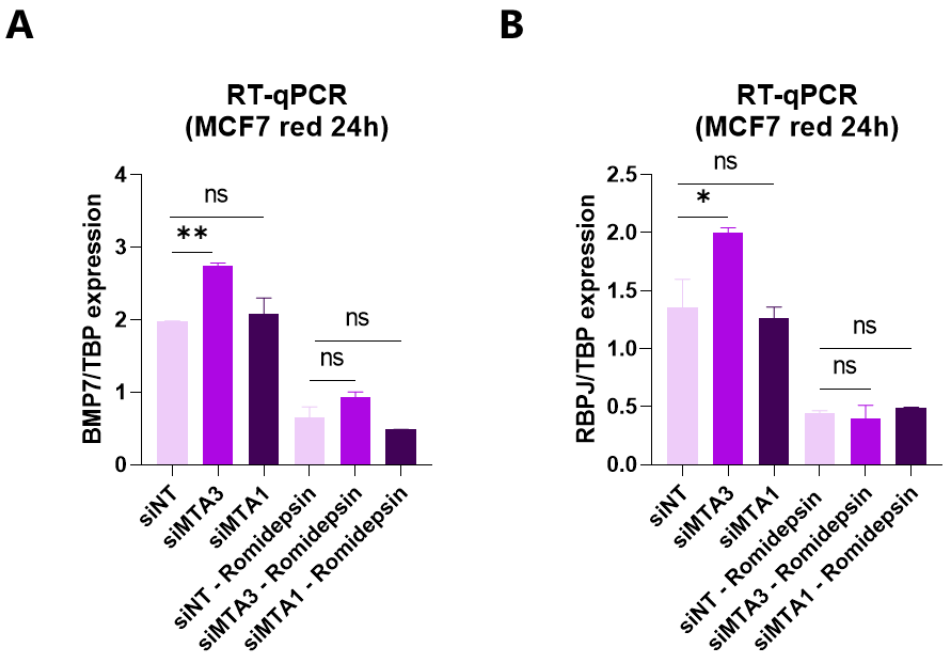

Figure 61. Validation of the expression upon HDAC treatment of the selected EMT genes. **(A)** RNA levels of BMP7 assessed in MCF7 cells depleted of MTA1 or MTA3 in combination with Romidepsin in medium with hormones. BMP7 levels were normalized against the reference gene TBP using RT-qPCR. Data is presented as the mean ± SEM (n=3). Statistical significance was evaluated using a One-Way ANOVA multiple comparison test (Tukey's). **(B)** RNA levels of RBPJ assessed in the same conditions as in (A).

4. Targeting the NuRD complex in conditions where there is an imbalance between MTA1 and MTA3 can prevent migration

4.1. HDAC inhibitors can target the NuRD complex to prevent migration

After demonstrating the importance of the NuRD complex in cell migration and invasion under conditions of an MTA3 and MTA1 imbalance, our research led us to inquire whether by targeting the NuRD complex, we could potentially impede the process of EMT. The NuRD complex is made of different subunits among those, histone deacetylases HDAC1 and HDAC2 are key components of this complex. In the clinic, there are several HDAC inhibitors, with different targets, mainly used for hematological tumors, epilepsy and bipolar disorders. To evaluate the potential of HDAC inhibitors in mitigating cell migration, we conducted a wound healing assay assessing the impact of Romidepsin (20 nM) and Valproic Acid (VPA) (5 mM) on MCF7 cells depleted of MTA3 or MTA1. Romidepsin is known to exhibit specificity towards Class I HDACs, having a high affinity for HDAC1 and 2. However, VPA targets Class I and Class IIa HDACs, having less affinity than Romidepsin for HDAC1, as it has a broader target [254].

Migration experiments were carried out in medium with and without hormones. The results obtained in medium with hormones, revealed that Romidepsin alone did not exert any influence on the migratory behavior of the cells (Figure 62 A and B). Interestingly, when MTA3 was depleted, the cells displayed increased migration compared to the non-depleted cells. However, when MTA3 depletion was combined with the HDAC inhibitor Romidepsin, the drug effectively reversed the increased migration induced by MTA3 depletion. When cells were depleted of MTA1, cells migrated slightly less than the control. Surprisingly, cells depleted of MTA1 treated with Romidepsin, exhibited the highest migration.

The results obtained in medium without hormones, revealed that Romidepsin alone did not exert any influence on the migratory behavior of the cells (Figure 62 C and D). MTA3-depleted cells treated with Romidepsin exhibited decreased cell migration compared to cells with MTA3 depletion alone, although their migration rate remained higher than the control (siNT). The fact that the migration capacity of MTA3-depleted cells is reverted with Romidepsin, but still lower than the control, suggests that estrogen, and probably ER, is crucial for the proper functioning of the NuRD complex. Cells depleted of MTA1 treated with Romidepsin exhibited the highest migration, just as in medium with hormones.

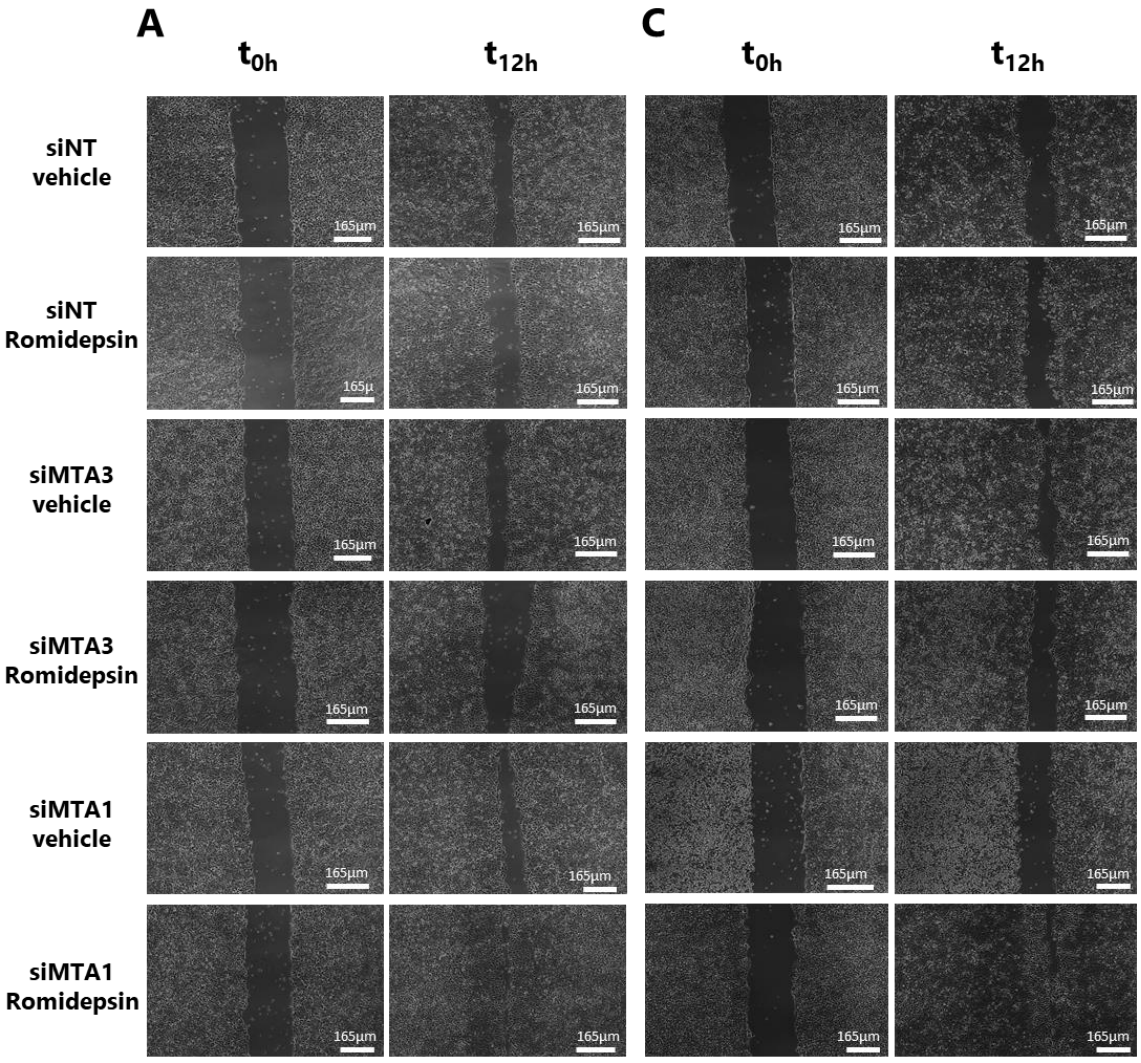
A
t_{0h}
t_{12h}
siNT vehicle
siNT Romidepsin
siMTA3 vehicle
siMTA3 Romidepsin
siMTA1 vehicle
siMTA1 Romidepsin
165µm
C
t_{0h}
t_{12h}

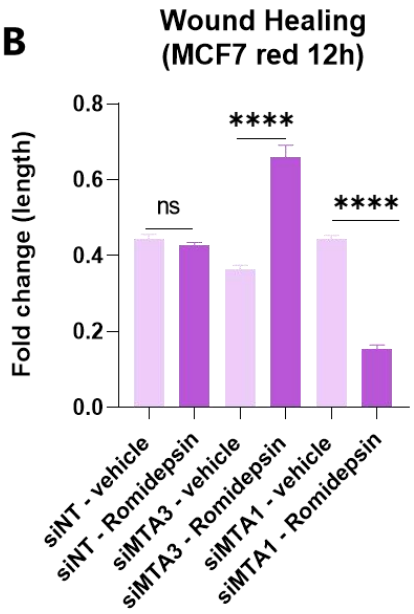
B
Wound Healing (MCF7 red 12h)
Fold change (length)
0.8
0.6
0.4
0.2
0.0
ns
****
****
siNT - vehicle
siNT - Romidepsin
siMTA3 - vehicle
siMTA3 - Romidepsin
siMTA1 - vehicle
siMTA1 - Romidepsin

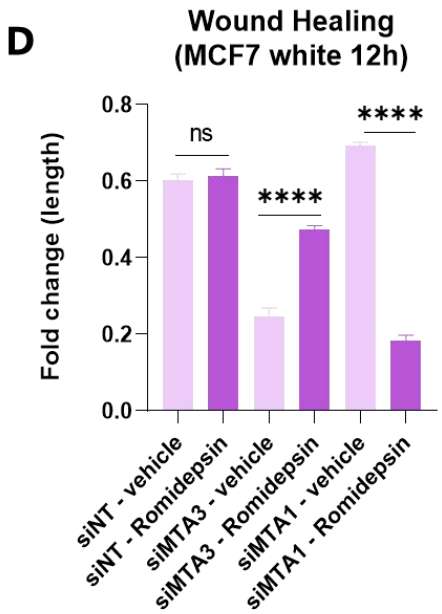
D
Wound Healing (MCF7 white 12h)
Fold change (length)
0.8
0.6
0.4
0.2
0.0
ns
****
****
siNT - vehicle
siNT - Romidepsin
siMTA3 - vehicle
siMTA3 - Romidepsin
siMTA1 - vehicle
siMTA1 - Romidepsin

Figure 62. Evaluation of Romidepsin, an HDAC inhibitor, on cell migration in the presence of MTA1 and MTA3 imbalance. **(A)** A wound healing experiment was conducted using MCF7 cells treated with Romidepsin in medium with hormones, showing that reduced wound closure was observed when MTA3 was silenced. In contrast, MCF7 cells with MTA1 silenced and treated with Romidepsin in medium with hormones, exhibited higher migration rates. Images were captured at the experiment's outset and 12 h after creating the wound, with a scale bar representing a distance of 165 µm. **(C)** The data is presented as the mean ± SEM (n=3). The bar chart visually illustrates the change in wound length 12 h after the initial wound creation compared to the initial measurement. Statistical significance was assessed using a One-Way ANOVA multiple comparison test (Tukey's). **(B)** In MCF7 cells treated with Romidepsin in medium without hormones, a migration assay was conducted, demonstrating decreased wound closure when MTA3 was depleted. Conversely, cells with silenced MTA1 and treated with Romidepsin in medium without hormones showed higher migration rates. Images were captured at the experiment's outset and 12 h after creating the wound under the same conditions as described in (A). **(D)** The quantification of wound healing results in (B) follows the same parameters as described in (C).

These results suggest that HDAC1 inhibitor Romidepsin is effective in preventing cell migration when low levels of MTA3 are exhibited. However, depletion of MTA1 in combination with Romidepsin exhibited higher migration, in medium with and without hormones.

Migration assay was also carried out using VPA (5 mM) in MCF7 cells. The results of this migration assay in medium with hormones, showed that VPA *per se* does not have any influence on cell migration (Figure 63 A and B). However, the combined depletion of MTA3 and the treatment with VPA was able to reverse the enhanced migration caused by MTA3 depletion. Conversely, when MCF7 cells were depleted of MTA1 and concurrently treated with VPA, there was a notable increase in migration compared to the condition without VPA.

The results of this migration assay in medium without hormones, showed that VPA *per se* does not have any influence on cell migration (Figure 63 C and D). Depletion of MTA3 in combination with VPA treatment resulted in significantly decreased migration compared to MTA3 depletion alone, although their migration rate remained higher than the control (siNT). Remarkably, there were no significant differences between the effects of MTA1 depletion and VPA treatment on cell migration.

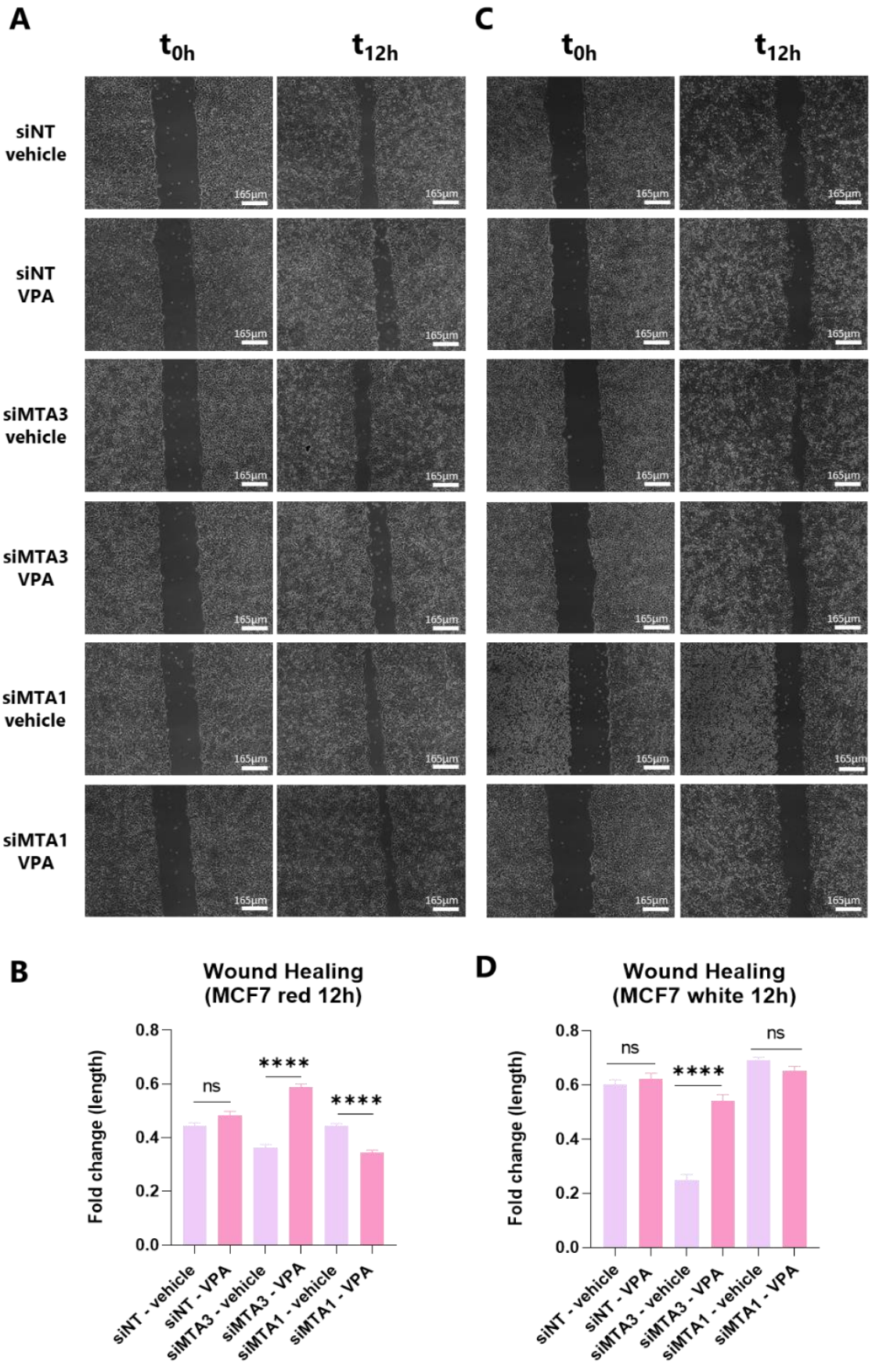
A
t_{0h}
t_{12h}
siNT vehicle
siNT VPA
siMTA3 vehicle
siMTA3 VPA
siMTA1 vehicle
siMTA1 VPA
165µm
C
t_{0h}
t_{12h}
B
Wound Healing (MCF7 red 12h)
Fold change (length)
0.0
0.2
0.4
0.6
0.8
ns
****
****
siNT - vehicle
siNT - VPA
siMTA3 - vehicle
siMTA3 - VPA
siMTA1 - vehicle
siMTA1 - VPA
D
Wound Healing (MCF7 white 12h)
Fold change (length)
ns
****
ns

Figure 63. Assessment of VPA, an HDAC inhibitor, on cell migration under MTA1 and MTA3 imbalance conditions. **(A)** A wound healing experiment was performed with MCF7 cells, indicating that reduced wound closure occurred when MTA3 was suppressed, and cells were treated with VPA in medium with hormones. Conversely, MCF7 cells, with silenced MTA1 and treated with VPA, exhibited enhanced migration rates. Images were captured at the beginning of the experiment and 12 h after the wound was created, with a scale bar representing a distance of 165 µm. **(C)** The data is displayed as the mean ± SEM (n=3). The bar chart visually represents the change in wound length 12 h after the initial wound creation compared to the initial measurement. Statistical significance was determined using a One-Way ANOVA multiple comparison test (Tukey's). **(B)** A migration assay was conducted in MCF7 cells to evaluate wound closure in medium without hormones where MTA3 was depleted and VPA was administrated. In contrast, cells with silenced MTA1 and treated with VPA did not exhibit changes in migration rates. Images were taken at the start of the experiment and 12 h after the wound creation, under the same conditions described in (A). **(D)** The quantification of wound healing results in (B) follows the same criteria as described in (C).

These results suggest that VPA effectively reverses the migratory potential of MCF7 cells, when MTA3 is depleted. However, depletion of MTA1 in combination with VPA did not exhibit higher migration in medium with hormones, but no significant differences could be appreciated in medium without hormones. These differences reinforce the role of ER in modulating cell migration and its possible implications upon treatment with HDAC inhibitors. This observation underscores a potential connection between estrogens, or ER, and their interaction with HDAC1.

DISCUSSION II

Metastatic breast cancer is a multifactorial process that presents an intricate cascade of events, often involving molecular mechanisms (e.g., EMT), genetic and epigenetic modifications [255]. Indeed, epigenetic changes have emerged as significant contributors to the development of resistance to the treatments leading to breast cancer progression and metastasis [256]. Despite the clinical success of aromatase inhibitors (AIs) in treating HR-positive breast cancer, resistance to these drugs presents a therapeutic challenge [257]. Our work aimed to elucidate the lack of response to AIs in patients who progressed to metastatic disease. In this study we have delved into the relationship between chromatin modifications and transcriptional regulators promoting metastasis.

The use of Fit-Seq technology enabled the examination of formalin-fixed paraffin-embedded (FFPE) samples. This analysis revealed substantial changes in chromatin states in the primary tumor compared to the metastatic setting. The analysis of the annotated genes from paired samples (primary and metastatic tumors) highlighted a substantial upregulation of genes in the primary tumor and a downregulation of genes in the metastatic setting (Figure 37 B). This suggests a dynamic process where specific genes were switched off or exhibited reduced expression during therapy. The PCA analysis indicated a shift in the epigenomic landscape during metastatic progression for the majority of patients (Figure 37 C). This difference in distance between the two timepoints suggests a substantial variance between the primary and metastatic tumors. This reinforces the idea that there exist epigenetic modifications of transcriptional activity during the course of treatment. This indicates that metastatic tumors accumulate these epigenetic alterations, leading to distinguish from their primary original tumors.

This epigenetic analysis was focused on understanding the transcription factors (TFs) responsible for the downregulation of genes in the metastatic setting. Consequently, we studied the common genes that had significantly changed their expression. This analysis revealed significant changes in transcriptional regulator pathways, linked to histone modification, histone methylation and peptide methylation (Figure 38). The comparison of the genes identified in these 3 pathways pointed out 14 TF candidates that could explain the lack of response to the treatment that derived to metastasis (Figure 39 A).

To further filter this set of 14 genes, we compared them with unpublished Nanostring data performed with a list of poor prognosis markers, from the same patients. From these 14 genes, only GATA3 appeared in the list of poor prognosis markers. Therefore, GATA3 emerged as a potential candidate to be involved in the development of the metastasis. This finding was surprising as GATA3 is typically known for its roles in maintaining epithelial cell differentiation and suppressing metastasis [258, 259].

GATA3 has only been linked to metastasis in its loss of expression or mutations. Indeed, mutations in GATA3 that affect its DNA-binding capacity are commonly identified in breast cancer as this gene is one of the 3 most mutated ones and its mutation is observed in more than 10% of breast cancers [260, 261].

Indeed, MCF7 cell line carries a heterozygous frameshift mutation (an insertion at position 1566, D336fs) in the second zinc finger of GATA3, resulting in the synthesis of a truncated protein [260]. This mutation's precise role remains uncertain. Studies have indicated that the truncated GATA3 protein in MCF7 cells has impaired interaction with chromatin, leading to its easy release from the nucleus. They have also reported that this mutation may confer protection against the regulated turnover of GATA3 in MCF7 cells [262]. However, other studies indicated that the GATA3 mutation might enhance tumor growth *in vivo* [263]. Hence, the involvement of GATA3, whether mediated by wild-type or mutated, in promoting migration remains unelucidated and, thus, needs further investigation.

Regarding GATA3 loss of expression, it has been reported that, during the progression of luminal breast cancer, GATA3 expression gradually diminishes. Reduced GATA3 expression is closely associated with adverse indicators such as higher histologic grade, poor differentiation, positive lymph nodes, ER negativity, PR negativity, and HER2 overexpression, all of which signal a poor prognosis [264, 265]. However, from Nanostring data, we have observed that GATA3 expression was not reduced in the metastatic setting in all patients (Figure 39 B). Altogether, the published reports alongside with our findings prompted our interest in exploring the role of GATA3 as a TF in the metastatic setting.

Recent studies have demonstrated that the loss of function of GATA3 promotes breast cancer metastasis by regulating G9A and metastatic tumor antigen (MTA) family proteins [246]. The complex that GATA3 forms with MTA proteins is known as the Nucleosome Remodeling and Deacetylase (NuRD) complex, which plays a critical role in breast cancer

progression by regulating chromatin assembly and reorganization [266]. It has been proposed that the NuRD complex, when composed of GATA3, G9A, and MTA3, plays a role in inhibiting the invasive potential of breast cancer cells *in vitro* and suppressing breast cancer metastasis *in vivo* [246]. That publication claimed that during breast cancer progression, a downregulation of GATA3, G9A, and MTA3 takes place, which results in elevated ZEB2 expression. ZEB2, in turn, would repress the expression of G9A and MTA3 and allow MTA1 to bind to the NuRD complex. Therefore, NuRD (MTA1) would affect mammary epithelial cell fate and contribute to breast cancer metastasis inducing EMT [267]. The induction of EMT plays a crucial role in the acquisition of migratory and invasive capabilities by cancer cells, facilitating metastatic dissemination [268]. However, the molecular mechanism underlying the dual role of NuRD (MTA3) and NuRD (MTA1), in breast cancer progression is still unknown. It is important to emphasize that the mechanistic interplay between these components has not been explored within the context of resistance to AIs.

In our study, it was identified that cumulative signal intensity from Fit-Seq reads for MTA1 increased in metastatic tumors whereas, MTA3 signal was slightly reduced in the metastatic setting (Figure 40). This imbalance between the primary and metastatic tumor could be the reason for metastasis development. From these findings, we studied, *in vitro*, if the variations in the levels of MTA1 or MTA3 could impact the invasive and migratory capabilities of breast cancer cells. Therefore, in this thesis we hypothesized that GATA3/NuRD (MTA1) complex might promote a metastatic phenotype whereas GATA3/NuRD (MTA3) might promote a non-metastatic one in the context of AIs resistance. However, the specific mechanisms underlying the increased presence of MTA1 in metastatic patients or the reasons behind the decreased levels of MTA3 during metastasis goes beyond the scope of this work.

Our first experimental assay unveiled an intricate interplay between MTA1 and MTA3 observed in non-invasive breast cancer cells (MCF7 cells). The depletion of MTA1 resulted in a pronounced increase in both MTA3 mRNA and protein levels. Conversely, silencing MTA3 demonstrated a slight increase in MTA1 protein levels, but a substantial rise in MTA1 mRNA levels (Figure 41). These findings reinforce the dynamic interdependence and regulatory cross-talk between MTA1 and MTA3 within the NuRD, as previously observed [246].

Further, we elucidated the interactions of HDAC1 with ER and GATA3 as part of the NuRD complex. Our findings revealed that GATA3 and ER interact with HDAC1 regardless of the levels of MTA1 and MTA3 (Figure 42). Previous research demonstrated that GATA3 is physically associated with G9A and that it only interacts with MTA3 within the NuRD complex [246]. They also reported that MTA1 and MTA3 interact with HDAC1. Contradictory to the Si, Wenzhe et al. (2015) [246] results, our findings suggest that GATA3 could form a complex with MTA3 and MTA1 within the NuRD complex. This is not surprising as MTA1 and MTA3 have GATA domains. MTA1 and MTA3, despite being in different chromosomes, 14q32.32 and 2p21, respectively, hold a 69% identity. MTA1 and MTA3 have the same functional domains which are the bromo adjacent homology (BAH) domain, an EGL-27 domain, a SANT domain and a GATA type zinc finger (ZnF) domain [269]. While previous research by Si, Wenzhe et al. (2015) [246] has established the link between GATA3 and the NuRD complex, with MTA3, the specific interaction of GATA3 with MTA1 within the NuRD complex remained unexplored. Consequently, our primary focus centered on investigating this specific interaction.

After confirming the influence between MTA1 and MTA3 expression, our investigation focused on assessing the impact of the MTA1 and MTA3 imbalance on cell proliferation. However, no significant alterations in cell proliferation were detected upon depletion of either MTA1 or MTA3, regardless of the growth conditions (Figure 43). The outcome of our study aligns with the observations of Dannenmann, C. et al. (2008) in which they reported no significance effect on proliferation in MTA1-overexpressed ovarian cells (OVCAR-3) [270].

Nevertheless, our investigation revealed distinct effects of MTA1 and MTA3 on cell migration. When MTA3 was depleted, migration increased, the opposite effect occurred when MTA1 was silenced (Figure 44). When the complementary experiment was performed, elevated MTA3 levels were linked to reduced migration, while increased MTA1 levels were associated with enhanced migration (Figure 45). This effect was observed in all tested conditions, regardless of the presence of hormones, implying that it appears to be hormone-independent. This finding further validates the previously mentioned interplay mechanism wherein the depletion of MTA3 leads to the association of MTA1 with the NuRD complex, promoting the expression of EMT genes, like ZEB2 [246]. This finding underscores the significance of these proteins in influencing migratory behavior, highlighting the potential

relevance of these factors in the metastatic cascade. Numerous studies support the role of MTA1 and MTA3 in migration [271], but our results validate this concept, demonstrating a clear influence on cell migration based on the balance between MTA1 and MTA3 within the NuRD complex. This phenomenon has also been observed in ovarian cancer, where MTA1 expression was enhanced during cancer progression, while MTA3 exhibited an opposite effect potentially preventing EMT [270]. Nevertheless, it has also been reported in colorectal cancer that elevated levels of MTA3 are linked to the regulation of malignant progression [272]. Additionally, MTA3 is an oncogene and a prognostic factor in lungs [273].

Our *in vitro* validation through invasion assays using MCF7 cells under distinct hormonal conditions, provided compelling evidence of the impact of MTA1 and MTA3 imbalances on cell invasiveness. Under red medium (media with hormones), altering the expression of MTA1 or MTA3 did not significantly modify cell invasiveness, compared to the control group. This suggests that under standard estrogenic conditions, the sole depletion of MTA1 or MTA3 does not confer invasive properties to MCF7 cells (Figure 46). However, under white media (media without hormones), the depletion of MTA3 led to heightened cell invasiveness compared to the control and the MTA1-depleted condition (Figure 47). This observation implicates that the depletion of MTA3, leading to NuRD (MTA1) complex, confers invasive capacities. In contrast, the silencing of MTA1 did not significantly affect cell invasiveness compared to the control groups, which goes in line with our migration results, suggesting that, when MTA1 is downregulated, the NuRD complex is bound to MTA3 and, consequently, it lacks invasive capacity. The observed behavioral difference between mediums, with and without hormones, suggests a potential involvement of estrogens, or ER, in this biological process.

This might suggest that patients treated with AIs, when having low levels of MTA3, could confer invasive capacity to the cells through the NuRD (MTA1) complex. Thus, these findings reveal that the effect of NuRD (MTA1) complex inducing invasion might be contrasted in cells growth with estradiol. These findings are not surprising as it has been reported that MTA1 is a potent co-repressor of ERE transcription, by blocking the ability of estradiol to stimulate ER-mediated transcription. MTA1 can also interact with the endogenous ER [274].

Additionally, an overexpression on MTA1 levels, concurrent with MTA3 depletion, significantly increased invasiveness. Conversely, increased MTA3 expression, while silencing MTA1, did not significantly alter invasiveness (Figures 49 and 50). These results underlined that cell invasiveness effect could be enhanced in conditions of hormone deprivation, thus, with AI treatment.

Taking previous findings into consideration, we studied the implication of ER in the migration and invasion capacities of the NuRD complex when the levels of MTA1 and MTA3 were altered. Our findings pointed out the involvement of ER in modulating the interplay between MTA1 and MTA3 in the NuRD complex. Silencing experiments targeting ER, MTA1, and MTA3 revealed unexpected patterns in protein expression levels (Figure 51), challenging the findings of the existence of a dynamic interdependence and regulatory cross-talk between MTA1 and MTA3 within the NuRD complex (Figure 41). A possible interpretation for this unexpected pattern in protein expression levels of MTA1 and MTA3 could be due to the strong dependency of MCF7 to ER and MTA3 to grow [275]. Unpublish data from our group suggests that MTA3 might impair apoptosis induced by Skip/TGF-β pathway, exclusively occurring in ER-positive tumors. Consequently, the simultaneous silencing of ER and MTA3 could allow apoptosis induced by TGF-β, facilitating this apoptotic environment. In such a scenario, the expected upregulation of MTA1 protein levels might not occur.

Simultaneous depletion of ER and MTA3 resulted in a reduction in MTA1 levels which suggest that ER could be involved in the regulation of MTA1 and MTA3 cross-talk. Double silencing of ER and MTA1 did not increase MTA3 levels, which reinforces the idea that ER has a regulatory role in mediating the dynamic interplay between MTA1 and MTA3. These results go in line with what has been reported that silencing of ER resulted in the loss of MTA3 transcript in breast cancer cells [276]. This underscores the necessity of ER for endogenous MTA3 expression. Although in our results MTA3 protein levels were not significantly downregulated upon silencing of ER (Figure 51), there was a discernible trend indicating a potential impact of ER on MTA3 protein expression.

Our *in vitro* studies, examining cell migration under both red (medium with hormones) and white (without hormones) conditions, further emphasized the critical role of ER in altering migration in MCF7 cells in the presence of MTA1 and MTA3 imbalance. Silencing ER alone did not influence cell migration compared to the control group, which was expected

as MCF7 cell line is strongly dependent on ER and estrogens to grow [275]. Similarly, the absence of ER in combination with depletion of MTA3, reversed the migratory potential observed when silencing MTA3 alone (Figure 52). This double silencing leads to no overexpression in MTA1, suggesting that NuRD (MTA1) complex, when ER is depleted, cannot exhibit migratory capacity. Depletion of ER, alongside MTA1, led to a reduction in cell migration compared to MTA1 depletion alone. This effect on migration could be causative of the breakage of the dynamic interdependence and regulatory cross-talk between MTA1 and MTA3 within the NuRD complex. This effect is not surprising as we have proven in Figure 42, that HDAC1, from the NuRD complex, can directly interact with ER regardless of the levels of MTA1 and MTA3.

Regarding the impact of ER in invasion in the NuRD complex, we observed that cells exhibiting MTA1 overexpression concurrent with MTA3 depletion displayed enhanced invasion, which was reversed upon simultaneous depletion of ER regardless of the used medium (Figure 53 and 54). Conversely, when MTA1 was depleted and MTA3 overexpressed, cells exhibited unaltered invasive capacities, regardless of the hormone presence in the medium. These results emphasize the role of ER in disrupting the cross-talk between MTA1 and MTA3 within the NuRD complex. ER also seems to mediate the effect of NuRD (MTA1) complex on cell invasion. The fact that invasion is reverted when ER and MTA3 are depleted, despite MTA1 levels being overexpressed, lead us to think that when ER and MTA3 are initially depleted, they might interrupt the cross-talk between MTA1 and MTA3. Subsequently, although MTA1 is later overexpressed, it seems to be insufficient to bind to the NuRD complex forming the NuRD (MTA1). Consequently, ER might not be able to access and bind to the chromatin and, thus, initiate invasive actions.

Our next goal was to unravel the role of GATA3 within the NuRD complex dynamics, particularly its involvement in regulating cell migration when there is a protein imbalance between MTA1 and MTA3. Notably, GATA3 depletion led to decreased levels of MTA1 and MTA3. These results reinforce our idea that GATA3 could be part of the NuRD (MTA1) and NuRD (MTA3) complexes. The depletion of MTA1 resulted in increased levels of GATA3. In contrast, silencing of MTA3 resulted in decreased levels of GATA3, achieving same protein levels as silencing of GATA3 alone (Figure 55). It is noteworthy that these observations hint an interdependent relationship among these proteins. Double silencing of MTA1 and GATA3, resulted in an increase MTA3 protein level. Conversely, simultaneous

depletion of MTA3 and GATA3 resulted in a decrement in MTA1 levels regarding the observed levels when MTA3 was depleted alone. This breakage of the already confirmed dynamic interplay between MTA1 and MTA3 within the NuRD complex (Figure 41) gave further evidence of the existence of a cross-talk between GATA3, MTA1 and MTA3 within the NuRD complex (Figure 55).

The assessment of cell migration revealed that GATA3, MTA1, and MTA3 levels have an impact on migratory capacity of the cells. In the presence of medium with hormones (red), silencing GATA3 significantly reduced cell migration. However, there are other studies that have reported that the loss of GATA3 expression leads to a more migratory and invasive phenotype in breast and in bladder cancers [277, 278]. Nevertheless, the fact that we did not observe this phenotype might be because GATA3 alone was partially silenced and some GATA3 expression remained (Figure 55). However, this technical problem does not invalidate the other results, as the double silencing affected the cross-talk between MTA1 and MTA3. The simultaneous suppression of both MTA3 and GATA3 resulted in a pronounced reduction in migration, surpassing the observed effect when GATA3 was silenced alone. These findings suggest a critical role for GATA3 in counteracting cell migratory potential under conditions where NuRD complex is bound to MTA1. The simultaneous depletion of MTA1 and GATA3 further decreased migration compared to silencing MTA1 alone, indicating the significance of GATA3 in modulating migratory behavior of MCF7 within the NuRD complex. Similar trends were observed under hormone-depleted conditions (Figure 56). This effect on migration could be causative of the breakage of the dynamic interdependence and regulatory cross-talk between MTA1 and MTA3 within the NuRD complex.

Regarding the impact of GATA3 in invasion within the NuRD complex, we observed that cells exhibiting MTA1 overexpression, concurrent with MTA3 depletion, displayed enhanced invasion, which was reversed upon simultaneous depletion of GATA3 regardless of the used medium (Figure 57 and 58). Conversely, when MTA1 and GATA3 were depleted, simultaneously to MTA3 overexpression, cells did not exhibit any increase in invasive potential in medium with hormone. However, in medium without hormones, the concurrently silencing of GATA3 reduced invasive capacities compared to the condition that MTA1 was silenced and MTA3 was overexpressed. These findings highlight the role of GATA3 in disrupting the cross-talk between MTA1 and MTA3 within the NuRD complex.

The reversal of invasion upon depletion of GATA3 and MTA3, despite elevated MTA1 levels, suggests that the initial depletion of GATA3 and MTA3 potentially disrupts the interaction between MTA1 and MTA3. As a result, although MTA1 becomes overexpressed later on, it appears insufficient to establish binding within the NuRD complex, forming the NuRD (MTA1) complex. Altogether, the interplay among GATA3, MTA1, and MTA3 revealed intricate dynamics, where the depletion of one protein influenced the levels of the others. This underscores the relevance of these proteins within the NuRD complex regulation. Our findings are aligned with prior reports that have exclusively detailed the involvement of GATA3/NuRD (MTA3) in suppressing the processes of EMT and cellular invasion [246].

Moreover, the observed trends in mediums with and without hormones suggest that the impact of GATA3 on cell migration and invasion might be independent from estrogen-related pathways. Therefore, our findings reinforce our hypothesis that GATA3 could bind to MTA1 and form the NuRD (MTA1) complex, which seems to be responsible for the observed migratory and invasive actions. However, in previous research, it has been asserted that a strong association exists between GATA3 and ER. A meta-analysis indicated that GATA3 participates within the ER pathway regulating tumorigenesis and the tumor progression [279].

We further studied the simultaneous effect of ER and GATA3 by using MDA-MB-231 which is a more aggressive breast cancer cell line that does not express ER nor GATA3 [278]. We aimed to elucidate whether our phenotypical observations in MCF7 cells was exclusively dependent on ER-positive and GATA3-positive cells or not. The depletion of MTA3 in MDA-MB-231 cells exhibited reduced cell migration in medium with hormones and no differences were observed in medium without hormones. The downregulation of MTA1 in medium with hormones resulted in increased cell migration relative to the depletion of MTA3, but still less migration than the control was observed. However, silencing MTA1, in medium without hormones, exhibited more cell migration (Figure 59).

The MDA-MB-231 cell line exhibited different migratory behavior compared to MCF7 cells. This reversal of cellular behavior upon imbalance between MTA1 and MTA3, suggests there is an interplay between MTA1, MTA3, ER and GATA3 in MCF7 cells, being necessary the expression of ER and GATA3. These results suggest that this cross-talk seems not to be present in triple negative tumors, highlighting the complexity of these interactions

and its dependence on the tumor type. It seems that the migratory promotor effect observed in NuRD (MTA1) complex will exclusively occur in ER-positive and GATA3-positive cells. This finding reinforces the idea that the migratory effect of NuRD (MTA1) complex could be dependent on ER context, meaning that MTA1 does not have a migratory role in ER-negative cells. However, when MTA3 is bound to the NuRD (MTA3) complex, it could induce migration in ER-negative cell lines, but it seems to hinder cell migration in ER-positive cell lines. This finding reinforces the possible dual role of MTA3 in promoting, or impairing, metastasis in a context-dependent manner. Indeed, MTA3 overexpression has been liked to carcinogenesis through Wnt signaling pathway in colorectal cancers [272].

Altogether, these findings suggest that both GATA3 and ER seem to be necessary for the actions of NuRD complex either bound to MTA1 or MTA3. Additionally, it seems that ER and GATA3, directly or indirectly, break the dynamic interplay of MTA1 and MTA3 reverting the migratory and invasive capacities of the NuRD complex. Finally, the apparent mandatory presence of ER and GATA3 could be due to a physical interaction with the chromatin by regulating the binding of the NuRD complex, changing their action on migration and invasion.

Once the phenotype was characterized, we conducted RNA-Sequencing on MCF7 cells depleted of MTA1 or MTA3. Our RNA-Sequencing analysis demonstrated significant alterations in gene expression upon depletion of either MTA1 or MTA3. The comparative analysis between siMTA3 and the control group (siNT), depicted in a volcano plot (Figure 60 A), identified 68 genes significantly upregulated and 64 genes downregulated, with a p-value equal or lower to 0.00001. The results of the GSEA showed that among the upregulated pathways, only EMT exhibited significance. In contrast, the downregulated pathways comprised Estrogen Response (Early and Late) and KRAS Signaling (Figure 60 B).

These results confirm that, when MCF7 cells are depleted of MTA3, genes related to EMT are upregulated. This suggests that the phenotype of the NuRD (MTA1) complex could be due to the activation of the EMT, exhibiting more migratory and invasive capacities. However, cells not only activate the EMT, but also downregulated ER signaling pathways and KRAS signaling. Therefore, it seems that the NuRD (MTA1) is able to repress the estrogen regulated pathways. This suggests that these pathways are blocked regardless of the presence of estrogens in the medium, thus, cells might not be responsive to anti-ER therapies as they seem to grow in a complete ER independent manner. Regrading ER, these results

suggest that GATA3/NuRD (MTA1) complex could bind to ER chromatin binding sites and impair transcriptional activity of ER. Therefore, MTA1, would inhibit transcriptional program of ER agreeing with previous studies from Mazumdar, A. et al. (2001) [274].

In the context of MTA3 silencing, the downregulation of KRAS signaling pathways appears logical, given their role in promoting cell proliferation, which is suppressed when NuRD binds to MTA1. Among the genes affected in this pathway, endothelin 2 (EDN2), stands out for its contribution to cell proliferation associated with KRAS signaling (Table 24 in Annex). In this scenario, MTA1 enhances migration and invasion, halting cell proliferation to facilitate metastasis. Additionally, our findings in cell proliferation (Figure 43), demonstrated that the imbalance between MTA1 and MTA3 does not impact cell proliferation [280]. Moreover, the NuRD (MTA1) phenotype seems to be related with KRAS signaling, suggesting an activation of genes repressing the KRAS pathway, enhancing cell migration and invasion. Under these conditions of low levels of MTA3, the NuRD (MTA1) MCF7 cells seem to become insensitive to medium without hormones reinforcing the relationship between EMT and the lack of response to AIs treatment.

Similarly, the comparison of the RNA expression of siMTA1 with the control group was illustrated in a volcano plot (Figure 60 C) and identified 48 highly significant genes upregulated and 57 that were highly downregulated, with a p-value equal or lower than 0.00001. The conducted GSEA revealed that among the upregulated pathways, five of them were significant, including Late Estrogen Response and EMT, also found to be significant in the siMTA3 analysis. This reaffirms the context-dependent nature of the MTA1 and MTA3 imbalance. However, there were no significant pathways identified in the downregulated genes (Figure 60 D). These findings suggest that the dynamic interdependence and regulatory cross-talk between MTA1 and MTA3 within the NuRD complex contributes to the regulation of key pathways associated with breast cancer progression, particularly EMT and estrogen response.

From the RNA-Seq results we further validated a few genes found upregulated in the siMTA3 versus siNT condition. Specifically, our aim was to investigate the gens from the EMT pathway to identify the ones that contribute to the observed phenotype upon MTA3 depletion. Among the identified genes implicated in the EMT pathway, our selection for *in vitro* validation through RT-qPCR included RBPJ and BMP7. RBPJ have been reported to promote cell proliferation and invasion in glioblastoma multiforme (GBM) [281]. BMP7 has

been reported to counteract EMT induced by TGF-β [282]. We explored the expression of these genes in MCF7 cells experiencing an imbalance between MTA1 and MTA3. Concurrently, we subjected these cells to treatment with the HDAC inhibitor, Romidepsin, considering the involvement of HDACs (1 and 2) as subunits of the NuRD complex. Our observations revealed that the highest levels of RBPJ and BMP7 were achieved in conditions where MTA3 was depleted. In contrast, RBPJ and BMP7 levels were comparable to the control when MTA1 was depleted. However, upon treatment with Romidepsin, the gene levels exhibited a consistent decrease across all three conditions compared to the siNT alone (Figure 61 A and B). This experiment confirmed the results from the RNA-Seq, that an imbalance of MTA1 and MTA3 is implicated in EMT and opens the door to therapeutic exploration to inhibit the NuRD complex through HDAC inhibitors. Nevertheless, the mechanism by which the NuRD (MTA1) upregulates the expression of these genes remains unexplored in this work.

The NuRD complex, comprised of various subunits including histone deacetylases HDAC1 and HDAC2, has emerged as a significant regulator of gene expression and cellular processes by repressing key genes in cancer progression and metastasis [283]. After understanding the dynamics of the NuRD complex, we explored whether it could be a therapeutic target in breast cancer. For that purpose, the specific inhibition of HDAC1 and HDAC2 was investigated. Our investigation delved into the effects of HDAC inhibitors, namely Romidepsin and Valproic Acid (VPA), on MCF7 cell migration in relation to MTA1 and MTA3 protein imbalance. It is known that Romidepsin, has a high affinity towards Class I HDACs specially HDAC1 and HDAC2 [284], whereas Valproic acid (VPA), targets Class I and Class IIa HDACs [285].

Interestingly, when treating MCF7 cells with Romidepsin and simultaneously, depleting the levels of MTA3, the increased migration induced by MTA3 depletion was reversed (Figure 62). These results indicate the potential efficacy of Romidepsin in preventing cell migration in cases exhibiting low MTA3 levles. However, when depleting MTA1 and treating cells with Romidepsin, unexpectedly heightened migration rates have been observed. This behavior has been observed regardless of the hormone levels, but the reversion of MTA3 depletion was more accentuated in medium with hormones. Our data suggest that upon stratification of patients on MTA1 and MTA3 levels, if Romidepsin is administered, it should be given as a monotherapy rather than in combination with AIs.

However, additional *in vivo* experiments should be performed to validate the beneficial role of combining this treatment with anti-ER therapies.

Remarkably, these results point out a differential potential effectiveness of Romidepsin based on MTA1 and MTA3 levels. It seems that when Romidepsin is administered and MTA3 levels are low, MTA1 might not be able to bind to the NuRD complex and exhibit its reported migratory activity. In contrast, our findings revealed that, with low levels of MTA1 and, upon administration of Romidepsin, the NuRD (MTA3) complex seems to acquire migratory capacity. This underscores a potential dual role of MTA3 within the NuRD complex going in line with previously reported papers that indicated MTA3 as a tumor progression and poor prognosis marker [286].

Similarly, VPA showed differential effects on cell migration upon MTA1 and MTA3 levels. When MTA3 was depleted, and cells were treated with VPA, it effectively reversed enhanced migration caused by MTA3 depletion (Figure 63). This finding underscores the potential of VPA in impeding cell migration in low MTA3 conditions regardless of the presence of hormones. It seems that when VPA is administered, and MTA3 levels are low, MTA1 might not be able to bind to the NuRD complex and exhibit its reported migratory activity. Conversely, in the context of MTA1 silencing, VPA treatment paradoxically resulted in increased migration rates only in medium with hormones. These findings suggest that with low levels of MTA1 and upon VPA administration, the NuRD (MTA3) complex seems to acquire migratory capacity only when there are hormones present in the medium. The differences observed between mediums with and without hormones may indicate the role of additional factors in modulating cell migration. This observation underscores a potential connection between estrogens, or ER, and their interaction with HDAC 1 or 2. Furthermore, it implies that combining VPA with hormone therapies, such as AIs, could be a viable approach, only if this combinatory treatment shows no side effects nor toxicity.

These findings highlight the necessity of meticulous patient selection and thorough assessment of MTA1 and MTA3 levels before commencing HDAC1 inhibitor-based therapies. The discrepancies observed in migration patterns in response to Romidepsin and VPA treatment underscore the importance of personalized approaches in selecting the appropriate HDAC1 inhibitor based on the NuRD complex composition. Moreover, these results could shed light on previous HDAC clinical trial failure on solid tumors (prostate cancer) [287]. Therefore, these findings suggest that for targeting the NuRD complex, *in*

vivo studies are needed. However, there is a need for patient stratification based on MTA1 and MTA3 expression levels for optimal therapeutic outcomes in metastatic breast cancer. Nevertheless, further understanding of efficacy and limitations of these therapeutic strategies is needed. In addition, these phenotypic behaviors could also be assessed in other breast cancer subtypes or even in other cancer types.

CONCLUSIONS II

CONCLUSIONS II

The main conclusions of this chapter, dedicated to the identification of epigenetic features influencing resistance to aromatase inhibitors in luminal breast cancer patients progressing towards metastasis, are the following:

1. Epigenetic analysis performed in paired samples (primary and metastases) of patients resistant to endocrine treatment underscored epigenetic dynamics in treatment response and metastases progression.

2. The epigenetic analysis revealed transcriptional regulators, among which GATA3 emerged as a pivotal transcription factor significantly implicated in breast cancer metastasis.

3. The NuRD complex plays opposite roles in ER-positive tumors regulating migration and invasion depending on the MTA protein bound to the complex.

4. In ER-positive and GATA3-positive cells, both GATA3 and ER seem to be necessary for the enhanced migratory and invasive phenotype of the NuRD (MTA1) complex, whereas NuRD (MTA3) might promote a non-metastatic phenotype in the context of aromatase inhibitors resistance.

5. In ER-negative and GATA3-negative cells, the NuRD (MTA3) complex led to enhanced migratory capabilities, whereas the migratory capabilities of NuRD (MTA1) complex were lessened.

6. GATA3/NuRD (MTA1) complex promotes metastasis facilitating the expression of genes that activate epithelial-mesenchymal transition and represses ER transcriptional activity.

7. Targeting NuRD complex with HDAC inhibitors in conditions where there is an imbalance between MTA1 and MTA3, can prevent cells migration in MCF7 cells unveiling its potential for personalized medicine.

METHODS

Experimental models

NeoLetExe clinical trial

Blood-serum samples, fresh frozen (FF) tissue, and immunohistochemistry (IHC) slides were collected from the first 30 patients enrolled in the NeoLetExe clinical trial. Sample collection occurred at three key timepoints: before the initiation of any treatments (baseline), after 2 months of receiving the first treatment, and after 4 months from the start of the clinical trial, while patients were still undergoing treatment with the second drug. These samples were sourced from the Clinical Research Unit within the Division of Medicine at Akershus University Hospital.

In this study, various parameters were assessed for each patient. These parameters encompassed biochemical data, measurement of tumor size using calipers, pre-biopsy breast MRIs, follow-up MRIs after 2 months of treatment, another follow-up at 4 months, and imaging just before the final surgical procedure. All biopsies were obtained through surgical methods under anesthesia and were subsequently subjected to pathological examination to determine the status of ER, PR, HER2, and Ki67 expression. From the biopsies, a portion of the tissue was rapidly frozen using liquid nitrogen and stored at -80°C for further analysis.

Additionally, several clinical data variables such as age, body mass index (BMI), breast cancer type, tumor grade, residual tumor, treatment sequence, relapse, presence of metastasis at diagnosis, decease, decease related to breast cancer and response were provided. This last variable encompassed three values: partial response (PR), stable disease (SD), and complete response (CR).

Primary and metastatic samples

For the metastatic project, we obtained five formalin-fixed paraffin-embedded (FFPE) samples derived from the primary tumors of luminal breast cancer patients. These patients underwent a treatment regimen consisting of 2 years of tamoxifen followed by, at least, 3 years of aromatase inhibitor therapy. Subsequently, the patients were closely monitored for this period, during which they developed metastatic tumors. FFPE samples from these metastatic sites were also collected for analysis. All these tissue samples were sourced from Vall d'Hebron Hospital in Barcelona, Spain. Additionally, mRNA from both the primary tumor and metastatic tumor tissues were extracted and analyzed using the NanoString nCounter® platform.

Ethic disclaimer

The utilization of patient samples was carried out in adherence to established methods and policies for informed patient consent, which had received approval from the Bioethics committees of Clinical Research Unit within the Division of Medicine at Akershus University Hospital and from the Bioethics committees of Vall d'Hebron Research Institute**.**

Cell culture

Breast cancer cell lines used in the thesis were breast adenocarcinoma MCF7 cells (ER-positive, HER-2-negative); MCF7-AR cells (ER-positive, HER-2-negative, AR-positive); MCF7-Luc cells (ER-positive, HER2-negative); and metastatic breast carcinoma MDA-MB-453 cells (ER-negative, HER-2-negative and AR-positive). All these cancer cell lines were purchased from the American Type Culture Collection (ATCC). MDA-MB-231 cells (ER-negative, HER2-negative) were generously provided by Dr. Jesús Pérez Losada from the Cancer Research Center at the University of Salamanca, Spain. All cell lines were cultured in Dulbecco's Modified Eagle's Medium (DMEM) (Gibco, 21969) supplemented with 10% heat-inactivated Fetal Bovine Serum (FBS) (Gibco, 10270106), 1% L-glutamine (GlutaMAX 100X) (Gibco, 35050061), 1% Penicillin-Streptomycin (Gibco, 10378016) and 1% of Sodium Pyruvate (100 mM) (Gibco, 11360070). This was the standard culture conditions, unless otherwise specified. The cells were maintained at 37°C in a 5% CO2 environment. Cells were regularly tested (every 2 weeks) for mycoplasma infection.

Methods

Fixed-tissue chromatin immunoprecipitation (Fit-Seq)

To conduct fixed-tissue chromatin immunoprecipitation (Fit-Seq), two sections of 10-µm thickness of formalin-paraffin fixed tissue (FFPE) were needed. Each tissue section was processed independently until the chromatin immunoprecipitation step. FFPE tissue sections were washed with xylene (PanReac, 251768) by incubating the samples at room temperature (RT) for 10 min on a rotating platform, followed by centrifugation at 14000 g at RT for 8 min and a total of 3 washes. Then, samples were rehydrated through a gradient of ethanol/water solutions (95/5, 80/20, 70/30, 50/50, 20/80, 0/100). After each wash, samples were incubated for 10 min at 4°C in a rotator platform end-to-end and centrifuged for 5 to 20 min at 4°C and 14000 g. The samples were resuspended in 500 µl of 1% (wt/vol) sodium dodecyl sulfate (SDS) lysis buffer and it was incubated in the shaker overnight at 65°C at 900 rpm. The resulting material was sonicated through 9 cycles of 30s ON and 30s OFF at low intensity (4 mA) (diagenoide, Bioruptor plus). After sonication, samples were centrifuged for 20 min at 14000 g at 4°C and the supernatant was collected to perform the chromatin immunoprecipitation (ChIP) protocol, with 10 µl of chromatin taken aside as an input. Additionally, a chromatin shearing test was conducted to verify the effective sonication of the chromatin. To accomplish this, 25 µL of chromatin were mixed with 75 µL of TE pH 8 and chromatin was reverse cross-linked overnight at 65°C. Subsequently, the samples were mixed with 6x loading buffer (Thermo scientific, R0611) and loaded onto a 2% agarose gel. Gel was prepared by mixing agarose with 1x TAE and with GelRed (Biotium, 41003). For this experiment, the 1 kb to 100 bp Gene ruler (Thermo scientific, SM0321) was used as a marker.

Magnetic beads Dynabeads A (Invitrogen, 10001D) (100 µl/ChIP) were pre-blocked and coupled with 10 µg of antibodies against H3K27actyl (abcam, 4729) in a total volume of 1 ml of PBS/BSA buffer and incubated at 4°C overnight on an end-to-end rotator platform. After washing the beads with PBS/BSA, they were resuspended with sonicated chromatin and topped up (until 2 mL) with a 1% (wt/vol) SDS lysis buffer. Beads, chromatin and the coupled antibody were incubated overnight at 4°C on an end-to-end rotator platform. Then, beads were washed 5 times with RIPA buffer and DNA from the beads and from the input was eluted with an elution buffer. Eluted samples were treated with 10 µg of RNAse A (Invitrogen, AM2271) and were incubated at 37°C for 30 min at 900 rmp on the shaker. Reverse crosslink was performed by adding proteinase K at a final concentration of 1 µg/µl,

followed by overnight incubation at 65°C at 900 rpm on the shaker. All buffers are detailed in Table 12.

Samples were purified by performing an ethanol purification, which consists on adding phenol-chloroform-isoamyl (Sigma-Aldrich, 77617), 2 volumes of 3M Na-acetate (Invitrogen, AM9740) pH 5.5, 440 µl of 100% ethanol and 2 µl of glycogen (as a carrier) (Invitrogen, 10814-010). Samples were left overnight at -80°C and were, finally, washed twice with 70% ethanol before being resuspended in 10 mM tris HCl, pH 8.

The quantification of soluble chromatin was performed fluorometrically using QubitTM dsDNA HS Assay Kit (Invitrogen, Q32851) and measured with Qubit® 2.0 Fluorometer (Invitrogen). DNA libraries were prepared by the Center for Genomic Regulation (CRG) in Barcelona using ThruPLEX-FD kits (Takara, R400674) following the manufacturer's protocols. Subsequently, these libraries were subjected to sequencing on an Illumina Nextseq 2000 instrument with a coverage of 50 million of reads per sample with a read length of 50 bp single end.

Bioinformatic analysis of Fit-Seq

Bioinformatic analyses were performed on the Consorci de Serveis Universitaris de Catalunya (CSUC) High Performance Computing (HPC) server. This cluster of machines consists of 2 elements: a shared-memory Bull Sequana X800 of 16 processors and a Bull Sequana X550 of heterogeneous-distributed-memory, integrated by 60 computing nodes with a total of 2688 computing cores. In total the cluster has 13.44 TB of memory and 240 TB of disk. The obtained results were downloaded to a HP-15s-fq machine running on Intel i7-1165G7 processor at 2.80GHz and Windows 10 Home. The memory of this machine is 12GB and the GPU is an Intel Iris Xe Graphics, which packs 5.8GB of memory.

Reads in FASTQ files were first analyzed through a quality control process, using the fastqc package (version 0.11.9) to obtain, among others, the number of reads. Next, optical duplicated reads were filtered out using fastx-toolkit (version 0.0.14). Once filtered, FASTQ reads were aligned to the hg19 human genome (index file hg19.4.bt2) using bowtie2 (version 2.4.2) and converted to BAM format using samtools view (version 1.7). Then, files from different runs were merged using samtools merge, duplicated were removed using samtools markdup and, finally, the final BAM file was converted to BED using samtools bamToBed. After this process, files were ready to proceed with the peak calling. This process was carried

out with the sicer2 package (version 1.0.3) with the hg19 human genome as species (-s argument) and the input file as control (-c argument).

To assess overlapping between SICER peak calling, bed files were uploaded to a Jupyter notebook (Python 3.8.8 and Conda 4.11.0). Datasets were read, processed and saved using Pandas (version 1.2.4). Afterwards, files were uploaded to RStudio (R 4.0.3) to compute the overlapping using BiocManager (version 1.30.17), GenomicRanges (version 1.42.0), readxl (version 1.4.0) and ChIPpeakAnno (version 3.24.2). Functions GRanges and makeVennDiagram were used to plot the Venn diagrams showing the overlapping between peaks. To perform the filtering of unique peaks, bed files were uploaded to Jupyter notebook and to a local database with sqlite3 (version 2.6.0). Data was overlapped using sql-like queries with pandasql (version 0.7.3). Resulting files containing the overlapped and the non-overlapping peaks were downloaded in bed format. Bed files to be annotated were uploaded to RStudio and processed with tidyverse (version 1.3.1) and dplyr (version 1.1.4). Peaks were annotated using TxDb.Hsapiens.UCSC.hg19.knownGene (version 3.2.2) alongside annotatePeak function from ChIPseeker (version 1.26.2). Venn diagram representing the non-overlapping genes was plotted using makeVennDiagram function from the ChIPpeakAnno package. Gene Set Enrichment Analysis (GSEA) used the annotated files with gseGO function from clusterProfiler (version 3.18.1).

To perform the comparation between the GSEAs of the primary and metastatic tumors, the resulting enriched pathways from both datasets were sorted in descending order of the net enrichment score (NES). Then, a column was created containing the position of each pathway and both datasets were joined using the pathway name. Next, a new column with the difference between the position in the primary and in the metastatic dataset was calculated. The resulting dataframe was ordered using the difference in ranking. All these operations were performed using tidyverse and dplyr libraries. Then a barplot was represented using ggplot2 package (version 3.4.4). From the selected pathways from a GSEA, enrichment plots were represented using the gseaplot function from the enrichplot package (version 1.14.2).

To perform the signal intensity distribution, first bam files need to be converted to bigwig files using bamCoverage function from deepTools package (version 3.5.0) using a bin size for the output of 10 (binSize parameter), normalizing using bases per million (BPM) (normalizeUsing parameter), extending each read by a fragment size of 150 (extendReads

parameter) and centering the reads (centerReads parameter). The input for the heatmap is a matrix that is produced by the computeMatrix function (deepTools package). At the same time, the computeMatrix function needs the bigwig files of all the patients and a bed file containing which regions are going to be analyzed (R argument). This bed file is produced by merging the bed files for the different patients, sorting and only keeping the first 3 columns. This process is all made using bash commands (cat, sort and cut). For the computeMatrix function, the reference point used is the transcription start site (TSS) (referencePoint argument) and 1000 base pairs will be analyzed before the beginning and after the end of each region of the bed file (beforeRegionStartLength and afterRegionStartLength arguments). The results were visually depicted utilizing GraphPad Prism software (version 8).

To plot a principal component analysis (PCA), the function plotPCA (deeptools package) will be used. This function needs a npz file, which will be created with the multiBigwigSummary function (deeptools package). This function takes as input all the big wig files from all the patients and a bed file with all the patients' peak callings merged, sorted and without duplicates (BED argument).

Fresh frozen (FF) tissue chromatin immunoprecipitation (ChIP)

From the NeoLetExe clinical trial, we conducted ChIP analysis using fresh-frozen (FF) tissue samples. Specifically, we examined two sets of samples: baseline samples and samples obtained from patients who had undergone exemestane treatment for 2 months. These patients exhibited favorable or intermediate clinical outcomes and presented with high or moderate levels of androgen receptor (AR) expression.

To perform FF-ChIP-Seq, 80 mg of fresh-frozen tissue were used. The tissue was first pulverized by a hammer and liquid nitrogen (LN2). Following this, the tissue was resuspended in a 1% formaldehyde solution and briefly swirled, allowing it to undergo fixation for 10 min at RT. To stop the formaldehyde fixation process, glycine was added at a final concentration of 125 mM. The samples were placed on a rotator platform at RT for 5 min. After formaldehyde fixation, the fixed tissue samples were collected by centrifugation at 500 g for 5 min at 4°C. The resulting pellet was washed 3 times with 1.5 mL of ice-cold PBS-cOmplete buffer. After each wash with PBS, the tissue was dounced using a tight pestle.

Next, the crosslinked tissue pellet was lysed with 1 mL of LB1, and it was left to rock on a rotator platform for 10 min at 4°C. The samples were subsequently centrifuged at 2000 g for

5 min at 4°C. The isolated nuclei were obtained by resuspending the pellet in 1 mL of LB2 and rocking it on a rotator platform for 5 min at 4°C. The pellet containing the nuclei was again centrifuged at 2000 g for 5 min at 4°C. Finally, the pellet containing the isolated nuclei was resuspended in 200 µL of LB3. All buffers are detailed in Table 12.

Next, the samples underwent sonication through 15 cycles of 30s ON and 30s OFF at low intensity (4 mA) (diagenoide, Bioruptor plus). Following sonication, the samples were centrifuged at 14000 g for 20 min at 4°C. The supernatant was collected for to perform the ChIP protocol, while a 10 µl aliquot of chromatin was set aside to be used as an input control. The chromatin shearing test to verify the effective sonication of chromatin was performed. However, for this particular FF ChIP, beads were conjugated with 10 µg of antibodies targeting the AR (Santa Cruz, sc-816). Following quantification using a QuBit instrument, DNA libraries were prepared by the CRG in Barcelona using the New England Biolabs (NEB) library preparation kit. Subsequently, these libraries were subjected to sequencing on an Illumina Nextseq 2000 instrument with a coverage of 50 million of reads per sample with a read length of 50 bp single end.

Bioinformatic analysis of FF-ChIP-Seq

For the post-processing and analysis of the FF-ChIP-Seq files, the same pipeline was followed as in section Bioinformatic analysis of Fit-Seq.

Exploratory data analysis on NeoLetExe patient data

Data regarding different clinical variables such as age, body mass index (BMI), breast cancer type, tumor grade, ER status, HER2 status, residual tumor, the treatment sequence, relapse, presence of metastasis at diagnosis, decease, and decease related to breast cancer was provided by Prof. Jürgen Geisler. This dataset contained anonymized information for 100 patients and was uploaded to a Jupyter Notebook and processed using pandas. Then different barplots were depicted using the seaborn package (version 0.13.0).

Biochemical NeoLetExe patient data

Data containing the levels of estrogen, letrozole, exemestane and 17-HEXE at different timepoints was uploaded to a Jupyter Notebook and processed with pandas. Regarding estrogen levels comparation, a line plot with a confidence interval corresponding to the standard error was plotted using the lineplot function from seaborn.

For the ratio between 17-HEXE and exemestane, it was calculated using standard python operations and it was plotted using the barplot function from seaborn with the treatment response as hue. Similarly, a barplot for the levels of exemestane and 17-HEXE was plotted, and each patient was colored with red or blue by creating a custom seaborn color palette with different shades of blue and red.

siRNA mediated silencing

Transient silencing of MTA1 and MTA3 was performed using short-interfering RNAs (siRNAs) (Table 14). MCF7 and MDA-MB-231 cell lines were reverse transfected with 50 pmols/well of siRNA using Lipofectamine RNAiMAX Transfection Reagent (Invitrogen, 13778150). For each well of a 6-well plate, a mixture containing 50 pmols of either siMTA1, siMTA3, or siNT (Non-targeted) (Ambion, 4390844, which served as a negative control) was prepared. This mixture was combined with 150 µL of 1x Opti-MEM (Gibco, 11058-021) and 9 µL of lipofectamine RNAiMax. The resulting mixture was allowed to incubate for 20 min at RT. Subsequently, the cells were seeded to achieve 50% confluence upon transfection in a 6-well plate. These cells were seeded with DMEM at 10% FBS (without Penicillin-Streptomycin). 6 h after seeding, the cell culture medium was replaced with DMEM containing 5% FBS. Depending on the specific experimental requirements, cells were cultured for varying durations between 24 and 72 h. The specific culture times for each experiment, such as western blot analysis, wound healing assays, invasion assays, proliferation assays, RNA-Seq, RT-qPCR, ChIP-Seq, or immunoprecipitation (IP), are detailed in their respective sections.

RNA-Seq isolation and RNA extraction

For the RNA-Seq analysis in the metastatic project, MCF7 cells were transfected with siRNA (siMTA1, siMTA3 and siNT (Table 14)). After 48 h, RNA from these cells was isolated using the manufacturer's instructions provided by the RNeasy Plus Mini kit (Qiagen, 74134). Following RNA isolation, RNA was quantified using Nanodrop. Isolated RNA was sent to sequencing at BGI Genomics.

For the RNA-Seq analysis within the NeoLetExe project, MCF7-AR cells were seeded in a 6-well plate with a 50% confluence. These cells were subjected to various treatments, including vehicle (DMSO), 17-HEXE at 5 µM, exemestane at 1 µM, and a combination of exemestane and 17-HEXE at 1 and 5 µM, respectively. After 24 h incubation, RNA was isolated using the RNeasy Plus Mini kit (Qiagen, 74134), again following the manufacturer's

instructions. Following RNA isolation, RNA was quantified using Nanodrop. Isolated RNA was sent to sequencing at BGI Genomics.

Bioinformatic analysis of RNA-Seq

To generate gene read counts from the RNA-Seq data to then calculate differentially expressed genes, first FASTQ files were mapped to the human genome using STAR mapper (version 2.7.0a) in the HPC server. Then, using the resulting mapped BAM file and the gtf file from the ENSMBL database, read counts per gene and per condition were calculated in R using the featureCounts function from the Rsubread package (version 1.22.2).

To identify significantly upregulated and downregulated genes, different volcano plots were depicted using R. The first step was to read a gtf file containing all the genes in the ENSEMBL database. This file was read using the import function from the rtracklayer package (1.54.0). Subsequently, a dataframe containing the sample id and the conditions was created and the file containing the individual read counts was also uploaded. Then, a matrix was created merging the conditions with the expression dataframes by using the DESeqDataSetFromMatrix from the DESeq2 package (version 1.34.0) and the differential expression analysis was performed using the DESeq function. Finally, the volcano plot was represented using the EnhancedVolcano function from the EnhancedVolcano package (version 1.13.2). The upregulated and downregulated genes, which had a -log10(p-value) bigger than 5 and a log2(fold change) bigger than 1 or smaller than -1, were colored in red.

Next, from the upregulated and downregulated genes a GSEA was performed using the pathways related to cancer hallmarks from the MSigDB database. This was done using the msigdbr function from the msigdbr package (version 7.5.1) and by specifying “Homo Sapiens” as species and “C6” as category, which corresponds to the cancer hallmarks section. As the number of upregulated and downregulated genes was too low to perform the GSEA, the threshold of the p-value was set to 0.05, which is equivalent to a -log10(p-value) of, approximately, 1.30. The resulting pathways were sorted by descending order of the NES and plotted using the geom_bar function from ggplot2.

RT-qPCR

After RNA isolation, the RNA was converted to complementary DNA (cDNA) by employing the high-capacity reverse transcriptase kit (Applied Biosystems, 4368814), following the manufacturer's protocol. The resulting cDNA was then distributed into a 96-

well plate, mixed with PowerSYBR Green PCR Master Mix (Applied biosystems, 4367659), and also mixed with their corresponding primers (Table 17). RT-qPCR was carried out following the manufacturer's protocol. The cycle thresholds (Cts) obtained from the RT-qPCR analysis were subsequently standardized using the Cts of the housekeeping genes. The results were visually depicted utilizing GraphPad Prism software.

Nanostring

Total RNA (150 ng) was shipped to the NanoString nCounter® Human mRNA Expression Assay analysis. This RNA came from paired FFPE samples of metastases (n=5) and primary tumors (n=5). RNA was incubated in the presence of mRNA specific probes. To account for minor differences in hybridization and purification efficiencies raw data was adjusted using a technical normalization factor calculated from 6 internal positive spike controls present in each reaction. Background hybridization was corrected by deducting the negative control mean plus 2 standard deviations calculated from 8 negative controls. The results were visually depicted utilizing GraphPad Prism software.

Luciferase assay from serum of NeoLetExe patients

To conduct the luciferase assay for NeoLetExe patient serum, engineered MCF7 cell line were used. This specific cell line was genetically modified to include a luciferase reporter cassette downstream of the TFF1 promoter [221]. For the luciferase assay, MCF7-Luc cell line was seeded into a white transparent 96-well plate (PerkinElmer) at a density of 10000 cells per well. The cells were cultured in DMEM supplemented with 10% FBS. After a 24 h incubation period, the culture medium was replaced with white DMEM (Gibco, 31053-028) which contains high glucose, but it does not contain phenol red nor antibiotics. White DMEM was supplemented with 2% charcoal stripped FBS (Gibco, 12676029), 1% L-glutamine and with 1% of sodium pyruvate. Medium was changed every day for 72 h, to ensure that the experiment was performed in an estrogen-depleted conditions. Following this estrogen-depletion period, the medium was substituted with white DMEM without FBS. Instead, we introduced 20% of the serum obtained from patients at various timepoints, including baseline, 2 months into treatment, or 4 months into treatment. In some experiments, specific drugs such as fulvestrant and bicalutamide (Table 16) at 1 µM were added at this stage. The patient serum was cultured for 48 h under these conditions. After the 48-h incubation period, luciferase activity was assessed using the Dual-Glo luciferase

Assay System (Promega, E2920), following the manufacturer's protocol. Luciferase activity was quantified using a luminometer (Thermo Scientific).

Luminescence data was uploaded to a Jupyter notebook and plotted in a boxplot alongside the treatment (vehicle or fulvestrant). This was done using the boxplot function from seaborn. Statistical significance was checked with a t-test using the ttest_ind function from the stats module of the scipy package (version 1.7.1). The same data was plotted but without grouping by treatment and displaying the values of the ratio between the luminescence with fulvestrant and vehicle. This was displayed as a heatmap for the 25 patients. This heatmap was colored in Microsoft Excel (version 16.79.2) by using color scales. The same method was used to plot the heatmap for the comparison between the vehicle and bicalutamide.

The response to bicalutamide was plotted in two bars with the % of reduction of the tumor. This % of reduction was calculated, not only according to MRI data, but also to clinical parameters such as: clinical breast examination (size), histopathological results from tumor biopsies and histopathological yp TNM results. The combination of all these factors creates a classification of 3 levels: 25-50% reduction, 50-90% reduction and 90-100% reduction. The results were visually depicted utilizing GraphPad Prism software.

Generation of stable MCF7-AR cell line and plasmid overexpression

A stable MCF7 cell line overexpressing AR was established. Using the pLENTI6.3/AR-GC-E2325 (addgene, 85128) plasmid that was kindly provided by the research group of Dr. Rogelio González Sarmiento. The generation of viral particles involved transfecting HEK293T cells with the following plasmids: 10 µg of pMDLg, 6 µg of pVSV-G, 5 µg of pRSV, and 15 µg of plasmids (Table 15) and the use of lipofectamine 3000 (Invitrogen, L3000-015) according to the manufacturer's instructions. Cell culture supernatant was collected at 3 timepoints: 24, 48, and 72 h, and subsequently passed through 0.45 µm PVDF filters (GE Healthcare, 10462100) to remove any cellular debris. This supernatant, containing the viral particles, was supplemented with 8 µg/mL of polybrene (Sigma, H9268) and used to replace the medium in MCF7 cells when they reached approximately 60% confluence. This procedure was the same for the generation of a stable cell line and for the overexpression of MTA1 and MTA3. For the empty condition, viral particles without DNA were generated.

For the generation of MCF7-AR stable cell line, after 24 h of the infection, MCF7 cells were washed with PBS and were selected by exposure to 2 mg/mL of blasticidin (Sigma, 203350)

over a period of 2 weeks. The expression of AR was confirmed through immunoblot analysis using antibodies specific to AR.

Migration: Wound healing

To initiate the wound healing assay, MCF7 cells were reverse transfected with siRNA (siMTA1, siMTA3, siNT, siER and siGATA3 (Table 14)) and overexpressed (MTA1, MTA3 and empty (Table 15)). After 48 h, the cells were detached using trypsin (TrypLE Express) (Gibco, 12604-013) and subsequently reseeded in a 12-well plate at a density of $4.5 \cdot 10^5$ cells/mL. Within this experimental setup, each well was equipped with a culture-insert chamber featuring 3 compartments (ibidi, 80369). This chamber was utilized to ensure consistent and replicable wound creation between different experimental conditions. Following cell seeding, medium was replaced either with DMEM 5% FBS (with phenol red) or with DMEM medium without hormones supplemented with 5% FBS (charcoal stripped medium). None of the two mediums contained antibiotic. After 24 h, the ibidi chambers were gently removed. If any specific drug treatment was required as part of the experimental design (Romi at 20 nM and VPA at 5 mM (Table 16)), they were introduced at this stage. Then, the 12-well plate was placed in a Nikon Eclipse TE2000 microscope, and images were acquired from each well at 20 min intervals for a total observation period of 24 h to monitor and evaluate cell migration.

The migration assay was assessed using ImageJ software (version 1.53) to measure alterations in wound length. Precisely, the length of the wound was determined initially and at 12 or 24 h. To calculate the ability of the cells to migrate and close the wound, the fold change by comparing the wound's length at each of the specified time intervals to its original size was calculated. The results, illustrating this fold change, were visually depicted utilizing GraphPad Prism software.

Invasion assay with collagen spheroids

To perform the invasion assay, spheroids were prepared using 25000 of the previously transfected MCF7 cells. MCF7 cells were transfected with specific siRNA (siMTA1, siMTA3, siER, siGATA3 and siNT (Table 14)) and overexpressed (MTA1, MTA3 and empty (Table 15)). Subsequently, 800 µL of cell suspension were mixed with 200 µL of methylcellulose (Sigma, M7027). From this mixture, approximately 40 drops, each containing 25 µL, were carefully dispensed onto the lid of a P100 petri dish that had been filled with 1x PBS to provide appropriate humidity conditions. These spheroids were then

incubated upside-down for 48 h. After this incubation period, 8 to 10 spheroids were pipetted all together into an Eppendorf tube. It is worth noticing that during spheroid recovering, the pipette tip should be cut to prevent spheroid damage. Subsequently, the recovered spheroids were mixed with bovine type I collagen solution (Advanced BioMatrix, 5005) to achieve a final concentration of 1.5 mg/mL. Throughout this process, the mixture of spheroids and collagen was maintained on ice to prevent premature solidification. This mixture (8 to 10 spheroids per well well) was then carefully transferred to a 24-well plate and allowed to solidify for 30 min at 37°C in an incubator. Following solidification, 500 µL of either DMEM with 5% FBS with hormones or DMEM with 5% charcoal-stripped medium without hormones were added to the corresponding well according to the studied condition. The 24-well plate was subsequently placed into a Nikon Eclipse TE2000 microscope, and imaging of each well were captured at intervals of 30 min for a total duration of 72 h to monitor and evaluate cell invasion.

Invasion analysis involved the utilization of ImageJ software to assess changes in spheroid size. Specifically, spheroid's area at the initial time points and subsequently at 24, 48, and 72 h post-invasion were measured. To quantify the alteration in spheroid size over time, the fold change comparing the area to its initial size at each time interval was calculated. The results, depicting the fold change, were graphically presented using GraphPad Prism software.

Histological studies of Ki67 and AR

The paraffin embedded blocks were cut into 2-3 µm thick sections. Hematoxylin-eosin, Ki67 and androgen receptor (AR) immunohistochemical straining were performed using the Discovery Ultra instrument (Roche, 05987750001) in the Comparative Molecular Pathology Unit at the Cancer Research Center (CIC, Salamanca). Paraffin–embedded sections were dewaxed and then subjected to Tris EDTA [pH 8.0] for heat– induced antigen retrieval. They were subsequently incubated for 40 min with the AR and Ki67 primary antibody (Table 13). For standard staining, the Discovery OmniMap anti-Rb HRP detection system (Roche, 760-4311) was used for detection and hematoxylin was used for counterstaining, as indicated by the manufacturer.

Images were scanned at 20X magnification using an Olympus BX51 microscope coupled to an Olympus DP70 digital camera. Tumor sections were analyzed blindly by a pathologist to ensure proper working of the staining, while giving a semiquantitative score. For the

histological quantifications of immunohistochemical (IHC) slides, QuPath software (version 0.4.3) was employed. In the QuPath, the cell detection command (using default parameters) was used to identify all cells based on the optical density of nuclear hematoxylin staining. Next, cell intensity classification (using default parameters) was used to determine the population of positive and negative stained cells.

Western Blot (WB)

MCF7 cells were seeded in a 100 mm Petri dish (Thermo Fisher Scientific) at a cell density of 10^6 cells/mL. Cells were detached by mechanical forces after being washed twice with PBS solution supplemented with cOmplete protease inhibitor cocktail tablet. Cell suspension was centrifuged at 1000 g for 5 min at 4°C and supernatant was discarded. Proteins were extracted from the cell pellet by lysing it with WB RIPA buffer (Table 11) for 30 min on an end-to-end rotator platform at 4°C. Cell lysate was precleared by centrifugation at 13400 rpm at 4°C for 30 min. Total protein was quantified by performing Bradford protein assay (Bio-rad, 5000006) following manufacturer's protocol. Protein concentration was determined by measuring absorbance at 595 nm in the spectrophotometer and interpolating the sample's absorbance value with BSA calibration curve.

Equal amount of protein was diluted in NuPAGE™ LDS sample buffer (4X) (Novex by life technologies, NP0008) with 10% DTT. Samples were denaturalized for 5 min at 95°C and separated by electrophoresis using Mini-PROTEAN TGX Precast polyacrylamide 4-20% (Bio-rad, 456-1096 and 456-1093) gel run at 110 V for 70 min in running buffer (Table 11). Separated proteins were transferred onto a nitrocellulose membrane using the iBlot Dry Blotting System (Thermo Fisher, IB21001) at 23 V for 6 min. Protein transference was confirmed by staining the membranes with Ponceau S solution (Sigma, P7170). Membranes were blocked for at least 1 h at RT with 5% BSA in TBS-T (Table 11). Membrane incubation with primary antibodies (Table 13) diluted in blocking solution was carried out overnight at 4°C on a shaker.

Membranes were washed 3 times with TBS-T and incubated for 1 h at RT with the anti-rabbit or anti-mouse IgG, horseradish Peroxidase-linked (HRP) antibody (Table 13). Immunoreactive bands were revealed using chemiluminescent SuperSignal West Pico PLUS chemiluminescent substrate (Thermo Fisher Scientific, 34580) or SuperSignal West Femto (Thermo Fisher Scientific, 34094). Chemo-luminescence was measured using an iBright Imaging System (Invitrogen).

Image analysis of protein quantification of western blots was performed by Image Lab software (version 6.1). This software allows detection of the bands, normalization to the housekeeping protein level and graphical representations. The graphs and the statistical analysis were carried out using GraphPad Prism software.

Immunoprecipitation (IP)

For the immunoprecipitation (IP) procedure, MCF7 cells were reverse transfected with siRNA (siMTA1, siMTA3 and siNT (Table 14)). After this step IP was performed using the Pierce™ Crosslink IP Kit (Thermo Scientific, 26147), following the manufacturer's instructions. In summary, 5 µg of antibodies HDAC1 (Table 13), and control antibodies, rabbit IgG, were crosslinked to Protein A/G beads (Thermo Scientific, 1861760) in individual binding columns. MCF7 cells were lysed using IP Lysis/Wash buffer, and 500 µg of total protein from the cell lysate were loaded into each binding column for the immunoprecipitation. The protein lysate and the antibody-conjugated beads were incubated together at 4°C overnight, followed by 3 washes with IP Lysis/Wash Buffer. Proteins that were selectively pulled down by the corresponding antibodies were eluted using elution Buffer and western blot analysis was carried out.

Chromatin pellet: Protein detection in chromatin isolation

MCF-7 cells were seeded at a cell density of 10^6 cells in 100 mm Petri dish and treated with vehicle (DMSO), DHT at 100 nM, exemestane at 15 µM and 17β-hidroexemestane at 5 µM (Table 16) for 0, 2, 4 and 24 h, with cells cultured in DMEM 5% FBS. After that time, cells were scraped with 1x PBS-cOmplete and the pellet was centrifuged at 300 g for 5 min at 4°C.

Cells were then incubated for 10 min in cold buffer A. Then, nuclei were collected by low-speed centrifugation (1300 g, for 5 min at 4°C). Subsequently, nuclei underwent a single wash with buffer A (Table 12), but without Triton X-100, followed by low centrifugation. Nuclei were lysed for 30 min on ice with occasional vortexing in buffer B (Table 12).

Subsequently, cells were washed 3 times with buffer B by performing a low-speed centrifugation between washes. Chromatin was sonicated in buffer B for a total of 15 cycles of 30s ON and 30s OFF at low intensity (4 mA) (Bioruptor plus, Diagenode) to share DNA. Chromatin was pelleted by centrifugating it at 16000 g for 5 min at 4°C. Chromatin pellet was then resuspended in buffer B and in (4x) loading buffer NuPAGE™ LDS (Novex by

life technologies, NP0008) with 10% DTT. Chromatin pellets were subsequently loaded in a Mini-PROTEAN TGX Precast polyacrylamide 4-20% (Bio-rad, 456-1096 and 456-1093) gel, following the WB protocol. For the chromatin pellet, the antibodies used were AR and H3 (Table 13).

Image analysis of protein quantification of western blots was performed by Image Lab software. This software allows detection of the bands, normalization to the housekeeping protein level and graphical representations. The graphs and the statistical analysis were carried out using GraphPad Prism software.

Proliferation assays: Crystal violet

Cells were cultured for various durations, ranging from 24 h to 72 h, with cell density adjusted according to the experiment's timeline. For the first condition, cells were treated with either vehicle (DMSO or/and Chloroform), exemestane (15 µM), 17-HEXE (5 µM) or the combination of both exemestane (1, 5 or 15 µM) and 17-HEXE (5 µM). Cells were cultured in DMEM medium at 5% FBS. These experiments were conducted in both MCF7 cells and MCF7-AR cells. For the second condition, MCF7 cells were transfected with specific siRNA (siMTA1, siMTA3 and siNT (Table 14)) and cultured for 48 h in DMEM medium at 5% FBS (with hormones). To check cell viability, cells were rinsed once with PBS. Subsequently, the cells were fixed using a 2% (v/v) formaldehyde solution (PanReac, AppliChem, 252931) and agitated on an orbital shaker at RT for 20 min. Following fixation, the cells underwent 3 washes with MilliQ water and were then stained using a 0.25 mg/ml crystal violet solution (Sigma, C6158). Staining was allowed for 30 min on an orbital shaker at RT. Afterward, excess crystal violet was removed, and the cells were rinsed 6 times with miliQ water and left to air dry upside-down overnight. Stained cells were subsequently dissolved in a 10% (v/v) acetic acid solution (Sulpeco Analytical Products, 1.00063). Cell viability was determined by measuring the absorbance at 590 nm using a microplate reader (Infinite 200 PRO, Tecan). The graphs and the statistical analysis were carried out using GraphPad Prism software.

Proliferation assay: Incucyte

Proliferation assay was carried out by using a time-course imaging on IncuCyte (version 2020C). MCF7-AR cells were seeded at 40000 cells/well in a 24-well plate and monitored for 24 h and for other experiment’s durations (7.5 days) cell density was adjusted accordingly. Cells were treated with either vehicle (DMSO and Chloroform), exemestane (1

µM), 17-HEXE (5 µM) or the combination of both exemestane (1 µM) and 17-HEXE (5 µM). For the experiment for 7.5 days, cells were re-treated every 48 h. Cells were cultured in DMEM medium at 5% FBS. Cell growth and cell death were monitored using 9 images per well. This enabled us to monitor in real-time with IncuCyte imaging system by using phase-contrast images. IncuCyte analysis was performed using artificial intelligence cell count, cell live, cell death and eccentricity. The graphs and the statistical analysis were carried out using GraphPad Prism software.

Statistical analyses

Statistical analyses were conducted using GraphPad Prism software (version 8.0). Each figure legend provides information on the number of biological replicates (n), the specific statistical tests employed, and the corresponding statistical significance. For data with parametric distributions, Student's t-test was applied when comparing two experimental groups, while one-way ANOVA was used for comparisons involving more than two experimental groups with a single control group. For comparisons between more than two experimental groups with all other groups, Tukey's Honestly-significant-difference (HSD) test was employed based on the experimental design. When analyzing interactions between two factors, we employed 2-way ANOVA, followed by Tukey's HSD test for making multiple comparisons, depending on the nature of the analysis. Throughout the analysis, the level of statistical significance was denotated as follows: * for p-values < 0.05, ** for p-values < 0.01, and *** for p-values < 0.001. The presented data is expressed as the mean ± SEM or SD.

Materials

Laboratory Solutions and Reagents

Table 10. List of reagents used.

Reagents	Brand
Sodium Dodecyl Sulfate (SDS)	Sigma, L3771
EDTA	Sigma, E5134
Tris-HCl	Sigma, T-1503
Ethanol	Merck, 1.00983.2511
HEPES	Sigma, H3375
KOH	Sigma, P-5958
LiCl	Sigma, 71380
NP-40	Merck, 492016
Na-deoxycholate	Sigma, D6750
Proteinase & Phosphate inhibitor cocktail	cOmplete Ultra tablets (Roche, 05892970001)
KCl	Sigma, P9333
Glycine	Sigma, G6761
Glycerol	Sigma, G6376
NaCl	Sigma, 71380
Triton X-100	Sigma, T8787
EGTA	Sigma, E4378
N-lauroyl sarcosine	Sigma, L5125
$MgCl_2$	Sigma, M8266
Sucrose	Sigma, S0389
Dithiothreitol (DTT)	Roche, 10708984001
Formaldehyde	Thermo Scientific, 28908
NaF	Thermo Scientific, 424325000
Na3VO4	Sigma, S6508
ß-glycerophosphate	Sigma, G5422
KH_2PO_4	Sigma, P5655
Na_2HPO_4	Sigma, S9763
Tween-20	Panreac Applichem, A4974,0500
Yeast extract	Sigma, Y1625
Tryptone	Sigma, T7293
Ampicillin	ChemCruz, H1022
Kanamycin	Sigma, K1377
Bovine Serum Albumin (BSA)	Sigma, A7906

The specific composition of the regularly used buffers can be found in Table 11. For the preparation of these buffers, we utilized purified water obtained from the Milli-Q Reagent Grade Water Ultrafiltration System (Millipore). Buffers were also filtrated to be sterilized.

Table 11. List and composition of most commonly used buffers.

Solution or reagent	Composition
1x PBS	2.68 mM KCl, 1.47 mM KH_2PO_4, 137 mM NaCl, 7.98 mM Na_2HPO_4
20x TBS	0.5 M Tris, 1 M NaCl, 0.05 M KCl [pH 8]
1x TBS-T	1x TBS, 0.1% (v/v) Tween-20
50x TAE	2M Tris, 0.05 M EDTA [pH 8]
LB	0.5% yeast extract, 1% tryptone, 1% NaCl
Agar LB ampicillin	LB, 2% agar, ampicillin 0.125 mg/mL
LB ampicillin	LB, ampicillin 0.125 mg/mL
TE [pH 8]	10 mM Tris-HCl, 1 mM EDTA
10x SDS-PAGE	0.25M Tris, 2M glycine, 0.5% SDS
Running buffer	1x SDS-PAGE
Blocking solution	5% BSA mixed in TBS-T
RIPA buffer (WB, IP)	25 mM Tris-HCl [pH 7,6], 150 mM NaCl, 1% NP-40, 1% Triton X-100, 1% Na-deoxycholate, 0.1% SDS, 1 mM NaF, 1 mM Na3VO4, 1 mM ß-glycerophosphate. Added from fresh, proteinase & phosphate inhibitor cocktail (Roche, 05892970001)
PBS-cOmplete	1x PBS (10 mL) mixed with 1 tablet of Proteinase & Phosphate inhibitor cocktail (Roche, 05892970001)

For the preparation of these buffers, we utilized purified water obtained from the Milli-Q Reagent Grade Water Ultrafiltration System (Millipore), unless stated otherwise. Buffers were also filtrated to be sterilized.

Table 12. List and composition of buffers from chromatin studies.

Buffer name	Method	Composition
1% SDS lysis buffer	Fit-Seq	1% (wt/vol) SDS, 10 mM EDTA [pH 8], 50 mM Tris-HCl [pH 8]
PBS/BSA buffer	Fit-Seq, FF-ChIP	10 mM PBS, 83,6 µM BSA
RIPA buffer	Fit-Seq	50 mM Hepes-KOH [pH 7.6], 0.5M LiCl, 1% (vol/vol) NP-40, 0.7% (wt/vol) Na-deoxycholate, 1 mM EDTA. Added from fresh, proteinase & phosphate inhibitor cocktail
Elution buffer	Fit-Seq	50 mM Tris-HCl [pH 8], 1% SDS, 1 mM EDTA
LB1	FF-ChIP	1% glycerol, 50 mM Hepes-KOH [pH 7.6], 140 mM NaCl, 0.5% NP-40, 0.25% Triton X-100, 1 Mm EDTA [pH 8]. Added from fresh, proteinase & phosphate inhibitor cocktail
LB2	FF-ChIP	10 mM Tris-HCl [pH 7.5], 200 mM NaCl, 0.5 mM EGTA [pH 8], 1 mM EDTA [pH 8]. Added from fresh, proteinase & phosphate inhibitor cocktail
LB3	FF-ChIP	0.5% N-lauroyl sarcosine, 10 mM Tris-HCl [pH 7.5], 100 mM NaCl, 0.1% Na-deoxycholate, 0.5 mM EGTA, 1 mM EDTA [pH 8]. Added from fresh, proteinase & phosphate inhibitor cocktail and 1% Triton X-100.
Buffer A	Chromatin pellet	0,1 % Triton X-100, 10 mM Hepes [pH 7.9], 10 mM KCl, 1.5 mM $MgCl_2$, 0.34 M sucrose, 10 % glycerol, 1 mM DTT. Added from fresh, proteinase & phosphate inhibitor cocktail
Buffer B	Chromatin pellet	3 mM EDTA, 0.2 mM EGTA, 1 mM DTT. Added from fresh, proteinase & phosphate inhibitor cocktail

Table 13. List of antibodies.

Antibody	Method	Dilution	Brand
AR (D6F11) XP Rabbit	WB	1:100	Cell Signaling, 5153
AR (N-20)	FF	10 µg	Santa Cruz, sc-816
H3	WB	1:5000	Abcam, ab1791
MTA1 (D17G10)	WB	1:100	Cell signaling, 5646
MTA3 (428C2a)	WB	1:500	Santa Cruz, sc-81325
GATA3	WB	1:100	BD Pharmigen, 558686
ERα (D8H8)	WB	1:100	Cell Signaling, 8644
HDAC1	IP, WB	5 µg, 1:1000	Active motif, 40967
Normal rabbit IgG	IP	5 µg	Santa Cruz, sc-2027
AR (SP107)	IHC	1:50	Vitro, 710QD3
Ki67	IHC	1:50	Master diagnostica, MAD000310
H3K27Acetyl	Fit-Seq	10 µg	abcam, 4729
Anti-rabbit IgG	WB	1:2000	Cell Signaling, 7074
GAPDH (14C10)	WB	1:1000	Cell Signaling, 2118

Table 14. List of predesigned siRNA. These sequences were designed and purchased from MISSION Merck.

Name	Sequence (5'-3')
siMTA3 (SASI-HS01-00211926)	CCUAAUAGCAGUGUAGAU
siMTA1 (SASI-HS01-00239682)	CGGACAUUCAGCCAAGAUUU
siER (SASI-HS01-00078592)	GUUUGUGUGCCUCAAAUCU
siGATA3 (SASI-HS01-00153931)	CUCUGGAGGAGGAAUGCCA

Table 15. List of the plasmids.

Vector	Description	Brand
MTA1	Human cDNA clone in mammalian expression	Genomic-online, ABIN4478335
MTA3	Human cDNA clone in mammalian expression	Genomic-online, ABIN4478336
AR	Lentiviral plasmid (pLENTI6.3/AR-GC-E2325)	Adgene, 85128

Table 16. List of drugs.

Drugs	Brand
DMSO	Sigma, D2650
Chloroform	Thermo scientific, 268320025
Fulvestrant	Sigma, I4409
Bicalutamide	Sigma, B9061
Dihydrotestosterone (DHT)	Sigma, 521-18-6
Exemestane	Sigma, PZ0006
17β-Hydroxy Exemestane	Toronto Research Chemicals, H942340
Romidepsin	Selleckchem, S3020
Valproic acid (VPA)	Selleckchem, S3944

Table 17. List of oligonucleotides.

Name	Sequence
BMP7_Fw	5’ GCGCGAGATCCTCTCCATTT 3’
RBPJ_Fw	5’ CACTCCTGTGCCTGTGGTAG 3’
MTA1_Fw	5’ CCTCCAGCAACCCATACCTG 3’
MTA3_Fw	5’ CCACGTTCCAGCCTCAGAAT 3’
UBC_Fw	5’ ATTTGGGTCGCGGTTCTTG 3’
TBP_Fw	5’ GCCAGCTTCGGAGAGTTCTG 3’

ANNEX

Table 18. TNM staging clinical T (cT) and pathological (pT) [53].

T	Definition
Tx	Evaluation of the primary tumor is not possible
T0	No evidence of primary tumor
Tis	Tumor *in situ* (DCIS, LCIS, Paget's disease)
T1	Primary tumor ≤ 2 cm
T1mi	Primary tumor ≤ 1 mm
T1a	Primary tumor > 1 mm and ≤ 5 mm
T1b	Primary tumor > 5 mm and ≤ 1 cm
T1c	Primary tumor > 1 cm and ≤ 5 cm
T2	Primary tumor > 2 cm and ≤ 5 cm
T3	Primary tumor > 5 cm
T4	Tumor of any size with extension to the chest wall and/or skin
T4a	Chest wall involvement, not only pectoral muscle adherence/invasion
T4b	Ulceration and/or ipsilateral satellite nodules and/or edema
T4c	T4a+T4b
T4d	Inflammatory carcinoma

Table 19. TNM staging clinical N (cN) [53].

N	Definition
Nx	Regional nodes cannot be or have not been evaluated
N0	Absence of regional lymph node metastases
N1	Presence of mobile ganglia in axillary levels I and II
N2	Presence of mobile axillary nodes at levels I, II or presence of clinically detected nodes in the homolateral internal mammary chain
N2a	Presence of axillary nodes at levels I and II that are clinically fixed or filled
N2b	Clinically apparent metastases in ipsilateral internal mammary chain nodes in the absence of clinically apparent axillary nodes
N3a	Metastases in ipsilateral infraclavicular lymph nodes
N3b	Clinically apparent metastases in ipsilateral nodes of the internal mammary chain together with clinically apparent axillary nodes
N3c	Metastases in ipsilateral supraclavicular nodes

- Level I: lateral and inferior axillary nodes to the pectoralis minor muscle.
- Level II: axillary nodes posterior to the pectoralis minor muscle.
- Level III: axillary nodes medial to the pectoralis minor muscle and infraclavicular.

Table 20. TNM staging: N pathological (pN) [53].

pN	Definition
pNx	The lymph node regions have not been or could not be evaluated
pN0	Histological (H&E) absence of regional lymph node metastases
pN0(i-)	Absence of regional metastases, after histological and IHC evaluation
pN0(i+)	Presence of malignant cells in regional node(s) not larger than 0.2 mm (detected by H&E or IHC)
pN1mi	Micro metastasis (greater than 0.2 mm and/or accumulations greater than 200 cells, but none greater than 2.0 mm)
pN1a	Metastasis in 1-3 axillary nodes, at least one is greater than 2.0 mm
pN1b	Internal mammary chain metastasis with micro or macro metastases detected by selective sentinel node biopsy but not clinically detected
pN1c	Metastasis in 1-3 axillary lymph nodes and in an internal mammary chain with micro or macro metastases detected by selective sentinel lymph node biopsy, but not detected clinically
pN2a	Metastasis in 4-9 axillary nodes (at least one is greater than 2.0 mm)
pN2b	Clinically detected internal mammary chain metastasis(s) in the absence of axillary metastatic involvement
pN3a	Metastasis in 10 or more axillary nodes (at least one is greater than 2.0 mm); or metastasis in infraclavicular lymph nodes (axillary level III)
pN3b	Metastasis greater than 2 mm in one or more positive axillary nodes and involvement of the clinically apparent internal mammary chain; or metastatic involvement (> 2 mm) in 4 or more axillary nodes as well as in the internal mammary chain, with macro or micro metastases detected by selective biopsy, but not clinically apparent
pN3c	Metastasis in ipsilateral supraclavicular axillary nodes

Table 21. TNM staging: M [53].

M	Definition
Mx	Distant metastases cannot be evaluated or have not been evaluated
M0	Absence of distant metastases
M0(i+)	No clinical or radiographic evidence of distant metastasis, but existence of tumor cell deposits detected molecularly or microscopically in blood, bone marrow, or non-regional adenopathy, which are not larger than 0.2 mm in a patient without signs/symptoms of metastasis
M1	Presence of distant metastases

Table 22. NeoLetExe eligibility criteria. General inclusion and exclusion criteria of NeoLetExe trial [140].

Inclusion criteria	Exclusion criteria
Patients diagnosed with locally advanced primary breast cancer (defined by T3-T4 and/or N2-N3 status)	Triple-negative breast cancer
Large T2 tumors: primary tumors > 4 cm in diameter	HER-2 positive status
Postmenopausal status: age > 55 years or age > 50 years and at least 2 years of amenorrhea. In addition to LH- and FSH- and plasma estradiol levels in the postmenopausal range	Life-threatening metastasis (advanced visceral metastasis, brain-metastasis, elevated liver enzymes, defined as > 3 times normal values)
ER-positive status (at least 10% of cancer cells)	Any previous therapy for breast cancer within the last 12 months
HER-2 negative status	Treatment with drugs that may interfere with endocrine therapy of breast cancer
No or limited distant metastasis	-

Table 23. List of upregulated genes by RNA-Seq for 17-HEXE and Exemestane combinations. Significantly upregulated genes in three conditions: 17-HEXE&Exe vs Ctrl, 17-HEXE vs Ctrl and Exe vs Ctrl.

17-HEXE & Exe

Pathway description	Symbol
Hypoxia	IGFBP1
Hypoxia	TPD52
Hypoxia	ERRFI1
Hypoxia	JUN
Hypoxia	EDN2
Hypoxia	ANXA2
Hypoxia	TIPARP
Hypoxia	SDC2
Hypoxia	IGFBP3
Hypoxia	SLC2A3
Hypoxia	F3
Hypoxia	AKAP12
Hypoxia	P4HA1
Hypoxia	P4HA2
Hypoxia	HMOX1
Hypoxia	TGM2
Hypoxia	TMEM45A
Androgen Response	HOMER2
Androgen Response	ADAMTS1
Androgen Response	STK39
Androgen Response	SORD
Androgen Response	ELL2
Androgen Response	FADS1
Androgen Response	FKBP5
Xenobiotic Metabolism	MCCC2
Xenobiotic Metabolism	IGFBP1
Xenobiotic Metabolism	ABCC3
Xenobiotic Metabolism	CYB5A
Xenobiotic Metabolism	DDC
Xenobiotic Metabolism	AKR1C2
Xenobiotic Metabolism	CROT
Xenobiotic Metabolism	SERPINA6
Xenobiotic Metabolism	PTGR1
Xenobiotic Metabolism	PDK4
Xenobiotic Metabolism	CYP1A1
Xenobiotic Metabolism	HMOX1
Xenobiotic Metabolism	XDH
Xenobiotic Metabolism	PTGES
TNF-alpha Signaling via NF-kB	DUSP5
TNF-alpha Signaling via NF-kB	JUN
TNF-alpha Signaling via NF-kB	CEBPD
TNF-alpha Signaling via NF-kB	GADD45A
TNF-alpha Signaling via NF-kB	TIPARP
TNF-alpha Signaling via NF-kB	SIK1
TNF-alpha Signaling via NF-kB	SLC2A3
TNF-alpha Signaling via NF-kB	F3
TNF-alpha Signaling via NF-kB	TLR2
TNF-alpha Signaling via NF-kB	BIRC3
mTORC1 Signaling	RIT1
mTORC1 Signaling	PSMD12
mTORC1 Signaling	GOT1
mTORC1 Signaling	P4HA1
mTORC1 Signaling	ME1
mTORC1 Signaling	SORD
mTORC1 Signaling	CD9
mTORC1 Signaling	SLC2A3
mTORC1 Signaling	SLC7A11
mTORC1 Signaling	FADS1
Apoptosis	JUN
Apoptosis	GUCY2D
Apoptosis	GADD45A
Apoptosis	SLC20A1
Apoptosis	PMAIP1
Apoptosis	HMOX1
Apoptosis	EMP1
Apoptosis	BIRC3
Estrogen Response Early	SEC14L2
Estrogen Response Early	TIPARP
Estrogen Response Early	SCNN1A
Estrogen Response Early	PMAIP1
Estrogen Response Early	TSKU
Estrogen Response Early	SYBU
Estrogen Response Early	PTGES
Estrogen Response Early	TGM2
Estrogen Response Early	FKBP5
KRAS Signaling Up	AKAP12
KRAS Signaling Up	ANO1
KRAS Signaling Up	ALDH1A3
KRAS Signaling Up	KIF5C
KRAS Signaling Up	IGFBP3
KRAS Signaling Up	EMP1
KRAS Signaling Up	F13A1
KRAS Signaling Up	CROT
KRAS Signaling Up	BIRC3
KRAS Signaling Dn	NUDT11
KRAS Signaling Dn	HSD11B2
KRAS Signaling Dn	CLPS
KRAS Signaling Dn	TG
KRAS Signaling Dn	AKR1B10
KRAS Signaling Dn	EDN2
KRAS Signaling Dn	ZBTB16
KRAS Signaling Dn	TFCP2L1
Epithelial Mesenchymal Transition	JUN
Epithelial Mesenchymal Transition	GADD45A
Epithelial Mesenchymal Transition	CALD1
Epithelial Mesenchymal Transition	IGFBP3
Epithelial Mesenchymal Transition	SNAI2
Epithelial Mesenchymal Transition	TGM2

17-HEXE

Pathway description	Symbol
Hypoxia	IGFBP1
Hypoxia	ERRFI1
Hypoxia	EDN2
Hypoxia	ANXA2
Hypoxia	SDC2
Hypoxia	AK4
Hypoxia	SLC2A3
Hypoxia	F3
Hypoxia	AKAP12
Hypoxia	P4HA1
Hypoxia	HMOX1
Hypoxia	PLIN2
Hypoxia	ANGPTL4
Hypoxia	TGM2
Hypoxia	TMEM45A
Androgen Response	AKAP12
Androgen Response	ALDH1A3
Androgen Response	AZGP1
Androgen Response	ADAMTS1
Androgen Response	STK39
Androgen Response	SORD
Androgen Response	ELL2
Androgen Response	FADS1
Androgen Response	FKBP5
Xenobiotic Metabolism	IGFBP1
Xenobiotic Metabolism	ABCC3
Xenobiotic Metabolism	NQO1
Xenobiotic Metabolism	DDC
Xenobiotic Metabolism	SSR3
Xenobiotic Metabolism	HMOX1
Xenobiotic Metabolism	AKR1C2
Xenobiotic Metabolism	SERPINA6
Xenobiotic Metabolism	XDH
Xenobiotic Metabolism	PTGES
TNF-alpha Signaling via NF-kB	NFKBIA
TNF-alpha Signaling via NF-kB	CEBPD
TNF-alpha Signaling via NF-kB	GADD45A
TNF-alpha Signaling via NF-kB	SIK1
TNF-alpha Signaling via NF-kB	SLC2A3
TNF-alpha Signaling via NF-kB	F3
TNF-alpha Signaling via NF-kB	BIRC3
mTORC1 Signaling	RIT1
mTORC1 Signaling	GOT1
mTORC1 Signaling	P4HA1
mTORC1 Signaling	ME1
mTORC1 Signaling	SORD
mTORC1 Signaling	AK4
mTORC1 Signaling	SLC2A3
mTORC1 Signaling	SLC7A11
mTORC1 Signaling	FADS1
Apoptosis	GUCY2D
Apoptosis	GADD45A
Apoptosis	SLC20A1
Apoptosis	HMOX1
Apoptosis	EMP1
Apoptosis	BIRC3
Estrogen Response Early	SEC14L2
Estrogen Response Early	SCNN1A
Estrogen Response Early	AQP3
Estrogen Response Early	TSKU
Estrogen Response Early	SYBU
Estrogen Response Early	PTGES
Estrogen Response Early	TGM2
Estrogen Response Early	FKBP5
KRAS Signaling Up	AKAP12
KRAS Signaling Up	ANO1
KRAS Signaling Up	ALDH1A3
KRAS Signaling Up	EMP1
KRAS Signaling Up	F13A1
KRAS Signaling Up	ANGPTL4
KRAS Signaling Up	BIRC3
KRAS Signaling Dn	NUDT11
KRAS Signaling Dn	ZC2HC1C
KRAS Signaling Dn	HSD11B2
KRAS Signaling Dn	CLPS
KRAS Signaling Dn	TG
KRAS Signaling Dn	AKR1B10
KRAS Signaling Dn	EDN2
KRAS Signaling Dn	ZBTB16
KRAS Signaling Dn	TFCP2L1
KRAS Signaling Dn	SLC5A5
Epithelial Mesenchymal Transition	IL32
Epithelial Mesenchymal Transition	FAP
Epithelial Mesenchymal Transition	GADD45A
Epithelial Mesenchymal Transition	CALD1
Epithelial Mesenchymal Transition	SNAI2
Epithelial Mesenchymal Transition	TGM2

EXE

Pathway description	Symbol
Hypoxia	AKAP12
Hypoxia	IGFBP1
Hypoxia	TPD52
Hypoxia	EDN2
Hypoxia	P4HA1
Hypoxia	SDC2
Hypoxia	IGFBP3
Hypoxia	SLC2A3
Hypoxia	TGFBI
Hypoxia	F3
Hypoxia	TMEM45A
Androgen Response	TPD52
Androgen Response	AKAP12
Androgen Response	ALDH1A3
Androgen Response	AZGP1
Androgen Response	HPGD
Androgen Response	HOMER2
Androgen Response	ADAMTS1
Androgen Response	STK39
Androgen Response	SORD
Androgen Response	ELL2
Androgen Response	FADS1
Androgen Response	FKBP5
Xenobiotic Metabolism	IGFBP1
Xenobiotic Metabolism	DDC
Xenobiotic Metabolism	CROT
Xenobiotic Metabolism	SERPINA6
Xenobiotic Metabolism	XDH
Xenobiotic Metabolism	PTGES
TNF-alpha Signaling via NF-kB	GADD45A
TNF-alpha Signaling via NF-kB	SLC2A3
TNF-alpha Signaling via NF-kB	F3
mTORC1 Signaling	P4HA1
mTORC1 Signaling	SORD
mTORC1 Signaling	SLC2A3
mTORC1 Signaling	FADS1
Apoptosis	GADD45A
Apoptosis	SLC20A1
Apoptosis	EMP1
Estrogen Response Early	SEC14L2
Estrogen Response Early	SCNN1A
Estrogen Response Early	SYBU
Estrogen Response Early	PTGES
Estrogen Response Early	FKBP5
KRAS Signaling Up	AKAP12
KRAS Signaling Up	ALDH1A3
KRAS Signaling Up	IGFBP3
KRAS Signaling Up	EMP1
KRAS Signaling Up	F13A1
KRAS Signaling Up	CROT
KRAS Signaling Dn	NUDT11
KRAS Signaling Dn	CLPS
KRAS Signaling Dn	TG
KRAS Signaling Dn	AKR1B10
KRAS Signaling Dn	EDN2
KRAS Signaling Dn	ZBTB16
KRAS Signaling Dn	SLC5A5
Epithelial Mesenchymal Transition	GADD45A
Epithelial Mesenchymal Transition	CALD1
Epithelial Mesenchymal Transition	IGFBP3
Epithelial Mesenchymal Transition	SNAI2
Epithelial Mesenchymal Transition	TGFBI

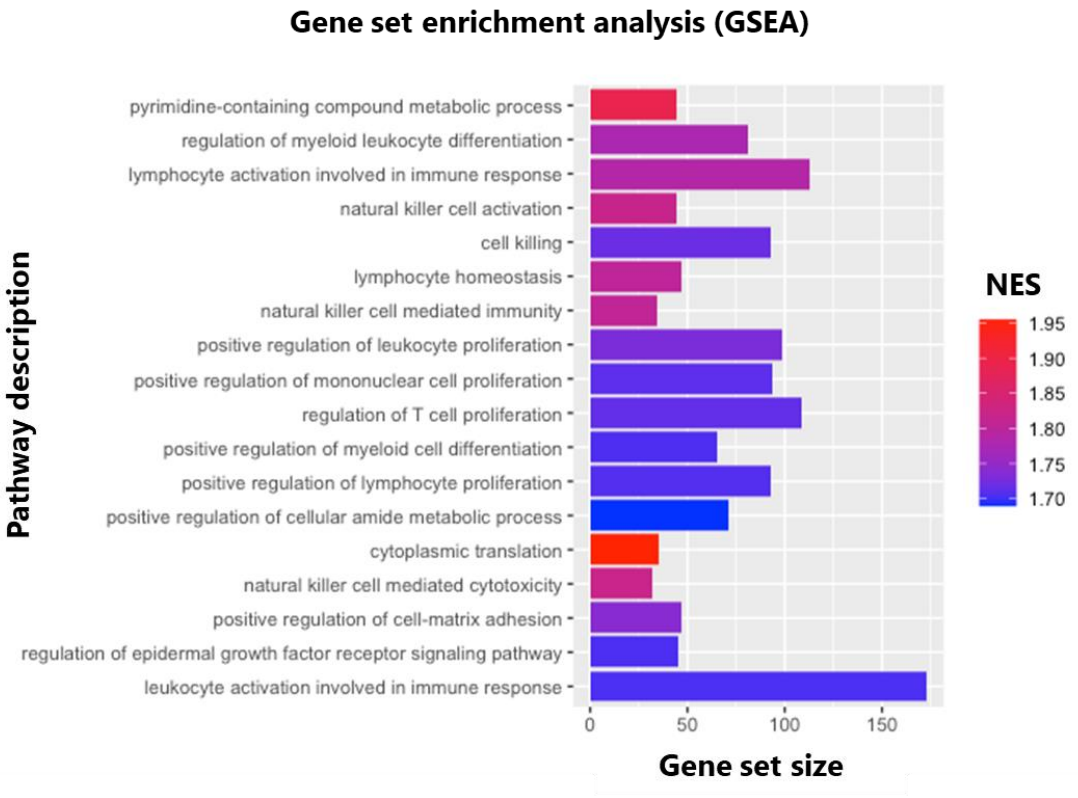

Figure 64. Gene Set Enrichment Analysis (GSEA) of the pathways with the biggest win in NES ranking between primary and metastatic tumors. Pathways with the biggest win of rank between primary and metastatic tumor for the GSEA of common genes from the cancer signature gene set. The length of the bars represents the gene set size of each pathway and the color is the Net Enrichment Score (NES).

Table 24. List of upregulated and downregulated genes by RNA-Seq for siMTA1 and siMTA3 combinations. Significantly upregulated and downregulated genes in two conditions: siMTA1 vs siNT and siMTA1 vs siNT.

siMTA1 vs siNT

Gene name	Expression
CNN3	Up
NIBAN1	Up
H3-3A	Up
ERO1B	Up
MCFD2	Up
SEPTIN10	Up
TMEM45A	Up
CLSTN2	Up
RPL22L1	Up
TAPT1	Up
SLC7A11	Up
RETREG1	Up
CDH18	Up
GPX8	Up
ST8SIA4	Up
SLC36A1	Up
BOD1	Up
CCND3	Up
HMGCLL1	Up
AGR2	Up
AGR3	Up
GRB10	Up
DNAJB9	Up
MET	Up
CALU	Up
PDIA4	Up
CYRIB	Up
SLC1A1	Up
RLN2	Up
SLC31A1	Up
AKR1C3	Up
TMEM26	Up
NRBF2	Up
PTPMT1	Up
BANF1	Up
PPP2R1B	Up
KCNJ8	Up
NELL2	Up
DDIT3	Up
TC2N	Up
IFI27L2	Up
CHAC1	Up
RSL24D1	Up
NTN1	Up
ADM2	Up
DYNLT3	Up
ATG4A	Up
RAB39B	Up

Gene name	Expression
DDAH1	Down
PDZK1	Down
SUCO	Down
RNASEL	Down
NPAS2	Down
FAM117B	Down
IKZF2	Down
TNS1	Down
AMOTL2	Down
RHOBTB3	Down
HLA-DRB1	Down
TNFRSF21	Down
FRK	Down
TNS3	Down
ARPC1A	Down
PODXL	Down
ATP6V0A4	Down
PPP1R3B	Down
MTUS1	Down
KRT8P3	Down
MYORG	Down
IER5L	Down
LOXL4	Down
H19	Down
SYT12	Down
P2RY2	Down
TSKU	Down
YAP1	Down
LINC02732	Down
KRT80	Down
KRT8	Down
KRT18	Down
CBX5	Down
CPM	Down
SLC5A8	Down
NHLRC3	Down
GNPNAT1	Down
RDH11	Down
MTA1	Down
RASGRP1	Down
CLDN9	Down
PHKB	Down
SMTNL2	Down
FAM222B	Down
RAB11FIP4	Down
KRT13	Down
KRT15	Down
KRT19	Down
DLX3	Down
TRIM47	Down
GREB1L	Down
SLC25A23	Down
KCNN4	Down
TGM2	Down
MGAT3	Down
STK26	Down
ZNF185	Down

siMTA3 vs siNT

Gene name	Expression
GRHL3	Up
PGM1	Up
NPR1	Up
TSTD1	Up
NIBAN1	Up
H3-3A	Up
ERO1B	Up
TRIB2	Up
MCFD2	Up
C1D	Up
SEPTIN10	Up
MALL	Up
RPRM	Up
ITGB6	Up
H3P6	Up
ITM2C	Up
OXTR	Up
MME	Up
RPL22L1	Up
CLDN1	Up
TAPT1	Up
RBPJ	Up
NPNT	Up
FAT4	Up
TLR2	Up
OTULINL	Up
RETREG1	Up
CENPH	Up
ST8SIA4	Up
SLCO4C1	Up
SLC36A1	Up
BOD1	Up
CCND3	Up
FUT9	Up
CCNC	Up
PDGFA-DT	Up
IGFBP3	Up
CYP3A5	Up
CALU	Up
PDIA4	Up
HMBOX1	Up
SDR16C5	Up
TMEM65	Up
CYRIB	Up
SLC1A1	Up
RFK	Up
NRBF2	Up
HHEX	Up
PTPMT1	Up
BANF1	Up
SESN3	Up
PPP2R1B	Up
CADM1	Up
NELL2	Up
DNAJC22	Up
NTN4	Up
IFI27L2	Up
CCPG1	Up
MT1X	Up
RPS27AP16	Up
HS3ST3A1	Up
CAVIN1	Up
LINC00511	Up
JAG1	Up
CYP24A1	Up
BMP7	Up
COL4A5	Up
LONRF3	Up

Gene name	Expression
TMEM222	Down
IPP	Down
TSPAN1	Down
TENT5C	Down
PDZK1	Down
FCGR1A	Down
ANXA9	Down
MTA3	Down
LINC01293	Down
SLC9A2	Down
LINC01963	Down
EFHD1	Down
PRICKLE2-DT	Down
BLOC1S4	Down
HMGCS1	Down
TENT2	Down
CXXC5	Down
SLC26A2	Down
ANXA6	Down
TNFRSF21	Down
FRK	Down
KLHDC10	Down
ATP6V0A4	Down
MTUS1	Down
ZHX2	Down
SPIN1	Down
STX17	Down
C9orf152	Down
IER5L	Down
UBAC1	Down
ARHGAP19	Down
TRIM6	Down
SLC1A2	Down
ALDH3B2	Down
P2RY2	Down
PGM2L1	Down
AMOTL1	Down
METTL7A	Down
SYT1	Down
SLC25A30	Down
TMEM30B	Down
RHOV	Down
ARPP19	Down
NPTN	Down
ALPK3	Down
UNC45A	Down
NUDT21	Down
CDH1	Down
HSBP1	Down
KRT13	Down
DCAF7	Down
RNF152	Down
LRG1	Down
CCDC124	Down
HOMER3	Down
KCNN4	Down
MYADM	Down
BTBD3	Down
MAPRE1	Down
PREX1	Down
SUSD2	Down
MGAT3	Down
GLA	Down
ZNF185	Down

RESUMEN EN CASTELLANO

Resumen de la introducción

El cáncer de mama es una enfermedad compleja y heterogénea que afecta a millones de mujeres en todo el mundo, siendo el cáncer más frecuente entre mujeres. Este tipo de cáncer se caracteriza por el crecimiento descontrolado de células malignas en el tejido mamario. Su etiología implica factores genéticos, ambientales y hormonales que contribuyen a su desarrollo. Los subtipos de cáncer de mama, determinados por marcadores moleculares como los receptores hormonales (receptor de estrógenos (ER) y el receptor de progesterona (PR)) y el receptor del factor de crecimiento humano tipo 2 (HER2), guían las estrategias terapéuticas. Los tumores positivos para ER, PR o HER2 permiten tratamientos dirigidos específicos que mejoran la efectividad de las terapias. Además, la investigación sobre los mecanismos moleculares, la heterogeneidad tumoral y la resistencia a los tratamientos es fundamental para desarrollar terapias más eficaces y personalizadas.

Este trabajo se centra en pacientes luminales, caracterizados por la expresión del ER. La vía de señalización del estrógeno y su interacción con el ER desempeñan un papel crucial en el desarrollo y progresión del cáncer de mama, especialmente en los tumores considerados cómo ER-positivo. El estrógeno, una hormona sexual femenina, se une al ER y desencadena una cascada de eventos que modulan la expresión génica y promueven la proliferación celular. La activación del ER por el estrógeno implica complejas interacciones con coactivadores y correpresores, regulando genes clave involucrados en el crecimiento y la supervivencia celular. Sin embargo, esta vía de señalización puede ser atacada terapéuticamente mediante la inhibición del ER o mediante la inhibición de la síntesis de estrógeno.

Las pacientes luminales suelen ser tratadas con terapia hormonal dirigidas a inhibir estas vías. Los tratamientos antiestrógenos o terapia endocrina, como el tamoxifeno o los inhibidores de la aromatasa (IAs), son fundamentales debido a la dependencia de estas células tumorales a los estrógenos para crecer. No obstante, hay que tener en cuenta que la estrategia terapéutica varía en función del subtipo tumoral y de si se trata de terapia neoadyuvante (antes de la cirugía) o adyuvante (después de la cirugía). En particular, dentro de los inhibidores de aromatasa destacan el letrozol y el exemestano, los cuales disminuyen la producción de estrógeno y, por lo general, se administran a mujeres postmenopáusicas.

No obstante, la resistencia a estos tratamientos y las recaídas sigue siendo un desafío clínico importante. Por ello, cabe resaltar la necesidad de comprender mejor los mecanismos moleculares subyacentes al cáncer de mama. En ocasiones la ineficacia de las terapias y las recaídas dan lugar al cáncer de mama metastásico. Dicho proceso es complejo y comienza con la invasión local del tejido circundante y se extiende a través de los vasos sanguíneos o linfáticos, culminando en la diseminación de células tumorales a órganos distantes. La metástasis involucra procesos celulares intrincados, incluida la transición epitelial-mesenquimal (EMT), que otorga a las células la capacidad de migración e invasión. Además, las interacciones dinámicas entre las células y su entorno, incluidas las células asociadas al cáncer y los cambios epigenéticos, también influyen en la metástasis.

Este trabajo está enfocado en descifrar los mecanismos de resistencia y a desarrollar estrategias terapéuticas más efectivas y personalizadas para frenar la progresión del cáncer de mama. Dicha resistencia puede surgir de diversas formas, incluyendo alteraciones genéticas, cambios en las vías de señalización, o la interacción compleja del tumor con su microambiente. Los mecanismos de resistencia a la terapia endocrina involucran vías de señalización clave como PI3K/Akt/mTOR, receptor de factor de crecimiento similar a la insulina 1 (IGF-1R), y modificaciones epigenéticas.

En concreto, las modificaciones epigenéticas, como la metilación del ADN, las modificaciones de histonas y los cambios en la estructura de la cromatina, tienen un impacto significativo en la activación o represión de genes clave asociados con el cáncer de mama. Estos cambios pueden alterar la disposición física del ADN y la accesibilidad a ciertos genes, influyendo en la progresión tumoral y la respuesta a tratamientos. Estas modificaciones pueden actuar como interruptores moleculares que influyen en la transcripción génica y, en consecuencia, en el comportamiento de las células tumorales. Por ello, la comprensión de estos mecanismos epigenéticos en el cáncer de mama es esencial para el desarrollo de terapias dirigidas específicas que puedan revertir estos cambios y restaurar la regulación normal de la expresión génica.

No obstante, con la identificación de biomarcadores moleculares que pueden servir como indicadores pronósticos y predictivos del tratamiento, los médicos pueden tomar decisiones terapéuticas más individualizadas y precisas, asegurando la efectividad de la terapia. Los avances en la investigación molecular han mejorado la comprensión de las características

tumorales, los biomarcadores del cáncer de mama y han llevado al desarrollo de terapias individualizadas para los pacientes.

Objetivos de la tesis

Esta tesis de doctorado se dedicó al estudio de los mecanismos de respuesta a los inhibidores de aromatasa y tuvo dos objetivos principales, cada uno explorado en capítulos individuales. Las preguntas planteadas fueron las siguientes:

1. Descubrir novedosos mecanismos de respuesta a los inhibidores de aromatasa en pacientes con cáncer de mama luminal. El objetivo principal es identificar un subgrupo de pacientes que muestren una respuesta preferencial a un inhibidor de aromatasa particular y entender la resistencia cruzada entre dos inhibidores de aromatasa distintos.

2. Elucidar los factores responsables del cese de la respuesta al tratamiento, el desarrollo de resistencia y el posterior desarrollo de metástasis tras la administración de inhibidores de aromatasa en pacientes con cáncer de mama luminal.

Capítulo I: estudio de los mecanismos de respuesta a los inhibidores de aromatasa en cáncer de mama luminal

El primer proyecto de esta tesis se dedicó a descubrir nuevos mecanismos de respuesta y resistencia cruzada a inhibidores de aromatasa en pacientes con cáncer de mama luminal. Los objetivos principales de este estudio fueron los siguientes:

1. Elucidar los mecanismos de respuesta a los inhibidores de aromatasa dentro del ensayo clínico NeoLetExe.
2. Identificar un subgrupo específico de pacientes que muestre una potencial predilección por respuestas favorables a los inhibidores de aromatasa.
3. Explorar la falta de respuesta, o la resistencia cruzada, a los inhibidores de aromatasa.

Resumen de los resultados I

Después de investigar dos IAs: exemestano y letrozol, se encontró que el tratamiento secuencial con exemestano seguido de letrozol demostró resultados clínicos superiores, reflejados en una disminución en el Ki67 (marcador de proliferación celular) en los pacientes pertenecientes al ensaño clínico NeoLetExe. Tras descubrir que la secuencia Exe-Let estaba correlacionada con un menor niveles de Ki67, planteamos la hipótesis de que este efecto podría deberse a diferencias entre estos fármacos para inhibir efectivamente la enzima aromatasa. Los resultados sugirieron una eficacia comparable de letrozol y exemestano en la inhibición de la actividad de la aromatasa, como se evidenció por la reducción consistente en los niveles de estrógeno en ambos grupos a los 2 y 4 meses. Por lo tanto, nuestra hipótesis inicial quedó descartada sugiriendo un mecanismo alternativo que diese explicación a la mejora clínica observada en pacientes tratados con Exe-Let.

Entonces decidimos explorar si el 17-HEXE (metabolito activo del exemestano) estaba desempeñando un papel clave en la mejora clínica observada. Para ello, primero se confirmó que tanto el exemestano como el 17-HEXE (su metabolito activo) estaban presentes en el suero de los pacientes, validando que el exemestano se estaba metabolizaba en 17-HEXE, pero se observó alta variabilidad entre pacientes. Por lo tanto, nuestro análisis subraya una considerable variabilidad en el metabolismo del exemestano entre individuos. Una vez confirmado que el exemestano se metabolizaba en 17-HEXE, exploramos si el 17-HEXE o exemestano, ambos presentes en el suero de los pacientes, podían interactuar y activar el Receptor de Andrógenos (AR). Esta interacción se evaluó, *in vitro*, realizando un ensayo de luciferasa y un ensayo llamado pellet de cromatina. Dichos resultados demostraron que tanto el exemestano como el 17-HEXE tienen afinidad, que se pueden unir y activar el AR. En consecuencia, dichos resultados sugieren que el beneficio clínico observado en determinados podría estar relacionada con la acción del exemestano o su metabolito 17-HEXE a través del AR.

Además, en este análisis se observa que los pacientes con una alta proporción de 17-HEXE en relación con el exemestano (más del 20%) tienden a activación del AR, hecho que parece estar vinculado con a una respuesta clínica más favorable. No obstante, después de este descubrimiento quisimos ampliar ampliamos nuestro estudio para explorar si la eficacia del tratamiento podría estar influenciada por los niveles de AR. Evaluamos el % de células AR-positivas en pacientes NeoLetExe y examinamos los niveles de Ki67 antes y después

del tratamiento con exemestano. Encontramos que pacientes con mayor % de células AR-positivas tuvieron respuestas más favorables, reflejadas en un menor niveles de Ki67 después del tratamiento. Estos resultados sugieren un umbral potencial entre 15-20% de células AR-positivas para predecir la respuesta al exemestano.

Para comprender mejor el papel del AR, investigamos qué genes o sitios de unión eran regulados por el AR en pacientes tratados con exemestano mediante ChIP-Seq. Este análisis dividió los pacientes en dos grupos. El Grupo 1, consistía en pacientes con un % intermedio de células AR-positivas y el Grupo 2-3 comprendía pacientes con un % notablemente alto de células AR-positivas. Investigaciones adicionales mediante GSEA resaltaron que las vías asociadas con la apoptosis y la regulación negativa de RAS estaban exclusivamente enriquecidas en pacientes del Grupo 2-3 después de dos meses de tratamiento con exemestano. Estos datos sugieren que la reprogramación de la unión de AR a la cromatina, tras el tratamiento con exemestano, parece llevar a una regulación al alza de vías relacionadas con la inhibición del crecimiento celular y la regulación a la baja de la señalización de Ras, lo que sugiere una posible explicación para la respuesta más favorable observada en estos pacientes. A raíz de estos resultados, proponemos un modelo celular para explicar por qué se exhibe una mejor respuesta al exemestano en tumores con un % más alto de células que expresan AR.

Basado en estos resultados, nos propusimos validar *in vitro* si el 17-HEXE, el exemestano o la combinación de ambos fármacos contribuyen a la inhibición del crecimiento celular, a través del AR. Los resultados revelaron que la combinación de 17-HEXE y exemestano mostraron una reducción significativa en la proliferación celular en células de cáncer de mama que sobreexpresan el AR, sugiere un posible efecto sinérgico entre estos compuestos.

Conclusiones I

En este capítulo dedicado a descubrir los mecanismos de respuesta a los inhibidores de aromatasa en pacientes con cáncer de mama luminal, se obtuvieron las siguientes conclusiones:

1. El tratamiento con exemestano seguido de letrozol demostró resultados clínicos superiores, validados por una menor variación del Ki67 en el grupo NeoLetExe.

2. El análisis bioquímico confirmó que el exemestano presenta una inhibición similar de la aromatasa que el letrozol, evidenciada por la reducción de los niveles de estrógeno en la sangre de los pacientes.

3. Tanto el exemestano como el 17-HEXE interactúan con el AR, confirmado mediante ensayos de luciferasa y la precipitación de cromatina.

4. Una alta proporción de células positivas para AR mostró una respuesta más favorable al tratamiento con exemestano, manifestada por una reducción en el Ki67, al alterar la unión del AR a la cromatina y aumentar las vías de apoptosis.

5. Se demostró un efecto sinérgico y mayor citotoxicidad de la combinación de 17-HEXE con exemestano en células de cáncer de mama que sobreexpresan el AR.

Capítulo II: identificación de los factores de transcripción responsables del desarrollo de metástasis en pacientes luminales tratados con inhibidores de aromatasa

El segundo proyecto de investigación de este doctorado se dedicó a investigar los factores responsables del desarrollo de resistencia al tratamiento con inhibidores de aromatasa en pacientes con cáncer de mama luminal. Los principales objetivos de este estudio fueron los siguientes:

1. Comprender los mecanismos subyacentes a la pérdida de respuesta a los inhibidores de aromatasa.
2. Descubrir las disparidades existentes entre los tumores primarios y metastásicos en relación con su exposición al tratamiento con inhibidores de aromatasa.
3. Explorar los reguladores de la transcripción que contribuyen a la aparición de metástasis en pacientes sometidos a terapia con inhibidores de aromatasa.

Resumen de los resultados II

Nuestro trabajo se enfocó en dilucidar la falta de respuesta a IAs en pacientes con progresión a enfermedad metastásica. Para estudiar dicha resistencia, se recolectaron muestras de tumores primarios luminales y de las metástasis desarrolladas en estos pacientes después de recibir terapia con IA para analizarlas y comprender los mecanismos moleculares de la resistencia al tratamiento. Utilizando la tecnología Fit-Seq, examinamos las muestras y encontramos cambios sustanciales en los estados de la cromatina entre tumores primarios y metastásicos. El análisis reveló una considerable regulación al alza de genes en el tumor primario y una regulación a la baja en el entorno metastásico, sugiriendo un proceso dinámico en el que genes específicos se apagan o muestran expresión reducida durante la terapia.

Centrándonos en comprender los factores de transcripción responsables de la regulación a la baja en el entorno metastásico, identificamos cambios significativos en vías reguladoras, relacionadas con la modificación de histonas y con la regulación de unión a la cromatina. De estos, GATA3 surgió como un candidato potencial involucrado en la metástasis, sorprendente por su papel conocido en mantener la diferenciación celular y suprimir la metástasis. Sin embargo, se ha observado que la pérdida de función de GATA3 promueve la metástasis del cáncer de mama regulando proteínas de la familia MTA, formando el complejo NuRD, el cual juega un papel crítico en la progresión del cáncer de mama al regular

la organización de la cromatina. No obstante el mecanismo molecular subyacente al rol dual de NuRD (MTA3) y NuRD (MTA1) en la progresión del cáncer de mama en el contexto de tratamiento con inhibidores de aromatasa.

En nuestro estudio, observamos una interacción entre MTA1 y MTA3 en células de cáncer de mama no invasivas (células MCF7). La depleción de MTA1 resultó en un aumento notable de los niveles de proteína y RNA de MTA3, y viceversa. Además, elucidamos las interacciones de HDAC1 con ER y GATA3 como parte del complejo NuRD. Por lo referente a la proliferación, no se detectaron alteraciones significativas en tras la eliminación de MTA1 o MTA3, independientemente de las condiciones de crecimiento.

Sin embargo, la depleción de MTA3 aumentó la migración, mientras que la depleción de MTA1 tuvo el efecto opuesto. Además, niveles elevados de MTA3 se relacionaron con una migración reducida, a diferencia de los niveles altos de MTA1 que se asociaron con una migración aumentada, independientemente de la presencia de hormonas. En ensayos de invasión, se evidenció en condiciones sin hormonas, la depleción de MTA3 aumentó la capacidad celular invasiva. Estos hallazgos sugieren que la depleción de MTA3, llevando al complejo NuRD (MTA1), confiere capacidad invasiva. Los experimentos demostraron que la presencia de estrógenos podría influir en este proceso biológico. Entonces, en pacientes tratados con inhibidores de aromatasa y bajos niveles de MTA3, el complejo NuRD (MTA1) podría conferir capacidad invasiva a las células. La implicación de ER en la modulación de la interacción entre MTA1 y MTA3 en el complejo NuRD se demostró en experimentos de silenciamiento, lo que sugiere un papel regulatorio de ER en esta dinámica. La presencia o ausencia de ER afectó significativamente la migración e invasión celular en relación con los niveles de MTA1 y MTA3.

El objetivo siguiente fue comprender el papel de GATA3 dentro de la dinámica del complejo NuRD, particularmente su implicación en la regulación de la migración celular cuando existe un desequilibrio proteico entre MTA1 y MTA3. La depleción de GATA3 resultó en niveles reducidos de MTA1 y MTA3, fortaleciendo la idea de que GATA3 podría formar parte de los complejos NuRD (MTA1) y NuRD (MTA3). Además, se observó que GATA3, MTA1 y MTA3 afectan la capacidad migratoria celular. No obstante, la supresión simultánea de MTA1 y GATA3 disminuyó aún más la migración, indicando la relevancia de GATA3 en la regulación de la migración en el complejo NuRD. Se exploró también el efecto de GATA3 en la invasión, mostrando que su depleción, junto con MTA1 sobre

expresado y MTA3 silenciado, revirtió la invasión, resaltando el papel de GATA3 en la interacción entre MTA1 y MTA3 en el complejo NuRD.

Seguidamente, se estudió la expresión génica, mediante RNA-Seq, al silenciar MTA1 o MTA3 revelaron alteraciones en, destacando la transición epitelial-mesenquimal (EMT) y la respuesta estrogénica. Esto sugiere que la formación del complejo NuRD (MTA1) podría activar la EMT, aumentando las capacidades migratorias e invasivas. De este experimento seleccionamos 2 genes candidatos: RBPJ and BMP7, los cuales aumentaron su expresión en condiciones de depleción de MTA3.

Finalmente, se exploró la inhibición del complejo NuRD mediante inhibidores de HDAC. La administración de Romidepsin revirtió la migración aumentada por la depleción de MTA3, sugiriendo su eficacia en condiciones de baja MTA3. Sin embargo, la depleción de MTA1 y el tratamiento con Romidepsin mostraron una migración incrementada, sugiriendo un potencial dual de MTA3 en el complejo NuRD. El VPA revirtió efectivamente la migración aumentada por la depleción de MTA3, resaltando su potencial en impedir la migración en condiciones de baja MTA3. Ambos tratamientos mostraron respuestas diferenciales según las condiciones de los niveles de MTA1 y MTA3, señalando la necesidad de estratificación de pacientes antes de utilizar terapias HDAC.

Conclusiones II

Las principales conclusiones de este capítulo, dedicado a la identificación de características epigenéticas que influyen en la resistencia a inhibidores de aromatasa en pacientes con cáncer de mama luminal que avanzan hacia metástasis, son las siguientes:

1. Las modificaciones epigenéticas en muestras emparejadas (primarias y metastásicas) son responsables de la resistencia al tratamiento endocrino, subrayando la dinámica epigenética en la respuesta al tratamiento y la progresión metastásica.

2. El análisis epigenético reveló reguladores de la transcripción, entre los cuales GATA3 surgió como un factor de transcripción crucial significativamente implicado en la metástasis del cáncer de mama.
3. El complejo NuRD y su dinámica de interacción entre MTA1 y MTA3 regulan la migración e invasión celular in vitro.

4. En células ER-positivas y GATA3-positivas, tanto GATA3 como ER parecen ser necesarios para el fenotipo migratorio e invasivo ensaltado del complejo NuRD (MTA1), mientras que NuRD (MTA3) podría promover un fenotipo no metastásico en el contexto de la resistencia a inhibidores de aromatasa.

5. En células ER-negativas y GATA3- negativas, el complejo NuRD (MTA3) aumentó las capacidades migratorias, mientras que las capacidades migratorias del complejo NuRD (MTA1) se vieron disminuidas.

6. El complejo NuRD influye en la transición epitelial a mesenquimal (EMT), sugiriendo los mecanismos para la evolución metastásica.

7. Las implicaciones terapéuticas que apuntan a las HDACs del complejo NuRD han surgido como un posible objetivo terapéutico.

ACKNOWLEDGEMENTS

Aquesta tesis no ha estat un camí fàcil ni ple de roses, però al arribar al final i veure el que he aconseguit m'enorgulleix molt. Al llegir-la no només veig figures i experiments, sinó que veig, sang, suor, llàgrimes, riures, mil moments (bons i dolents), però sobretot, moltes i moltes hores. Tots aquests records m'han fet evolucionar tant a nivell personal com professional i estic i estaré molt agraïda.

Com no podia ser d'una altra manera, voldria començar donant les gràcies al meu director de tesis, **Toni Hurtado**. La seva acollida al grup i el seu suport han estat fonamentals per al meu creixement professional i personal durant aquests anys. A més, el seu equip i la seva experiència han enriquit enormement el meu coneixement i la meva perspectiva. No puc expressar prou amb paraules la meva gratitud cap a tu. Et vull donar les gràcies pel temps que has dedicat a orientar-me, per ensenyar-me a plantejar les preguntes adequades i, sobretot, per haver-te implicat tant en treballar amb mi per tirar endavant aquest projecte. Agraeixo de tot cor la teva confiança en mi, per brindar-me aquesta oportunitat i donar-me suport durant tot aquest temps. Gràcies per ser aquest investigador excepcional, líder, mentor i persona a qui tots respectem i admirem.

Laboratorio TH - BCN

Voldria continuar donant les gràcies als companys de Barcelona. A ti **José Ángel**, gracias por todo el apoyo y paciencia que tuviste conmigo cuando llegué ya que estaba muy asustada de empezar esta etapa. Teniéndote a ti como compañero de laboratorio me dabas mucha tranquilidad y sabía que si trabajábamos juntos conseguiríamos tirar todos los proyectos hacía adelante, porque, por ejemplo, ninguno de los dos se resignaba a aceptar que no tuviéramos acceso a determinados aparatos. Te admiro mucho, sobre todo a nivel profesional y vas a conseguir todo lo que te propongas.

La següent incorporació al grup va ser l'**Helena Brunel**, la misteriosa bioinformàtica del grup que sempre havíem de veure a través d'una pantalla degut al Covid-19. Gràcies per tot el suport en els meus inicis de bioinformàtica i deixar les bases perquè pogués anar creant i executant els meus primers scripts, sentint-me com una Hacker.

I would like to also thank **Alice** for making me company the last months in the lab in Barcelona and made me realize that I was able to teach and transmit my knowledge to someone else and that I enjoyed it.

Laboratorio BCN

A Barcelona compartíem espai amb altres grups, entre els quals, estava el liderat per la **Rosa Aligué**. Moltes gràcies per totes les coses que ens vas deixar quan estàvem establint el laboratori. Gràcies a tu vam poder seguir endavant amb els experiments i sempre estaves disposada a ajudar-nos.

No podía no dar las gracias a **Rodrigo**, el torbellino, del laboratorio. Gracias por todas esas charlas en cultivos, juntamente con José Ángel, donde nos cuestionábamos la ciencia y nuestro propósito en la vida. Te admiro mucho como persona, tienes una fortaleza y una determinación envidiables, no lo olvides.

Cuando pienso en el laboratorio de Barcelona pienso en ti, **Tula**. Gracias por aguantar mis inseguridades y darme consejos unos tras otros sin esperar nada a cambio de mí. Gracias por dedicarme todo el tiempo que necesitaba y más, aunque eso luego supusiera tener que ir corriendo, o llegar tarde a la guardería a buscar a tu peque. Gracias por tus consejos, tu apoyo y hacerme de mami en el laboratorio. Todo era mucho más fácil sabiendo que podía contar con tu sabiduría y experiencia. Gracias a ti me di cuenta de lo bueno que es compartir los resultados de los experimentos y discutirlos durante horas con un café o con un tupper.

Finalmente, quiero agradecer a **Jon, Edgar, Julia y Maribel** por los incontables consejos que me distes sobre cómo afrontar el PhD e intentar no cometer errores. Gracias por amenizar las horas en el laboratorio.

Un cop adaptada al laboratori de Barcelona, tocava enfrontar-me a la disjuntiva de si seguir amb el projecte que tant m'il·lusionava i haver de mudar-me a Salamanca o si abandonar. He de dir que aquella va ser una decisió presa amb el cor i no racional, sinó...qui sap on estaria ara. Va ser molt dur marxar de casa quan tot just havia tornat. Em vaig imaginar milions de vegades com seria Salamanca, ciutat que vaig haver de buscar al mapa per saber on estava, i ni en els millors dels meus somnis m'imaginava la rebuda que he tingut aquí. Qui m'anava a dir que acabaria tenint amics d'aquells que se senten com a família i que t'estimen i et recolzen incondicionalment.

Laboratorio L2-L3 – Salamanca

Me gustaría empezar el capítulo de Salamanca hablando de **Antonio Abad**. Ese nombre se me va a quedar por siempre grabado, ya que, sin saberlo, fue la contraseña que me abrió las puertas a la familia de los Bustelinos y Dosilinos. Cuando llegué al CIC por primera vez, con las pipetas en la mano, me di cuenta de que había llegado antes de tiempo, que ahí todavía nadie conocía a Toni Hurtado y que nadie esperaba mi llegada. Mientras entraba en pánico, recordé que me habían dicho que si me pasaba esto que dijera que quería hablar con Antonio Abad, quien, supuestamente si sabía de mi llegada. Sorpresa, él tampoco tenía ni idea de quien era ni que hacía allí. Es aquí donde Antonio Abad cambió el curso de mi estancia en Salamanca para siempre. Antonio podría haberme dicho mil cosas para sacarse el "marrón" de encima. No obstante, me acogió con la mayor naturalidad. Apartó 4 papeles y me dio una poyata, un escritorio y una familia. Muchas gracias Antonio, por tomar esa decisión. Gracias por ese tour por el centro de 3 horas (sigo pensando que eso día vi más salas de las que realmente hay en el CIC). Gracias también a ti por toda la ayuda con los animales, eres un gran profesional y mejor persona.

No obstante, todo esto no hubiese sido posible sin **Xosé Bustelo**. Te estaré eternamente agradecida por acogerme y abrirme las puertas de tu laboratorio o más bien dicho, de tu familia profesional que hay en el L2 y L3. Gracias también a **Mercedes Dosil** por dejarme dar prácticas y darme cuenta de lo bonita que es la docencia y la transmisión de conocimientos.

Quiero empezar dándole las gracias a **Isa**, aún me acuerdo de ese correo a las 10 de la noche del viernes después de conocerme de 2 días para informarme de que ibais a cenar, y si quería unirme. Parece una tontería, pero para mí en eso momento no lo fue. Ahí me percaté de que la gente de ese laboratorio era increíble, sobre todo, a nivel humano. Gracias Isa por todo, eres de las personas más especial y única (con el mejor de los sentidos) que conozco. Gracias por todo el apoyo incondicional, por hacerme querer ser mejor persona día a día. Gracias por enseñarme a no tener miedo a decir lo que uno quiere o piensa, aunque no sea del todo políticamente correcto, gracias por los viernes de pádel "que iniciaste", por los viajes, por las risas…por convertirte en mi mayor apoyo.

Lucía, que decir de ti, eres pura bondad; pura luz. Eres un corazón con patas que haces mejor a los demás, tanto a nivel profesional como personal. Eres mi post-doc de confianza. Te

admiro profundamente y vas a llegar donde tu te propongas. Solo espero estar allí para poder ayudarte a conseguir tus sueños y brindar por ti. Gracias por sacar siempre tiempo para escucharme y darme consejos y opinión tanto personal como profesional. Gracias por enseñarme a que hay que tener una vida balanceada entre el trabajo y la vida personal y ocio y que el hecho de salir a las mil no es una limitación para ellos. Gracias por hacerme sentir tan querida y querer parecerme más a ti.

Quiero darle las gracias a mi queridísimo **Javi**. Gracias por todo lo que me has enseñado, no solo a nivel profesional, sino también en el ámbito personal. Eres la mezcla perfecta entre ser trabajador y divertido, siempre encontrando el equilibrio adecuado y en el momento justo. Aprecio profundamente la filosofía de vida que compartes y que me has enseñado. Gracias por las risas inolvidables. Cada vez que pienso en ti, recuerdo mil tonterías de las que nos hemos reído juntos, ya sea en las noches de películas, en los días en el gimnasio, durante las clases de pádel o en esos emocionantes viajes y excursiones en coche. Sea cual sea el plan, tú logras que sea divertido y memorable. Estoy deseando seguir haciendo planes contigo en el futuro, sabiendo que cada encuentro será una garantía de diversión y buenos momentos. Muchas gracias por todo lo que me has dado, tanto dentro como fuera del laboratorio. Tu influencia positiva en mi vida ha sido invaluable, y estoy agradecida por contar contigo como un amigo y mentor excepcional.

A **Natalia**, no puedo expresar lo agradecida que estoy por todo el apoyo que me has brindado. Tu corazón es verdaderamente valioso, y me considero afortunada de contar con alguien como tú en mi vida. Siempre has estado dispuesta a ayudar, escucharme y ofrecer tu opinión, y eso ha hecho una diferencia significativa en mi camino. Admiro enormemente tus innumerables cualidades. Eres fuerte, valiente y una luchadora incansable. Tu gran sentido del humor ha iluminado incluso los días más oscuros. Es un privilegio tener a alguien con tu positividad y determinación a mi lado. Estoy deseando seguir viviendo mil aventuras contigo. Gracias por ser una fuente constante de apoyo, inspiración y alegría.

A **Sonia**, quiero expresarte mi más profundo agradecimiento por tu paciencia infinita al diseñar oligos y por estar siempre ahí para escucharme. Eres la viva imagen de la lucha y la determinación, nunca aceptando un no como respuesta. Cada vez que pienso en ti, recuerdo mil aventuras y momentos inolvidables. Me siento increíblemente afortunada de tener a una persona tan apasionada y valiente como tú en mi vida. Eres única, una verdadera "loquita" que añade alegría y energía a cada situación. Las aventuras que hemos vivido son solo el

comienzo, y estoy emocionada por las que aún nos esperan. Gracias por tu apoyo y ayuda, tanto a nivel profesional como personal. Admiro enormemente tu fuerza y tu actitud inquebrantable ante cualquier obstáculo. Estoy segura de que llegarás muy lejos, porque no hay desafío que no puedas superar.

Quiero expresarte mi sincero agradecimiento a **Maribel** por tu inestimable apoyo y comprensión. A lo largo de nuestro tiempo juntas, tus charlas en cultivos y los valiosos consejos que me has brindado han sido de una ayuda inigualable. Siempre me ha reconfortado saber que podía contar contigo, una persona tan sabia y experimentada, en caso de que los experimentos no salieran como esperábamos. A nivel personal, mi admiración hacia ti crece aún más, si cabe. Ojalá pudieras verte con los ojos con los que yo te veo. Eres una persona increíblemente fuerte, luchadora, resiliente, buena, entregada y comprensiva. Gracias por ser una inspiración constante.

Quiero agradecerle esta tesis a una persona extraordinaria, la más bondadosa del laboratorio: **Rosa**. Tu corazón bondadoso ha sido un regalo para todos nosotros. Siempre estás dispuesta a ayudar y a ofrecer una sonrisa reconfortante en los momentos más desafiantes. Tu actitud positiva y compasiva ha creado un ambiente en el laboratorio que va más allá de los experimentos. Tu presencia ha dejado una huella imborrable en cada uno de nosotros.

Quería tomarme un momento para agradecer a **Rubén**. Gracias por ser la chispa de alegría en el laboratorio. Eres indudablemente el más gracioso, siempre con una broma o comentario ingenioso que logra sacarnos una sonrisa incluso en los días más agitados. Me hubiera encantado pasar más tiempo contigo en el laboratorio, pero estoy convencida de que nos quedan mil momentos que vivir fuera. Tu buen corazón y tu humor contagioso hacen que cada momento contigo sea especial.

No quiero dejar pasar la oportunidad de expresar mi más profundo agradecimiento a **Laura**, el equilibrio perfecto entre la locura y la cordura (Gómez Gaspar S., 2022). Este es elmo, el momento de agradecerte todo lo que has hecho por mi durante este tiempo. Eres el alma de la fiesta, siempre irradiando alegría con tu risueña energía y tu cálida acogida. Eres una fuente constante de inspiración en mi vida. Tu capacidad de discernir entre el bien y el mal me han fascinado, sobre todo tu espíritu justiciero y crítico. Has hecho cada momento especial y memorable. Gracias por toda la ayuda, soporte y comprensión que me has brindado. Tu apoyo ha sido un pilar fundamental en los momentos difíciles, y estoy

agradecida por tener a alguien tan solidaria en mi vida. Tengo muchas ganas de seguir viviendo mil momentos y risas contigo.

Laboratorio 7 – TH – Salamanca

Un cop instal·lada i feliç a Salamanca, tocava mudar-se de nou. Aquest cop era menys dolorós, ja que era creuar el passadís i muntar el laboratori 7. Des de Barcelona rebia el suport telemàtic del **Darek**. I would like to acknowledge Darek, our esteemed bioinformatician, whose unwavering support and expertise in analysis have been invaluable to the group's research endeavors from whom I gained such immense knowledge. I am sure it will be a major asset throughout my career.

In parallel, two exceptional students landed on the laboratory. I would like to give a special acknowledgment to **Inês** and **Ioanna**, whose dedication and effort made working together a rewarding experience. Their commitment and contributions greatly enriched our collaborative efforts.

No podría olvidarme de **María**, muchas gracias por tu valiosa contribución al proyecto del capítulo II. Gracias por el tiempo, esfuerzo y horas compartidas tratando de descifrar los resultados juntas.

Finalmente quiero dar las gracias a **David**, que ha sido la última incorporación al laboratorio. Te paso el relevo de llevar el laboratorio L7-TH, pero sé que lo dejo en buenas manos y estoy convencida de que lo harás genial. Eres una gran persona y un muy trabajador, así que lo tienes todo de cara para que este PhD te vaya fenomenal. Siempre que necesites cualquier cosa de mí, espero que sepas que puedes contar conmigo.

Otros Laboratorios del CiC

Si hay laboratorio 7-TH, eso significa que hay un L7-MD. Quiero dar mis gracias más sentidas a **Irene**. Solo tengo palabras de agradecimiento para ti. Gracias por hacer la convivencia en el laboratorio tan fácil, por siempre tener una sonrisa y una palabra amable. Eres pura bondad y de esas persones que solo se merece que le pasen cosas buenas. Te admiro muchísimo y te tengo muchísimo cariño. Te deseo lo mejor, pero estoy convencida de que nuestros caminos se volverán a cruzar pronto, al final y al cabo, eres mi doble.

El L7 no hubiese sido lo mismo sin ti, **Morena**. Gracias por aportar tu experiencia y tu criterio. Gracias por encomendarnos tu espíritu crítico. Gracias por los incontables consejos sobre cómo optimizar las técnicas y divagar sobre porque no se estaban obteniendo los resultados esperados.

No se puede hablar del L7, sin hablar de ti **Alejandra**. Eres la dulzura personificada. Siempre dispuesta a ayudar, siempre risueña. Gracias por estar siempre allí dispuesta a darme energía positiva y darme ese empujón final para continuar tirando hacia adelante. Con esta personalidad, con tu espíritu luchador y resiliencia vas a conseguir todo lo que te propongas. Aunque la vida se ponga dura, no dejes que te cambie porque esa sonrisa y optimismo tuya alegra los días.

En el CIC he tenido la suerte de compartir espacio con muchos otros laboratorios repletos de gente increíble y que han sido de gran ayuda. Entre todos ellos quiero dar un agradecimiento especial al laboratorio 5 de **Sandra Blanco**. Quiero empezar dando mi profundo agradecimiento a Sandra por su valiosa contribución en los lab meetings y por todo el soporte y mentoring recibido. Gracias por tu compromiso y generosidad en compartir su experiencia, que ha sido de inestimable valor para este proyecto. A parte de Sandra, quiero agradecer a otros miembros del laboratorio 5 como **Paz, Borja, Ana y otros miembros del L5.** Gracias por vuestra dedicación, conocimiento y perspectivas enriquecieron enormemente las discusiones durante nuestros lab meetings. Vuestros consejos, comentarios y apoyo fueron fundamentales para el desarrollo de este trabajo.

Quiero dar las gracias a **Judith** por estar siempre dispuesta a ayudarme, hasta el último momento con los papeleos de la tesis. Hemos compartido muchos momentos y viajes que siempre tendré grabado en mi memoria. Te admiro mucho y me siento muy afortunada de haberte conocido.

També voldria donar les gràcies a **Óscar (Polli).** Moltes gràcies per tenir sempre una paraula amable i un somriure pels passadissos. Ets el clar exemple de si la vida et dona llimones, fes llimonada i aquesta filosofia de vida es contagiosa. Amb aquesta resiliència i bon cor que tens segur que arribaràs on et proposis. Gràcies per fer-me sentir més a prop de casa quan els dies eren eterns al CIC.

Raquel (L5), no puedo hablar del L5 sin mencionarte, porque para mí has sido una revelación en el mejor sentido posible. Tu bondad profunda ha sido un apoyo inquebrantable,

siempre dispuesta a tenderme la mano, pero, sobre todo, esforzándote por calmarme y devolverme al suelo cuando más lo necesitaba. Lo haces sin esperar nada a cambio, ¡tu generosidad es infinita! Gracias por soportar mis podcasts y por llenar mis días de risas. Tu comprensión hacia mí es extraordinaria. El tiempo nos dará perspectiva, miraremos hacia atrás y reiremos de estos días, agradecidas por todo lo que el doctorado nos ha enseñado, no solo profesionalmente, sino también sobre nosotras mismas. Estoy convencida de que esto es solo el comienzo, que nos esperan innumerables momentos por vivir y viajes por hacer juntas.

A **Marta** (L5), mi más sincero agradecimiento por tu presencia constante y tu inigualable bondad. Tu inocencia y generosidad han iluminado cada interacción y han dejado una huella imborrable en este camino. Los viajes compartidos han sido momentos inolvidables, y sé que quedan muchos más por explorar juntas. Tu disposición inquebrantable para ayudar y los momentos de charlas espontáneas en los pasillos han sido un bálsamo en momentos de necesidad.

Agradezco sinceramente a **Javi** (L8, Zama) por tu inestimable apoyo durante la realización de esta tesis. Tu contribución va más allá de lo académico. Quiero destacar y agradecer especialmente los inolvidables viernes de pádel que se convirtieron en espacio para la diversión y la amistad. Esos momentos de relax fueron clave para recargar energías y enfrentar los desafíos que surgieron en el camino de esta investigación. Además, agradezco de corazón todos los momentos de fiesta que compartimos. Tu compañía ha hecho que este viaje académico sea mucho más memorable y enriquecedor.

A **Sergio** (L10) quisiera expresarte mi más profundo agradecimiento por todo lo que has hecho. Gracias, en primer lugar, por tu comprensión, por esas charlas en las que el tiempo parecía volar y al final dejaban una sensación de alivio y comprensión. Tu paciencia y disposición para escucharme han sido invaluables durante este proceso. Quiero agradecerte también por tu bondad genuina, siempre dispuesto a ayudarme en cada paso del camino. Tu generosidad al dejarlo todo para brindarme tu apoyo y responder a mis dudas no tiene precio. Ha sido una verdadera suerte tenerte en mi vida. Eres una de esas personas que sabes que quieres conservar para siempre.

Mil gracias **Maqui**. No puedo más que expresar mi profundo agradecimiento por tu presencia, aunque haya sido por un tiempo breve, tu vitalidad, energía y positividad han

dejado una huella imborrable en mi vida. Es asombroso cómo tu alegría contagiosa ha iluminado incluso los días más grises. A pesar de la distancia física y de haber compartido poquito tiempo, siento como si te conozco de toda la vida.

A las nuevas incorporaciones del L2 (**Leire**, **Gonzalo**, **Ana** y **Alejandra**), quiero expresar mi más sincero agradecimiento a cada uno de vosotros por ser parte de este equipo. La incorporación de nuevos miembros ha traído un aire fresco y renovado, y ha sido un verdadero placer contar con vuestro soporte en esta recta final de tesis. No obstante, en especial, quiero dirigir unas palabras de agradecimiento a **Cristi**. Gracias por tu apoyo y por esas risas tan necesarias, ha sido reconfortante. Tu calidad humana y dedicación al trabajo no han pasado desapercibidas, sigue así y serás imparable.

Servicios colaboradores

Quisiera expresar mi profundo agradecimiento a todos vosotros, ya que este trabajo no habría sido posible sin vuestra invalorable contribución. Sois la viva prueba de que la ciencia es un esfuerzo conjunto, un trabajo en equipo que se sostiene gracias a la dedicación y colaboración de individuos excepcionales como vosotros.

En particular, quiero extender mi gratitud al **servicio de Microscopia**, y más específicamente a **Ana**. Gracias por ser el alma de este servicio y del CIC entero. Tu sabiduría y voz de la razón han sido fundamentales, tanto a nivel profesional como personal. Aprecio enormemente tu disposición constante y el hecho de que siempre estuviste allí cuando te necesité.

Asimismo, este trabajo tampoco habría sido posible sin el **servicio de Patología Molecular** (**Susana**, **Telmo**, **Tania**, **Jairo**, **Ángel** y al resto de personal), pero quiero dirigir un agradecimiento especial a **Mamen**. No tengo palabras suficientes para expresar mi agradecimiento por todo el apoyo y soporte que he recibido de tu parte. Eres una fuente de inspiración y compartir sesiones de patología contigo ha sido un auténtico lujo y placer. Cada día aprendí algo nuevo a tu lado. Además de ser una profesional excelente, eres una persona maravillosa. Gracias por enseñarme a conocerme y a gestionar mis emociones. Ojalá algún día pueda ver la vida con tu clarividencia.

Moltes gràcies al servei de oncologia de **l'Hospital de la Vall d'Hebron** i al **Hospital Akerhus** per les mostres que ens han permès realitzar aquesta investigació i que tenen un valor incalculable.

Amigos de fuera del labo

A **Mercedes**, mi suerte manchega, una auténtica caja de sorpresas, siempre llena de buen rollo, positividad, energía y vitalidad. No hay encuentro contigo que no esté marcado por risas contagiosas y, por supuesto, ¡muchos perreitos! Tu filosofía de vida es un regalo. Gracias por ser un faro de buen rollo y por compartir esa energía tan contagiosa. Esto solo ha sido el principio, así que prepárate, porque ni Oscar ni yo queremos que te libres tan fácilmente de nosotros.

Quiero dedicarte unas palabras llenas de agradecimiento a **Mari**, por ser una fuente constante de risas y planes divertidos. Tu gracia y alegría contagiosa han añadido un toque especial a cada encuentro. Siempre estás dispuesta a adaptarte y a hacer de cualquier situación algo divertido. Gracias por ser esa chispa de alegría del grupo y por convertir cada momento compartido en algo especial.

A ti **Laura Zeballos**. Cuando me enteré de mi mudanza a Salamanca, la única perspectiva positiva que vislumbré fue que tú estarías allí, y que nuestros caminos se cruzarían nuevamente. ¡Qué suerte la mía! Te admiro profundamente y te quiero aún más. Gracias por ser esa vía de escape en Salamanca, esa burbuja en la que el tiempo se detiene y podemos hablar abiertamente de todo. Agradezco enormemente tu disposición para escucharme, apoyarme y brindarme consejos. Cada encuentro contigo deja la sensación de que el tiempo nunca es suficiente. Me muero de ganas de poder tener más tiempo libre para compartir y disfrutar más momentos contigo. Eres un 10 como persona, y no te puedes ni imaginar lo inmensamente feliz que me has hecho sentir. Gracias por ser una parte tan valiosa de mi vida.

No vull oblidar-me de donar-te les gràcies a tu, **Neus**. Gràcies, gràcies i més gràcies. Per tot. Per ser-hi sempre, per escoltar els meus podcasts, per fer que la distància sigui molt fàcil, per retrobar-nos com si el temps no hagués passat. Saps que aquesta etapa no ha estat fàcil per a mi, però saber que podia comptar amb el teu suport i afecte ho ha fet tot una mica més fàcil i agradable.

Voldria expressar el meu agraïment a altres persones que han estat fonamentals en aquesta etapa de la meva vida. Als amics del cole, al Núcleo, a les nenis/Merceditas/Seaguls (Ari, Andrea i Mire) i als meus nens (Edu i Guillle) sou la viva imatge del des de sempre i per sempre. Sou una de les raons que han fet que vulgui tornar a Bacelona, a casa, i que marxar hagi estat tant dur. A la **Mire**, **Ari** i **Andrea**, no puc deixar de reconèixer la importància que teniu en la meva vida. Agraeixo la vostra confiança constant, la comprensió de la complexitat del món de la ciència i, sobretot, seguir convidant-me a plans, fins i tot quan he hagut de rebutjar-los per alimentar les meves cèl·lules. Gràcies per la vostra empenta i per sentir-vos orgulloses de mi. Sou les millors, i us estimo amb bogeria. Als meus nens, **Edu** i **Guille**, la vostra presència sempre al meu costat ha estat un regal impagable. Ja sigui per riure, parlar de la vida o desfogar-me, sé que puc comptar amb vosaltres. Gràcies per oferir-me un suport incondicional que fa que cada dia sigui més fàcil.

A la familia de l'Oscar

Moltes gràcies, **Raquel**, **Xavi**, **Mila** i **Tata Rosa**, per ser una part tan important en la nostra vida. Vull expressar la meva profunda gratitud pel suport que ens heu brindat durant aquests anys. Sé que ha estat difícil veure com l'Oscar i jo ens anàvem, i agraeixo de tot cor la vostra comprensió i suport incondicional. Gràcies per ser sempre una font de suport a la qual puc recórrer en tot moment. És un luxe saber que podem comptar amb vosaltres i sentir la vostra presència en els moments més importants. Estic agraïda per poder sentir la vostra estima i orgull cap a mi. És un regal saber que puc comptar amb una família tan especial com la vostra.

A la meva familia

Moltes gràcies, **mama**, **papa**, **Marta**, **Marina**, **Marcel**, **Elsa**, **tieta**, **Xavier** i **Iaia Mercè**, per ser el pilar de la meva vida. Les vostres aportacions han estat incomparables i vull expressar el meu agraïment més sincer. Gràcies per sempre impulsar-me a ser una millor persona, a perseguir els meus somnis i a lluitar per ells. Cada consell que he rebut i cada valor que m'heu inculcat han estat vitals en la meva trajectòria. Espero que us sentiu tan orgullosos de mi com me'n sento jo de vosaltres. Sense el vostre suport incondicional, aquest camí no hauria estat possible. Estic profundament agraïda per tot el que heu fet per mi. Us estimo moltíssim i agraeixo cada sacrifici, cada paraula d'ànim i cada gest de amor que heu compartit amb mi. Gràcies per tot.

Oski

No podia acabar els agraïments sense dedicar una menció especial a tu, **Oski**. Només tu i jo sabem tot el que hi ha darrere d'aquesta tesis. Gràcies infinits cops per tot allò que has fet per mi durant aquests anys. Has estat una font constant de suport, tirant del carro quan jo no podia més. La teva confiança en mi, fins i tot quan jo dubtava de mi mateixa, no té preu. Agraeixo profundament l'amor que em dones i tan bé com ho fas. Gràcies per recórrer 1600 km cada setmana només per regalar-me el millor dels somriures. La teva dedicació i sacrifici no han passat desapercebuts, i ho valoro enormement. Agraeixo les hores de paciència i suport (bioinformàtic també) que has dedicat al meu projecte. Estar al meu costat, tant en els moments bons com en els difícils, sense esperar res a canvi m'han demostrat novament que ets una gran persona i que soc molt afortunada de tenir-te a la meva vida. Gràcies per fer-me brillar i fer-me millor persona. No sé si algun dia podré agrair-te prou tot el que has fet i significat per a mi en aquesta boja aventura que és la tesis. Estic convençuda que sense tu, no ho hauria aconseguit. T'estimo.

REFERENCES

REFERENCES

1. Sung, H., et al., *Global Cancer Statistics 2020: GLOBOCAN Estimates of Incidence and Mortality Worldwide for 36 Cancers in 185 Countries.* CA: A Cancer Journal for Clinicians, 2021. **71**(3): p. 209-249.
2. Bray, F., et al., *Global cancer transitions according to the Human Development Index (2008-2030): a population-based study.* Lancet Oncol, 2012. **13**(8): p. 790-801.
3. Bray, F., et al., *Global cancer statistics 2018: GLOBOCAN estimates of incidence and mortality worldwide for 36 cancers in 185 countries.* CA Cancer J Clin, 2018. **68**(6): p. 394-424.
4. Houghton, S.C. and S.E. Hankinson, *Cancer Progress and Priorities: Breast Cancer.* Cancer Epidemiol Biomarkers Prev, 2021. **30**(5): p. 822-844.
5. Torre, L.A., et al., *Global Cancer in Women: Burden and Trends.* Cancer Epidemiol Biomarkers Prev, 2017. **26**(4): p. 444-457.
6. Rossouw, J.E., et al., *Risks and benefits of estrogen plus progestin in healthy postmenopausal women: principal results From the Women's Health Initiative randomized controlled trial.* Jama, 2002. **288**(3): p. 321-33.
7. Howlader N, et al. *SEER Cancer Statistics Review, 1975-2019.* . 2019 [cited 2023 26/02/2023]; Available from: https://seer.cancer.gov/statistics/preliminary-estimates/.
8. Heer, E., et al., *Global burden and trends in premenopausal and postmenopausal breast cancer: a population-based study.* Lancet Glob Health, 2020. **8**(8): p. e1027-e1037.
9. Wojtyla, C., et al., *European trends in breast cancer mortality, 1980–2017 and predictions to 2025.* European Journal of Cancer, 2021. **152**: p. 4-17.
10. Hu, K., et al., *Global patterns and trends in the breast cancer incidence and mortality according to sociodemographic indices: an observational study based on the global burden of diseases.* BMJ Open, 2019. **9**(10): p. e028461.
11. Carioli, G., et al., *Trends and predictions to 2020 in breast cancer mortality in Europe.* The Breast, 2017. **36**: p. 89-95.
12. Coleman, M.P., et al., *Cancer survival in five continents: a worldwide population-based study (CONCORD).* The Lancet Oncology, 2008. **9**(8): p. 730-756.
13. Maajani, K., et al., *The Global and Regional Survival Rate of Women With Breast Cancer: A Systematic Review and Meta-analysis.* Clinical Breast Cancer, 2019. **19**(3): p. 165-177.
14. McGuire, K.P., *Breast Anatomy and Physiology*, in *Breast Disease: Diagnosis and Pathology*, A. Aydiner, A. İğci, and A. Soran, Editors. 2016, Springer International Publishing: Cham. p. 1-14.
15. Skandalakis, J.E., *Skandalakis' surgical anatomy: the embryologic and anatomic basis of modern surgery*. Vol. 2. 2004: PMP.
16. Hassiotou, F. and D. Geddes, *Anatomy of the human mammary gland: Current status of knowledge.* Clinical anatomy, 2013. **26**(1): p. 29-48.
17. Thomsen, S. and D. Tatman, *Physiological and pathological factors of human breast disease that can influence optical diagnosis.* Annals of the New York Academy of Sciences, 1998. **838**: p. 171-193.
18. Ellis, H. and V. Mahadevan, *Anatomy and physiology of the breast.* Surgery (Oxford), 2013. **31**(1): p. 11-14.
19. Evan, G.I. and K.H. Vousden, *Proliferation, cell cycle and apoptosis in cancer.* Nature, 2001. **411**(6835): p. 342-8.
20. Graña, X. and E.P. Reddy, *Cell cycle control in mammalian cells: role of cyclins, cyclin dependent kinases (CDKs), growth suppressor genes and cyclin-dependent kinase inhibitors (CKIs).* Oncogene, 1995. **11**(2): p. 211-9.
21. Akram, M., et al., *Awareness and current knowledge of breast cancer.* Biological Research, 2017. **50**(1): p. 33.
22. Sever, R. and J.S. Brugge, *Signal transduction in cancer.* Cold Spring Harb Perspect Med, 2015. **5**(4).

23. Feng, Y., et al., *Breast cancer development and progression: Risk factors, cancer stem cells, signaling pathways, genomics, and molecular pathogenesis.* Genes Dis, 2018. **5**(2): p. 77-106.
24. Campeau, P.M., W.D. Foulkes, and M.D. Tischkowitz, *Hereditary breast cancer: new genetic developments, new therapeutic avenues.* Hum Genet, 2008. **124**(1): p. 31-42.
25. Kamińska, M., et al., *Breast cancer risk factors.* Prz Menopauzalny, 2015. **14**(3): p. 196-202.
26. Brewer, H.R., et al., *Family history and risk of breast cancer: an analysis accounting for family structure.* Breast Cancer Res Treat, 2017. **165**(1): p. 193-200.
27. Colditz, G.A., et al., *Family history and risk of breast cancer: nurses' health study.* Breast Cancer Res Treat, 2012. **133**(3): p. 1097-104.
28. Hsieh, C.C., et al., *Age at menarche, age at menopause, height and obesity as risk factors for breast cancer: associations and interactions in an international case-control study.* Int J Cancer, 1990. **46**(5): p. 796-800.
29. Washbrook, E., *Risk factors and epidemiology of breast cancer.* Women's Health Medicine, 2006. **3**(1): p. 8-14.
30. Sun, Y.S., et al., *Risk Factors and Preventions of Breast Cancer.* Int J Biol Sci, 2017. **13**(11): p. 1387-1397.
31. Dall, G.V. and K.L. Britt, *Estrogen Effects on the Mammary Gland in Early and Late Life and Breast Cancer Risk.* Front Oncol, 2017. **7**: p. 110.
32. Eliassen, A.H., et al., *Endogenous steroid hormone concentrations and risk of breast cancer among premenopausal women.* J Natl Cancer Inst, 2006. **98**(19): p. 1406-15.
33. Ban, K.A. and C.V. Godellas, *Epidemiology of breast cancer.* Surg Oncol Clin N Am, 2014. **23**(3): p. 409-22.
34. Hamajima, N., et al., *Alcohol, tobacco and breast cancer--collaborative reanalysis of individual data from 53 epidemiological studies, including 58,515 women with breast cancer and 95,067 women without the disease.* Br J Cancer, 2002. **87**(11): p. 1234-45.
35. Makarem, N., et al., *Dietary fat in breast cancer survival.* Annu Rev Nutr, 2013. **33**: p. 319-48.
36. Bauer, S.R., et al., *Plasma vitamin D levels, menopause, and risk of breast cancer: dose-response meta-analysis of prospective studies.* Medicine (Baltimore), 2013. **92**(3): p. 123-131.
37. Zubor, P., et al., *Why the Gold Standard Approach by Mammography Demands Extension by Multiomics? Application of Liquid Biopsy miRNA Profiles to Breast Cancer Disease Management.* Int J Mol Sci, 2019. **20**(12).
38. Sawaki, M., T. Shien, and H. Iwata, *TNM classification of malignant tumors (Breast Cancer Study Group).* Jpn J Clin Oncol, 2019. **49**(3): p. 228-231.
39. Harris, L.N., et al., *Use of Biomarkers to Guide Decisions on Adjuvant Systemic Therapy for Women With Early-Stage Invasive Breast Cancer: American Society of Clinical Oncology Clinical Practice Guideline.* Journal of Clinical Oncology, 2016. **34**(10): p. 1134-1150.
40. Prat, A., et al., *Concordance among gene expression-based predictors for ER-positive breast cancer treated with adjuvant tamoxifen.* Ann Oncol, 2012. **23**(11): p. 2866-2873.
41. Shegekar, T., S. Vodithala, and A. Juganavar, *The Emerging Role of Liquid Biopsies in Revolutionising Cancer Diagnosis and Therapy.* Cureus, 2023. **15**(8): p. e43650.
42. Veronesi, U., et al., *Breast cancer.* The Lancet, 2005. **365**(9472): p. 1727-1741.
43. Page, K., et al., *Next Generation Sequencing of Circulating Cell-Free DNA for Evaluating Mutations and Gene Amplification in Metastatic Breast Cancer.* Clinical Chemistry, 2017. **63**(2): p. 532-541.
44. Sawaki, M., T. Shien, and H. Iwata, *TNM classification of malignant tumors (Breast Cancer Study Group).* Japanese Journal of Clinical Oncology, 2018. **49**(3): p. 228-231.
45. Hortobagyi, G.N., S.B. Edge, and A. Giuliano, *New and Important Changes in the TNM Staging System for Breast Cancer.* American Society of Clinical Oncology Educational Book, 2018(38): p. 457-467.
46. Amin, M.B., et al., *AJCC cancer staging manual*. Vol. 1024. 2017: Springer.

47. Łukasiewicz, S., et al. *Breast Cancer—Epidemiology, Risk Factors, Classification, Prognostic Markers, and Current Treatment Strategies—An Updated Review*. Cancers, 2021. **13**, DOI: 10.3390/cancers13174287.
48. Bednarek, A.K., et al., *Analysis of telomerase activity levels in breast cancer: positive detection at the in situ breast carcinoma stage.* Clinical cancer research: an official journal of the American Association for Cancer Research, 1997. **3**(1): p. 11-16.
49. Segal, R., et al., *Structured exercise improves physical functioning in women with stages I and II breast cancer: results of a randomized controlled trial.* Journal of clinical oncology, 2001. **19**(3): p. 657-665.
50. Moran, M.S., et al., *Society of Surgical Oncology–American Society for Radiation Oncology consensus guideline on margins for breast-conserving surgery with whole-breast irradiation in stages I and II invasive breast cancer*. International Journal of Radiation Oncology* Biology* Physics, 2014. **88**(3): p. 553-564.
51. Jacquillat, C., et al., *Results of neoadjuvant chemotherapy and radiation therapy in the breast-conserving treatment of 250 patients with all stages of infiltrative breast cancer.* Cancer, 1990. **66**(1): p. 119-129.
52. Neuman, H.B., et al., *Stage IV breast cancer in the era of targeted therapy: does surgery of the primary tumor matter?* Cancer: Interdisciplinary International Journal of the American Cancer Society, 2010. **116**(5): p. 1226-1233.
53. Singletary, S.E., et al., *Revision of the American Joint Committee on Cancer staging system for breast cancer.* J Clin Oncol, 2002. **20**(17): p. 3628-36.
54. Perou, C.M., et al., *Molecular portraits of human breast tumours.* Nature, 2000. **406**(6797): p. 747-52.
55. Sørlie, T., et al., *Gene expression patterns of breast carcinomas distinguish tumor subclasses with clinical implications.* Proceedings of the National Academy of Sciences, 2001. **98**(19): p. 10869-10874.
56. Prat, A. and C.M. Perou, *Deconstructing the molecular portraits of breast cancer.* Molecular oncology, 2011. **5**(1): p. 5-23.
57. Eroles, P., et al., *Molecular biology in breast cancer: intrinsic subtypes and signaling pathways.* Cancer treatment reviews, 2012. **38**(6): p. 698-707.
58. Ades, F., et al., *Luminal B breast cancer: molecular characterization, clinical management, and future perspectives.* Journal of clinical oncology, 2014. **32**(25): p. 2794-2803.
59. Prat, A., et al., *Prognostic significance of progesterone receptor-positive tumor cells within immunohistochemically defined luminal A breast cancer.* J Clin Oncol, 2013. **31**(2): p. 203-9.
60. Xu, C., et al., *FOXA1 Expression Significantly Predict Response to Chemotherapy in Estrogen Receptor-Positive Breast Cancer Patients.* Annals of Surgical Oncology, 2015. **22**(6): p. 2034-2039.
61. Prat, A., et al., *Molecular Features and Survival Outcomes of the Intrinsic Subtypes Within HER2-Positive Breast Cancer*. JNCI: Journal of the National Cancer Institute, 2014. **106**(8).
62. Plasilova, M.L., et al., *Features of triple-negative breast cancer: Analysis of 38,813 cases from the national cancer database.* Medicine, 2016. **95**(35).
63. Wang, D.-Y., et al., *Molecular stratification within triple-negative breast cancer subtypes.* Scientific Reports, 2019. **9**(1): p. 19107.
64. Khan, M.Z.I., et al., *An overview on Estrogen receptors signaling and its ligands in breast cancer*. European Journal of Medicinal Chemistry, 2022. **241**: p. 114658.
65. Osborne, C.K. and R. Schiff, *Mechanisms of endocrine resistance in breast cancer.* Annu Rev Med, 2011. **62**: p. 233-47.
66. Boon, W.C. and E.R. Simpson, *Chapter 33 - Neuroendocrine Inherited or Induced Aromatase Enzyme Deficits*, in *Handbook of Neuroendocrinology*, G. Fink, D.W. Pfaff, and J.E. Levine, Editors. 2012, Academic Press: San Diego. p. 723-737.
67. Simpson, E.R., *Sources of estrogen and their importance.* The Journal of Steroid Biochemistry and Molecular Biology, 2003. **86**(3): p. 225-230.
68. Gruber, C.J., et al., *Production and actions of estrogens.* N Engl J Med, 2002. **346**(5): p. 340-52.

69. Zhu, B.T., et al., *Quantitative Structure-Activity Relationship of Various Endogenous Estrogen Metabolites for Human Estrogen Receptor α and β Subtypes: Insights into the Structural Determinants Favoring a Differential Subtype Binding.* Endocrinology, 2006. **147**(9): p. 4132-4150.
70. Ng, H.W., et al. *Versatility or Promiscuity: The Estrogen Receptors, Control of Ligand Selectivity and an Update on Subtype Selective Ligands*. International Journal of Environmental Research and Public Health, 2014. **11**, 8709-8742 DOI: 10.3390/ijerph110908709.
71. Richardson, H., et al., *Baseline estrogen levels in postmenopausal women participating in the MAP.3 breast cancer chemoprevention trial.* Menopause, 2020. **27**(6): p. 693-700.
72. Samavat, H. and M.S. Kurzer, *Estrogen metabolism and breast cancer.* Cancer Lett, 2015. **356**(2 Pt A): p. 231-43.
73. Falk, R.T., et al., *Estrogen Metabolites Are Not Associated with Colorectal Cancer Risk in Postmenopausal Women.* Cancer Epidemiology, Biomarkers & Prevention, 2015. **24**(9): p. 1419-1422.
74. Fata, J.E., Z. Werb, and M.J. Bissell, *Regulation of mammary gland branching morphogenesis by the extracellular matrix and its remodeling enzymes.* Breast Cancer Res, 2004. **6**(1): p. 1-11.
75. Vrtačnik, P., et al., *The many faces of estrogen signaling.* Biochem Med (Zagreb), 2014. **24**(3): p. 329-42.
76. Lee, H.-R., et al., *Treatment with bisphenol A and methoxychlor results in the growth of human breast cancer cells and alteration of the expression of cell cycle-related genes, cyclin D1 and p21, via an estrogen receptor-dependent signaling pathway.* Int J Mol Med, 2012. **29**(5): p. 883-890.
77. Edwards, D.P., *REGULATION OF SIGNAL TRANSDUCTION PATHWAYS BY ESTROGEN AND PROGESTERONE.* Annual Review of Physiology, 2004. **67**(1): p. 335-376.
78. Haque, M.M. and K.V. Desai, *Pathways to endocrine therapy resistance in breast cancer.* Frontiers in endocrinology, 2019. **10**: p. 573.
79. Ascenzi, P., A. Bocedi, and M. Marino, *Structure–function relationship of estrogen receptor α and β: Impact on human health.* Molecular Aspects of Medicine, 2006. **27**(4): p. 299-402.
80. Li, X., et al., *Single-chain estrogen receptors (ERs) reveal that the ERalpha/beta heterodimer emulates functions of the ERalpha dimer in genomic estrogen signaling pathways.* Mol Cell Biol, 2004. **24**(17): p. 7681-94.
81. García-Becerra, R., et al. *Mechanisms of Resistance to Endocrine Therapy in Breast Cancer: Focus on Signaling Pathways, miRNAs and Genetically Based Resistance*. International Journal of Molecular Sciences, 2013. **14**, 108-145 DOI: 10.3390/ijms14010108.
82. Lewis, J.S. and V.C. Jordan, *Selective estrogen receptor modulators (SERMs): Mechanisms of anticarcinogenesis and drug resistance.* Mutation Research/Fundamental and Molecular Mechanisms of Mutagenesis, 2005. **591**(1): p. 247-263.
83. Hamilton, K.J., et al., *Chapter Four - Estrogen Hormone Biology*, in *Current Topics in Developmental Biology*, D. Forrest and S. Tsai, Editors. 2017, Academic Press. p. 109-146.
84. Musgrove, E.A. and R.L. Sutherland, *Biological determinants of endocrine resistance in breast cancer.* Nat Rev Cancer, 2009. **9**(9): p. 631-43.
85. Fuentes, N. and P. Silveyra, *Estrogen receptor signaling mechanisms.* Adv Protein Chem Struct Biol, 2019. **116**: p. 135-170.
86. Stice, J.P. and A.A. Knowlton, *Estrogen, NFκB, and the Heat Shock Response.* Molecular Medicine, 2008. **14**(7): p. 517-527.
87. Heldring, N., et al., *Estrogen receptors: how do they signal and what are their targets.* Physiol Rev, 2007. **87**(3): p. 905-31.
88. Ratajczak, T., *Protein coregulators that mediate estrogen receptor function.* Reprod Fertil Dev, 2001. **13**(4): p. 221-9.
89. Hurtado, A., et al., *Regulation of ERBB2 by oestrogen receptor-PAX2 determines response to tamoxifen.* Nature, 2008. **456**(7222): p. 663-6.

90. Stender, J.D., et al., *Genome-wide analysis of estrogen receptor alpha DNA binding and tethering mechanisms identifies Runx1 as a novel tethering factor in receptor-mediated transcriptional activation.* Mol Cell Biol, 2010. **30**(16): p. 3943-55.
91. Kushner, P.J., et al., *Estrogen receptor pathways to AP-1.* J Steroid Biochem Mol Biol, 2000. **74**(5): p. 311-7.
92. Björnström, L. and M. Sjöberg, *Mechanisms of Estrogen Receptor Signaling: Convergence of Genomic and Nongenomic Actions on Target Genes.* Molecular Endocrinology, 2005. **19**(4): p. 833-842.
93. Revankar, C.M., et al., *A transmembrane intracellular estrogen receptor mediates rapid cell signaling.* Science, 2005. **307**(5715): p. 1625-30.
94. Harrington, W.R., et al., *Estrogen Dendrimer Conjugates that Preferentially Activate Extranuclear, Nongenomic Versus Genomic Pathways of Estrogen Action.* Molecular Endocrinology, 2006. **20**(3): p. 491-502.
95. Bennesch, M.A. and D. Picard, *Minireview: Tipping the balance: ligand-independent activation of steroid receptors.* Mol Endocrinol, 2015. **29**(3): p. 349-63.
96. Nilsson, S., et al., *Mechanisms of estrogen action.* Physiol Rev, 2001. **81**(4): p. 1535-65.
97. Spring, L.M., et al., *Neoadjuvant Endocrine Therapy for Estrogen Receptor-Positive Breast Cancer: A Systematic Review and Meta-analysis.* JAMA Oncol, 2016. **2**(11): p. 1477-1486.
98. Dao, K.-L. and R.N. Hanson, *Targeting the Estrogen Receptor using Steroid–Therapeutic Drug Conjugates (Hybrids).* Bioconjugate Chemistry, 2012. **23**(11): p. 2139-2158.
99. Musa, A.M., M. Omar F. Khan, and S.J. Cooperwood, *Medicinal Chemistry and Emerging Strategies Applied to the Development of Selective Estrogen Receptor Modulators (SERMs).* Current Medicinal Chemistry, 2007. **14**(11): p. 1249-1261.
100. Prossnitz, E.R. and M. Barton, *Estrogen biology: New insights into GPER function and clinical opportunities.* Molecular and Cellular Endocrinology, 2014. **389**(1): p. 71-83.
101. Belachew, E.B. and D.T. Sewasew, *Molecular Mechanisms of Endocrine Resistance in Estrogen-Positive Breast Cancer.* Front Endocrinol (Lausanne), 2021. **12**: p. 599586.
102. Belachew, E.B. and D.T. Sewasew, *Molecular Mechanisms of Endocrine Resistance in Estrogen-Receptor-Positive Breast Cancer.* Frontiers in Endocrinology, 2021. **12**.
103. Hanker, A.B., D.R. Sudhan, and C.L. Arteaga, *Overcoming Endocrine Resistance in Breast Cancer.* Cancer Cell, 2020. **37**(4): p. 496-513.
104. Pan, H., et al., *20-Year Risks of Breast-Cancer Recurrence after Stopping Endocrine Therapy at 5 Years.* New England Journal of Medicine, 2017. **377**(19): p. 1836-1846.
105. Waks, A.G. and E.P. Winer, *Breast Cancer Treatment: A Review.* Jama, 2019. **321**(3): p. 288-300.
106. Patel, H.K. and T. Bihani, *Selective estrogen receptor modulators (SERMs) and selective estrogen receptor degraders (SERDs) in cancer treatment.* Pharmacology & Therapeutics, 2018. **186**: p. 1-24.
107. Fisher, B., et al., *Effect of preoperative chemotherapy on local-regional disease in women with operable breast cancer: findings from National Surgical Adjuvant Breast and Bowel Project B-18.* Journal of Clinical Oncology, 1997. **15**(7): p. 2483-2493.
108. Korde, L.A., et al., *Neoadjuvant Chemotherapy, Endocrine Therapy, and Targeted Therapy for Breast Cancer: ASCO Guideline.* Journal of Clinical Oncology, 2021. **39**(13): p. 1485-1505.
109. Burstein, H.J., *Systemic Therapy for Estrogen Receptor-Positive, HER2-Negative Breast Cancer.* N Engl J Med, 2020. **383**(26): p. 2557-2570.
110. Coates, A.S., et al., *Tailoring therapies--improving the management of early breast cancer: St Gallen International Expert Consensus on the Primary Therapy of Early Breast Cancer 2015.* Ann Oncol, 2015. **26**(8): p. 1533-46.
111. Sledge, G.W., Jr., et al., *The Effect of Abemaciclib Plus Fulvestrant on Overall Survival in Hormone Receptor-Positive, ERBB2-Negative Breast Cancer That Progressed on Endocrine Therapy-MONARCH 2: A Randomized Clinical Trial.* JAMA Oncol, 2020. **6**(1): p. 116-124.
112. Cardoso, F., et al., *70-Gene Signature as an Aid to Treatment Decisions in Early-Stage Breast Cancer.* N Engl J Med, 2016. **375**(8): p. 717-29.

113. Jameera Begam, A., S. Jubie, and M.J. Nanjan, *Estrogen receptor agonists/antagonists in breast cancer therapy: A critical review.* Bioorg Chem, 2017. **71**: p. 257-274.
114. Davies, C., et al., *Relevance of breast cancer hormone receptors and other factors to the efficacy of adjuvant tamoxifen: patient-level meta-analysis of randomised trials.* Lancet, 2011. **378**(9793): p. 771-84.
115. Martinkovich, S., et al., *Selective estrogen receptor modulators: tissue specificity and clinical utility.* Clinical Interventions in Aging, 2014. **9**: p. 1437-1452.
116. Shang, Y., et al., *Cofactor dynamics and sufficiency in estrogen receptor-regulated transcription.* Cell, 2000. **103**(6): p. 843-52.
117. Ellis, M.J., et al., *Fulvestrant 500 mg Versus Anastrozole 1 mg for the First-Line Treatment of Advanced Breast Cancer: Overall Survival Analysis From the Phase II FIRST Study.* J Clin Oncol, 2015. **33**(32): p. 3781-7.
118. Cristofanilli, M., et al., *Fulvestrant plus palbociclib versus fulvestrant plus placebo for treatment of hormone-receptor-positive, HER2-negative metastatic breast cancer that progressed on previous endocrine therapy (PALOMA-3): final analysis of the multicentre, double-blind, phase 3 randomised controlled trial.* Lancet Oncol, 2016. **17**(4): p. 425-439.
119. McDonnell, D.P. and S.E. Wardell, *The molecular mechanisms underlying the pharmacological actions of ER modulators: implications for new drug discovery in breast cancer.* Current Opinion in Pharmacology, 2010. **10**(6): p. 620-628.
120. Hernando, C., et al., *Oral Selective Estrogen Receptor Degraders (SERDs) as a Novel Breast Cancer Therapy: Present and Future from a Clinical Perspective.* Int J Mol Sci, 2021. **22**(15).
121. Slamon, D.J., et al., *Phase III Randomized Study of Ribociclib and Fulvestrant in Hormone Receptor–Positive, Human Epidermal Growth Factor Receptor 2–Negative Advanced Breast Cancer: MONALEESA-3.* Journal of Clinical Oncology, 2018. **36**(24): p. 2465-2472.
122. Brueggemeier, R.W., J.C. Hackett, and E.S. Diaz-Cruz, *Aromatase Inhibitors in the Treatment of Breast Cancer.* Endocrine Reviews, 2005. **26**(3): p. 331-345.
123. Corbin, C.J., et al., *Isolation of a full-length cDNA insert encoding human aromatase system cytochrome P-450 and its expression in nonsteroidogenic cells.* Proc Natl Acad Sci U S A, 1988. **85**(23): p. 8948-52.
124. Molehin, D., et al., *Regulation of aromatase in cancer.* Molecular and Cellular Biochemistry, 2021. **476**(6): p. 2449-2464.
125. Miller, W.R., *Aromatase inhibitors: mechanism of action and role in the treatment of breast cancer.* Seminars in Oncology, 2003. **30**: p. 3-11.
126. Kang, H., et al., *Potent aromatase inhibitors and molecular mechanism of inhibitory action.* European Journal of Medicinal Chemistry, 2018. **143**: p. 426-437.
127. Early Breast Cancer Trialists' Collaborative, G., *Aromatase inhibitors versus tamoxifen in early breast cancer: patient-level meta-analysis of the randomised trials.* The Lancet, 2015. **386**(10001): p. 1341-1352.
128. Ellis, M.J., et al., *Randomized phase II neoadjuvant comparison between letrozole, anastrozole, and exemestane for postmenopausal women with estrogen receptor-rich stage 2 to 3 breast cancer: clinical and biomarker outcomes and predictive value of the baseline PAM50-based intrinsic subtype--ACOSOG Z1031.* J Clin Oncol, 2011. **29**(17): p. 2342-9.
129. Johannessen, D.C., et al., *Endocrine and clinical effects of exemestane (PNU 155971), a novel steroidal aromatase inhibitor, in postmenopausal breast cancer patients: a phase I study.* Clinical Cancer Research, 1997. **3**(7): p. 1101-1108.
130. Kaufmann, M., et al., *Exemestane Is Superior to Megestrol Acetate After Tamoxifen Failure in Postmenopausal Women With Advanced Breast Cancer: Results of a Phase III Randomized Double-Blind Trial.* Journal of Clinical Oncology, 2000. **18**(7): p. 1399-1411.
131. Landry, K.K., A.F. David, and D. Zeruesenay, *In Vitro Cytochrome P450-Mediated Metabolism of Exemestane.* Drug Metabolism and Disposition, 2011. **39**(1): p. 98.
132. Wang, L.-Z., et al., *Validation of a Rapid and Sensitive LC-MS/MS Method for Determination of Exemestane and Its Metabolites, 17β-Hydroxyexemestane and 17β-Hydroxyexemestane-17-O-β-D-Glucuronide: Application to Human Pharmacokinetics Study.* PLOS ONE, 2015. **10**(3): p. e0118553.

133. Ariazi, E.A., et al., *Exemestane's 17-hydroxylated metabolite exerts biological effects as an androgen.* Molecular cancer therapeutics, 2007. **6**(11): p. 2817-2827.
134. Takagi, K., et al., *Increased intratumoral androgens in human breast carcinoma following aromatase inhibitor exemestane treatment.* Endocrine-related cancer, 2010. **17**(2): p. 415.
135. Sobral, A.F., et al., *Unravelling exemestane: From biology to clinical prospects.* The Journal of Steroid Biochemistry and Molecular Biology, 2016. **163**: p. 1-11.
136. Bhatnagar, A.S., *The discovery and mechanism of action of letrozole.* Breast Cancer Research and Treatment, 2007. **105**(1): p. 7-17.
137. Haynes, B.P., et al., *The pharmacology of letrozole.* The Journal of Steroid Biochemistry and Molecular Biology, 2003. **87**(1): p. 35-45.
138. Lønning, P.E., *Aromatase inhibitors and inactivators in breast cancer.* Bmj, 2001. **323**(7318): p. 880-1.
139. Lønning, P.E. and J. Geisler, *Experience with Exemestane in the Treatment of Early and Advanced Breast Cancer.* Expert Opinion on Drug Metabolism & Toxicology, 2008. **4**(7): p. 987-997.
140. Bahrami, N., et al., *The NEOLETEXE trial: a neoadjuvant cross-over study exploring the lack of cross resistance between aromatase inhibitors.* Future Oncology, 2019. **15**(32): p. 3675-3682.
141. Chang, M., *Tamoxifen resistance in breast cancer.* Biomol Ther (Seoul), 2012. **20**(3): p. 256-67.
142. Hoskins, J.M., L.A. Carey, and H.L. McLeod, *CYP2D6 and tamoxifen: DNA matters in breast cancer.* Nature Reviews Cancer, 2009. **9**(8): p. 576-586.
143. Giuliano, M., et al., *Biological mechanisms and clinical implications of endocrine resistance in breast cancer.* Breast, 2011. **20 Suppl 3**: p. S42-9.
144. Ottaviano, Y.L., et al., *Methylation of the estrogen receptor gene CpG island marks loss of estrogen receptor expression in human breast cancer cells.* Cancer Res, 1994. **54**(10): p. 2552-5.
145. Fleischer, T., et al., *DNA methylation at enhancers identifies distinct breast cancer lineages.* Nature Communications, 2017. **8**(1): p. 1379.
146. Harrod, A., et al., *Genome engineering for estrogen receptor mutations reveals differential responses to anti-estrogens and new prognostic gene signatures for breast cancer.* Oncogene, 2022. **41**(44): p. 4905-4915.
147. Karmakar, S., et al., *Distinctive functions of p160 steroid receptor coactivators in proliferation of an estrogen-independent, tamoxifen-resistant breast cancer cell line.* Endocrine-Related Cancer, 2011. **18**(1): p. 113-127.
148. Zhou, Y., et al., *Enhanced NFκB and AP-1 transcriptional activity associated with antiestrogen resistant breast cancer.* BMC Cancer, 2007. **7**(1): p. 59.
149. Dawson, S.J., E. Provenzano, and C. Caldas, *Triple negative breast cancers: clinical and prognostic implications.* Eur J Cancer, 2009. **45 Suppl 1**: p. 27-40.
150. Massarweh, S., et al., *Tamoxifen resistance in breast tumors is driven by growth factor receptor signaling with repression of classic estrogen receptor genomic function.* Cancer Res, 2008. **68**(3): p. 826-33.
151. Turczyk, L., et al., *FGFR2-Driven Signaling Counteracts Tamoxifen Effect on ERα-Positive Breast Cancer Cells.* Neoplasia, 2017. **19**(10): p. 791-804.
152. Vora, Sadhna R., et al., *CDK 4/6 Inhibitors Sensitize PIK3CA Mutant Breast Cancer to PI3K Inhibitors.* Cancer Cell, 2014. **26**(1): p. 136-149.
153. Bai, J., Y. Li, and G.-J. Zhang, *Cell cycle regulation and anticancer drug discovery.* Cancer Biology & Medicine, 2017. **14**: p. 348.
154. Mireia Cruz De los, S., P.D. Mihnea, and A.C. George, *The role of exosomal long non-coding RNAs in cancer drug resistance.* Cancer Drug Resistance, 2019. **2**(4): p. 1178-1192.
155. Li, D., et al., *Tumor-associated macrophages secrete CC-chemokine ligand 2 and induce tamoxifen resistance by activating PI3K/Akt/mTOR in breast cancer.* Cancer Science, 2020. **111**(1): p. 47-58.

156. Jiménez-Garduño, A.M., et al., *IL-1β induced methylation of the estrogen receptor ERα gene correlates with EMT and chemoresistance in breast cancer cells.* Biochemical and Biophysical Research Communications, 2017. **490**(3): p. 780-785.
157. Alamolhodaei, N.S., et al., *MiR 221/222 as new players in tamoxifen resistance.* Curr Pharm Des, 2016. **22**(46): p. 6946-55.
158. Chen, M.-J., et al., *MiR-148a and miR-152 reduce tamoxifen resistance in ER+ breast cancer via downregulating ALCAM.* Biochemical and Biophysical Research Communications, 2017. **483**(2): p. 840-846.
159. Huang, D., et al., *Mechanisms of resistance to selective estrogen receptor down-regulator in metastatic breast cancer.* Biochim Biophys Acta Rev Cancer, 2017. **1868**(1): p. 148-156.
160. Franke, T.F., et al., *The protein kinase encoded by the Akt proto-oncogene is a target of the PDGF-activated phosphatidylinositol 3-kinase.* Cell, 1995. **81**(5): p. 727-736.
161. Beeram, M., et al., *Akt-induced endocrine therapy resistance is reversed by inhibition of mTOR signaling.* Annals of Oncology, 2007. **18**(8): p. 1323-1328.
162. Baselga, J., et al., *Buparlisib plus fulvestrant versus placebo plus fulvestrant in postmenopausal, hormone receptor-positive, HER2-negative, advanced breast cancer (BELLE-2): a randomised, double-blind, placebo-controlled, phase 3 trial.* Lancet Oncol, 2017. **18**(7): p. 904-916.
163. Fribbens, C., et al., *Plasma ESR1 Mutations and the Treatment of Estrogen Receptor–Positive Advanced Breast Cancer.* Journal of Clinical Oncology, 2016. **34**(25): p. 2961-2968.
164. Giessrigl, B., et al., *Fulvestrant induces resistance by modulating GPER and CDK6 expression: implication of methyltransferases, deacetylases and the hSWI/SNF chromatin remodelling complex.* British Journal of Cancer, 2013. **109**(10): p. 2751-2762.
165. Zhang, Y., et al., *Elevated insulin-like growth factor 1 receptor signaling induces antiestrogen resistance through the MAPK/ERK and PI3K/Akt signaling routes.* Breast cancer research, 2011. **13**(3): p. 1-16.
166. Baldwin, A.S., *Control of oncogenesis and cancer therapy resistance by the transcription factor NF-κB.* The Journal of clinical investigation, 2001. **107**(3): p. 241-246.
167. Rao, X., et al., *MicroRNA-221/222 confers breast cancer fulvestrant resistance by regulating multiple signaling pathways.* Oncogene, 2011. **30**(9): p. 1082-1097.
168. Yang, J., et al., *Estrogen receptor-α directly regulates the hypoxia-inducible factor 1 pathway associated with antiestrogen response in breast cancer.* Proceedings of the National Academy of Sciences, 2015. **112**(49): p. 15172-15177.
169. Sledge, G.W., et al., *Past, present, and future challenges in breast cancer treatment.* J Clin Oncol, 2014. **32**(19): p. 1979-86.
170. Li, S., et al., *Endocrine-therapy-resistant ESR1 variants revealed by genomic characterization of breast-cancer-derived xenografts.* Cell Reports, 2013. **4**: p. 1116-1130.
171. Fox, E.M., et al., *Autocrine IGF-I/insulin receptor axis compensates for inhibition of AKT in ER-positive breast cancer cells with resistance to estrogen deprivation.* Breast Cancer Research, 2013. **15**(4): p. R55.
172. Collins, L., et al., *Androgen receptor expression in breast cancer in relation to molecular phenotype: results from the Nurses' Health Study.* Modern Pathology, 2011. **24**: p. 924-931.
173. Macedo, L.F., et al., *Combination of Anastrozole with Fulvestrant in the Intratumoral Aromatase Xenograft Model.* Cancer Research, 2008. **68**(9): p. 3516-3522.
174. Augusto, T.V., et al., *Acquired resistance to aromatase inhibitors: where we stand!* Endocrine-Related Cancer, 2018. **25**(5): p. R283-R301.
175. Chen, S., *An "Omics" Approach to Determine the Mechanisms of Acquired Aromatase Inhibitor Resistance.* OMICS: A Journal of Integrative Biology, 2011. **15**(6): p. 347-352.
176. Wang, X., et al., *The Role of Amphiregulin in Exemestane-Resistant Breast Cancer Cells: Evidence of an Autocrine Loop.* Cancer Research, 2008. **68**(7): p. 2259-2265.
177. Arpino, G., et al., *Crosstalk between the Estrogen Receptor and the HER Tyrosine Kinase Receptor Family: Molecular Mechanism and Clinical Implications for Endocrine Therapy Resistance.* Endocrine Reviews, 2008. **29**(2): p. 217-233.

178. Beaver, J.A. and B.H. Park, *The BOLERO-2 trial: the addition of everolimus to exemestane in the treatment of postmenopausal hormone receptor-positive advanced breast cancer.* Future Oncology, 2012. **8**(6): p. 651-657.
179. Hole, S., et al., *Aurora kinase A and B as new treatment targets in aromatase inhibitor-resistant breast cancer cells.* Breast Cancer Research and Treatment, 2015. **149**(3): p. 715-726.
180. Khatri, R., et al., *Aromatase Inhibitor–Mediated Downregulation of INrf2 (Keap1) Leads to Increased Nrf2 and Resistance in Breast Cancer.* Molecular cancer therapeutics, 2015. **14**(7): p. 1728-1737.
181. Kubo, M., et al., *Inhibition of the proliferation of acquired aromatase inhibitor-resistant breast cancer cells by histone deacetylase inhibitor LBH589 (panobinostat).* Breast Cancer Research and Treatment, 2013. **137**(1): p. 93-107.
182. Hanamura, T., et al., *Androgen metabolite-dependent growth of hormone receptor-positive breast cancer as a possible aromatase inhibitor-resistance mechanism.* Breast Cancer Research and Treatment, 2013. **139**(3): p. 731-740.
183. O'Shaughnessy, J., et al., *Abiraterone acetate, exemestane or the combination in postmenopausal patients with estrogen receptor-positive metastatic breast cancer.* Ann Oncol, 2016. **27**(1): p. 106-13.
184. Rechoum, Y., et al., *AR collaborates with ERα in aromatase inhibitor-resistant breast cancer.* Breast Cancer Research and Treatment, 2014. **147**(3): p. 473-485.
185. Tilghman, S.L., et al., *Proteomic signatures of acquired letrozole resistance in breast cancer: suppressed estrogen signaling and increased cell motility and invasiveness.* Molecular & Cellular Proteomics, 2013. **12**(9): p. 2440-2455.
186. Mayer, I.A., et al., *Stand up to cancer phase Ib study of pan-phosphoinositide-3-kinase inhibitor buparlisib with letrozole in estrogen receptor-positive/human epidermal growth factor receptor 2-negative metastatic breast cancer.* J Clin Oncol, 2014. **32**(12): p. 1202-9.
187. Hortobagyi, G.N., et al., *Ribociclib as first-line therapy for HR-positive, advanced breast cancer.* New England Journal of Medicine, 2016. **375**: p. 1738-1748.
188. Schech, A.J., et al., *Histone deacetylase inhibitor entinostat in combination with a retinoid downregulates HER2 and reduces the tumor initiating cell population in aromatase inhibitor-resistant breast cancer.* Breast Cancer Research and Treatment, 2015. **152**(3): p. 499-508.
189. Das, P.M., et al., *Chromatin immunoprecipitation assay.* Biotechniques, 2004. **37**(6): p. 961-9.
190. Park, P.J., *ChIP–seq: advantages and challenges of a maturing technology.* Nature Reviews Genetics, 2009. **10**(10): p. 669-680.
191. Latchman, D.S., *Transcription factors: An overview.* The International Journal of Biochemistry & Cell Biology, 1997. **29**(12): p. 1305-1312.
192. Furey, T.S. and P. Sethupathy, *Genetics. Genetics driving epigenetics.* Science, 2013. **342**(6159): p. 705-6.
193. Hinshelwood, R.A. and S.J. Clark, *Breast cancer epigenetics: normal human mammary epithelial cells as a model system.* Journal of molecular medicine, 2008. **86**: p. 1315-1328.
194. Shilatifard, A., *Chromatin modifications by methylation and ubiquitination: implications in the regulation of gene expression.* Annu. Rev. Biochem., 2006. **75**: p. 243-269.
195. Shanmugam, M.K., et al., *Role of novel histone modifications in cancer.* Oncotarget, 2017. **9**(13).
196. Wade, P.A., *Transcriptional control at regulatory checkpoints by histone deacetylases: molecular connections between cancer and chromatin.* Hum Mol Genet, 2001. **10**(7): p. 693-8.
197. Chun, P., *Histone deacetylase inhibitors in hematological malignancies and solid tumors.* Archives of Pharmacal Research, 2015. **38**(6): p. 933-949.
198. Kouzarides, T., *Histone methylation in transcriptional control.* Current opinion in genetics & development, 2002. **12**(2): p. 198-209.

199. De Smet, C., A. Loriot, and T. Boon, *Promoter-Dependent Mechanism Leading to Selective Hypomethylation within the 5' Region of Gene MAGE-A1 in Tumor Cells.* Molecular and Cellular Biology, 2004. **24**(11): p. 4781-4790.
200. Steinhauser, S., et al., *A comprehensive comparison of tools for differential ChIP-seq analysis.* Briefings in Bioinformatics, 2016. **17**(6): p. 953-966.
201. Nakato, R. and T. Sakata, *Methods for ChIP-seq analysis: A practical workflow and advanced applications.* Methods, 2021. **187**: p. 44-53.
202. Koboldt, D.C., et al., *The next-generation sequencing revolution and its impact on genomics.* Cell, 2013. **155**(1): p. 27-38.
203. Zhu, J., et al., *Genome-wide chromatin state transitions associated with developmental and environmental cues.* Cell, 2013. **152**(3): p. 642-54.
204. Rabbani, B., et al., *Next generation sequencing: implications in personalized medicine and pharmacogenomics.* Mol Biosyst, 2016. **12**(6): p. 1818-30.
205. Luque-Bolivar, A., et al., *Resistance and Overcoming Resistance in Breast Cancer.* Breast Cancer (Dove Med Press), 2020. **12**: p. 211-229.
206. Spear, B.B., M. Heath-Chiozzi, and J. Huff, *Clinical application of pharmacogenetics.* Trends Mol Med, 2001. **7**(5): p. 201-4.
207. Waks, A.G. and E.P. Winer, *Breast Cancer Treatment.* Jama, 2019. **321**(3): p. 316.
208. Parsons, J. and C. Francavilla, *'Omics Approaches to Explore the Breast Cancer Landscape.* Front Cell Dev Biol, 2019. **7**: p. 395.
209. Mehta, S., et al., *Predictive and prognostic molecular markers for cancer medicine.* Therapeutic Advances in Medical Oncology, 2010. **2**(2): p. 125-148.
210. Taneja, P., et al., *Classical and Novel Prognostic Markers for Breast Cancer and their Clinical Significance.* Clinical Medicine Insights: Oncology, 2010. **4**: p. CMO.S4773.
211. Naito, Y. and T. Urasaki, *Precision medicine in breast cancer.* Chin Clin Oncol, 2018. **7**(3): p. 29.
212. Collins, F.S. and H. Varmus, *A new initiative on precision medicine.* N Engl J Med, 2015. **372**(9): p. 793-5.
213. Semiglazov, V.F., et al., *Phase 2 randomized trial of primary endocrine therapy versus chemotherapy in postmenopausal patients with estrogen receptor-positive breast cancer.* cancer, 2007. **110**(2): p. 244-254.
214. Lønning, P.E., et al., *Activity of exemestane in metastatic breast cancer after failure of nonsteroidal aromatase inhibitors: a phase II trial.* Journal of Clinical Oncology, 2000. **18**(11): p. 2234-2244.
215. Steele, N., et al., *Exemestane in metastatic breast cancer: effective therapy after third-generation non-steroidal aromatase inhibitor failure.* The Breast, 2006. **15**(3): p. 429-435.
216. Geisler, J., *Differences between the non-steroidal aromatase inhibitors anastrozole and letrozole–of clinical importance?* British journal of cancer, 2011. **104**(7): p. 1059-1066.
217. Lønning, P., *Lack of complete cross-resistance between different aromatase inhibitors; a real finding in search for an explanation?* European journal of cancer, 2009. **45**(4): p. 527-535.
218. Dixon, J.M., T.J. Anderson, and W.R. Miller, *Neoadjuvant endocrine therapy of breast cancer: a surgical perspective.* Eur J Cancer, 2002. **38**(17): p. 2214-21.
219. Geisler, J., et al., *Influence of neoadjuvant anastrozole (Arimidex) on intratumoral estrogen levels and proliferation markers in patients with locally advanced breast cancer.* Clin Cancer Res, 2001. **7**(5): p. 1230-6.
220. Ariazi, E.A., et al., *Exemestane's 17-hydroxylated metabolite exerts biological effects as an androgen.* Molecular Cancer Therapeutics, 2007. **6**(11): p. 2817-2827.
221. Wang, S., et al. *High Throughput Chemical Screening Reveals Multiple Regulatory Proteins on FOXA1 in Breast Cancer Cell Lines*. International Journal of Molecular Sciences, 2018. **19**, DOI: 10.3390/ijms19124123.
222. Gao, L., et al., *The beneficial androgenic action of steroidal aromatase inactivators in estrogen-dependent breast cancer after failure of nonsteroidal drugs.* Cell Death & Disease, 2019. **10**(7): p. 494.

223. Bahrami, N., et al., *Lack of cross-resistance between non-steroidal and steroidal aromatase inhibitors in breast cancer patients: the potential role of the adipokine leptin.* Breast Cancer Res Treat, 2021. **190**(3): p. 435-449.
224. World Health, O., *Guide to cancer early diagnosis*. 2017, Geneva: World Health Organization.
225. Varela, C.L., et al., *Exemestane metabolites: Synthesis, stereochemical elucidation, biochemical activity and anti-proliferative effects in a hormone-dependent breast cancer cell line.* Eur J Med Chem, 2014. **87**: p. 336-45.
226. Kamdem, L.K., D.A. Flockhart, and Z. Desta, *In vitro cytochrome P450-mediated metabolism of exemestane.* Drug Metab Dispos, 2011. **39**(1): p. 98-105.
227. Amaral, C., et al., *Exemestane metabolites suppress growth of estrogen receptor-positive breast cancer cells by inducing apoptosis and autophagy: A comparative study with Exemestane.* Int J Biochem Cell Biol, 2015. **69**: p. 183-95.
228. Amaral, C., et al., *Steroidal aromatase inhibitors inhibit growth of hormone-dependent breast cancer cells by inducing cell cycle arrest and apoptosis.* Apoptosis, 2013. **18**(11): p. 1426-1436.
229. Cepa, M., et al., *New steroidal aromatase inhibitors: Suppression of estrogen-dependent breast cancer cell proliferation and induction of cell death.* BMC Cell Biology, 2008. **9**(1): p. 41.
230. Peterson, A., et al., *In vitro metabolism of exemestane by hepatic cytochrome P450s: impact of nonsynonymous polymorphisms on formation of the active metabolite 17β-dihydroexemestane.* Pharmacol Res Perspect, 2017. **5**(3): p. e00314.
231. Kanaya, N., et al., *AroER tri-screen™ is a novel functional assay to estimate both estrogenic and estrogen precursor activity of chemicals or biological specimens.* Breast Cancer Res Treat, 2015. **151**(2): p. 335-45.
232. Evans, T.R., et al., *Phase I and endocrine study of exemestane (FCE 24304), a new aromatase inhibitor, in postmenopausal women.* Cancer Res, 1992. **52**(21): p. 5933-9.
233. Gao, W., C.E. Bohl, and J.T. Dalton, *Chemistry and structural biology of androgen receptor.* Chem Rev, 2005. **105**(9): p. 3352-70.
234. Park, S., et al., *Androgen receptor expression is significantly associated with better outcomes in estrogen receptor-positive breast cancers.* Annals of Oncology, 2011. **22**(8): p. 1755-1762.
235. Moinfar, F., et al., *Androgen receptors frequently are expressed in breast carcinomas: potential relevance to new therapeutic strategies.* Cancer, 2003. **98**(4): p. 703-11.
236. Birrell, S.N., et al., *Androgens induce divergent proliferative responses in human breast cancer cell lines.* The Journal of Steroid Biochemistry and Molecular Biology, 1995. **52**(5): p. 459-467.
237. Hwang, J.H., et al., *Cordycepin promotes apoptosis by modulating the ERK-JNK signaling pathway via DUSP5 in renal cancer cells.* Am J Cancer Res, 2016. **6**(8): p. 1758-71.
238. Liu, T., et al., *The suppression of DUSP5 expression correlates with paclitaxel resistance and poor prognosis in basal-like breast cancer.* Int J Med Sci, 2018. **15**(7): p. 738-747.
239. Roufayel, R., et al., *BH3-Only Proteins Noxa and Puma Are Key Regulators of Induced Apoptosis.* Life (Basel), 2022. **12**(2).
240. Hunter, K.W., N.P. Crawford, and J. Alsarraj, *Mechanisms of metastasis.* Breast Cancer Res, 2008. **10 Suppl 1**(Suppl 1): p. S2.
241. Chen, W., et al., *Organotropism: new insights into molecular mechanisms of breast cancer metastasis.* npj Precision Oncology, 2018. **2**(1): p. 4.
242. Park, M., et al., *Breast Cancer Metastasis: Mechanisms and Therapeutic Implications.* Int J Mol Sci, 2022. **23**(12).
243. Weigelt, B., J.L. Peterse, and L.J. van 't Veer, *Breast cancer metastasis: markers and models.* Nat Rev Cancer, 2005. **5**(8): p. 591-602.
244. Heerboth, S., et al., *EMT and tumor metastasis.* Clin Transl Med, 2015. **4**: p. 6.
245. Brabletz, T., et al., *EMT in cancer.* Nat Rev Cancer, 2018. **18**(2): p. 128-134.

246. Si, W., et al., *Dysfunction of the Reciprocal Feedback Loop between GATA3- and ZEB2-Nucleated Repression Programs Contributes to Breast Cancer Metastasis.* Cancer Cell, 2015. **27**(6): p. 822-36.
247. Karamanou, K., et al., *Epithelial-to-mesenchymal transition and invadopodia markers in breast cancer: Lumican a key regulator.* Seminars in Cancer Biology, 2020. **62**: p. 125-133.
248. Chen, J., et al., *CCL18 from tumor-associated macrophages promotes breast cancer metastasis via PITPNM3.* Cancer Cell, 2011. **19**(4): p. 541-55.
249. Lyko, F. and R. Brown, *DNA methyltransferase inhibitors and the development of epigenetic cancer therapies.* J Natl Cancer Inst, 2005. **97**(20): p. 1498-506.
250. Cejas, P., et al., *Chromatin immunoprecipitation from fixed clinical tissues reveals tumor-specific enhancer profiles.* Nature Medicine, 2016. **22**(6): p. 685-691.
251. Font-Tello, A., et al., *FiTAc-seq: fixed-tissue ChIP-seq for H3K27ac profiling and super-enhancer analysis of FFPE tissues.* Nature Protocols, 2020. **15**(8): p. 2503-2518.
252. Siv, G., et al., *Breast tumors escape endocrine therapy by ER-independent mechanisms triggered by the coordinated activities of HER2/HER3 and deacetylated FOXA1*. bioRxiv, 2020: p. 2020.09.22.308569.
253. Chou, J., S. Provot, and Z. Werb, *GATA3 in development and cancer differentiation: cells GATA have it!* J Cell Physiol, 2010. **222**(1): p. 42-9.
254. McClure, J.J., X. Li, and C.J. Chou, *Advances and Challenges of HDAC Inhibitors in Cancer Therapeutics.* Adv Cancer Res, 2018. **138**: p. 183-211.
255. Tan, T., et al., *Epigenetic modification regulates tumor progression and metastasis through EMT (Review).* Int J Oncol, 2022. **60**(6).
256. Smith, B.N. and N.A. Bhowmick *Role of EMT in Metastasis and Therapy Resistance*. Journal of Clinical Medicine, 2016. **5**, DOI: 10.3390/jcm5020017.
257. Ma, C.X., et al., *Mechanisms of aromatase inhibitor resistance.* Nature Reviews Cancer, 2015. **15**(5): p. 261-275.
258. Kouros-Mehr, H., et al., *GATA-3 maintains the differentiation of the luminal cell fate in the mammary gland.* Cell, 2006. **127**(5): p. 1041-55.
259. Asselin-Labat, M.L., et al., *Gata-3 is an essential regulator of mammary-gland morphogenesis and luminal-cell differentiation.* Nat Cell Biol, 2007. **9**(2): p. 201-9.
260. Usary, J., et al., *Mutation of GATA3 in human breast tumors.* Oncogene, 2004. **23**(46): p. 7669-7678.
261. Brigham, et al., *Comprehensive molecular portraits of human breast tumours.* Nature, 2012. **490**(7418): p. 61-70.
262. Adomas, A.B., et al., *Breast tumor specific mutation in GATA3 affects physiological mechanisms regulating transcription factor turnover.* BMC Cancer, 2014. **14**: p. 278.
263. Gustin, J.P., et al., *GATA3 frameshift mutation promotes tumor growth in human luminal breast cancer cells and induces transcriptional changes seen in primary GATA3 mutant breast cancers.* Oncotarget, 2017. **8**(61): p. 103415-103427.
264. Yoon, N.K., et al., *Higher levels of GATA3 predict better survival in women with breast cancer.* Human pathology, 2010. **41**(12): p. 1794-1801.
265. Kouros-Mehr, H., et al., *GATA-3 links tumor differentiation and dissemination in a luminal breast cancer model.* Cancer cell, 2008. **13**(2): p. 141-152.
266. Huang, W., et al., *CUL4B Promotes Breast Carcinogenesis by Coordinating with Transcriptional Repressor Complexes in Response to Hypoxia Signaling Pathway.* Adv Sci (Weinh), 2021. **8**(10): p. 2001515.
267. Zhang, H., L.C. Stephens, and R. Kumar, *Metastasis tumor antigen family proteins during breast cancer progression and metastasis in a reliable mouse model for human breast cancer.* Clin Cancer Res, 2006. **12**(5): p. 1479-86.
268. Kalluri, R. and R.A. Weinberg, *The basics of epithelial-mesenchymal transition.* The Journal of clinical investigation, 2009. **119**(6): p. 1420-1428.
269. Kumar, R. and R.A. Wang, *Structure, expression and functions of MTA genes.* Gene, 2016. **582**(2): p. 112-21.

270. Dannenmann, C., et al., *The metastasis-associated gene MTA1 is upregulated in advanced ovarian cancer, represses ERβ, and enhances expression of oncogenic cytokine GRO.* Cancer Biology & Therapy, 2008. **7**(9): p. 1460-1467.
271. Basta, J. and M. Rauchman, *Chapter 3 - The Nucleosome Remodeling and Deacetylase Complex in Development and Disease*, in *Translating Epigenetics to the Clinic*, J. Laurence and M.V. Beusekom, Editors. 2017, Academic Press: Boston. p. 37-72.
272. Jiao, T., et al., *MTA3 regulates malignant progression of colorectal cancer through Wnt signaling pathway.* Tumor Biology, 2017. **39**(3): p. 1010428317695027.
273. Li, H., et al., *Overexpression of MTA3 correlates with tumor progression in non-small cell lung cancer.* PloS one, 2013. **8**(6): p. e66679.
274. Mazumdar, A., et al., *Transcriptional repression of oestrogen receptor by metastasis-associated protein 1 corepressor.* Nature Cell Biology, 2001. **3**(1): p. 30-37.
275. Şerban, C., C. Anca Maria, and R. Marius, *The Story of MCF-7 Breast Cancer Cell Line: 40 years of Experience in Research.* Anticancer Research, 2015. **35**(6): p. 3147.
276. Fujita, N., et al., *Hormonal Regulation of Metastasis-Associated Protein 3 Transcription in Breast Cancer Cells.* Molecular Endocrinology, 2004. **18**(12): p. 2937-2949.
277. Li, Y., et al., *Loss of GATA3 in bladder cancer promotes cell migration and invasion.* Cancer Biol Ther, 2014. **15**(4): p. 428-35.
278. Yan, W., et al., *GATA3 inhibits breast cancer metastasis through the reversal of epithelial-mesenchymal transition.* J Biol Chem, 2010. **285**(18): p. 14042-51.
279. Wilson, B.J. and V. Giguère, *Meta-analysis of human cancer microarrays reveals GATA3 is integral to the estrogen receptor alpha pathway.* Molecular cancer, 2008. **7**: p. 1-8.
280. Eibl, G. and E. Rozengurt, *KRAS, YAP, and obesity in pancreatic cancer: A signaling network with multiple loops.* Semin Cancer Biol, 2019. **54**: p. 50-62.
281. Zhang, G., et al., *RBPJ contributes to the malignancy of glioblastoma and induction of proneural-mesenchymal transition via IL-6-STAT3 pathway*. Cancer Sci, 2020. **111**(11): p. 4166-4176.
282. Zeisberg, M., et al., *BMP-7 counteracts TGF-beta1-induced epithelial-to-mesenchymal transition and reverses chronic renal injury*. Nat Med, 2003. **9**(7): p. 964-8.
283. Basta, J. and M. Rauchman, *The nucleosome remodeling and deacetylase complex in development and disease.* Transl Res, 2015. **165**(1): p. 36-47.
284. VanderMolen, K.M., et al., *Romidepsin (Istodax, NSC 630176, FR901228, FK228, depsipeptide): a natural product recently approved for cutaneous T-cell lymphoma.* The Journal of Antibiotics, 2011. **64**(8): p. 525-531.
285. Nam, Y.S., et al. *Valproic Acid Inhibits Progressive Hereditary Hearing Loss in a KCNQ4 Variant Model through HDAC1 Suppression*. International Journal of Molecular Sciences, 2023. **24**, DOI: 10.3390/ijms24065695.
286. Wang, C., et al., *Overexpression of the metastasis-associated gene MTA3 correlates with tumor progression and poor prognosis in hepatocellular carcinoma.* Journal of Gastroenterology and Hepatology, 2017. **32**(8): p. 1525-1529.
287. Rana, Z., et al., *Understanding Failure and Improving Treatment Using HDAC Inhibitors for Prostate Cancer.* Biomedicines, 2020. **8**(2).